

Department of Naval Architecture, Ocean and Marine  
Engineering

University of Strathclyde, Glasgow

# **Estimation of Stress Intensity Factors in Ship Structural Connections**

By

**Enqian LIU**

A thesis presented in fulfilment of the requirements for the  
degree of Doctor of Philosophy

August 2021

©Enqian Liu


*I would like to dedicate this thesis to my loving parents*

## Declaration

This thesis is the result of the author's original research. It has been composed by the author and has not been previously submitted for examination which has led to the award of a degree.

The copyright of this thesis belongs to the author under the terms of the United Kingdom Copyright Acts as qualified by University of Strathclyde Regulation 3.50. Due acknowledgement must always be made of the use of any material contained in, or derived from, this thesis.

Enqian Liu

Signed:  Date: 30 August 2021

## Acknowledgements

First of all, I wish to express my limitless thank to my supervisor, Professor Nigel Barltrop. He made me realised that a Ph.D. research work is a kind of training in how to think, present an idea, argue, debate, listen to other people, find a problem, formulate and solve it, etc. Professor Barltrop always encouraged me when I felt confused in conducting the research. He guided me through the research with his extensive knowledge, experience and ever optimism. Without Professor Barltrop, this thesis could never have been accomplished.

I also want to express my limitless thank to my department NAOME, for the financial support during my Ph.D. study. I would like to thank to Ms. Thelma Will, Ms. Susan Pawson, and Mr. Ross Gilmour for their care and support on all the administrative details and IT problems solving.

Special thanks to my friend and mentor Dr Gerard for his unlimited help to improve my thesis grammatically and, his time and patience to proofread my thesis generously. His profound experience broadened my views to the wider world and gave countless encouragement and full support throughout.

I deeply thank my colleagues, Dr Li Xu and Dr Benqiang Lou for their kind help and valuable advice during my research. They helped me a lot on the start of my PhD on using ANSYS and MathCAD programmes and shared some of their experiences with me, which also benefited me a lot.

I need to warmly thank Dr Wei Shen for his technical help and worthwhile discussions using Finite Element software. He always solved my academic puzzles with an abundance of patience and compassion.

I would like to express my gratitude to all my friends in Glasgow. Many thanks to my schoolfellows Dr Mengshi Sun, Dr Zhiming Yuan, Dr Aijun Wang, my helpful friend Dr Lei Ju, and all my friends and colleagues in the department of NAOME for their kind assistance during my Ph.D. study.

Finally, I would like to express my deepest gratitude to my father Youguang and my mother Guixia, who have given me endless love, unconditional support, and firm encouragement. I would not be able to succeed without their selfless dedication and support.

Last, but not least, I would like to express my thank once again to all the people who helped me, give my grateful appreciation to the Department of Naval Architecture, Ocean and Marine Engineering and University of Strathclyde. I will never forget the fantastic time I have spent in Glasgow.

## **Abstract**

Stiffened plated structures such as ships and box girder bridges, result in connection details that contain sharp internal corners. Many failures in ship structure have been found to be associated with fatigue crack propagation at the side shell connections between longitudinal and transverse structure. According to elastic stress analysis, these sharp corners are geometric singularities that have an infinite stress in the corner.

A further complication of stiffened structures is that a crack may grow through intersections, e.g. of plates and stiffeners and changes of plate thickness before it causes a catastrophic structural failure. In this thesis, a new approach is developed to simplify the analysis of these issues. The singular stress contribution is, as usual, characterised by  $Y$ , the non-dimensional the stress intensity factor but within this method simplified analysis is used to calculate the  $Y$  values. The method combines a ratio of non-singular linearized ligament stresses to estimate the effect of large changes in crack length and changes in plate thickness with an empirical methods to estimate the local effect as the crack grows through a change of thickness. The method does not require an analysis of the actual singularity, so saving analysis time and, importantly, giving the engineer some feeling for the result and the possibility of a “back of the envelope” calculation for the SIF or  $Y$ .

This work is based on running finite element analyses, to determine the Stress Intensity Factor and  $Y$  and using the results to test the empirical or analytical methods.

The derived methods are useful both for assessment of existing structures and for design application. Comparing the results from the application of this new methodology with the FE method and existing fatigue analysis guidance, the new method is very much quicker and easier to apply. It is though less accurate than FE analysis and so is most appropriate for, (1) preliminary assessment, (2) reliability assessment where many structural and defect variations are to be considered and (3) for checking whether a more detailed analysis is producing sensible results.

For design calculations often a stress concentration factor or SCF is needed that can be used with an S-N curve. The actual predicted peak stress and hence SCF will, for finite element analysis, depend on the element size and will normally increase as the element size decreases. The existing guidance on determining an appropriate stress value for fatigue analysis of a sharp corner is commonly in terms of linearly extrapolating finite element calculated surface stresses from a number of plate thicknesses  $t$  away from the singularity to the corner. A simpler approach, developed for planar plates with sharp corners, assesses the stress on the basis of the dimensions of the corner. This thesis includes checks on the applicability, to more complicated 3-d geometry, of these previous recommendations for the assessment of corner singularities.

## Contents

Abstract .....	i
Contents .....	iii
List of Figures .....	viii
List of Tables .....	xix
Nomenclature .....	xxi
Chapter 1 Introduction.....	1
1.1 Background .....	1
1.2 Motivation and Aims .....	6
1.3 Outline contents of each chapter .....	8
Chapter 2 Literature Review .....	10
2.1 Cracks in Ships.....	10
2.1.1 Liberty Ships.....	10
2.1.2 Problem of Shell-Stiffener Connection.....	14
2.2 Design and assessment for fatigue and fracture .....	19
2.3 S-N curves .....	20
2.3.1 Stress Concentration Factor (SCF) Assessment based on S-N Curve classes .....	22
2.3.2 Hot-spot stress fatigue calculation.....	24
2.3.3 Relationship between hot-spot SCF and weld classification approach .....	27
2.3.4 Structural stress fatigue approach .....	28
2.4 Fracture Mechanics .....	33
2.4.1 The stress field associated with the SIF .....	36



Contents

---

2.4.2	Geometry Correction Factor Y .....	38
2.4.3	Published results for SIFs or Y values.....	39
2.4.4	Energy release rate $G$ .....	40
2.4.5	SIF Weight Function Method .....	40
2.4.6	Critical Distance Method.....	45
2.4.7	Additional Crack Size Method for Notches.....	48
2.4.8	Stress intensity for different crack sizes near a sharp corner and the effective additional crack size $ae$ .....	52
2.4.9	Calculation of SCF for fatigue life estimation from $as$ .....	54
2.4.10	Calculating K Values Using FEM .....	57
2.5	Summary .....	60
2.6	The work reported in this thesis.....	61
Chapter 3	A crack growing through a constant thicknesses plate .....	65
3.1	Introduction.....	65
3.2	FEA of plate thickness change.....	65
3.3	Estimation of the Y values for a constant thickness .....	68
3.3.1	Validation of FEA against Fett's published work for a constant thickness plate .....	68
3.3.2	Empirical estimation of the Y values for a constant thickness finite length cracked plate subject to tension.....	77
3.4	An alternative assessment of the SIF in a finite width plate subject to an axial force and moment .....	83
3.4.1	Introduction.....	83
3.4.2	Details of the approximate method for calculating SIFs in a finite width plate.....	84
3.4.3	The approximate method .....	86
3.4.4	Application of the method to a plate subject to in-plane bending .....	90

3.5	Conclusion .....	91
Chapter 4	Cracks growing through a change of plate thickness .....	93
4.1	Introduction.....	93
4.2	Flat plate with thickness change, results .....	98
4.3	Estimation of SIF values for crack growing through a change in thickness .....	99
4.3.1	Estimation of SIF values for crack growing through a change in thickness: Second empirical method .....	99
4.4	Investigation of $Y$ values for more crack lengths around $W/2$ .....	105
4.4.1	Estimation of SIF values for crack growing through a change in thickness Third empirical method .....	112
4.5	Conclusion .....	118
Chapter 5	Crack growing through “T-shape” connections.....	119
5.1	Empirical estimation of the $Y$ values for a flat stiffener attached to a panel .....	123
5.2	Results for a T section with $t_2 = t_1 / 2$ .....	127
5.3	Crack Growing in a T connection with different ratios of, stiffener to shell plate thickness.....	135
Chapter 6	Study of longitudinal stiffener connection to transverse structure with shell elements and membrane-only fracture mechanics elements .....	142
6.1	Single stiffener model .....	142
6.2	Simplified numerical model.....	149
6.2.1	Method based on the T section analysis .....	149
6.2.2	Modelling the intersection of the shell and frame stiffeners.....	154
6.2.3	Effect of flange and transverse frame on $Y$ values .....	162
6.2.4	Single stiffener shell model subject to stiffener bending.....	165
6.2.5	SIFs for small cracks.....	168

6.3	Conclusion for estimation of Y values in connections .....	169
Chapter 7	Study of three longitudinal stiffener connections to transverse structure with shell elements and membrane-only fracture mechanics elements ... ..	171
7.1	Finite element analysis of the three stiffener model .....	171
7.2	Simplified analysis of the three stiffener model .....	176
7.3	Conclusion of three stiffener simplified modelling .....	182
Chapter 8	Study of a longitudinal stiffener connection to transverse structure with solid elements and solid fracture mechanics elements .....	183
8.1	The solid model.....	183
8.2	Prediction of the bending SIFs in the plate after the stiffener has broken .....	192
8.3	Conclusions for simplified modelling of connection with plate bending included.....	197
Chapter 9	Comparison of Stress Concentration Factors calculated using stress extrapolation and singularity strength estimation .....	198
9.1	SCF Assessment from LEFM .....	199
9.2	Comparison of the different models.....	202
9.3	Results and Analysis .....	205
9.4	SCFs from stress extrapolation .....	215
9.5	Estimation of stress concentration factors SCFs.....	217
9.6	Conclusions related to stresses and SCFs in stiffener connection .....	219
Chapter 10	Conclusions and Recommendations .....	220
10.1	Introduction.....	220
10.2	General Conclusions .....	221
10.3	My Contributions from this study.....	224
10.4	Proposals for future research.....	225
Chapter 11	References and Bibliography.....	227

*Contents*

---

Appendix A	Validation of ANSYS using Fett (1998).....	235
A.1	Introduction.....	235
A.2	Stress intensity factor.....	235
A.3	The rectangular plate with an edge crack.....	236
A.4	The SIF values through FEA methods.....	241
A.5	The SIF results through Fett approach.....	248
A.6	Conclusion.....	252
Appendix B	Validation of ANSYS plate bending calculation using solid elements (with and without crack closure).....	253
B.1	Three Dimensional Analysis.....	253
B.2	Three-dimensional Analysis under tension loading.....	266
B.3	Model with Finite Element method.....	272
B.4	Solid Element Conclusions.....	276
Appendix C	Estimation of SIF values for crack growing through a change in thickness: First empirical method.....	278
Appendix D	References.....	288

## List of Figures

Figure 2-1 Fatigue failure of welded components (Shen, 2015).....	10
Figure 2-2 Liberty Cargo Ships (J, 2008) .....	11
Figure 2-3 Tanker breaking accident (“Liberty tanker”, 1943) (J, 2008) .....	12
Figure 2-4 S-N curves of a plate, a plate with a hole and a plate with longitudinal gussets under tensile stress (Schijve, 2009).....	20
Figure 2-5 Example of design S–N curves for welded joints (Standard, 2014) .	23
Figure 2-6 Loading details on welded attachment (BS7608, 2014).....	24
Figure 2-7 Different thickness based methods of extrapolating of surface stresses to a corner hot-spot .....	26
Figure 2-8 D curve and F2 curve by stress at $2 \times 10^6$ cycles (BS7608:2014 Figure 10) .....	28
Figure 2-9 A failure assessment diagram (Qian, 2016) .....	35
Figure 2-10 Fracture Modes.....	36
Figure 2-11 Coordinate system and stress component ahead of crack tip .....	37
Figure 2-12 Stress normal to the crack plane in Mode I when $\theta = 0$ (Wang, 1996) .....	38
Figure 2-13 The Weight Function method for calculating Stress Intensity Factors .....	42
Figure 2-14 Configurations of infinite sheet with centre crack .....	44
Figure 2-15 Configurations of infinite sheet with edge crack.....	44
Figure 2-16 Variation of $p$ (Singularity Power) at different corner angle (Xu and Barltrop, 2007b) .....	49
Figure 2-17 Stress decay away from singularity for different $p$ (with $\sigma_0 = 100MPa$ ) (Xu and Barltrop, 2007a).....	50

*List of Figures*

---

Figure 2-18 Simple plate with attachment leading to corner stress singularity (Xu and Barltrop, 2009) .....51

Figure 2-19 Power curve to represent reduction in  $ae$  for small cracks.....53

Figure 2-20 Left:  $a + ae$  values calculated from Hasebe & Ueda’s (1981)  $Y$  value; Right:  $(a + ae)^2$  values which are proportional to the SIF,  $K$  [Equation (2.29)].....54

Figure 2-21 E curve SCF for different  $as$  values from Xu et al (2013) .....55

Figure 2-22 D curve SCF for different  $as$  values from Xu et al (2013).....56

Figure 2-23 Coordinate at crack tip and path for displacement extrapolation (Bao et al., 2010).....58

Figure 3-1 Mesh Details and Boundary Conditions Support .....67

Figure 3-2 Mesh Details around Crack Tip.....68

Figure 3-3 Crack in rectangular plates under tension loading (Fett, 1998) .....71

Figure 3-4 Comparisons of  $F_t$ ’ values with FE method and Fett work.....73

Figure 3-5 The errors between Fett, (1998) and FEA:  $\left( \frac{Y_{FEA} - Y_{Fett}}{Y_{Fett}} \right) \%$ .....76

Figure 3-6 Comparisons of  $Y$  values with FE method and Fett, (1998).....77

Figure 3-7 Singular stress on ligament ( $\sigma_{si}$ ) (Stress: Pa).....78

Figure 3-8 Average Stress on ligament from singular stress ( $\sigma_{si\mu}$ ) (Stress: Pa) 79

Figure 3-9 Bending stress from singular stress ( $\sigma_{bmsi}$ ) (Stress: Pa) .....79

Figure 3-10 Average + Bending stress from singular stress ( $\sigma_{si\mu} + \sigma_{bmsi}$ ) (Stress: Pa) .....80

Figure 3-11 Axial stress from applied load ( $\sigma_{\mu a}$ ) (Stress: Pa).....81

Figure 3-12 Bending stress on ligament from applied load ( $\sigma_{bma}$ ) (Stress: Pa)..81

Figure 3-13 Axial and bending stress on ligament ( $\sigma_{\mu a} + \sigma_{bma}$ ) (Stress: Pa).....82

*List of Figures*

---

Figure 3-14 Comparison  $Y$  values between approximate method and Fett (Fett, 1998) results .....83

Figure 3-15 Edge crack subject to tension (Applied tension  $\sigma_0 = 1Pa$ ) .....84

Figure 3-16 Stress distributions and linear equivalent stresses for  $a/w = 0.5$  (Stress: Pa) .....88

Figure 3-17 Comparison of approximate method and Fett (1998) for applied axial stress. ....89

Figure 3-18 Estimated / Fett axial load  $Y$  value .....89

Figure 3-19 Comparison of approximate formula method  $[Y = 1.12 \cdot (\sigma_a / \sigma_{si})]$  and Fett (1998) for applied bending stress. ....90

Figure 3-20 Approximate formula method / Fett in-plane bending  $Y$  value .....91

Figure 4-1 Crack growing into different thickness plates .....93

Figure 4-2 View of plates and (through thickness) crack .....95

Figure 4-3 Crack growing through  $t_1$  plate .....96

Figure 4-4 Crack propagating through  $t_2$  plate.....97

Figure 4-5 SIF values for crack growing in different thickness plates .....98

Figure 4-6 The trends of  $Y$  curves at different  $t_1$  and  $t_2$  thicknesses with the step change at  $ac/at = 1$  shown by the dashed lines (Calculated value for  $ac/at = 1$  is only valid for  $ac/at < 1$ .  $Y$  values for more  $ac/at$  values were calculated later and are shown in Figure 4-11) ..... 100

Figure 4-7  $Y$ -value ( $Y$ ) for a plate with a thickness change divided by  $Y$ -value in a constant thickness (12mm) plate ( $Y_c$ ) for the same crack length from Figure 3-17 (Note this does not show the extrapolation to the cases where the crack has just penetrated the changed thickness)..... 101

Figure 4-8 Approximately of  $Y_e$  (dashed lines) and FEA (solid lines) of  $Y/Y_c$  constant thickness values ( $Y/Y_c$ ) for a crack from  $t_1$  to  $t_2$  (Note the approximate values allow for the step in the  $Y$  value at the change in thickness using  $Y_e$  [Equations (4.1) and (4.2)], that was not calculated for  $ac/at$  just greater than 1 in the FEA) ..... 103

*List of Figures*

---

Figure 4-9 Approximate (dashed lines) and FEA (solid lines) of  $Y$  values for a crack from  $t_1$  to  $t_2$ , log vertical axis (Note approximate values are extrapolated back to the step in the  $Y$  value at the change in thickness, using the function  $Ye$  [Equations (4.1) and (4.2)], that was not calculated for  $ac/at$  just greater than 1 in the FEA).....104

Figure 4-10 SIF values for crack lengths around  $W/2$  for different  $t_2$  thicknesses .....106

Figure 4-11  $Y$  values for crack lengths around  $at$  .....107

Figure 4-12 Ratio of  $Y$  value for changing in thickness to  $Y$  value for constant thickness just before crack reaches the thickness change .....108

Figure 4-13 Ratio of  $Y$  values for the crack just after it enters the thickness change .....109

Figure 4-14 Comparison of approximate and FEA results for  $Y/Y_c$  for edge cracked plate with thickness change from  $t_1$  to  $t_2$  .....110

Figure 4-15 Comparison of approximate  $Y$  and FEA results for  $Y$  for edge plate with thickness change from  $t_1$  to  $t_2$ .....111

Figure 4-16  $Y$  from simple linearized stress ratio calculation based on actual thicknesses .....113

Figure 4-17 Ratios of FE to Linear stress variation calculation  $t_2/t_1 < 1$  and empirical correction [ $Ye1(ac)$ ] [Equation (4.5)].....114

Figure 4-18 Ratios of FE to Linear stress variation calculation  $t_2/t_1 > 1$  and empirical correction [ $Ye2(ac)$ ] [Equation (4.6)].....115

Figure 4-19 Estimation of  $Y$  values for thickness changes, using linearized stresses of the remaining ligament with actual thicknesses and empirical correction equations [Equation (4.5) and Equation (4.6)].....116

Figure 4-20 Ratio of FEA results / simple method (Applied ligament linearized stress/semi infinite linearized singular stress, with Equation (4.5) and (4.6) correction) results.....117

Figure 5-1 Real T-shape structure.....119

Figure 5-2 Real T structure and equivalent plate for I-shape structure.....120



*List of Figures*

---

Figure 5-3 Crack growing through $t_1$ plate .....	120
Figure 5-4 Crack propagating through $t_2/h$ plate.....	121
Figure 5-5 General applied loads and supports of T-connection model.....	122
Figure 5-6 Mesh details around the crack tip.....	123
Figure 5-7 Edge crack subject to tension in T-shape model (Applied tension $\sigma_a = 1Pa$ ) .....	126
Figure 5-8 Stresses from applied external loads acting on remaining ligament $\sigma_a$ (left side) and semi-infinite plate singularity $\sigma_i$ (right side).....	127
Figure 5-9 Stress from singularity before linearization ( $\sigma_{si}$ ) (Stress: Pa) plotted against (non-dimensional) distance through the remaining ligament .....	128
Figure 5-10 Mean stress from singular stress on cracked section ( $\sigma_{si\mu}$ ) (Stress: Pa) .....	129
Figure 5-11 Bending stress from singular stress on cracked section ( $\sigma_{bmsi}$ ) (Stress: Pa) .....	129
Figure 5-12 Mean stress from applied load on cracked section ( $\sigma_{\mu a}$ ) (Stress: Pa) .....	130
Figure 5-13 Bending stress from applied load on cracked section ( $\sigma_{b\mu a}$ ) (Stress: Pa) .....	130
Figure 5-14 Approximate analysis of the T section [using Equation (5.1)] compared with FEA results ( $t_2/t_1=0.5$ ).....	131
Figure 5-15 Approximate analysis of the T section compared with FEA results ( $t_2/t_1=0.5$ ), effective width of shell plate in bending = $0.2 \cdot B$ .....	133
Figure 5-16 Approximate analysis of the T section compared with FEA results ( $t_2/t_1=0.5$ ), effective width of shell plate in bending = $0.6 \cdot B$ .....	134
Figure 5-17 Approximate analysis of the T section compared with FEA results region around $a/ds = 1$ ( $t_2/t_1=0.5$ ), effective width of shell plate in bending = $0.6 \cdot B$ .....	135

*List of Figures*

---

Figure 5-18  $Y$  values for different shell plate / stiffener thickness .....137

Figure 5-19 Local behaviour of shell plate in bending and web stresses concentrating in the remaining ligament.....138

Figure 5-20  $Y$  values with additional shell-plate/web relative thickness correction ( $Y$  in log-scale).....139

Figure 5-21 Ratio of  $Y$  values Approx/FEA result.....140

Figure 6-1 Illustration of stiffener structure on ship connection (Lou, 2013) ..143

Figure 6-2 Illustration of longitudinal cracked and shell web cracked (Thickness  $t = 12\text{mm}$ ).....144

Figure 6-3 Applied symmetric Boundary Conditions and loadings (10MPa) (Note: U-Fixed support means there is no displacement in  $Y$  direction, which is the movement in  $Y$  direction has been fixed) .....145

Figure 6-4 Details of mesh, fixed support, and applied loadings (10MPa) .....146

Figure 6-5 Mesh details around crack tip (Stiffener Model).....147

Figure 6-6 Membrane  $Y$  curve for crack in web and shell plate of single stiffener structure under tension loading .....148

Figure 6-7 Membrane  $Y$  curve for crack in flange of single stiffener structure under tension loading .....149

Figure 6-8 Comparison of  $Y$  values between stiffener simple method (including  $ae$ ) and FEA.....150

Figure 6-9 Graphical descriptions of some parameters.....151

Figure 6-10 Comparison of  $Y$  values with and without  $ae$  values to account for the singularity introduced by the frame stiffener to plate stiffener right angle connection .....152

Figure 6-11 Approximation of corner crack by semi-infinite plate and infinite plate cracks.....155

Figure 6-12 Result of approximation of corner crack by semi-infinite plate and infinite plate cracks (step height = 0.1m,  $as \approx 0.05\text{m}$ ).....156

Figure 6-13 Behaviour of  $ae/as$  at small  $a/as$  .....158

*List of Figures*

---

Figure 6-14  $ae$  calculated from FEA with simple method and power and exponential approximations to Hasebe and Ueda (1981) results (non-dimensionalized by  $as = 24\text{mm}$ ) .....159

Figure 6-15  $ae$  calculated from FEA with simple method and power and exponential approximations to Hasebe’s results (non-dimensionalized by  $as = 17\text{mm}$ ) .....161

Figure 6-16 FE analysis with frame and flange .....162

Figure 6-17 FE analysis with transverse frame removed.....163

Figure 6-18 FE analysis and simplified method with flange removed .....164

Figure 6-19 Flange removed  $ae$  values .....165

Figure 6-20  $Y$  comparison for bending moment and tension loading on single stiffener .....166

Figure 6-21 Membrane  $Y$  comparison for bending moment case  $as = 24\text{mm}$  ..167

Figure 6-22 Apparent crack size ( $a+ae$ ) for small cracks relevant to typical design fatigue life calculation .....169

Figure 7-1 Dimensions and Thickness ( $t=12\text{mm}$ ) of triple stiffeners model....172

Figure 7-2 Applied symmetric Boundary Conditions and loadings (10MPa) ..173

Figure 7-3 Details of mesh, supports, and applied loadings (10MPa) for three stiffeners model.....174

Figure 7-4 Mesh Details around crack tip.....175

Figure 7-5  $Y$  for crack on triple and single stiffener under tension loading.....176

Figure 7-6 Shell plate bending supporting a cracked stiffener .....177

Figure 7-7 Comparison of  $K$  values from simplified model and FEA with moment redistribution through plating to side stiffeners .....179

Figure 7-8 Comparison of  $K$  values from simplified model and FEA with moment and axial force redistribution .....181

Figure 8-1 Single Stiffener model with solid elements modelling the shell plate .....184

Figure 8-2 Dimensions and Thickness ( $t=12\text{mm}$ ) of solid elements model .....185

*List of Figures*

---

Figure 8-3 Applied boundary conditions and loading (100MPa) on solid elements.....	186
Figure 8-4 Details of mesh, support, and applied loadings (100MPa) on solid elements model.....	187
Figure 8-5 Comparisons of $Y$ values for shell model and middle plane with solid model.....	188
Figure 8-6 Absolute $Y$ values for different planes in solid model and shell model type (see Figure 8-7 for definition of surfaces).....	189
Figure 8-7 Description of $Y$ on Upper/Middle/Lower Surface of Solid Model.....	190
Figure 8-8 Ratio between bending $Y$ values and average $Y$ values (Bending $Y$ value is $(Y_1 - Y_2)/2$ , where $Y_1$ and $Y_2$ are the opposite surface $Y$ values).....	191
Figure 8-9 Connection with the stiffener just completely cracked .....	193
Figure 8-10 $Y$ values, including plate bending (linear scale) .....	195
Figure 8-11 $Y$ values, including plate bending (log scale) .....	196
Figure 9-1 Principal fine mesh model of the ship components.....	198
Figure 9-2 Stress distribution approaching a welded joint and the definition of the hot-spot stress (Maddox, 2003).....	200
Figure 9-3 Typical existing guidance on determining sharp corner stresses (Maddox, 2001).....	202
Figure 9-4 Structure parts definition in 3-D coordinates .....	204
Figure 9-5 Localization of the stress lines (X, Y and Z direction) .....	205
Figure 9-6 Displacement Plot under Tension Loading .....	206
Figure 9-7 Displacement Plot under Pure Bending Loading .....	207
Figure 9-8 Displacement Plot under Tension and Bending Combined Loading .....	208
Figure 9-9 Stress Concentration at bracket corner in Model 1 (Max Stress)....	209
Figure 9-10 Stress Concentration at vertical stiffener corner in Model 1 (Min Stress).....	210

*List of Figures*

---

Figure 9-11 Stresses on Line Y (Stress Line on longitudinal stiffener) under tension loading nominal stress= 100MPa .....211

Figure 9-12 Stresses on Line Y under Bending Moment (nominal flange stress = 100MPa).....212

Figure 9-13 Stresses on Line Y under Tension, compared with 1) expected decay for a corner ( $p = 0.455$ ) and 2) better (though not good) fit ( $p = 0.25$ ) ..213

Figure 9-14 Stresses on Line Z (on Flange) under Tension, compared with 1) expected decay for a corner ( $p = 0.455$ ) and 2) better (though not good) fit ( $p = 0.25$ ) .....214

Figure 9-15 FEA SCF results ( $SCF_{fe}$ ) extrapolated on transverse (y) line compared with predictions from the cruciform formula ( $SCF_p$ ) and the revised stiffener connection formula ( $SCF_r$ ).....218

Figure A-1 Crack in rectangular plates under pure tension (Fett, 1998) .....237

Figure A-2 the values of  $Y$  for various  $H/W$  in Fett work .....241

Figure A-3 SIF values for various  $H/W$  ratios in  $Y$ -Log scale from FEA methods .....245

Figure A-4  $Y$  values for various  $H/W$  ratios from FEA methods .....247

Figure A-5 Comparison of  $Y$  values with FEA and Fett work.....248

Figure A-6 SIF values for various  $H/W$  ratios from Fett work .....251

Figure A-7 Comparison of SIF values with FEA and Fett work .....252

Figure B-1 In-Plane and Out-Plane lateral forces on plate .....256

Figure B-2 Normalized geometry factor along the crack front ( $t=10\text{mm}$ ).....257

Figure B-3 Normalized geometry factor along the crack front ( $t=20\text{mm}$ ).....258

Figure B-4 Normalized SIF for no contact region plates with different mesh sizes .....259

Figure B-5 Normalized SIF for 6mm contact region plates with different mesh sizes .....260

Figure B-6 Coordinate around the crack tip.....261

*List of Figures*

---

Figure B-7 Normalized geometry factor along the crack front in contact case ( $t=10\text{mm}$ ) .....261

Figure B-8 Normalized geometry factor along the crack front in contact case ( $t=20\text{mm}$ ) .....262

Figure B-9 Normalized Geometry Factor along the crack front in contact and not contact cases ( $t=10\text{mm}$ ) .....263

Figure B-10 Normalized Geometry Factor along the crack front in contact and not contact cases ( $t=20\text{mm}$ ) .....264

Figure B-11 Geometry Factor for various thicknesses along the contacted crack .....265

Figure B-12 Geometry Factor for various thicknesses along the non-contacted crack .....266

Figure B-13 The regular plate with an edge crack .....267

Figure B-14 Geometry Factor in no contact cases in 20mm thickness .....270

Figure B-15 Geometry Factor in no contact cases in 10mm thickness .....271

Figure B-16 Comparisons of Geometry Factors in two thicknesses plates .....272

Figure B-17 crack plate calculation model .....273

Figure B-18 SIF values for the same model with solid element and shell element .....273

Figure B-19 Meshes on source area and target area .....274

Figure B-20 Boundary Conditions and Tension Loading details .....276

Figure C-1 SIF values for crack growing in different thicknesses plates in flat plate model .....279

Figure C-2 Estimating equivalent length of crack for the same SIF value .....280

Figure C-3 comparing the equivalent crack length for five thicknesses .....281

Figure C-4 Equivalent crack length ratios for five thicknesses .....282

Figure C-5 Estimation of crack length ratio when  $t_2/t_1=4$  .....284

Figure C-6 Estimation of crack length ratio when  $t_2/t_1=2$  .....285

Figure C-7 Estimation of crack length ratio when  $t_2/t_1=0.5$  .....286

*List of Figures*

---

Figure C-8 Estimation of crack length ratio when  $t_2/t_1=0.25$ .....286

## List of Tables

Table 2-1 Stress Intensity Factors for several common geometries (Roylance, 2001a).....	39
Table 3-1 Present non-dimensional factor $Y$ values against $a/W$ for different $t_2$ thicknesses (Results obtained from FEA).....	69
Table 3-2 $Y$ and $F_t$ values for $t_2=12\text{mm}$ plate with FEA method.....	70
Table 3-3 Comparing $F_t$ factors with FEA against Fett's results.....	72
Table 3-4 Comparing $Y$ factors with FEA against Fett's results.....	75
Table 3-5 Crack lengths in 1000mm width plate .....	78
Table 4-1 Thickness data .....	94
Table 5-1 Crack lengths in stiffener model.....	125
Table 5-2 Thickness data .....	136
Table 9-1 Different models of the single stiffener structure showing connection length: $L_c$ .....	203
Table 9-2 Hot-Spot Stress and SCF for each Model under Tension Loading ..	215
Table 9-3 Hot-spot Stress for each Model under Bending Moment (nominal flange stress = 100MPa).....	216
Table A-1 The values of Geometric function $Y \cdot (1 - a / W)^{3/2}$ for tension .....	238
Table A-2 the values of Geometric factor $Y$ under tension.....	240
Table A-3 SIF values for components with $H/W=1.5, 1.25, 1.00$ and $0.75$ through FEA.....	242
Table A-4 SIF values for components with $H/W=0.5, 0.4, 0.3$ and $0.25$ through FEA .....	244
Table A-5 the values of Geometric factor $Y$ from Finite Element Analysis methods .....	246



*List of Tables*

---

Table A-6 SIF values for components with $H/W=1.5, 1.25, 1.00$ and $0.75$ through Fett .....	249
Table A-7 SIF values for components with $H/W=0.5, 0.4, 0.3$ and $0.25$ through Fett .....	250
Table B-1 Elements Number on the front crack .....	253
Table B-2 Normalised stress intensity factor for extension loaded, $Y^0$ .....	254
Table B-3 The ratio between $Y_{max}$ and $Y^0$ .....	255
Table B-4 Geometric function for tension loading .....	269

## **Nomenclature**

<i>a, ac</i>	Crack size
<i>ae</i>	Additional Crack Size to represent a sharp corner
<i>as</i>	Corner singularity strength
<i>at</i>	Crack size at which thickness change
ABS	American Bureau of Ship
<i>b, B</i>	Dimension (normal to crack)
<i>bf</i>	Flange width
<i>ds</i>	Depth of stiffener
BCM	Boundary Collection Method
BSI	British Standards Institution
BV	Bureau Veritas
<i>C</i>	Paris crack growth law constant
CDM	Critical Distance Method
DNV	Det Norske Veritas
FDA	Fatigue Design Assessment
FEA	Finite Element Analysis

*Nomenclature*

---

FEM	Finite Element Method
$f, fr$	Empirical constants
$F_t$	Geometry factor equal to $Y$ (terminology of Fett 1998)
$F_t'$	A non-dimensional SIF used by Fett(1998), $F_t' = Y(1-a/W)^{3/2}$
FM	Fracture Mechanics
$G$	Energy release rate (per unit thickness)
GL	Germanischer Lloyd
$H$	Height of attachment
HHS	Hot-Spot Stress
IACS	International Association of Classification Societies
$I$	Second moment of area
$I_r$	Second moment of area of the remaining cross section of the stiffener
$I_p$	The plate second moment of area per unit width and represents the support provided in transverse bending
IIW	International Institute of Welding
ISSC	International Ships Structure Congress
$K, KI,$	Stress Intensity Factor (SIF)
$Kt$	Stress Concentration Factor
$L$	Attachment length

*Nomenclature*

---

$L_c$	The links between the crack and the end of stiffener
LEFM	Linear Elasticity Fracture Mechanics
LR	Lloyds' Register
$M$	Moment
	Subscripts
	$a$ from applied forces
	$si$ from cracked semi-infinite plate singularity
	$\mu$ mean
$p$	Corner singularity stress decay power
$P$	Force
	Subscripts
	$a$ from applied forces
	$si$ or $s$ from cracked semi-infinite plate singularity
	$\mu$ mean
$q$	$3p-0.5$
$qt$	Value of $a/as$ after which $ae \approx as$
$r$	Distance from crack tip
$t$	Thickness
$tf$	Thickness of flange
$tp$	Thickness of plate
$tw$	Thickness of web
TCD	Theory of Critical Distance

*Nomenclature*

---

$x$	Distance from the crack tip in the $x$ direction
SCF	Stress Concentration Factor
S-N	Stress Range – Number of Stress Cycles
SSC	Ship Structural Committee
$t, T$	Thickness
$t_1$	Thickness that crack starts growing in
$t_2$	Thickness that crack grows into
$t_2h$	Special case thickness of shell plate that is half the thickness of the stiffener web
$W$	Length of structure, in direction of crack, through which crack is growing
WF	Weight Function
$y$	Distance from centre of area
$Y$	Geometry Factor (non-dimensional SIF)
$Y_{fea}$	Geometry Factor values from Finite Element Analysis
$Y_{sf}$	Geometry Factor values from simple method excluding $ae$ values
$Y_c$	Constant value of $Y$ (used with other quantities such as $ae$ to define the SIF)
$Y_e$	Correction factor applied to $Y$
$Z$	Distance through plate thickness from surface
$\Delta$	A small change in the following quantity

*Nomenclature*

---

$\sigma$       Stress

Subscripts

*a* from applied forces

*si* or *s* from cracked semi-infinite plate singularity

$\mu$  mean

*bm* bending

$\sigma_0$       Nominal Stress

$\theta$       Corner angle (0 deg = crack, 90 deg = right angle corner, 180 deg = straight edge)

# **Chapter 1 Introduction**

## **1.1 Background**

The connections between the longitudinal stiffeners and the transverse web frames have for long time been regarded as weak points in the fatigue strength of a traditional marine structure design and there is difficulties to estimate fatigue life of these connections. The cause of structural failure can be due to negligence during design, construction or manufacturing. Poor workmanship, unsuitable materials and errors in stress analysis are examples that contribute to failure. Traditional failure criteria, that compare extreme load to strength, cannot adequately explain many structural failures that occur at stress levels lower than the ultimate strength of the material.

Fatigue, due to cyclic loading, is responsible for a great proportion of cracks occurring in ships and offshore structures. Consequently, fatigue failure of structural details is an important concern in operation of ships, both in the maintenance of existing vessels and in the design of new vessels. Research into fatigue started in the year of 1837 (Schütz, 1996), when Wilhelm Albert publishes the first article on fatigue and continues to this day. Fatigue alone can result in a structural failure but often it weakens the structure and leads to a failure by fracture caused by a combination of reduced remaining structure to resist the load and the remaining structural material failing at a load lower than the yield load as a result of the structure behaving in a more brittle way as a result of the presence of the crack.

A further contribution to failure may be the application of a new design or material, which produces an undesirable result. This type of failure is more difficult to prevent. One of the most notorious failures was due to the

introduction of a new design is the brittle fracture of the World War II Liberty ships. The Liberty ships were the first ships to have an all-welded hull. They could be fabricated faster and cheaper than earlier riveted designs but many of the ships sustained serious fractures as a result of the design change that made fatigue cracks more likely, reduced the steel toughness so encouraging brittle fracture and, by replacing the multiple riveted plates with continuous welded steel removed some crack arresting characteristic of the previous riveted construction. Now almost all steel ships are welded but sufficient knowledge was gained from the failures to generally avoid similar serious extensive problems, but fatigue cracks and occasional failures continued to occur (Manan, 2008).

Other examples of engineering structures that have fatigue and fracture problems are offshore platforms, railway track, aeroplanes and bridges.

To predict the combination of fatigue and fracture, a fracture mechanics theory was therefore introduced, as opposed to the use of the traditional fracture criteria. Fracture research began in the early 1920s by Griffith (Griffith, 1920). He applied the first law of thermodynamics to formulate a fracture theory based on a simple energy balance. According to the theory, a flaw crack becomes unstable and thus fracture occurs when the strain energy change that results from an increment of crack growth is sufficient to overcome the surface energy of the material.

Design by fracture mechanics requires knowledge of a critical crack size and a parameter which characterizes the tendency of a crack to grow. Such a parameter should be able to relate analysis results or laboratory test results to structural performance. Thus the response of a structure with cracks can be predicted from analysis in conjunction with laboratory test data. An important parameter is the stress intensity factor (SIF) and related non-dimensional Geometry Factor or “Y” value. The SIF is determined in terms of crack size, structural geometry and loading conditions. From the laboratory tests, fracture



toughness can be defined as the ability of the material to resist fracture in the presence of cracks. In a similar way laboratory tests determine the yield strength of a material which measures the resistance of the material to yield (Manan, 2008). The fracture mechanics method takes into account, at a crack tip, the theoretical stress singularity (a stress which becomes infinite at the corner).

During the 1970s and 80's, new grades of steel with improved weld-ability and increased tensile strength were used for ships and other structures. Unfortunately the fatigue resistance of these steels was no better than the lower strength steels but the higher design stresses that were allowed reduced the fatigue lives and led to considerable fatigue problems with ships which had previously not been specifically checked for fatigue at the design stage (Boardman, 1990).

Another development that was important for fatigue design was the advent of floating production, storage and offloading (FPSO) ships for oil and gas field development. These vessels are moored offshore and operated on location for the production life of an oil and gas field, typically up to 20 years (RONGRONG, 2007). Docking for inspection and repair is very costly for an FPSO, and design is thus aimed at uninterrupted operation.

Although metal fatigue has been studied for more than 170 years, many problems still remain unsolved due to the complexity of the subject. Fatigue refers to the failure of materials under repeated actions of stress fluctuations. The loads responsible for fatigue are generally not large enough to cause material yielding. Instead, failure occurs after a certain number of load or stress fluctuations. Several factors contribute to this marked reduction in fatigue strength: the notches caused by various discontinuities in geometry, residual stresses, deleterious microstructures in the Heat Affected Zone and internal weld defects such as extrusions, porosity and lack of fusion.

Fatigue strength assessment is mandated to evaluate and develop procedures for estimating the fatigue strength and providing recommendations. Unfortunately, the codified approaches developed so far have limitations, particularly when dealing with structural details with sharp internal corners which theoretically have a stress singularity for a linear elastic material. At the present time, independent estimations of fatigue life and fatigue crack propagation rates are made based using fatigue S-N curves and the fracture mechanics method, respectively. The development of finite element analyses, together with high-speed computers, allows more rational approaches for ship structural analyses but combining the results of finite element analysis and S-N curves or fracture mechanics is often difficult and the approximate assessment of some.

S-N approach and Fracture Mechanics (FM) approaches both use Finite Element Analysis (FEA), but complicated to set up and interpret. The  $\frac{t}{2} \sim \frac{3t}{2}$  method with linear stress fit is the effective option to interpret FEA results for S-N calculations.

There are several ways of using finite element methods in the fatigue design of steel structures: the local stress concepts such as the hot spot stress approach and the effective notch stress approach which are used with S-N curves and crack propagation analysis using fracture mechanics. The application range of these methods has extended greatly during the last decades. The geometrical complexities and irregularities as well as load transfer conditions in steel structures can cause difficulties to estimate correctly the load effects on the fatigue strength of structure components because often there is a theoretically singular stress even in the uncracked structure, which is approximated in some uncertain and mesh dependent way by the finite element analysis. In the case of large steel structures with complex details, such as welded joint components in orthotropic stiffener decks, an initial estimation of the fatigue life of the welded details may be obtained by applying S-N assessment method to the nominal

$(\frac{P}{A} + \frac{M \cdot y}{I})$  stresses. A refined local stress assessment method, which takes into account of the stress raising effects due to the geometry and loading conditions, might provide a more accurate overall estimate of the behaviour of the structure but for fatigue assessment the selection of mesh size and the choice of extrapolation method from locations close but away from the singular point of interest both have a large effect on the calculated fatigue life and the available guidance (e.g. DNV (DNV, 2015) or BS7608 (Standard, 2014) is limited. Furthermore there is a lack of methods that fall between the initial estimation and fully detailed FE modelling methods.

When fracture mechanics crack growth analysis is applied then finite elements that include the singularity may be used to calculate the SIF values from which the fatigue life can be estimated using e.g. BS7910. BS7910 is a British Standard code of practice for the assessment of flaws using fracture mechanics principles to guide the methods for assessing the acceptability of flaws in metallic structures. It is particularly relevant wherever structural integrity is important e.g. pipelines, shipbuilding, turbines, engines, vehicle manufacturing and pressure vessels and equipment. The technique is also referred to as an engineering critical assessment (ECA) or damage tolerance, and is complementary to other methods of weld quality assurance (BS, 2000). This method avoids the problem of deciding what stresses to use for the fatigue analysis as the singular stresses are represented within the analysis. However the meshes required for the analysis may be very fine, and hence time consuming to run, and many different analyses with different crack lengths are required in order to estimate the fatigue life.

For checking detailed FEA results for making preliminary assessments of structured details and for reliability modelling (often part of inspection planning), where large numbers of analyses are required, it is useful to be able to estimate the Stress Intensity Factor (SIF) or Geometric Factor ( $Y$ ) values. Presently, for practical stiffened plating details, approximate estimation methods

hardly exist. However some interesting work leading to simplified estimation of SIFs at sharp corners has been done by Lou (Lou, 2013).

## **1.2 Motivation and Aims**

According to statistics, more than 80% mechanical fracture accidents were caused by metal fatigue (Shen, 2015) and in the welding marine structures, more than 90% fracture accidents were caused by fatigue failure (Gürgen et al., 2016). Fatigue and fracture are the main failure modes of ship and marine structures. Therefore, it is the key things of the safety states estimation to make sure the marine structures can be operated safely. The fatigue can be generated in many circumstances, the material damage, loading from out-of-plane, erosion environment, geometric discontinuities, flaws on the structures and the residual stress, from which the residual stress will stimulate high level of residual stress with structural deformation and geometric discontinuities will cause the singularities, furthermore the stress concentration, from where crack initiating and propagating.

In the view of complex of microscopic fatigue, it's not easy to predict the failure in appropriate theoretical or numerical method, therefore nowadays, many fatigue approaches are on basis of macroscopic aspects, such as S-N curve approach, fracture mechanics approach and reliability analysis methods.

The overall scope of the study aims to develop a program for estimation of stress intensity factor in marine structures so that decision making during initial design and the through life management can be better planned, leading to the structures which can be kept adequately safe during their design life time.

There is a need for simplified approach to check whether or not detailed FEA fracture mechanics results are sensible and the simplification could be

applied with reliability analysis where very large numbers of analyses are required, followed by estimation of reliability life.

Some work, mainly on cruciform plates, has already been done by Xu, Lou and Barltrop (Xu et al., 2013). This work extends that to T sections and the estimation of the stress intensity factor for thickness changes and at plate junctions, how they are modified for different geometry size, and their overall effect on the structural fatigue life of the hull of marine structure.

The objectives of the current research are to study and find approximate physical or empirical SIF estimation methods for:

- 1) Cracks growing towards a change of plate thickness.
- 2) Cracks growing towards a T-connection.
- 3) Cracks growing in actual ship details.
- 4) The effect of parallel uncracked structure which, as the cracks grow, increasingly supports the cracked location.

The approximate methods should ideally have a physical basis and allow the estimation of SIFs from small to large cracks, so that a fatigue life can be estimated.

- To understand the distribution of stress intensity factors along such crack fronts with a finite element analysis program and study the fatigue propagation of through cracks in plates subjected to pure tension and bending loadings.
- To estimate numerically the stress intensity factor values for many crack geometries and loading cases of a welding model with single or triple stiffeners by using fracture mechanics i.e. LEFM approach and simplify the solution for complex structures through numerical simulation.

- To understand the effects of crack propagating in a constant thickness plate towards an edge, which is relatively simple but a useful starting point for understanding a crack propagating in a plate with a thickness change.
- To understand crack propagation in a stiffener towards a plate, and, importantly, when the crack grows into the plate.

### 1.3 Outline contents of each chapter

- Chapter 2 reviews some basic concepts and common problems and approaches to fatigue assessment, including S-N curves and linear elastic fracture mechanics (LEFM).
- Chapter 3 analyses a crack growing across a constant thickness plate and demonstrates that a simple analysis provides a (surprisingly) accurate assessment of the  $Y$  values.
- Chapter 4 extends the Chapter 3 analysis to a plate with a thickness change at right angles to the crack.
- Chapter 5 extended the method to a plate with a flat bar stiffener and the crack growing from the stiffener outstand and into the plate.
- Chapter 6 further extends the method to a connection between a plate, longitudinally stiffened by an angle stiffener, and a transverse frame with a flat bar stiffener.
- Chapter 7 considers three stiffeners connected side by side to the transverse frame with only the middle stiffener cracking.
- Chapter 8 returns to the single stiffener but now includes the plate bending effect.
- Chapter 9 presents the stresses on various lines through the single stiffener and estimates SCFs.

- Chapter 10 contains conclusions and recommendations
- Chapter 11 Bibliography
- The Appendices contain some validation of the ANSYS estimation of SIF values and an early attempt at quantifying the effect of a thickness change.

## Chapter 2 Literature Review

### 2.1 Cracks in Ships

#### 2.1.1 Liberty Ships

From the construction of the welded steel ‘Liberty’ ships, there have been many accidents in which the load-bearing capacity of steel ships was reduced or even completely lost due to the cracking damage. In addition to the failure of the welded components, the crack may even cause the fracture of the whole structure. Figure 2-1 shows the failure of component.



Figure 2-1 Fatigue failure of welded components (Shen, 2015)

For early steel ships, the plates were all connected by riveting and this prevented cracks growing from one plate to another. But welding leaves flaws,



adversely changes the material properties and adds stress in steel hulls, which can have serious consequences. Probably the best well-known examples of ship fatigue and fracture failures are in the Liberty cargo ships built during World War II (Lou, 2013). The American government decided to use the method of “welding” than the conventionally followed method of “riveting” for ship building (Taneja, 2016). The ships were called “Liberty ships”.

Between 1941 and 1945, Virtual Shipyard of the United States built about 2700 Liberty cargo ships, presented in Figure 2-2, 800 “Victory” ships, 320 oil tankers and other series of ships. In all, there are more than 5,200 ships, with a total cost of about \$83 billion (Shen, 2015). These ships were the first all-welded ships.

In addition to increasing the speed of construction, the use of welding also decreases construction costs. The number of skilled labourers required carrying out welding on the ship’s hull and the deck were thought to be significantly lesser than the numbers required to carry out using riveting. Some of the early ships experienced structural damage when cracks developed in their decks and hulls. Three of them catastrophically split in half when cracks formed, grew to critical lengths, and then rapidly propagated completely around the ships girths.

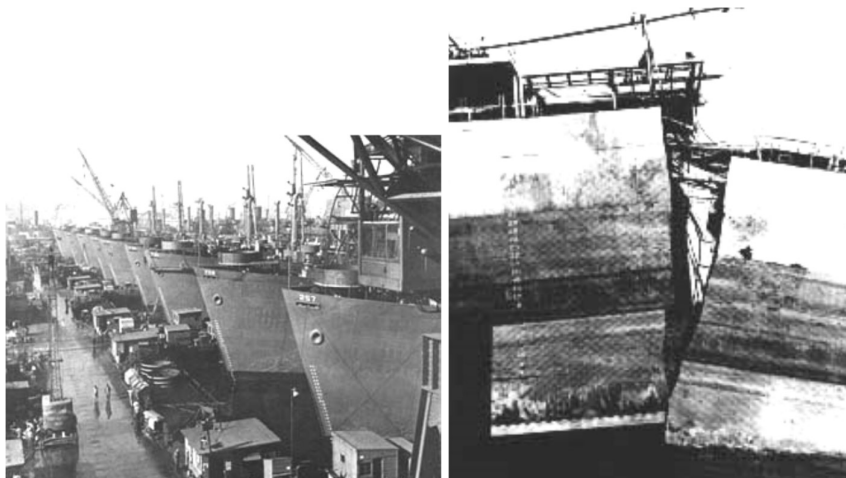


Figure 2-2 Liberty Cargo Ships (J, 2008)

The use of welding technology and poor metal material properties was leading to a large number of Liberty ships to break. There were 238 ships completely scrapped due to long-length cracks in several places, while 19 ships sank due to crack propagation during service. The average cost of these series ships was \$1.6 million for each ship. The accidents were caused due to the lack of fracture toughness of the welded joint (Tipper, 1948). The accident highlighted the importance of fracture toughness and marked the “birth of fracture mechanics” (Taneja, 2016). It was found that a large number of cracks occurred in the stress concentration area, such as the hatchway, and their rapid growth eventually led to brittle fracture, see Figure 2-3.

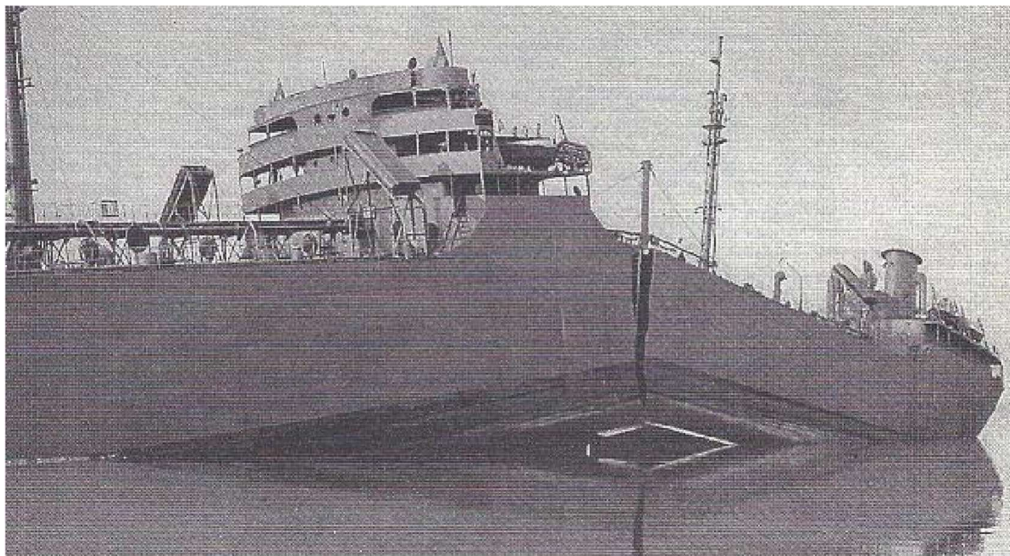


Figure 2-3 Tanker breaking accident (“Liberty tanker”, 1943) (J, 2008)

Generally, early Liberty Ship suffered hull and deck cracks. One common type of crack nucleated at the square corner of a hatch which coincided with a welded seam, both the corner and the weld acted as stress concentrators and small fatigue cracks probably become unstable and fractured (Arshad, 2015). It

is suspected that the shipyards often used inexperienced workers and new welding techniques to produce large numbers of ships in great haste. The primarily welded hull construction then allowed cracks to run for large distances unimpeded. It was believed that the unskilled welding caused micro-cracks in the weld itself, thus, resulting stress concentrations which contributed to the brittle fracture of the Liberty ships (Zhang, 2016).

Further work discovered that if the environmental temperature fell below a critical point, the mechanism of failure changed from ductile to brittle, and thus the hull could fracture relatively easily (Academy, 1996).

Unfortunately, cracks in welded structures may propagate unimpeded for large distances, which can lead to catastrophic failure. However, when structures are riveted, a crack ceases to propagate once it reaches the edge of a steel sheet (Callister and Rethwisch, 2018).

For most of ships, it should be noted that the most common type of cracks was one which began at the square corner of the opening hatch coincided with a weld. Thus, both the weld and stress concentrations acted as localised areas of high stresses.

The reasons of the failure of the Liberty ships could be summarized as,

- a) The material used did not have sufficient fracture toughness especially at lower temperatures.
- b) The standard of the welded joints was in general poor due to inexperienced welders; which meant there were micro cracks in the welds.
- c) The all-welded construction eliminated crack arresting plate boundaries which are present in riveted joints (Taneja, 2016).

The measures taken to correct those problems included (Arshad, 2015),

- 1) Lowering the ductile-to-brittle temperature of the steel to an acceptable level by improving steel quality, e.g., reducing sulphur and phosphorus impurity contents.
- 2) Rounding off hatch corners by welding a curved reinforcement strip on each corner. (Corners of windows and doors for all of today's marine and aircraft structures are rounded.)
- 3) Installing crack-arresting devices such as riveted straps and strong weld seams to stop propagating cracks. The remedial measure adopted was to use rivetted steel arrestor plates in areas of higher stress concentration thus arresting crack growth. In fact, Victory ship was an upgrade in ship design had arrestor plates to maintain a less stiff and stronger ship design that was better able to deal with fatigue.
- 4) Improving welding practices and establishing welding codes.

The studies on the Liberty Ship lead to recommendation for steel manufacture and material selection to reduce the fatigue fracture risk, although, with better steels, fast crack growth is now not so much of a problem but it can still occur.

### **2.1.2 Problem of Shell-Stiffener Connection**

The TAPS (Trans-Alaska Pipeline Service) trade ships are a particularly well known example of ships that have had serious fatigue problems, generally and at their connections between the side shell and transverse structure. These are the U.S. flagged vessels that run up and down the West Coast bringing crude oil from the Trans- Alaska Pipeline south to refineries in California and Puget Sound (BATE, 1999). (The 800 miles pipeline, which is operated by Alyeska Pipeline Service Company, carries crude oil from Alaska's North Slope to the ice-free Port of Valdez in Prince William Sound.) From Valdez, the oil is loaded into waiting tankers. Many of these tankers were built in the 1970s and

approximately half were single-hulled vessels (BATE, 1999). As these tankers faced retirement, service companies wrestled with how to deal keeping them safe and with double-hull regulations and anticipated lower production levels in the Alaska oil fields.

In the US Coast Guard's Structural Casualty Study of 1988 (Hughesi and Franklin, 1993), the TAPS tankers were identified as a population of ships with apparently inadequate fatigue resistance. The study reported that during the period 1984 to 1988, 59% of documented structural failures in US flag vessels over 10,000 tons occurred in the 13% of the population that served the TAPS route (1988). An investigation of the TAPS tankers reported at least 16 Class 1 fractures, several of which led to "significant pollution incidences" (Sipes et al., 1991). A Class 1 fracture was redefined to include any fracture in the oil or watertight boundary of a vessel's hull. The Class 1 structural failure includes internal fractures that are 10 feet or longer in length and the definition was also clarified to distinguish them from structural damage.

The oil tankers that operate on the TAPS route have exhibited a large number of structural fatigue cracks. These cracks can be attributed to the increase in use of high strength in tanker construction and to the harsh operating environment in the Gulf of Alaska (Franklin, 1993). The TAPS tankers have been examined in several studies on the subject of fatigue cracking.

Findings by the TAPS Study Group were based on an evaluation of the data that was assimilated from 200 Coast Guard vessel files, information contained in the Marine Safety Information System (MSIS), and data from the operators (Sipes et al., 1991). The analysis indicated that significant and potentially serious failures could occur on TAPS vessels at any time of the year. Generally, the more harsh the environment the more serious the event, i.e., all four Class 1 events were documented between October and March. Analyses in MSIS showed vessels with cargo blocks constructed of a combination of mild and high tensile steel (HTS) or solely of high tensile steel experienced

disproportionately higher numbers of structural failures than vessels built solely of mild steel. For single hull vessels, regardless of the type of steel, comprised 62.3% of those studied and accounted for nearly 80% of the failure events and for vessels built to full scantlings regardless of type of steel, suffered the same proportion of failures as vessels built to reduced scantlings (Sipes et al., 1991).

Data in MSIS showed that the 69 vessels subject to this Study comprised 28 separate vessel classes. The six vessels in the Atigun Pass Class, whose fractures were described in the deck, the bottom and in side shell longitudinal, accounted for 26.3% of the failure events (Franklin, 1993). The first SOHIO tanker, the Atigun Pass, was launched at Avondale on June 4, 1977, and two more quickly followed (1977). The vessel MOBIL ARCTIC (Not in Atigun Pass Class) accounted for 8 of the failure events, making a total of 24 (34.8%) vessels accounting for 72.9% of the documented failure events. The Atigun Pass Class vessels have experienced the most frequent occurrence of cracking, including two of the four documented Class 1 events reviewed by the TAPS Study Group (Sipes et al., 1991). These vessels experienced active cracking for which effective detail retrofits were not found to be possible. The vessels in the America Sun Class, for which the majority of cracks were found in either the bottom structures or at “rat holes” (small cut-outs) in various unspecified details, accounted for 12.8% of the documented events, and experienced active cracking for which repair solutions were pursued. Much of the past cracking has been attributed to poor initial design and construction, for which effective repair have been made. The MOBIL ARCTIC had several Class 2 fractures, for which the failures were less than 10 feet in length. The vessel was built with numerous structural deficiencies including misalignments of support members by as much as 3 inches, poor transitions and missing brackets. Deficiencies did not become apparent until after a fracture has occurred (Sipes et al., 1991).

The primary concern of most companies is the poor design of details, i.e., the transition pieces such as brackets that connect the main transverse and

longitudinal strength members where structural discontinuities exist. A vessel with poorly designed details is likely to be subject to a high incidence of cracking regardless of the specific environmental conditions. Analysis should not necessarily be aimed at increasing the strength scantlings of the vessel, but in reducing stress concentrations and in providing a better load path for the stresses.

In February 1990, the BROOKS RANGE experienced two fractures in the centre cargo tank, one in the base metal adjacent to the transverse erection butt joint near the centre vertical keel and the other outboard of the first crack in the weld erection joint in way of a longitudinal limber hole. In January 1990, the THOMPSON PASS had numerous side shell fractures in the starboard cargo tank, including an 8 inch crack. In July 1989, 3 individual fractures totalling 17 feet in length appeared along the toe of a transverse field-erection weld in the bottom plating of centre cargo tank (Sipes et al., 1991).

Regardless of how well designed a vessel maybe, or how thoroughly a detail is analysed and engineered for a particular arrangement, the poor welding technique or a poor weld will negate the best of detail designs and possibly lead to a structural failure.

There was a general accord among the TAPS operators that modern vessels, built around 1970-1990, which contain High Tensile Steels (HTS) have more problems than the older vessels constructed solely of mild steel. Particularly for vessels in the Atigun Pass class, the entire cargo block section consists of HTS. It was suggested that HTS has no place on large vessels because the technology employed in actual design and construction of these ships is not adequate to produce HTS vessels that will not have cracking problems. Many of the structural details used in larger vessels have been designed from historical experience and fabrication preferences, and without any specific analyses requirements or guidance contained in classification society rules (Sipes et al., 1991). It was the general consensus among the

operators that studies have shown that details that had proven satisfactory for older vintage mild steel construction are not necessarily satisfactory for newer vessel designs particularly those with High Tensile Steels. Some structural details on these larger vessels have proven to be inadequate and subject to failure.

One common detail that has been subject to failure on older vessels is lap joints. Fractures in lap joints are common in the transverse web structures in wing tanks. Generally, operators repaired fractured lap joints with butt-welded joints when possible (Sipes et al., 1991). Some operators have spent considerable resources to analyse details and have been successful in producing effective modification and repair solutions.

ABS discussed comparisons of wave data for the California to Alaska route, the Alaska to Yokohama route, and the New York to Rotterdam route. A most probable extreme wave height of approximately 33 feet, based upon data for the North Atlantic, was chosen as a norm for the comparison. While the wave severity for the New York to Rotterdam route nearly matched 33 feet, the wave severity for the Alaska to Yokohama route was approximately 39 feet, and that for the California to Alaska route approximately 40 feet (Sipes et al., 1991). This data supports the view that the environmental climate in the Gulf of Alaska can be considered more of a problem for tankers on the TAPS route than those in North Atlantic service. Ships in the North Atlantic service also have more routing options to avoid storms, whereas vessels in the TAPS trade do not.

Poorly designed details, poor weld workmanship, and fatigue appears to be the major causes of structural failures, especially in association with the use of high tensile steel. Corrosion is also another primary type of structural degradation that can lead to structural failures. Coating maintenance can be an effective way to slow corrosion and, hence stress corrosion cracking when employed in strict maintenance (Sipes et al., 1991).



To assess the possibility of cracks in the joint connection of ships, fatigue failure has to be investigated. This type of failure is still complicated to predict and when the various locations where it can occur, even on one ship joint connection, are considered it leads to a complicated and time consuming phenomenon to assess.

## **2.2 Design and assessment for fatigue and fracture**

For several decades, fatigue design procedures have been established for bridges, pressure vessels, etc., with fatigue strength criteria, S-N curves based on small scale testing of planar welded joints (Gurney, 1979) (Maddox, 1975). It becomes evident that offshore structures in this harsh environment had to be designed against fatigue with explicit procedures during the development of oil and gas fields in the North Sea in the early 1970's. In addition, the traditional approach to the fatigue analysis of notched structural components has been based on the classical S-N curve. The S-N curve is the most common way to present fatigue test data and design curves, as illustrated in Figure 2-4.

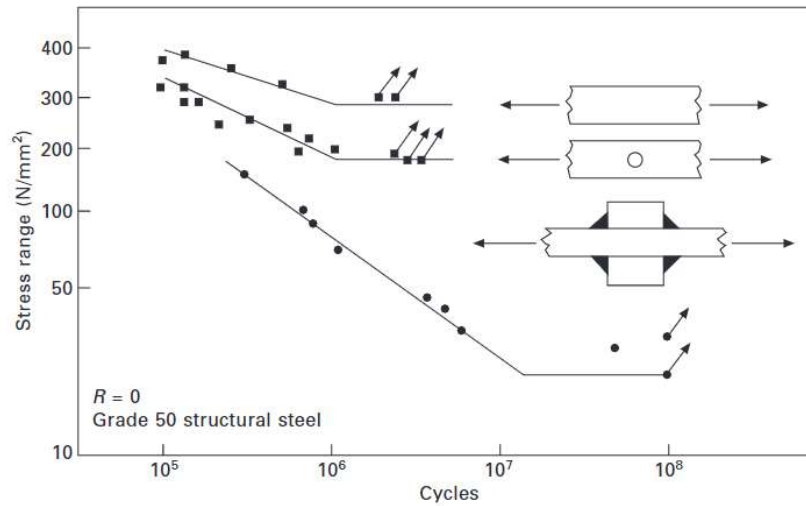


Figure 2-4 S-N curves of a plate, a plate with a hole and a plate with longitudinal gussets under tensile stress (Schijve, 2009)

S-N curves are not generally useful for more complicated design assessments, particularly when crack inspection frequency or structural reliability under fatigue decay with inspections is required to be considered during the design. For these analyses fracture mechanics fatigue calculations, which consider the time history of crack growth, are more helpful than S-N calculations. Fracture mechanics also allows the estimation of the crack size that will fail under any particular loading. Fracture mechanics is discussed in Section 2.4. S-N curves are discussed in Section 2.3.

### 2.3 S-N curves

Most offshore and ship structures are welded steel, and always bear alternating environmental loadings. Therefore, fatigue failure is considered as one of the major failure modes in structure engineering (Pradana et al., 2017)

(Fricke and Kahl, 2005). There are several well-founded fatigue design specifications (DNV1998, DNV2000) for welded connections in steel that should prove to be suitable to some extent. However, a feature of such specifications which is increasingly regarded as a disadvantage is that they are based on the use of the nominal applied stress. This proves to be a problem in the design of some structural configurations because of the difficulty of defining nominal stresses. The same problem frequently arises when stress information is obtained by finite element analysis (FEA). In view of this, there is growing interest in the use of hot-spot stresses for fatigue design (Maddox, 2001).

Common fatigue assessment methods include nominal stress method, hot spot stress method and notch stress method (Fricke, 2003). Nominal stress method can be conveniently applied to the fatigue calculation of various typical joints, but ignore the stress discontinuity effect caused by the connection structure, which will cause large errors in the analysis of complex welded joints. Hot Spot stress takes the maximum structural stress or geometric stress as the reference value for stress extraction, analyzes the stress concentration effect of structural geometric changes on welded structures, but ignores the non-linear stress caused by notches or cracks. Hot Spot stress method can express the fatigue strength of different types of welded joints through a basic S-N curve, which is convenient for engineering application and popularization (Shen et al., 2020a). Hot Spot stress was recommended to determine the stress at the corner in the traditional classification society specifications. For example, some classification societies suggested to use the surface stress values at  $0.5t$  and  $1.5t$  from the corner for linear extrapolation to obtain the stress value at corner (Shen et al., 2020b).

Fatigue resistance data for design are usually expressed in terms of S-N curves, relating nominal applied cyclic stress range  $S$  and the corresponding number of cycles  $N$  needed to cause failure. S-N curve methods are useful for assessing the fatigue lives of welded joints, therefore they are intended for

application at the design stage. For S-N curve approach, the stress distribution calculation is required, so that either the stress concentration or a nominal stress can be estimated. The Hot-Spot stress method is an extension of the S-N curve approach in that it makes use of S-N curves obtained from tests on actual welded joints (Maddox, 2003).

### 2.3.1 Stress Concentration Factor (SCF) Assessment based on S-N Curve classes

All the fatigue design specifications present a series of S-N curves for particular weld details, with a classification scheme linking a description of the welded joint with the appropriate design curve. The classification usually depends on the joint type, geometry, loading direction and mode of fatigue failure (Maddox, 2003). The S-N curves are derived from linear regression analysis of  $\log S$  versus  $\log N$  fatigue data to establish mean curves and statistical lower bound, usually mean -2 standard deviations of  $\log N$ .

The equation of the S-N curve has the form,

$$S^m \cdot N = A \quad (2.1)$$

where  $A$  and  $m$  are constants.  $m$  is often 3.  $A$  is a constant that depends on the structural detail and the required probability of failure in lab tests. For a typical ships detail and 2.3% failure probability (-2 standard deviation) and an 'F' attachment classification,  $A = 0.63 \times 10^{12}$  in MPa units (Barltrop, 2014). In codes and standards (Hobbacher, 1996a), it is now common to define S-N curves by the stress at  $2 \times 10^6$  cycles.

The S-N curves are modified for the thickness of the structural components (generally increased thickness reduces the allowable fatigue stress).

S-N curves are also modified for the corrosive marine environment and the presence or lack of coatings and electrical corrosion protection systems (DNVGL-RP-0416, March 2016). Corrosion reduces thickness, so increasing stress but also reduces the allowable fatiguing stress.

S-N curves for welded structures generally assume that the welds are in areas of large local tensile ‘residual’ stresses as a result of welding. Very occasionally an allowance is made for the reduction of residual stress over the lifetime of the structure.

Example S-N curves for welded joints are illustrated in Figure 2-5. Some structural details are presented in Figure 2-6.

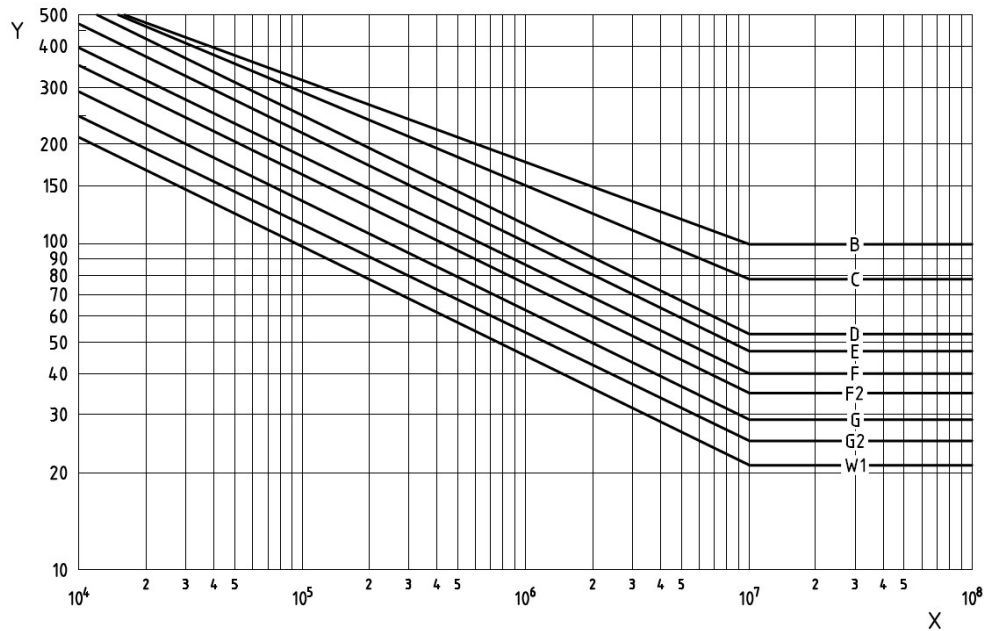


Figure 2-5 Example of design S–N curves for welded joints (Standard, 2014)

The fatigue cracks often initiate from the weld toe in the plate with welded details. Figure 2-6 gives diagrams that illustrate the geometrical features and

potential crack location for the loading direction shown which determines the class of nominal stress and hot spot stress.

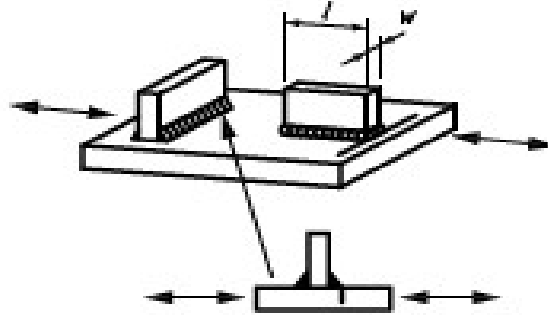


Figure 2-6 Loading details on welded attachment (BS7608, 2014)

Detail classifications are given for assessment based on applied nominal stress. For example, for the location of potential crack initiation at weld toe and with the length of attachment plate larger than 150mm, the fatigue class is F2 and the cycles to failure for any applied stress range can be directly read from the curve or, more usually, calculated from the formula that defines the curve. For some details there may not be an appropriate S-N curve and rules might specify an SCF to use with a particular S-N curve. In this case the methodology becomes similar to the Hot-spot stress approach.

### 2.3.2 Hot-spot stress fatigue calculation

Hot Spot stress takes the hot spot position as the reference value for stress extraction to analyze the stress concentration effect of structural geometric changes on welded structures (Hobbacher, 2016). Considering the reference stress can directly obtained by the strain gauge in engineering, Hot Spot stress method was conveniently applied and widely recommended (Niemi et al., 2006).

The Hot Spot stress approach has been widely used in engineering designs at present (Fricke and Petershagen, 1992). This approach utilizes more accurate stress analysis on different types of welded joints; therefore, it has higher precision and more extensive applicability (Niemi et al., 2006). On the other hand, it does not consider the local stress concentration caused by the weld toe itself and, hence, avoids the difficulty of determining the local geometry of the weld toe, as required in the notch stress approach. Therefore, the Hot Spot stress approach has been the most favorable option due to both accuracy and applicability in engineering designs. The traditional approach to derive the Hot Spot stress is using linear or quadratic extrapolation of surface stresses measured at two or three reference points in front of the weld toe (Hobbacher, 1996b) (Fricke, 2002).

When an assessment of the concentrated stress in a detail is made, e.g. by using finite element analysis then, to avoid double counting the stress concentration effect, it is appropriate to use this with the basic S-N curve for a butt weld instead of the S-N curve for that class of detail. This requires the workmanship standards to be similar for the actual weld and the reference butt weld. The S-N class for a butt weld is D (Standard, 2014). The S values corresponding to a D curve at  $2 \times 10^6$  is 90MPa. However, the estimation of hot-spot stresses from finite element analysis is often not straightforward because commonly used structural connections have sharp corners which imply theoretical infinite stresses and therefore infinite SCFs. These localized infinite stresses do not imply a zero fatigue life and the finite element analysis will in practice usually only provide an approximation to an infinite stress so the results of the analysis need careful interpretation. Codes of practice have introduced methods for interpreting the results of finite element analyses in these situations. Common recommendations (BS7608, 2014) are to calculate the stresses, where  $t$  is the plate thickness, from  $t$  and  $0.4t$  to the corner,  $1.5t$  and  $0.5t$  to the corner, as shown in Figure 2-7.

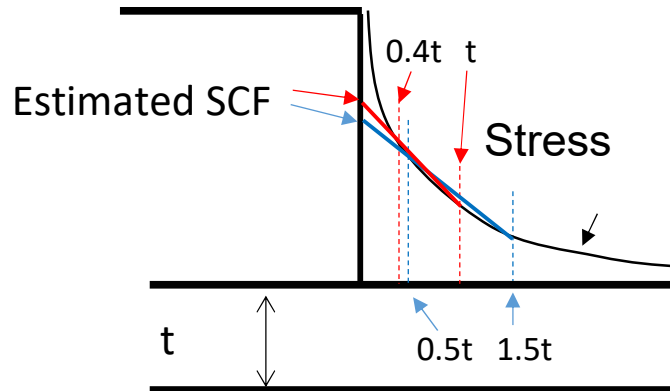


Figure 2-7 Different thickness based methods of extrapolating of surface stresses to a corner hot-spot

It is not clear that the extrapolation positions should depend on the thickness of the plate, however it does mean that the SCF calculated for geometrically similar specimen sizes will be the same. BS7608 (2014) notes alternative extrapolation methods, e.g. from fixed distances of 15mm and 5mm to the weld, or to simply use the stress at 5mm from the weld.

It is also possible to use the stresses through the thickness of the plate  $t$  to calculate the SCF. BS7608 (2014) describes a method, based on Dong (Dong, 2001), where the SCF is based on the linearized stress over the plate depth.

A further method uses the stress 1mm below the corner as the basis for the SCF.

Empirically Maddox (Maddox, 2001) shows the methods do generally give reasonable results, but suggests consideration should be given to applying the different methods with different S-N curves.

It is clear that different methods will result in significantly different SCFs and as none of the methods are theoretically based it is difficult to confidently apply them to new situations for which they have not been tested or calibrated.



### 2.3.3 Relationship between hot-spot SCF and weld classification approach

For the attachment example, corresponding to an F2 class, given above, the fatigue strength ‘S’ defined at  $2 \times 10^6$  cycles is 60MPa, as presented in Figure 2-8. This strength is the nominal (average across the loaded plate) stress. The curve is a minus 2 standard deviation curve, corresponding to a 2.3% failure probability with the specified stress and number of cycles.

The S-N curve for butt weld is a D curve, for which, the strength ‘S’ at  $2 \times 10^6$  cycles is 90MPa.

Arguably, the difference between these specimens is the local SCF in the F2 specimen. Therefore the SCF implied by the F2 curve is:

$$SCF = \frac{90MPa}{60MPa} = 1.5 \quad (2.2)$$

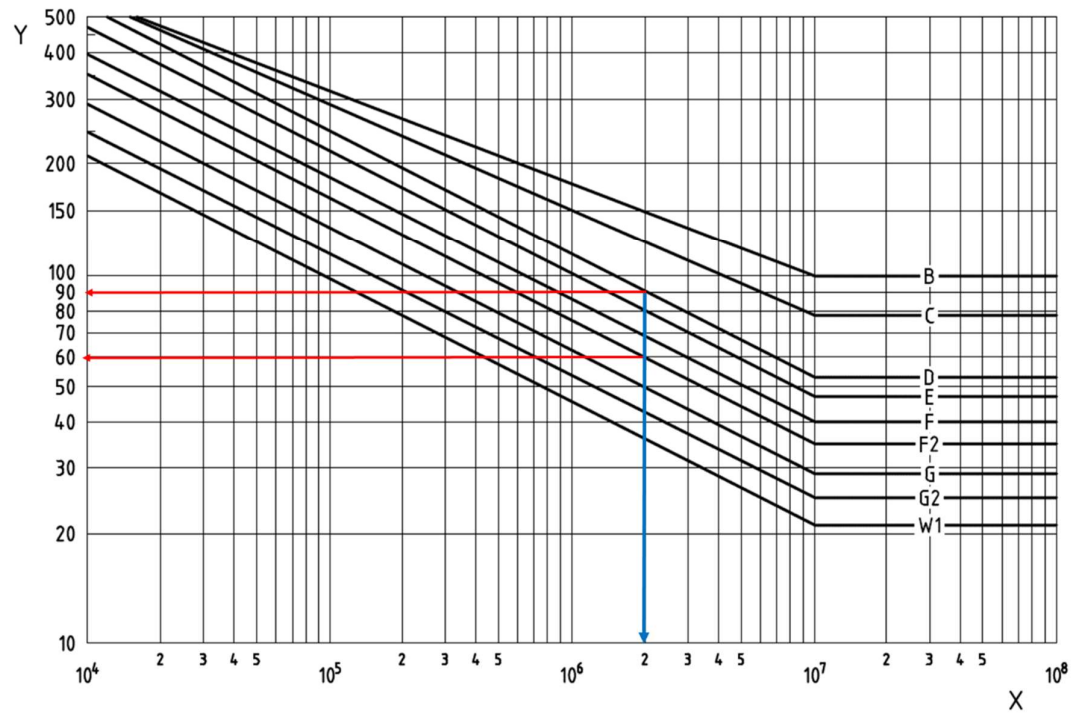


Figure 2-8 D curve and F2 curve by stress at  $2 \times 10^6$  cycles  
(BS7608:2014 Figure 10)

### 2.3.4 Structural stress fatigue approach

#### 2.3.4.1 Fatigue design based on rules, standards, codes and guidelines for ships

Fatigue analyses performed according to current rules and guidelines from the several classification societies are individually considered below. The fatigue assessment requires a broader consideration of the problem than the details considered in this thesis.

The primary objective of various Class rules, regulations and codes applicable to ship and offshore structures is to ensure that the design and analysis process results in the construction of the ship and offshore structures

that can resist both extreme loads and cyclic operating loads. ISSC (Garbatov et al., 2018) presented the fatigue analysis procedures from LR, DNV, ABS, and BV, within a comparative study of the fatigue assessment of a pad detail on a tanker, bulk cargo ship and an FPSO:

The Lloyd's Register Rules and Regulations for the Classification of Ships (Register, 2016a) indicate that the fatigue performance of the hull structure is to be assessed in accordance with the applicable ShipRight Fatigue Design Assessment (FDA) procedures (Register, June 2015).

The FDA procedures adopt a unit load approach to estimate the total stress response by combining the results of discrete unit load cases and the applied loads. The unit cases include hull girder global loadings, external hydrodynamic wave pressure loads, and internal cargo/water ballast inertia pressure loads. All these loads are further computed for any loading condition and sea state resulting from the hydrodynamic analysis and voyage simulation. The distribution and magnitude of internal inertia pressure loads are determined by simplified expressions for each ship motion.

The ShipRight Fatigue Design Assessment procedure (Register, June 2015) applies to oil tankers, LNG and LPG carriers, bulk and ore carriers and container ships and requires three possible levels of assessments:

FDA Level 1 (Register, 2009): the proposed joint configurations at critical areas are compared with the structural design configurations specified in the Structural Detail Design Guide, which can offer an improved fatigue life performance.

FDA Level 2 (Register, 2015) (Register, 2016b): this is a spectral direct calculation procedure based on parametric databases to compute the wave-induced loads and motions and simplified structural models which utilize LR's software. This procedure is intended for the analysis of secondary stiffener connections.

FDA Level 3 (Register, 2016d): this is a full spectral direct calculation procedure based on first principles computational methods, such as hydrodynamic load and ship motion analysis to determine the wave-induced loads and motions, and finite element analysis to determine the structural response. It is intended mainly for the analysis of primary structural details.

Both FDA Level 2 and FDA Level 3 adopt a hot spot stress approach in conjunction with the Palmgren-Miner cumulative damage rule. The LR hot spot reference design S-N curve represents the fatigue strength of the welded material in air, including the stress concentration due to the local notch at the weld toe. It consists of two slopes modified as per the Haibach correction at the  $10^7$ -stress cycle and a reduction factor for corrosive operational environments (Garbatov et al., 2018). Additional stress concentration factors to account for construction tolerances and plate thickness effects may be applied (Register, 2016d). The mean stress correction is included to reduce the overall stress range when the stress cycle is in compression.

DNV and GL merged and their combined fatigue regulation came into force in January 2016 (Garbatov et al., 2018). It has been improved to be applicable also for other ship types, e.g. also for small and slender ships. The fatigue capacity part is also aligned with Common Structural Rules (CSR) that are agreed by a group of classification societies, but very much based on what has already been used by DNV and GL.

DNV was using the hot-spot stress approach and GL used the nominal stress approach with a stress concentration factor  $K$ . A revised thickness and size effect has been introduced where not only the base plate thickness is considered but also the length of transverse attachments, cruciform joints, and butt welds.

For consideration of corrosion a simplification has been made, the effect of which is however small. Other rules and standards use separate S-N curves for corrosive environments. But as measured corrosion progress scatters very

much in practice, the related damage contribution is taken as based on the S-N curve in the air and then multiplied by 2.0. The amount of time to be considered in a corrosive environment is defined based on compartment type and content and ranges between 0 and 5 years. For target lifetimes above 25 years, the formulation for the predicted lifetime is made independent of the target lifetime, assuming a regular maintenance regime.

The mean stress effect, which can be important when details are exposed to compression, is handled similarly to how it has been in DNV and in GL. The pronounced effect of residual stresses and its shakedown on the mean stress effect, as it is considered in CSR for bulk carrier and tanker, is not relevant for typical loading conditions of other ship types and accordingly not applied in DNV-GL rules. For container ships, more ship specific and more sophisticated considerations are possible according to DNV GL class guideline for fatigue and ultimate strength assessment of container ships (DNV, 2017a).

Bureau Veritas Rules concerning fatigue for steel ships involve a part dedicated to loads including fatigue loads defined in the framework of design load scenarios. In each scenario, Hot Spot Stress ranges are calculated according to a specified spectral approach. As dedicated to a structure where the operator specifications are generally very detailed this Classification rule is more focused on the objectives of the assessment including for fatigue than aiming to provide a comprehensive procedure to assess the structure (BV, 2016a). Within the objectives, different loads are involved due to waves, inertia, vortex shedding, and slamming. Fatigue life is addressed involving linear cumulating of damage or alternatively fracture mechanics. An assessment based on a fracture mechanics approach has been introduced to assess the validity of inspection planning. Fracture mechanics is applicable from flaw detection up to fracture criterion in terms of a Failure Assessment Diagram.

Fatigue strength corresponding to a cathodic protection condition for welded assemblies is involved. The effect of weld improvement (e.g. grinding to

improve the weld shape) is considered by using S-N curves with a lower slope and higher fatigue limit. The capacity of remaining fatigue life evaluation is addressed with fracture mechanics crack propagation analysis.

The stresses and S-N curve are based on the notch stress approach by the BV rules. (Veritas, 1998) (Veritas, 2000). Parametrical S-N curves may also be used to fit the results from component fatigue tests.

A comparative study between the rules of classification and FE extrapolation was performed as part of the work of Committee III.2 “Fatigue and Fracture”, of the International Ship and Offshore Structures Congress (ISSC) during the working period 2015–2018. It was shown that the calculated fatigue lives varied considerably between 1.8 and 20.7 years on the Panamax container ship studied, so there is clearly more work needed to properly define fatigue analysis methodology.

#### **2.3.4.2 S-N fatigue assessment summary**

In the view of the low fatigue performance of widely used welded joints, design stresses in welded structures are frequently governed by fatigue consideration and the majority of service failures are attributed to fatigue. There is the necessity for careful consideration of potential fatigue failure at the design stage, and for clear design guidance.

Even though this approach is empirical its widespread acceptance by codes of practice indicates it works reasonably well – at least it now requires fatigue to be considered at the design stage. However there are uncertainties in the application of the methodology with finite element analysis and the selection of the appropriate S-N class when finite element analysis is not being used. Some insights and improvements to the methodology can then be made by using fracture mechanics to better understand the particular problem.

There are particular challenges for ship structures with respect to fatigue design. Welded details in ships are complicated in several respects. The loading on ship structures is continually varying and the geometry of the welded connections can be very complex. The combined effect of these load components for fatigue strength assessment is not clear (RONGRONG, 2007).

## 2.4 Fracture Mechanics

S–N curves are useful for determining the number of load cycles-to-failure for a material, but they do not provide information on the rate of crack propagation at any time or the combination of the size of crack and applied stress that is likely to cause the material to suddenly fracture.

Fracture mechanics can help answer these questions, it has been around for a century and thus is relatively new (Anderson, 2017).

An important concept in fracture mechanics is the Stress Intensity Factor or SIF, which is usually give the symbol  $K$ .  $K$  is (approximately) proportional to stress and the square root of the crack length:

$$K=Y \cdot \sigma \sqrt{\pi a} \quad (2.3)$$

Where

$\sigma$  is the applied stress (which is conventionally calculated at some distance from the crack);

$a$  is the crack size (usually the crack length away from the surface for a surface piercing crack or half the crack length for a crack that does not pierce the surface.

$Y$  is a geometry factor (see Section 2.4.2). For simple cases of small cracks in simple geometry where the SCF is 1  $Y$  may be approximately 1. However for more complicated geometry (such as the connection details considered in this thesis) the  $Y$  value may vary considerably as the crack grows.

For simple geometry and loading  $K$  may be calculated analytically but for many practical problems numerical analysis, typically the finite element method, is used to calculate  $K$ . This thesis provides simplified methods for estimating  $K$  or  $Y$ .

$K$  can be used to calculate both fatigue crack growth and critical conditions likely to cause fracture.

For fatigue crack growth calculation the range of stress intensity, usually written as  $\Delta K$  is calculated for the particular crack size and stress range.

The crack growth per cycle ( $da/dN$ ) of applied stress intensity factor range ( $\Delta K$ ) is given by the Paris Erdogan Law (Paris and Erdogan, 1963).

$$\frac{da}{dN} = C \cdot \Delta K^m \quad (2.4)$$

Because the  $\Delta K$  value changes with crack length this equation has to be integrated, analytically or numerically, to determine the number of cycles for the crack to grow from an initial to a final size.

For sudden fracture the maximum applied  $K$  value, including built in stresses such as from welding, is used. For brittle material the applied  $K$  is compared with an experimentally determined critical  $K$  value. For more ductile behaviour the interaction with material yield needs to be considered and this is often done using a Failure Assessment Diagram or FAD as shown in Figure 2-9.  $Kr$  is related to the applied  $K$  divided by the critical  $K$  value for the material when it responds in a brittle manner.  $Lr$  is the applied load divided by the load that would result in a plastic failure in the remaining material at the cracked



section.  $K_r$  and  $L_r$  are calculated and plotted on the FAD. If the point plots above or to the right of the FAD then failure is predicted. If the point plots within the FAD failure is not predicted, though whether the structure is ‘Safe’ or not actually depends on the safety factors used in the calculation and the consequences of failure.

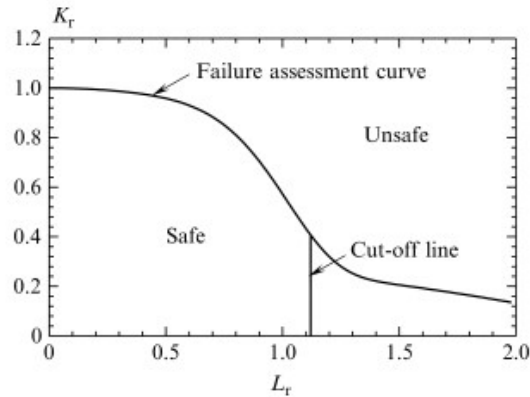


Figure 2-9 A failure assessment diagram (Qian, 2016)

An alternative method of dealing with the linear elastic or non-linear elastic behaviour, which can be used as an approximation to elastic-plastic behaviour is to use the ‘J-integral’. This has not been used in this thesis although when the material is behaving elastically it is the equivalent of  $G$ , discussed in Section 2.4.4 and it is also used as a method of calculating  $K$  values within a finite element analysis.

This thesis is primarily about the calculation of SIFs or  $K$  or the non-dimensional  $Y$  values. The predicted SIFs could be used for fatigue crack growth or fracture calculations.

### 2.4.1 The stress field associated with the SIF

The literature treats here types of crack loading, termed mode I, II and III (Roylance, 2001a), as shown in Figure 2-10.

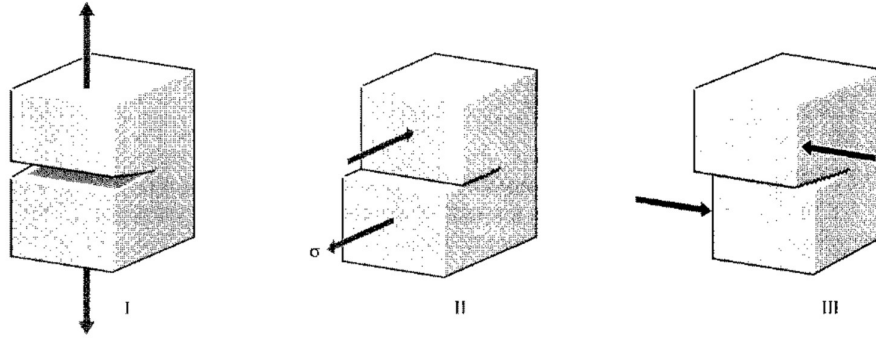


Figure 2-10 Fracture Modes

Mode I is a normal-opening mode and mode II and III are shear sliding modes. (This thesis is primarily concerned with Mode I cracks.)

In a polar coordinate axis with the origin at the crack tip as shown in Figure 2-11, it can be shown that the stress field in any linear elastic cracked body is given by

$$\sigma_{ij} = \frac{K_{I,II,III}}{\sqrt{2\pi r}} f_{ij}^{(I,II,III)}(\theta) + \text{other terms} \quad (2.5)$$

where  $\sigma_{ij}$  represents the stresses acting on a material element at a distance  $r$  from the crack tip and at an angle  $\theta$  from the crack plane and  $f_{ij}(\theta)$  is known trigonometric functions of  $\theta$  depending on Modes I, II and III. As  $r$  approaches zero, the leading term approaches infinity but the other terms remain constant or approach zero (Manan, 2008). The stress near the crack tip varies

with  $\frac{1}{\sqrt{r}}$  regardless of the configuration of the cracked body. It describes a stress singularity as stress is asymptotic to  $r$  equal to zero for Equation (2.5).

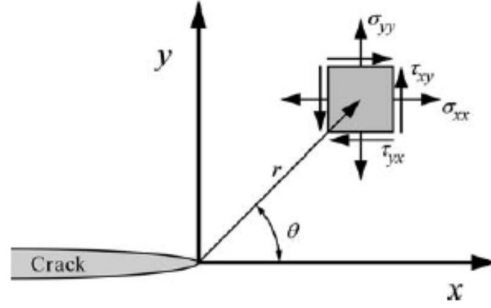


Figure 2-11 Coordinate system and stress component ahead of crack tip

The semi-inverse method shows the opening-mode stress to be (Anderson, 2017):

$$\sigma_x = \frac{K_I}{\sqrt{2\pi r}} \cos\left(\frac{\theta}{2}\right) \cdot \left[1 - \sin\left(\frac{\theta}{2}\right) \sin\left(\frac{3\theta}{2}\right)\right] \quad (2.6)$$

$$\sigma_y = \frac{K_I}{\sqrt{2\pi r}} \cos\left(\frac{\theta}{2}\right) \cdot \left[1 + \sin\left(\frac{\theta}{2}\right) \sin\left(\frac{3\theta}{2}\right)\right] \quad (2.7)$$

$$\tau_{xy} = \frac{K_I}{\sqrt{2\pi r}} \cos\left(\frac{\theta}{2}\right) \cos\left(\frac{3\theta}{2}\right) \sin\left(\frac{\theta}{2}\right) \quad (2.8)$$

On the crack plane where  $\theta$  equals zero, the stresses in the X and Y direction are equal, thus,

$$\sigma_{xx} = \sigma_{yy} = \frac{K_I}{\sqrt{2\pi r}} \quad (2.9)$$

Stresses away from the crack tip zone are governed by the remote boundary conditions and approach a constant value,  $\sigma^\infty$ .

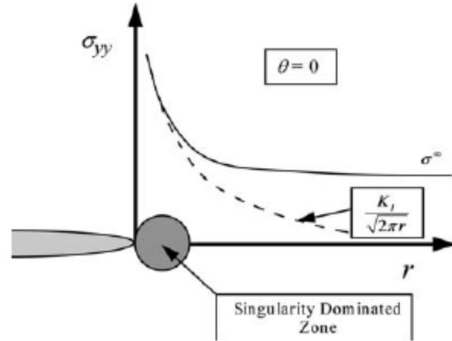


Figure 2-12 Stress normal to the crack plane in Mode I when  $\theta = 0$   
(Wang, 1996)

## 2.4.2 Geometry Correction Factor Y

Generally  $K$  is a function of the loading condition, crack size and shape, and other geometrical parameters.  $K$  is linearly related to stress and characteristic crack dimension. Normally  $K$  is defined as

$$K = Y \cdot \sigma_0 \sqrt{\pi a} \quad (2.10)$$

where  $\sigma_0$  is the remotely applied stress,  $a$  is the crack length and  $Y$  is the geometric factor which is a dimensionless constant that depends on crack geometry and mode of loading. The geometry correction factor  $Y$  usually referred to as non-dimensional SIF, is the most common form of representation for SIF solutions.

For the specific case of a central crack of width  $2a$  in a large sheet, the SIF values is  $K_I = \sigma_\infty \sqrt{\pi a}$ . And for an edge crack of length  $a$  in the edge of a large sheet  $K_I = 1.12 \cdot \sigma_\infty \sqrt{\pi a}$  (Roylance, 2001b).

### 2.4.3 Published results for SIFs or Y values

A lot of solutions for  $Y$  or  $K$  have been published. Some expressions for  $K_I$  for some simple geometries are given in Table 2-1. Many other SIF values (and plastic capacity for use in the FAD calculation) are available in compendia of SIFs and in standards such as BS7608(2019).

Type of Crack	SIF, $K_I$
Centre crack, length $2a$ , in an infinite plate	$\sigma_\infty \sqrt{\pi a}$
Edge crack, length $a$ in a semi-infinite plate	$1.12 \sigma_\infty \sqrt{\pi a}$
Central penny-shaped crack, radius $a$ , in infinite body	$2 \sigma_\infty \sqrt{\frac{a}{\pi}}$
Centre crack, length $2a$ in plate of width $W$	$\sigma_\infty \sqrt{W \cdot \tan\left(\frac{\pi a}{W}\right)}$
Two symmetrical edge cracks, each length $a$ , in plate of total width $W$	$\sigma_\infty \sqrt{W \cdot \left[ \tan\left(\frac{\pi a}{W}\right) + 0.1 \sin\left(\frac{2\pi a}{W}\right) \right]}$

Table 2-1 Stress Intensity Factors for several common geometries (Roylance, 2001a)

Within this thesis finite element solutions of SIF are used extensively to find simplified methods for estimating SIFs. The finite element methods needed validation and for that purpose some published SIF solutions were useful:

- 1) SIF solutions given by Fett (1998), for an edge cracked plate, constant thickness plate validated the analyses that, in this thesis, were extended to a plate with a crack growing through change in thickness and to a crack growing through a T section.
- 2) A paper by Hasebe & Ueda (HASEBE and UEDA, 1981) presents  $Y$  values in a semi-infinite plate with a crack growing from a step in the plate edge. This provided a useful comparison with the approximate assumption of Xu, Lou and Barltrop (2013) described in Section 2.4.7 that is used for the assessment of SCFs in various side shell connection arrangements in Chapter 6.

#### **2.4.4 Energy release rate $G$**

As an alternative to fracture occurring at a critical value of  $K$  a theory was developed on the basis of fracture occurring when a small length of crack growth released more strain energy ( $G$ ) from the structure than the energy that was needed to break that small length of structure. It was found that the energy release rate is proportional to  $K^2$  and that the  $K$  and  $G$  methods are equivalent to one another. In this thesis  $K$  is used rather than  $G$  (although for some work where  $K^2$  is important  $G$  might have been a more convenient choice).

#### **2.4.5 SIF Weight Function Method**

The Weight Function Method (WFM) originally developed by Bueckner (Bueckner, 1987), is a useful procedure that separates the calculation of the SIF into two parts:

- 1) The calculation of the SIF from a localized force per unit thickness of the crack applied to any particular part of the crack surface (this SIF is the weight function  $h(a,x)$  that, for a particular geometry, depends on the distance along the crack,  $x$ , and the length of the crack  $a$ ).
- 2) The calculation of the stress  $\sigma(x)$  along the line of the crack but in the uncracked structure.

The SIF for the actual applied force is obtained by integrating the product of the stress from 2) and the weighting function from 1).

The method relies on the equivalence of

- i) The overall applied stress distribution applied just above and below the section containing the crack and
- ii) that part of the distribution that is aligned with the crack being applied directly to the crack faces.

This equivalence is explained in Figure 2-13 where:

- a) Shows the applied stress (red) opening a crack and resulting in an SIF =  $K$ .
- b) Shows an additional stress field (white) that will just close the crack – this must be the opposite of the applied stress applied to the crack faces as that will balance the stress applied to the edge of the specimen that is aligned with the crack. Because the crack is closed the SIF is now 0 and the additional stress field has resulted in an SIF of  $-K$
- c) Therefore if the additional stress field from b) alone is reversed it will result in an SIF of  $K$ , equal to that of the stress applied in a) but only onto the crack faces.

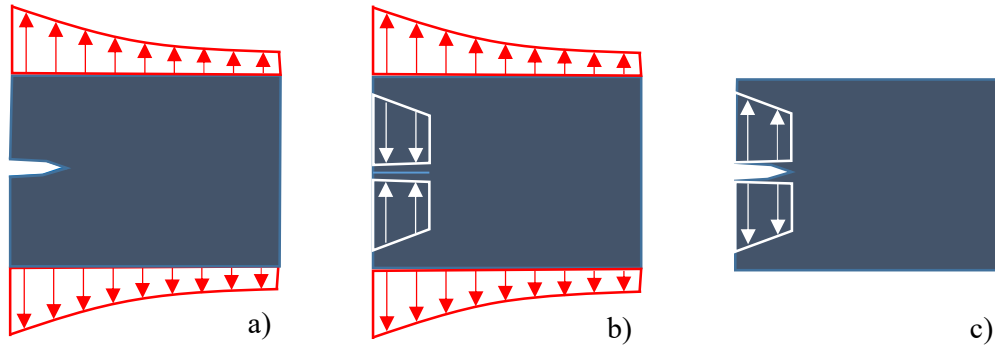


Figure 2-13 The Weight Function method for calculating Stress Intensity Factors

According to the weight function concept,

$$K_I = \int_0^a \sigma(x) h(a, x) dx \quad (2.11)$$

The weight function  $h(x, a)$  does not depend on the particular stress distribution, but only on the geometry of component. One possibility to derive the weight function is the evaluation of numerically determined crack opening profiles which may be obtained by FE computations. Providing the weight functions and stress distributions in the uncracked body are known, the SIF can be calculated for any complex stress pattern.

The WFM should give exact solution providing the correct  $h(a, x)$  is available and many different weight functions of either closed-form or approximate are available for simple configurations, i.e. centre crack or edge crack (Wu and Carlsson, 1991).

For the case of a two-dimensional problem of a cracked sheet containing a crack of length  $2a$  subjected to localized forces  $\pm P$  acting at points on the



crack surface and normal to the crack faces, the SIF is calculated by Equation (2.12) (Bao et al., 2010) (Shah, 1976).

$$K_I = \frac{P}{\sqrt{\pi \cdot a}} \left( \frac{a+x}{a-x} \right)^{\frac{1}{2}} = \frac{P}{\sqrt{\pi \cdot a}} G(x) \quad (2.12)$$

The Green's function  $G(x)$  is an earlier approach that is similar to the weight function method (Sih et al., 1962). In order to apply the method, it is necessary to know the appropriate Green's function and the distribution of stress along the crack site in the un-cracked solid. Once these are known, the technique will give exact solutions.

If a pressure  $p(x)$  acts normal to the crack faces,  $-a \leq x \leq a$ , there is

$$\begin{aligned} K_I &= \frac{1}{\sqrt{\pi a}} \int_{-a}^a p(x) G(x) dx \\ &= \int_{-a}^a p(x) \frac{1}{\sqrt{\pi a}} G(x) dx \\ &= \int_{-a}^a p(x) g(a, x) dx \end{aligned} \quad (2.13)$$

The Green's function  $G(x)$ , for this particular problem is

$$g(a, x) = \frac{1}{\sqrt{\pi a}} G(x) = \frac{1}{\sqrt{\pi a}} \sqrt{\frac{a+x}{a-x}} \quad (2.14)$$

Equation (2.13) is consentaneous with Equation (2.11). It is weight function for an infinite width with centre crack of length  $2a$  (Shah, 1976), see Figure 2-14.

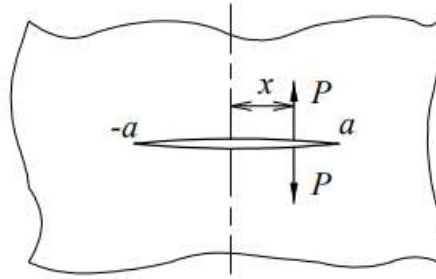


Figure 2-14 Configurations of infinite sheet with centre crack

For edge crack in a semi-infinite sheet, see Figure 2-15, the approximate form is used to express weight function by Equation (2.15) (Sih, 1973).

$$h(a, x) = \frac{1}{\sqrt{\pi a \left[ 1 - \left( \frac{x}{a} \right)^2 \right]}} \left[ 1.3 - 0.3 \left( \frac{x}{a} \right)^{\frac{5}{4}} \right] \quad (2.15)$$

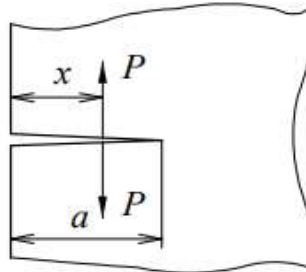


Figure 2-15 Configurations of infinite sheet with edge crack

A simple weight function used in this thesis is for a semi-infinite crack in an infinite body. This (for a pair of opposing forces) has the form:

$$h(c) = \frac{2P}{\sqrt{2\pi c}} \quad (2.16)$$

Where  $c$  is the distance from the crack tip to the position of the force  $P$ .

Note that care is needed with weight functions as the formulae provided in references sometimes relate to opposed force applied on both sides of the crack and sometimes to the force on one side only.

### 2.4.6 Critical Distance Method

Critical Distance Theories of Fracture defines failure criteria based on the stresses within a critical region surrounding the stress concentration, the size depending on the material (Neuber, 1958). This theory has seen an extensive development, providing answers to different scientific and engineering problems (Taylor, 2008) (Cicero et al., 2011) (Cicero et al., 2012). This theory is actually a group of methodologies that have in common the use of the material toughness and a length parameter, that is critical distance,  $L$ , that depends on the material. The theories are particularly applicable to small notches and cracks that are of the same order or smaller than the critical distance.

For brittle failure situations in cracked components, in which linear-elastic behaviour is dominant, fracture mechanics establishes that fracture occurs when the applied stress intensity factor ( $K$ ) is equal to the material fracture toughness  $K_{mat}$ ,

$$K=K_{mat} \quad (2.17)$$

The critical distance follows the Equation (2.18).

$$L = \frac{1}{\pi} \left( \frac{K_{mat}}{\sigma_0} \right)^2 \quad (2.18)$$

where  $K_{mat}$  is the material fracture toughness and  $\sigma_0$  is characteristic strength parameter, known as the inherent strength, which may or may not correspond to the plain-specimen strength (in static or cyclic loading).

For fatigue a critical distance may be defined using the threshold SIF and the fatigue limit stress (the limiting  $K$  and stress below which no cracking is observed in constant stress amplitude tests).

Taylor (Taylor, 2011) summarizes some useful conclusions that can be drawn from critical distance analysis:

“1) Defects which are much smaller in size than the critical distance  $L$  can be assumed to be harmless, having no effect on the failure loads for the failure mechanism under consideration. Defects much larger than  $L$  can be treated using standard techniques such as LEFM for cracks or the stress concentration factor  $Kt$  for notches. A dimensionless number obtained by dividing the linear size of the defect by  $L$  is thus useful in assessing defects.

2) Notches (and other stress concentration features in components) which have root radii smaller than  $L$  can be regarded as cracks. Features with root radii much larger than  $L$  exert the full effect of their  $Kt$  factor. A dimensionless number obtained by dividing the root radius by  $L$  is thus useful in assessing the effect of stress concentrations.

3) If the size of the body (defined by a relevant linear dimension) is similar to or less than  $L$ , the normal TCD methods cannot be used, and the failure behaviour can be expected to differ from that of larger bodies. Thus a dimensionless number consisting of the body size divided by  $L$  will be useful.

4) If the critical stress so as used in the linear elastic TCD is greater than the plain-specimen strength of the material (in the cyclic or static loading modes as appropriate) then a notch having a  $K_t$  factor equal to or less than the ratio of

critical stress to material strength will be harmless. Thus this ratio is a useful dimensionless number.”

There are four different versions of the Critical Distance Method (CDM) will be considered:

(a) The Point Method is the simplest methodology, and it affirms that fracture takes place when the stress at a distance of  $L/2$  from the notch tip is equal to the inherent strength  $\sigma_0$ . Therefore the resultant fracture criterion is,

$$\sigma\left(\frac{L}{2}\right) = \sigma_0 \quad (2.19)$$

(b) The Line Method, assumes that fracture occurs when the average stress along a certain distance,  $2L$ , reaches the inherent strength  $\sigma_0$ . Consequently, it follows,

$$\frac{1}{2L} \int_0^{2L} \sigma(r) dr = \sigma_0 \quad (2.20)$$

(c) The Imaginary Crack Method (ICM) in which an imaginary crack of length  $L$  is placed at the notch root and LEFM conditions assumed.

(d) Finite Fracture Mechanics (FFM) in which fracture conditions are derived by assuming a finite increment of crack growth, equal to  $2L$  (Taylor, 2008).

Modifications are required to the standard fracture mechanics approach if the crack concerned is a short crack, because short cracks tend to grow more quickly, and have lower threshold values, than longer cracks. The subject has been extensively researched, but no universally-acceptable solution has been reached as yet. Equation (2.21) (Taylor, 1996) involves a modification of the standard fracture mechanics equation to include a factor  $ae$ , that is,

$$\Delta K_I = \Delta \sigma \cdot \sqrt{\pi(a + ae)} \quad (2.21)$$

Critical distance methods have not been used in this thesis but it appears that they could be useful for analysing and better understanding ship details with small cracks or no cracks in sharp corners.

### 2.4.7 Additional Crack Size Method for Notches

A method described by (Xu, 2007) and Xu, Lou and Barltrop (2013) involves an equation that is identical to Equation (2.21). The interpretation of ‘*ae*’ in this work (and in this thesis) is of an increased effective defect size caused by a sharp notch or corner singularity.

The work can conveniently be split into two parts:

- 1) The calculation of a length *as* and power *p* that are scale and decay factors for the stresses in the vicinity of the notch/corner singularity.
- 2) The calculation of a length *ae*: an additional crack size that represents the effect of the notch/corner on the SIF.

*ae* and *as* were found, empirically, to be closely related. *ae* and *as* are discussed in the following sections.

#### 2.4.7.1 Estimation of stress field near cracks and sharp corners and characteristic size *as*

Williams (Williams, 1952) stated that, in the context of the elasticity theory, the asymptotic stress state near a sharp corner is singular and its degree of singularity is a function of the angle of the corner. Close to the singularity, the stress has the form,

$$\sigma = \frac{\sigma_0 \cdot \sqrt{\pi} \cdot (as)^p}{\sqrt{2\pi} \cdot (x)^p} \quad (2.22)$$

where  $p$  presents for different corner angles, is shown in Figure 2-16.  $x$  is the distance from the corner and  $as$  is a characteristic size of the singularity with units of length.

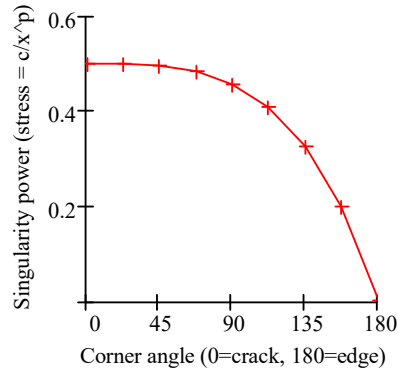


Figure 2-16 Variation of  $p$  (Singularity Power) at different corner angle (Xu and Barltrop, 2007b)

$as$  is an important parameter related to the geometry that, for a simple attachment or cruciform, is determined by the height (H) and length (L) of the attached plate, normally called unloaded plate, shown in Figure 2-18.

At distances larger than  $\frac{as}{10}$  from the singularity, a more complicated formula than Equation (2.22) is required to fit the stresses, which do not decay to zero.

Paris and Sih (1965) quote the following formula for the stress field ahead of a finite crack in an infinite plate:

$$\sigma(x) = \frac{\sigma_0 \cdot (x+a)}{\sqrt{x^2 + 2 \cdot a \cdot x}} \quad (2.23)$$

For a corner singularity, an equation which has the required characteristics near the singularity, decays to the correct applied stress value and is equal to Equation (2.23) for the case of  $p = 0.5$  is (Barltrop and Xu, 2011),

$$\sigma(x) = \frac{\sigma_0 (as + x)}{\left[ \left( 2 \left( \frac{1}{2p} \right) \cdot x \cdot as \left( \frac{1}{p} - 1 \right) \right)^q + x \left( \frac{q}{p} \right) \right]^{\frac{p}{q}}} \quad (2.24)$$

where,  $q = 3p - 0.5$

$\sigma_0$  is the nominal stress,

For a crack the angle is  $0^\circ$  and  $p = 0.5$  and the stress decreases at  $x(\text{m})$  from the crack tip in proportion to  $1/x^{0.5}$ . At  $90^\circ$ ,  $p$  is 0.455 and at  $45^\circ$ ,  $p = 0.326$ . For a straight edge the angle is  $180^\circ$  and, as expected, the singularity disappears with  $p = 0$ , implying a constant stress. Stress plots for different corner angles are shown in Figure 2-17.

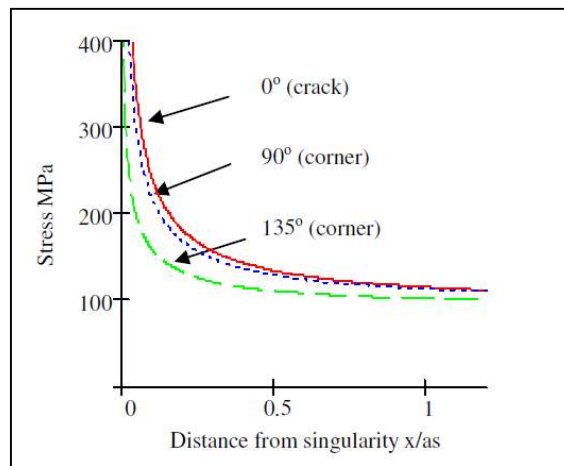


Figure 2-17 Stress decay away from singularity for different  $p$  (with  $\sigma_0 = 100 \text{ MPa}$ ) (Xu and Barltrop, 2007a)



For cruciform plates or attachments to the edge of plates,  $as$  can be obtained (approximately) from the specimen dimensions on the basis of curve fitting by Xu, Lou and Barltrop (Xu et al., 2013), see Equation (2.25).

$$as = \text{smallest of} \left( \frac{L}{25}, \frac{H}{2} \right) \quad (2.25)$$

$L$  is the length of the bracket, and  $H$  is its height. The thickness of  $t_o$  plate equals with  $t_p$  ( $t_o = t_p$ ), see Figure 2-18.

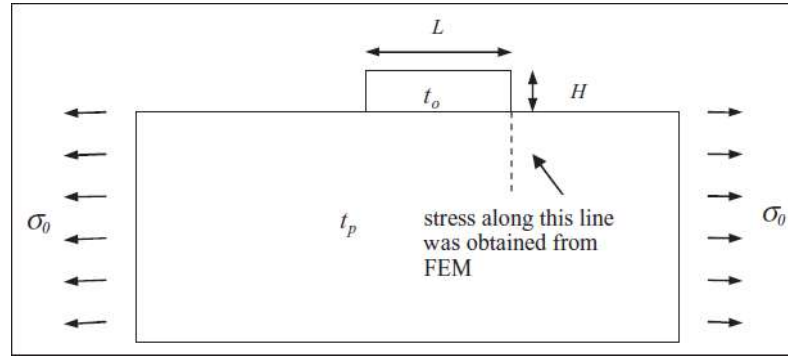


Figure 2-18 Simple plate with attachment leading to corner stress singularity (Xu and Barltrop, 2009)

For different thicknesses of the plate and outstand ( $t_o \neq t_p$ ),  $as$  was found

to be the minimum of  $\left( \frac{H}{2} \right) \left( \frac{t_p}{t_o} \right)^{0.87}$  and  $\left( \frac{L}{25} \right) \left( \frac{t_p}{t_o} \right)^{0.5}$ . That is,

$$as = \text{smallest of} \left[ \left( \frac{H}{2} \right) \cdot \left( \frac{t_p}{t_o} \right)^{0.87}, \left( \frac{L}{25} \right) \cdot \left( \frac{t_p}{t_o} \right)^{0.5} \right] \quad (2.26)$$

### 2.4.8 Stress intensity for different crack sizes near a sharp corner and the effective additional crack size $ae$

Xu, Lou and Barltrop (Xu et al., 2013) explain an interesting behaviour of the SIF that helps with its simple estimation – when the crack is larger than about  $as$  the SIF, instead of requiring a complicated formula for  $Y$  as a function of the crack size  $a$ , can be approximated by the simple equation with constant  $Y$  and  $ae$ .

$$\Delta K = Y \cdot \Delta\sigma \cdot \sqrt{\pi(a + ae)} \quad (2.27)$$

This equation appears to be the same as Equation (2.21) but it is simply representing the ordinary SIF, whereas Equation (2.21) is representing fundamentally different behaviour of small cracks.

For small cracks ( $a < qt \times as$ ) the  $ae$  value increases from 0 to the full  $as$  value as the crack size increases from 0 to  $qt \times as$  and equation 2.23 needs to be modified, e.g. Xu et al.(2013) by:

$$a + ae = \left(1 + \frac{1}{qt}\right) \cdot (qt \cdot as \cdot a^{qt})^{\frac{1}{1+qt}} \quad (2.28)$$

This formula defines a curve of  $a$  raised to power that, on a graph of  $a+ae$  against  $a$ , goes through the origin and is a tangent to the line  $a + as$  at  $qt \times as$ , as shown in Figure 2-19

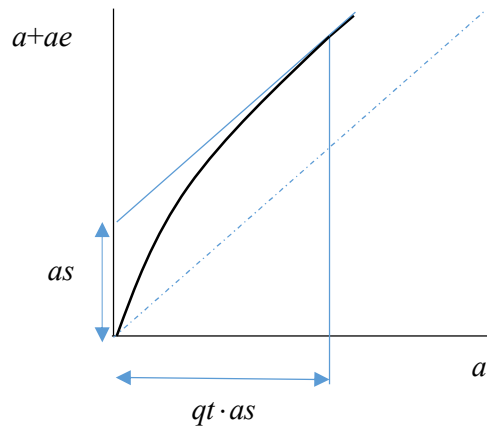


Figure 2-19 Power curve to represent reduction in  $ae$  for small cracks

$ae$  can be calculated from known SIF values and a fixed reference  $Y$  value (e.g. 1.12 for an edge crack):

$$a + ae = \frac{1}{\pi} \cdot \left( \frac{K}{Y \cdot \sigma} \right)^2 \quad (2.29)$$

Hasebe & Ueda (HASEBE and UEDA, 1981) have presented the geometry factor ( $Y$ ) results for a semi-infinite plate with a step in the edge. This work was not studied previously by Xu, Lou and Barltrop (2013) and the results are plotted as  $a+ae$  values (dimensioned here to a crack growing from a 0.1m step) against the actual crack size  $a$  in Figure 2-20 left. Here:

- i. The green dotted line is simply  $a = a$ , which is the result that would be expected if there were no step.
- ii. The red, solid, curve is the  $a + ae$  value calculated from Hasebe and Ueda's  $Y$  values.
- iii. The blue, dashed, curve is the  $a + ae$  curve calculated simply from  $ae = as$

where  $as = \frac{H}{2} = \text{step height}/2$

The  $ae$  value is well predicted as about half the step height. These results are investigated further in Chapter 6.

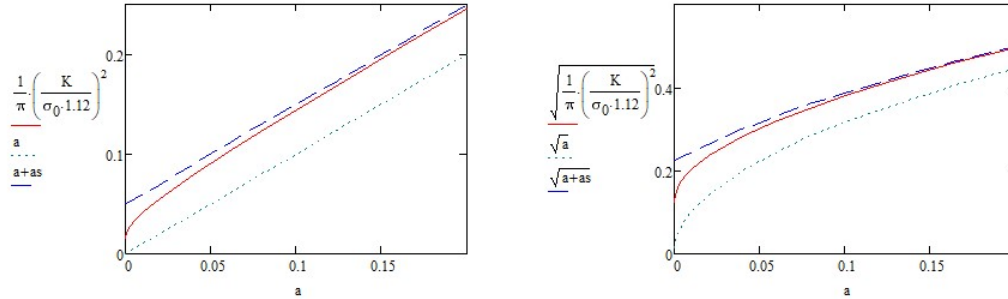


Figure 2-20 Left:  $a + ae$  values calculated from Hasebe & Ueda's (1981)  $Y$  value;  
Right:  $(a + ae)^2$  values which are proportional to the SIF,  $K$  [Equation (2.29)]

## 2.4.9 Calculation of SCF for fatigue life estimation from $as$

Give the singular stress field and a suitable weighting function the crack growth behaviour can be calculated using Paris' Law.

Xu et al (2013) used an approximate weighting function to represent the sharp corner that was taken as the average of the weighting functions for:

- 1 a crack growing from the edge of a semi-infinite plate and
- 2 a semi-infinite crack growing in an infinite plate.

This was argued to be an approximation to the actual weighting function.

The crack is assumed to propagate along the direction perpendicular to the loads, to start at the sharp corner.

Xu et al. (2013) then calculated the cycles to grow a crack from 0.15mm to 25mm in the singular stress field with a nominal stress range of 10MPa. They

compared the results, for the same range of crack growth, but with a uniform applied stress range of the same nominal stress of 10MPa. The stress concentration factor (Figure 2-21) was calculated as the cube root of the inverse ratio of the cycles to failure in the two calculations.

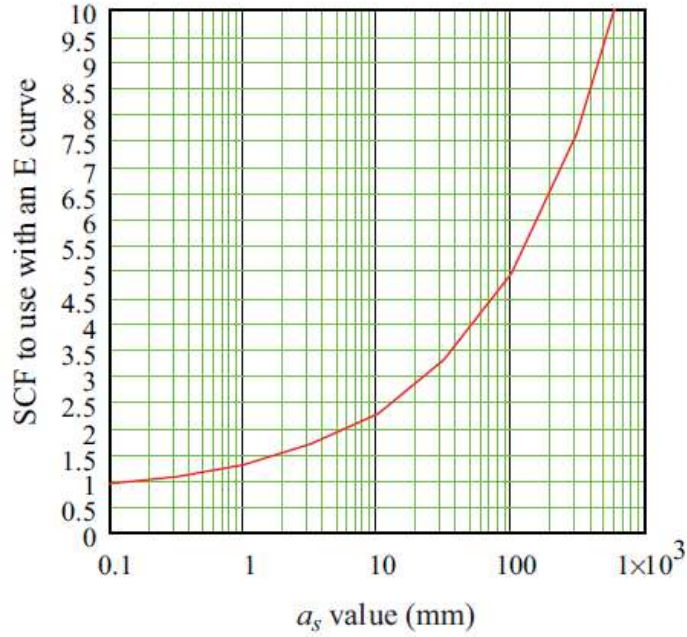


Figure 2-21 E curve SCF for different  $a_s$  values from Xu et al (2013)

Figure 2-22 is the Figure 2-21, E class curve adapted for a D class S-N curve and also shows a simple formula  $SCF_p$ , that closely follows the numerical results:

$$SCF_p = 0.55 \cdot \left( \frac{a_s}{mm} \right)^{0.48} + 0.9 \quad (2.30)$$

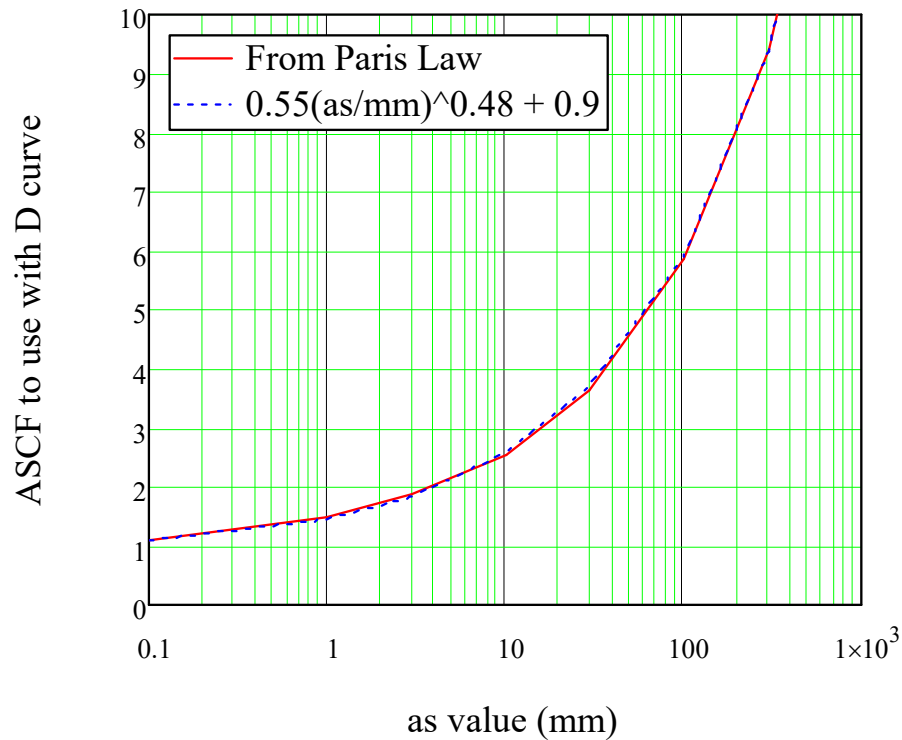


Figure 2-22 D curve SCF for different  $as$  values from Xu et al (2013)

For the related problem of the connection to the corner of an angle stiffener the same formula, with an  $as$  value allowing for the relative thicknesses of the attachment and the sum of the thicknesses of the flange and web was expected to result in good estimates of the SCF. However, for the small cracks in the angle stiffener connection that are relevant to an S-N curve calculation, where  $ae$  is much smaller than  $as$  (as in Figure 2-19), the Figure 2-22 curve was not found to give a good estimate and in Figure 60 of Barltrop & Xu (2011) there is an indication that a better estimate of the SCF for this case can be obtained by multiplying the effect of an SCF of 1.4 and an  $as$  value of connection length/190 instead of connection length/25.

That results in the following revised formula for the SCF ( $SCF_r$ ):

$$SCFr = 1.4 \times 0.55 \cdot \left( \frac{\frac{25}{190} \cdot as}{mm} \right)^{0.48} + 0.9 \quad (2.31)$$

## 2.4.10 Calculating K Values Using FEM

The numerical calculation of  $K$  in the finite element method (FEM) can be done using displacement matching methods and various energy based method. A displacement extrapolation and an energy based method are implemented in commercial FE software packages, e.g. ANSYS Workbench and ABAQUS.

### 2.4.10.1 Energy based method for calculation of $J$ in ANSYS

The J-integral is defined as “a certain integral evaluated along a contour traversing a region around the crack tip” (Hellen, 2001). The J-integral concept applied for both 2D and 3D crack tips. Under certain conditions e.g. LEFM and small scale yielding, the result of the J-integral can be considered equal to the energy release rate (Yoda, 1980). This equality is really important as it gives the possibility to calculate the J-integral value through a FEM software and then derive the Stress Intensity Factor from it.

The J-integral method is not suitable for evaluating SIF due to weld residual stresses because the J-integral is no longer path-independent in the presence of thermal strains, path dependent plastic strains, body forces within the integration area, and pressure on the crack surface (Seifi, 2012).

The displacement extrapolation method discussed below, not the J integral method, was used in this work.

### 2.4.10.2 Displacement extrapolation method for calculation of $K$ in ANSYS

According to the LEFM, the crack tip displacement field in the load direction for a 2D problem is presented in Equation (2.32) (Anderson, 2017),

$$u_y = \frac{K_I}{2G} \sqrt{\frac{r}{2\pi}} \sin\left(\frac{\theta}{2}\right) \left[ \kappa + 1 - 2 \cos^2\left(\frac{\theta}{2}\right) \right] - \frac{K_{II}}{2G} \sqrt{\frac{r}{2\pi}} \cos\left(\frac{\theta}{2}\right) \left[ \kappa - 1 - 2 \sin^2\left(\frac{\theta}{2}\right) \right] \quad (2.32)$$

where  $\kappa = \frac{3-\nu}{1+\nu}$  for plane stress (this is relevant for the thin plates analysed in this thesis) and  $\kappa = 3-4\nu$  for plane strain,

$G$  is shear modulus, and as for isotropic materials it is connected with the equation  $G = \frac{E}{2(1+\nu)}$ ,

$u_y$ ,  $r$ ,  $\theta$  are defined in crack tip coordinate, see Figure 2-23.

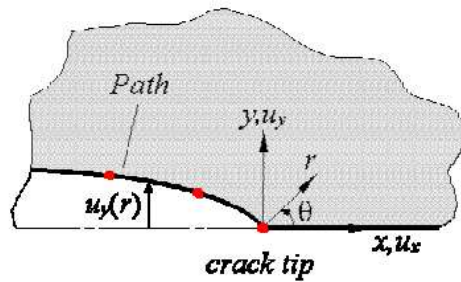


Figure 2-23 Coordinate at crack tip and path for displacement extrapolation (Bao et al., 2010)



The SIFs can be calculated from the FE solution according to the displacement extrapolation procedure using Equation (2.33)

$$K_I = \sqrt{2\pi} \frac{2G}{\kappa+1} \cdot \frac{\Delta u_y}{\sqrt{r}} \quad (2.33)$$

where  $\Delta u_y$  is the displacement between the corresponding nodes located on the upper and lower crack surfaces.  $r$  is the node coordinate. Away from the crack tip,  $\frac{\Delta u_y}{\sqrt{r}}$  can be fitted by a linear function of  $r$  in Equation (2.34),

$$\frac{\Delta u_y}{\sqrt{r}} = \alpha + \beta \cdot r \quad (2.34)$$

If the node is located infinitely close to the crack tip, there is

$$\lim_{r \rightarrow 0} \frac{\Delta u_y}{\sqrt{r}} = \alpha \quad (2.35)$$

Therefore,

$$K_I = \sqrt{2\pi} \frac{2G\alpha}{1+\kappa} \quad (2.36)$$

The displacement extrapolation is implemented in ANSYS code using the “KCALC” command can be called in the general postprocessor after defining the path and either the plane stress or the plane strain state for the 2D problem. A refined mesh is used in the region around the crack tip to capture the rapidly varying stress and deformation fields (Ahmed and Alshamma, 2016). Singularity elements at the crack tip mesh result in more accurate SIF calculation for linear elastic problems. The embedded procedure in the ANSYS software package uses the absolute value of the displacement when evaluating the SIF so the SIF values will always be positive or zero. (Also if the SIF is

evaluated by the J-integral approach, the value will also be positive or zero (Bao et al., 2010)).

## 2.5 Summary

The fatigue literature review above demonstrates both existing experienced and mature results and new ideas. It is not surprising that different approaches exist for fatigue analysis. However there is no universally correct or best method. The circumstances of any considered particular case determine the choice of approaches.

The nominal stress- S-N class approach (by Gurney, British Standard BS7910) is considered as robust with regarding to it is statistical foundation. However, it is only valid for details similar to those tested so it cannot represent all structural details and it does not provide guidance on crack growth rates.

Finite Element Analyses are often performed to evaluate the hot-spot stress but the results depend on the mesh size, the elements used and the interpretation of the calculated stress pattern. The method described by Maddox (Maddox, 2001) varies depending on the particular codes used because of uncertainty in the extrapolation procedures used to interpret the stress results.

The Fracture Mechanics approach is quick if there are published solutions e.g. by Fett (1998) but these have the disadvantage that there are a very large number of possible geometrical forms so often there is no available published solution.

Finite element analysis to determine the SIF,  $K$ , is generally applicable but it is often time consuming to set up the required analyses for a particular industrial application, such as the side shell connections that were one of the parts that cracked in the TAPS trade ships.

There are different approaches for fracture mechanics assessment of  $K$  or SIF values. However these require the crack to be modelled with very fine meshes around the crack tip and for fatigue, many different crack sizes need to be modelled, resulting in time consuming analyses.

Simplified estimation of SIFs are useful for practical engineering initial estimation and checking the results of more accurate analysis for these, more complicated, welded structures. Stress intensity factors are most often approximated using two-dimensional analysis from previous literature. However the literature does not provide insights into the behaviour of cracks emanating from corners, crossing thickness changes or growing through stiffeners and into plates.

Mathematically simple expressions to determine SIFs will simplify the calculations process and time dramatically. If the error between the FEM and the simplified approach is sufficiently small, it will help with the process of estimating the stress intensity factor for complex welding components. A simplified method that provides approximate SIF results could be utilized for rough calculations to decide whether more accurate calculations are required and, with some calibration, in reliability calculations where many thousands of computations required and for approximate checking of results of more accurate calculations.

## **2.6 The work reported in this thesis**

This PhD started with the intention of comparing the reliability of different structural details that had the same fatigue life. That required the assessment of SIF values and finally that part of the work became the subject of the PhD. So this thesis is aimed at the direct estimation of the SIF. However as the stress field is also estimated the work will also assist with S-N based fatigue

analysis. An understanding of the stress field can also be used by the analyst to help choose the mesh size in finite element analysis and, with suitable weight functions, can be used for fracture mechanics based assessment without the need for analysing the cracked structure. In particular this thesis will extend the previous work and produce simplified formulae for SIFs or  $Y$  values and SCFs for cracks growing through changes of plate thickness and through typical side shell connection details.

The analysis of a longitudinal to transverse stiffener connection is researched in several simpler stages that are reported chapter by chapter:

- Chapter 3 analyses a crack growing across a constant thickness plate and demonstrates that a simple analysis based on the ratio of the:
  - remaining ligament linear  $(\frac{P_a}{A} + \frac{M_a \cdot y}{I})$  crack tip stress from the applied loading] to the similarly calculated
  - $[(\frac{P_s}{A} + \frac{M_s \cdot y}{I})$  crack tip stress from the semi-infinite plate singular stress field, truncated to the extent of the ligament] provides a (surprisingly) accurate assessment of the  $Y$  values.
- Chapter 4 extends the Chapter 3 analysis to a plate with a thickness change at right angles to the crack. (The same semi-infinite stress pattern is used irrespective of the thickness change but the resultant force and moment  $P_s$  and  $M_s$ ) differ as a result of the different thicknesses. It was also necessary to introduce terms to account for the step change in the  $Y$  value at the thickness change. The method continued to work well, although the difference between the simple formula and the FEA was larger than for the constant thickness plate.
- Chapter 5 extended the method to a plate with a flat bar stiffener and the crack growing from the stiffener outstand and into the plate. The

extension is relatively minor, it simply affects the levers for the moment calculation for both the applied load and the reference singular stress.

- Chapter 6 further extends the method to a connection between a plate, longitudinally stiffened by an angle stiffener, and a transverse frame with a flat bar stiffener. The crack grows from the angle stiffener corner both into the stiffener flange and down the stiffener web. In this chapter only membrane stresses and SIFs or  $Y$  values are considered. The changes to the previous calculation are that
  - the applied loading affects the whole of the remaining ligament (including the uncracked flange), whereas
  - the singular load is only applied to and resisted by the uncracked part of the stiffener web and plate.
  - the singularity caused by the right angled corner between the stiffeners is accounted for by an estimated  $as$  and resulting crack size dependent  $ae$ .

Results are obtained for both tension and bending loads applied to the shell plate and stiffener. The results continue to be useful, although each additional complication reduces the overall accuracy. The singularity at the connection of a flat plate and angle appears to be significantly different to the singularity associated with a coplanar attachment to a flat plate.

- Chapter 7 considers three stiffeners connected side by side to the transverse frame with only the middle stiffener cracking. It was necessary to introduce an analysis of the redistribution effect as the middle stiffener loses stiffness relative to the outer stiffeners.
- Chapter 8 returns to the single stiffener but now includes the plate bending effect which becomes dominant once the longitudinal (shell) stiffener has cracked through. It shows that a simple assessment of the

plate bending SIF works reasonably well for this, web completely cracked, case.

- Chapter 9 presents the stresses on various lines through the single stiffener. The stresses confirm that the singularities at the intersection of the stiffeners are significantly different to the singularity at a coplanar attachment, with a much lower power law exponent. Nevertheless estimating  $as$  from the connection length results in a reasonable estimate of the stress concentration factor in comparison with, conventionally, linearly extrapolating the stress.
- Chapter 10 presents conclusions and recommendations
- The Appendices contain some validation of the ANSYS estimation of SIF values.

## **Chapter 3 A crack growing through a constant thicknesses plate**

### **3.1 Introduction**

This chapter analyses, using ANSYS FEA to predict the SIF for the well known case of an edge crack with different length/plate width (in the direction of the crack) values. After validating the FEA results against published SIF solutions a novel alternative method of estimating the SIFs based on the linearized stress in the remaining ligament is presented. This method is used in later chapters to estimate SIFs in more complicated geometry.

### **3.2 FEA of plate thickness change**

#### **3.2.1 Element types**

Finite element analysis for a range of thickness ratios were performed using ANSYS with ANSYS type 8-node Shell 93 elements around the crack, adapted to 6-nodes with singular properties at the crack tip. Away from the crack, where stress gradients were relatively small, the 4-node element type Shell 63 was used. This allowed a quicker solution with less mesh coarsening than if Shell 93 elements had been used everywhere. Comparisons with published results showed this modelling method to be satisfactory in this case.

### **3.2.2 Meshing**

In the geometry of a single edge crack, it is possible to utilize standard mesh generation tools to produce a crack tip surrounded by the required singular elements. Around the node at the crack tip a circular area is meshed by a designated number of triangular singular elements with quarter point nodes. Immediately beyond that mid-node element meshing using 8 node Shell93 is created automatically by the programs.

The remainder of the mesh was generated using the ANSYS APDL input meshing functions.

### **3.2.3 Constraints**

For one side of loading, there are X, Y and Z direction constraints at one keypoint and X, Y direction constraints at the opposite keypoint. For the other side of loading, there is only Y-direction constraint at the middle of line.

### **3.2.4 Material properties**

The Young's modulus is 210GPa.

The Poisson's Ratio is defined as 0.3.

### **3.2.5 Loading**

The membrane stress loading is  $1.0 \times 10^8$  Pascal applied along two, opposite, sides of the structure.



### 3.2.6 SIF calculation

The SIFs were calculated using the Linear Elastic Fracture Mechanics (LEFM) solution method., which is based on the deflections of the crack surfaces.

### 3.2.7 The model

The mesh details of the model and the application of boundary conditions are shown in Figure 3-1.

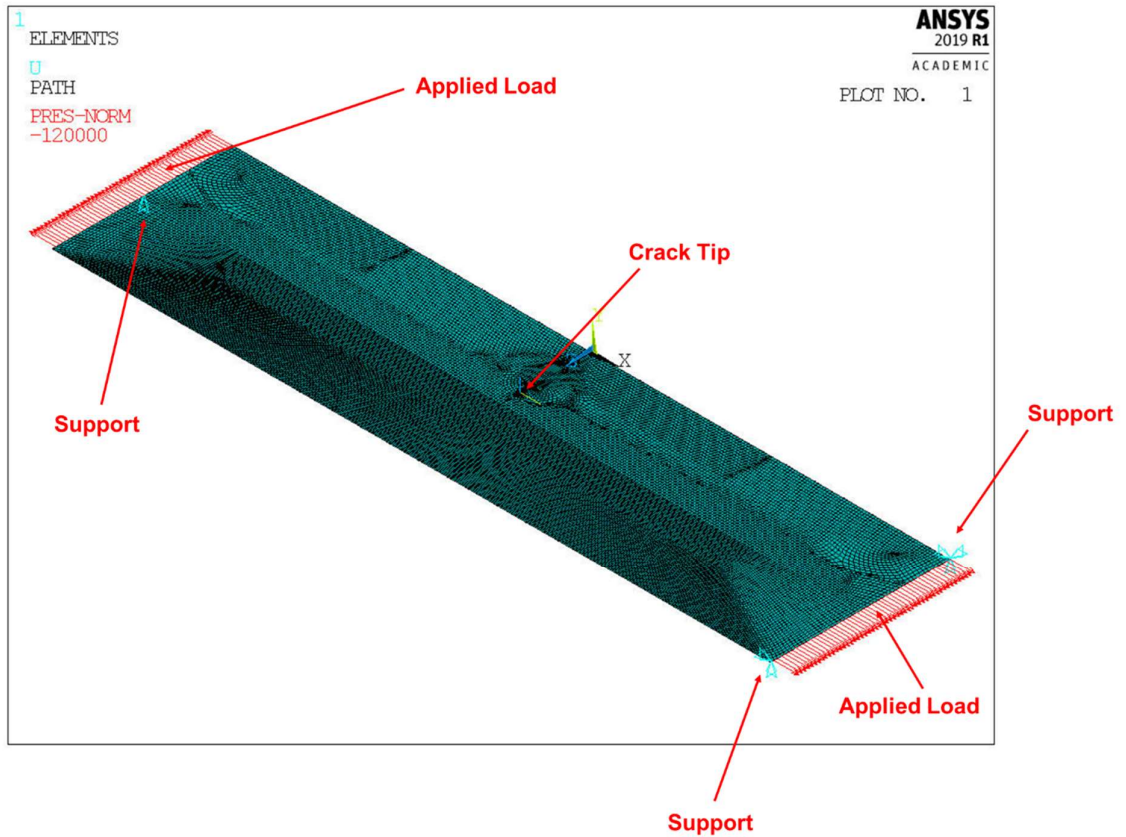


Figure 3-1 Mesh Details and Boundary Conditions Support

The mesh details around crack tip is shown in Figure 3-2.

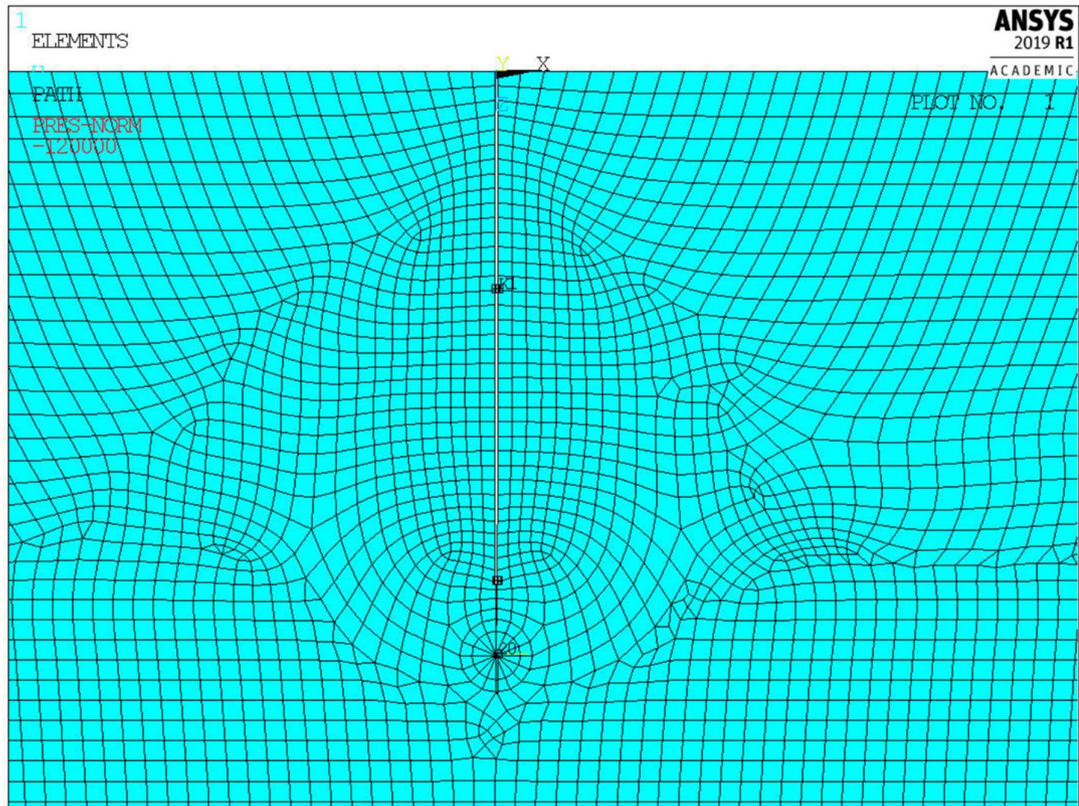


Figure 3-2 Mesh Details around Crack Tip

### 3.3 Estimation of the Y values for a constant thickness

#### 3.3.1 Validation of FEA against Fett's published work for a constant thickness plate

The values of  $F_t'$  factor can be validated against Fett, (1998) with the Geometric function for tension,  $F_t' = Y \cdot (1 - a/W)^{\frac{3}{2}}$  and  $Y$  values in Table 3-1. Note Fett uses the terminology  $F_t$  for the  $Y$  value and  $F_t'$  for the  $Y$  value

multipled by  $(1-a/W)^{\frac{3}{2}}$ . The values of  $Y$  and  $F_t'$  from FEA method against  $a/W$  for  $t_2 = t_1$  are presented in Table 3-2.

Y values against $a/W$					
Crack Length	$t_2 = 3\text{mm}$	$t_2 = 6\text{mm}$	$t_2 = 12\text{mm}$	$t_2 = 24\text{mm}$	$t_2 = 48\text{mm}$
$a = 100\text{mm}$	1.549	1.448	1.366	1.292	1.222
$a = 200\text{mm}$	3.071	2.562	2.123	1.731	1.398
$a = 250\text{mm}$	6.874	4.484	2.795	1.744	1.144
$a = 300\text{mm}$	14.657	7.562	4.034	2.281	1.411
$a = 350\text{mm}$	22.165	11.636	6.378	3.751	2.439
$a = 400\text{mm}$	41.124	21.814	12.161	7.333	4.92
$a = 450\text{mm}$	124.491	66.547	37.572	23.084	15.839

Table 3-1 Non-dimensional factor  $Y$  values against  $a/W$  for different  $t_2$  thicknesses (Results obtained from FEA)

Crack Length	Y Factor from FEA $Y = \frac{K_I}{\sigma \cdot \sqrt{\pi \cdot a}}$	$F_t'$ Factor from FEA $(F_t' = Y \cdot (1 - a/W)^{1.5})$
$a = 100\text{mm}$ $(a/W=0.2)$	1.366	0.977
$a = 200\text{mm}$ $(a/W=0.4)$	2.123	0.987
$a = 250\text{mm}$ $(a/W=0.5)$	2.795	0.988
$a = 300\text{mm}$ $(a/W=0.6)$	4.034	1.02
$a = 350\text{mm}$ $(a/W=0.7)$	6.378	1.048
$a = 400\text{mm}$ $(a/W=0.8)$	12.161	1.088
$a = 450\text{mm}$ $(a/W=0.9)$	37.572	1.188

Table 3-2 Y and  $F_t'$  values for  $t_2=12\text{mm}$  plate with FEA method

The values for  $F_t'$  factor under pure tension loadings for the rectangular plate with an edge crack are present in Fett (Fett, 1998). The ratio of  $H/W$  is 2.0 ( $H = 1000\text{mm}$  and  $W = 500\text{mm}$ ), see Figure 3-3 and Figure 4-2 and the  $F_t'$  factors against  $a/W$  at  $H/W = 2.0$  are able to be obtained using Linear Interpolation method from other  $H/W$  values, see Table 3-3.

The area of two sides of the Model in the condition of  $t_2=12\text{mm}$  is the thickness times the width of plate ( $0.012 \times [0.25+0.25]\text{m}^2$ ) and the forces on two sides of the model should be the stress multiplies the side area ( $10^7 \times 0.012 \times 0.5 \text{ N}$ ) based on Table 3-4.

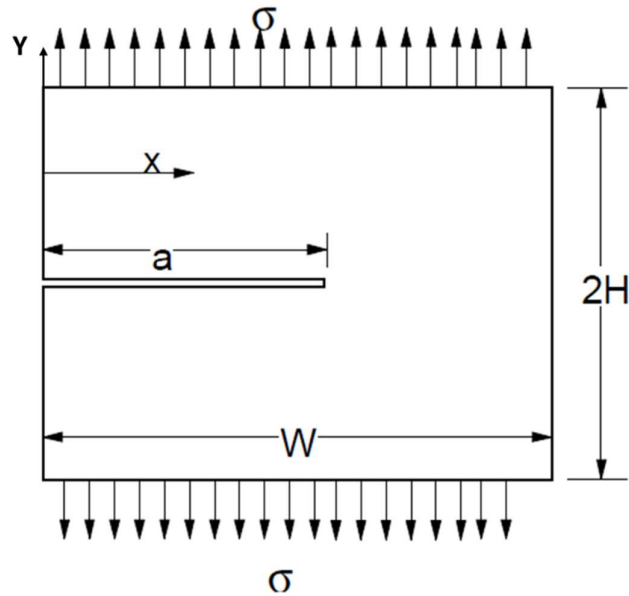


Figure 3-3 Crack in rectangular plates under tension loading (Fett, 1998)

Crack Length	$F_t'$ Factor from Fett	$F_t'$ Factor from FEA
$a = 100\text{mm}$ ( $a/W=0.2$ )	0.98	0.977
$a = 200\text{mm}$ ( $a/W=0.4$ )	0.981	0.987
$a = 250\text{mm}$ ( $a/W=0.5$ )	0.998	0.988
$a = 300\text{mm}$ ( $a/W=0.6$ )	1.02	1.02
$a = 350\text{mm}$ ( $a/W=0.7$ )	1.044	1.048
$a = 400\text{mm}$ ( $a/W=0.8$ )	1.068	1.088
$a = 450\text{mm}$ ( $a/W=0.9$ )	1.095	1.188

Table 3-3 Comparing  $F_t'$  factors with FEA against Fett's results

Figure 3-4 shows the result of  $F_t'$  values from two methods are in good agreement for the  $t_1 = t_2 = 12\text{mm}$  model.

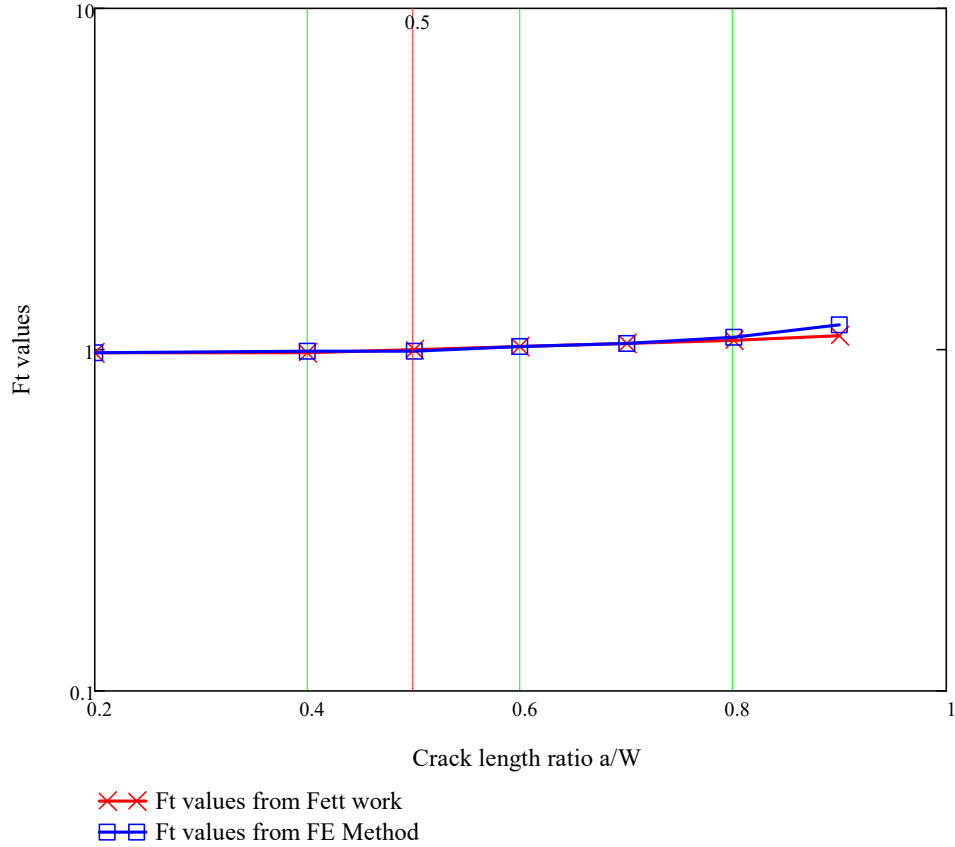


Figure 3-4 Comparisons of  $F_t'$  values with FE method and Fett work

On the basis of the Geometric Function for tension formula from Fett work,

$$Y = \frac{F_t'}{\left(1 - \frac{a}{W}\right)^{\frac{3}{2}}} \quad (3.1)$$

Finally the geometric correction factor  $Y$  is obtained from Equation (3.1), see Table 3-4. The values of non-dimensional form  $Y$  from the two methods are very close with the difference of -1.03% for a 250mm crack and 7.84% for a 450mm crack (where the crack has nearly severed the 500mm plate). See Figure 3-5, Figure 3-6 and Table 3-4.



Crack Length	Y Factor from Fett	Y Factor from FEA	$\left(\frac{Y_{FEA} - Y_{Fett}}{Y_{Fett}}\right)\%$
$a = 100\text{mm}$ ( $a/W=0.2$ )	1.37	1.366	-0.29%
$a = 200\text{mm}$ ( $a/W=0.4$ )	2.111	2.123	0.56%
$a = 250\text{mm}$ ( $a/W=0.5$ )	2.824	2.795	-1.03%
$a = 300\text{mm}$ ( $a/W=0.6$ )	4.033	4.034	0.02%
$a = 350\text{mm}$ ( $a/W=0.7$ )	6.352	6.378	0.41%
$a = 400\text{mm}$ ( $a/W=0.8$ )	11.944	12.161	1.78%
$a = 450\text{mm}$ ( $a/W=0.9$ )	34.627	37.572	7.84%

Table 3-4 Comparing Y factors with FEA against Fett's results

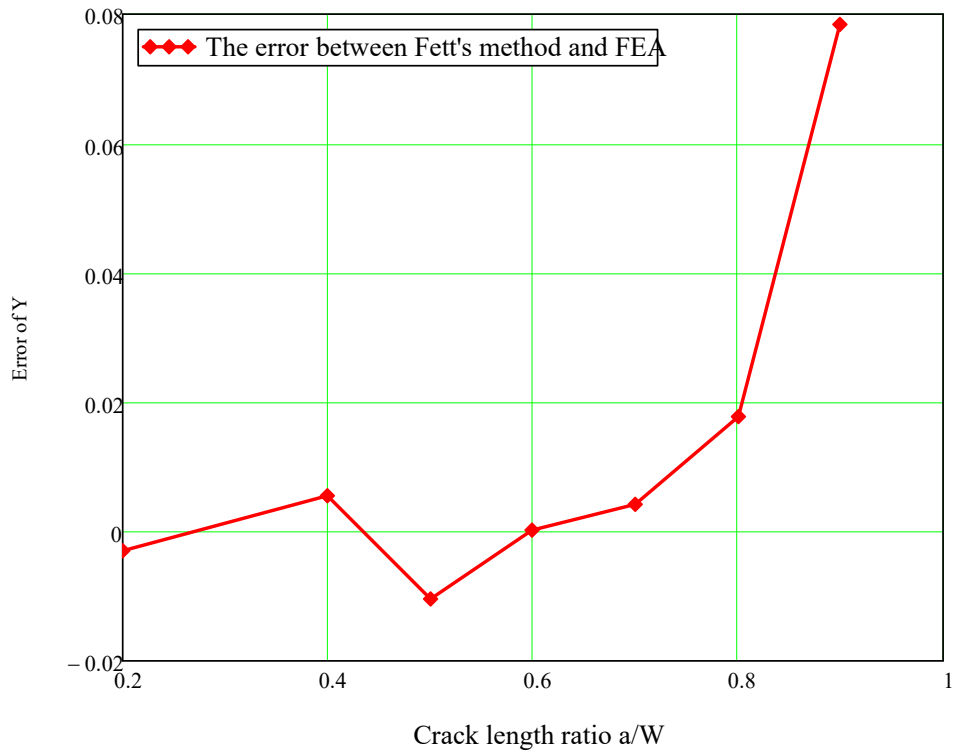


Figure 3-5 The errors between Fett, (1998) and FEA:  $\left( \frac{Y_{FEA} - Y_{Fett}}{Y_{Fett}} \right) \%$

Figure 3-5 and Figure 3-6 show similar errors between Fett and FEA as between the simplified method and FEA.

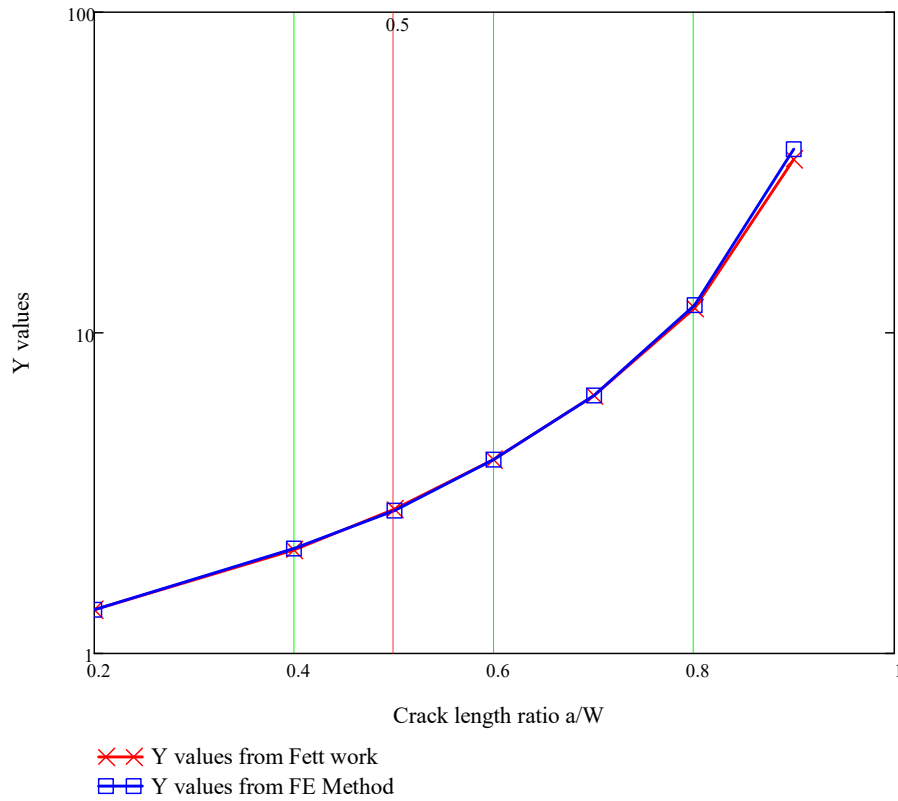


Figure 3-6 Comparisons of  $Y$  values with FE method and Fett, (1998)

According to the comparisons in the Table 3-4, it can be seen that the results of  $Y$  and  $F_t'$  values from Fett approach and FEA method are very close. The results from FEA approach are therefore validated based on Fett, (1998).

### 3.3.2 Empirical estimation of the $Y$ values for a constant thickness finite length cracked plate subject to tension

The geometric factor value  $Y$  is 1.12, inversely dependent on the radial distance from crack tip for initial crack (small crack,  $a/W = 0.01$ ). The crack size  $a$  is set up from 10mm to 990mm for the calculations, see Table 3-5.

Crack Length $a$ (in mm unit)										
10	100	200	300	400	500	600	700	800	900	990

Table 3-5 Crack lengths in 1000mm width plate

For particular  $a/W$ , the stresses on ligament is shown from step 1) to step 9).

1) The singular stress distribution in Figure 3-7 for a crack in an infinite plate is determined and assumed to apply over the finite plate size.

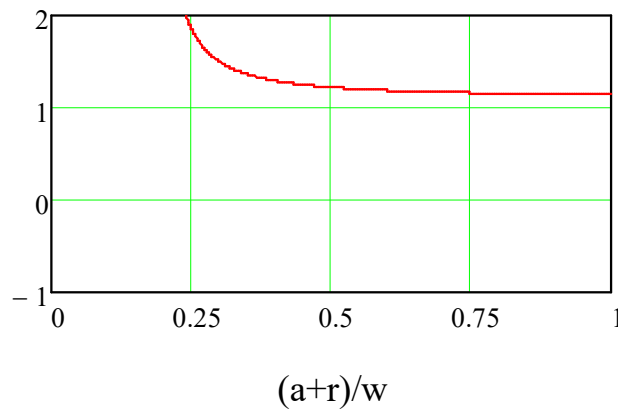


Figure 3-7 Singular stress on ligament ( $\sigma_s$ ) (Stress: Pa)

2) The mean ligament stress in step 1) is calculated and subtracted from step 1) so that the singular stress distribution now has a zero mean value in Figure 3-8.

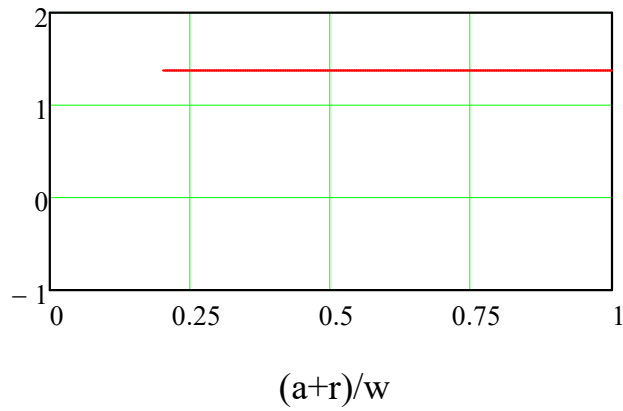


Figure 3-8 Average Stress on ligament from singular stress ( $\sigma_{si\mu}$ ) (Stress: Pa)

3) The moment about the ligament's centroid and the associated ligament stresses are calculated and subtracted from the result of step 2). The resulting of stress distribution now has zero force and zero moment, see Figure 3-9.

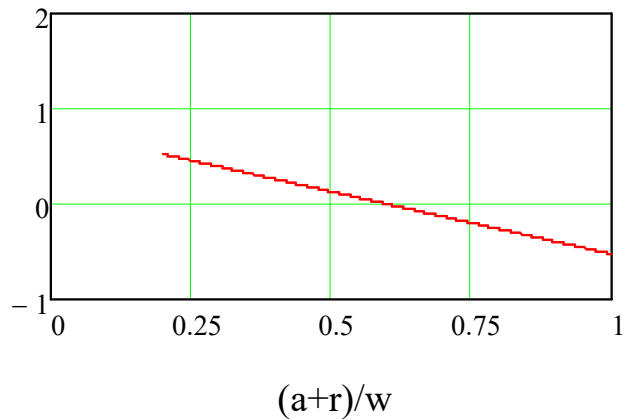


Figure 3-9 Bending stress from singular stress ( $\sigma_{bmsi}$ ) (Stress: Pa)

4) The original singular stress is characterized by the mean stress distribution plus the moment stress distribution and in particular by the sum of those values at the crack tip, Figure 3-10.

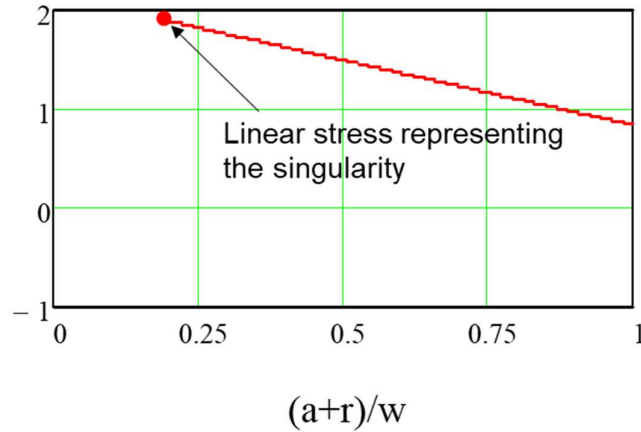


Figure 3-10 Average + Bending stress from singular stress ( $\sigma_{si\mu} + \sigma_{bmsi}$ )  
(Stress: Pa)

5) The applied stress on the plate is now integrated to determine a force and moment relative to the centre of area of the remaining ligament.

6) A uniform ligament stress is calculated for the applied force in Figure 3-11.

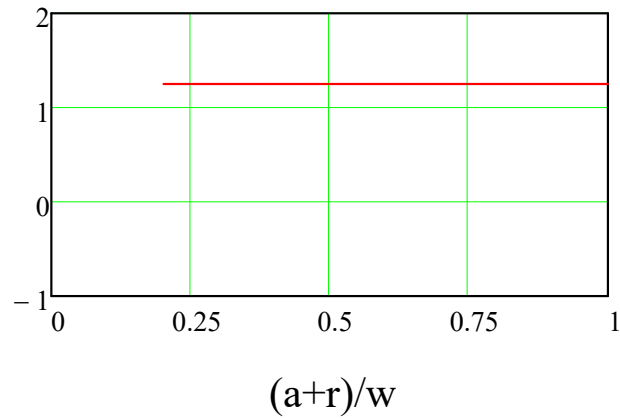


Figure 3-11 Axial stress from applied load ( $\sigma_{la}$ ) (Stress: Pa)

7) Using engineer's bending theory, a linearly varying ligament stress is calculated for the applied moment, in Figure 3-12.

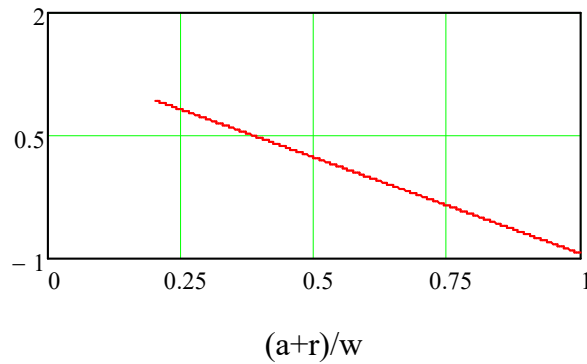


Figure 3-12 Bending stress on ligament from applied load ( $\sigma_{bml}$ ) (Stress: Pa)

8) These are combined and stress representing the applied load is taken as the stress from step 6) and plus the stress from step 7) at the crack tip, see Figure 3-13.

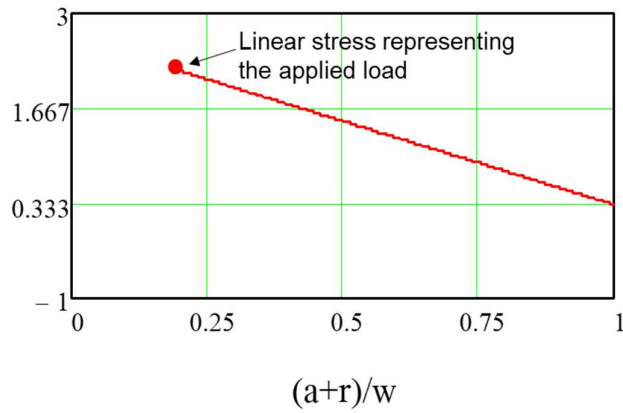


Figure 3-13 Axial and bending stress on ligament ( $\sigma_{\mu a} + \sigma_{bma}$ ) (Stress: Pa)

9) The  $Y$  value is calculated as  $1.12 \times$  the stress representing the applied load (in Figure 3-10)/the stress representing the singular stress (in Figure 3-13).

Steps 1) to 9) are repeated for each crack size and the graph of  $Y$  value against  $a/W$  results. This is shown in Figure 3-14 along with the results from Fett work (Fett, 1998).

When considering the stress correction ratio alone at the crack tip in the ligament, there is,

$$\begin{aligned} \text{Ratior} &= \frac{\text{nominal axial stress} + \text{bending stress from applied load}}{\text{infinite plate formula nominal stress} + \text{bending stress from singular stress}} \\ &= \frac{\sigma_{\mu a} + \sigma_{bma}}{\sigma_{si\mu} + \sigma_{bmsi}} \end{aligned}$$

Estimation of  $Y$  values around crack tip is using the ratio of underlying mean stress plus the bending stress,

$$Ynr = 1.12 \cdot \text{Ratior} \quad (3.2)$$



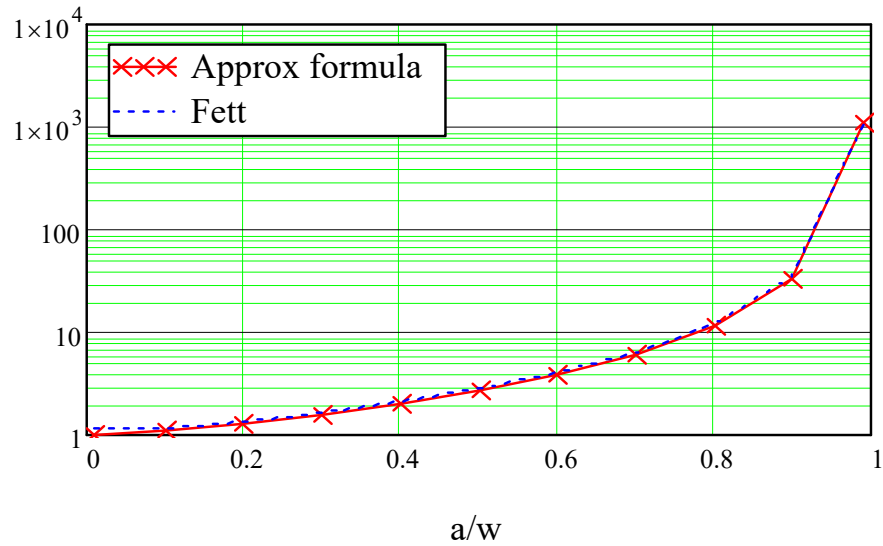


Figure 3-14 Comparison  $Y$  values between approximate method and Fett (Fett, 1998) results

### 3.4 An alternative assessment of the SIF in a finite width plate subject to an axial force and moment

#### 3.4.1 Introduction

To enable the simple estimation of  $Y$  values for more complicated structured, a method of simply estimating the  $Y$  values for a finite length cracked plate was developed.

The method is based on applying engineer's bending theory to the remaining ligament for the plate in Figure 3-15. The ligament length  $b = w - a$  and the variation of  $a$  represents the crack length. The total width of the plate  $w = 1$  m and since it is assumed that the plate is semi-infinite, the plate is infinite long and has finite width. The loading applied on both sides of the plate is the uniform stress, 1Pa.



However, for finite plate widths (where the width is in the direction of the crack) it is interesting to use an alternative method of estimating  $K$  using a linearized crack tip stress calculated from the mean applied stress and linear bending stress at the crack tip, in conjunction with the stress field formula for a finite (through thickness) crack in an infinite plate quoted by Paris and Sih (Paris and Sih, 1965). This resulted in surprisingly accurate SIF values for cracks in wide finite width plates subject to axial tension or bending.

The Paris and Sih formula for a through thickness crack in an infinite plate subject to a constant stress is,

$$\sigma(x) = \frac{\sigma_0 \cdot (x+a)}{\sqrt{x^2 + 2 \cdot a \cdot x}} \quad (3.4)$$

### 3.4.2.1 Singular stress distribution based on Paris and Sih (1965)

For this work an edge crack in a semi-infinite is of interest and the above formula is empirically but simply modified, two methods were used as discussed in Section 3.4.2.1 and Section 3.4.2.2.

- a) The stress at the crack tip (where  $x$  is much smaller than  $a$ ) is 1.12 times the Paris and Sih value (because the  $Y$  value for an edge crack is 1.12 times that for an internal crack).
- b) The stress at distance ( $x$  is much larger than  $a$ ) decays to the applied stress  $\sigma_0$ .

The modified stress distribution, which has these characteristic, for an edge crack in a semi-infinite plate is:

$$\sigma(x) = \frac{\sigma_0 \cdot (x+a)}{\sqrt{x^2 + \frac{1}{1.12} \cdot 2 \cdot a \cdot x}} \quad (3.5)$$

### 3.4.2.2 Other singular stress fields fitted to small cracks in semi-infinite plate

To determine the sensitivity to the assumed singular stress field the following alternatives were also used within the approximate methodology for estimating  $Y$  values and the final results were compared with Fett (Fett, 1998).

$$\sigma(x) = \frac{1.12 \cdot \sigma_0}{\sqrt{2 \cdot \pi \cdot x}} \quad (3.6)$$

$$\sigma(x) = \max\left(\frac{1.12 \cdot \sigma_0 \cdot \sqrt{\pi \cdot a}}{\sqrt{2 \cdot \pi \cdot x}}, \sigma_a\right) \quad (3.7)$$

$$\sigma(x) = \frac{1.12 \cdot \sigma_0 \cdot (x+a)}{\sqrt{x^2 + 2 \cdot a \cdot x}} \quad (3.8)$$

The first alternative gave very poor results for small  $a/w$ . The second alternative was a lot better but underestimated  $Y$  values at  $a/w$  of about 0.2. The third alternative gave results similar to the method described in 3.4.2.1 but were not as good, so it was concluded that the results are sensitive to the singular stress distribution that is used and that the distribution given in 3.4.2.1 was suitable.

### 3.4.3 The approximate method

The method first of all applies the modified Paris and Sih formula to the plate of finite width:  $w$ . It is argued that if this stress pattern were applied the

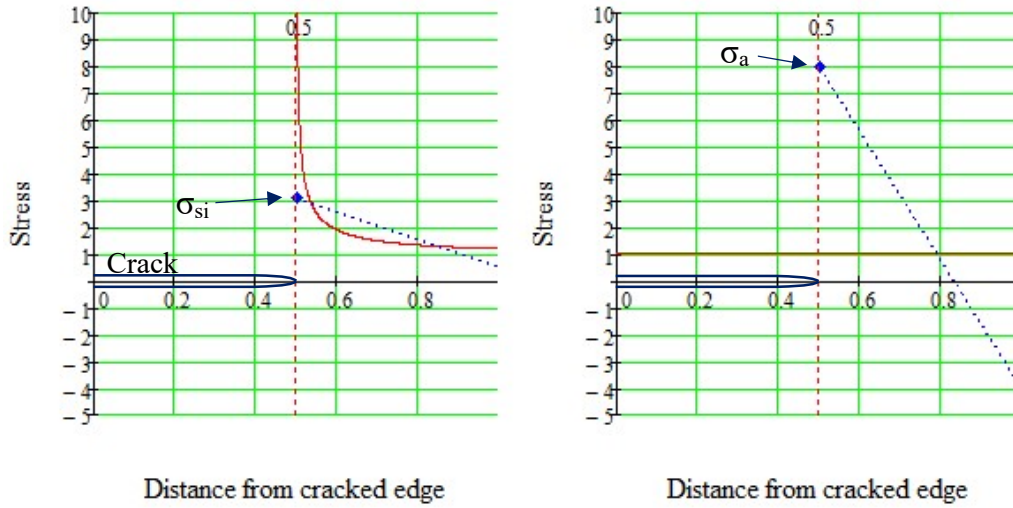
plate would have the expected SIF of 1.12 except perhaps for large  $a/w$  just before the crack breaks through.

Figure 3-16 shows stresses for a 1m width plate that has half cracked through i.e.  $a/w = 0.5$ , so the remaining ‘ligament’ is half the plate width. The crack is shown in dark blue.

Figure 3-16a shows, for a unit applied stress  $\sigma_0$ , the modified Paris and Sih ligament stress as a solid red line. It is simply truncated at the end of the plate where  $a/w = 1$ . Also shown, as a blue dotted line, is a linear stress profile that has the same force and moment about the centre of the remaining ligament. The linear stress profile has a stress of  $\sigma_s$  at the crack tip.

Figure 3-16b shows, in red, an applied unit stress of  $\sigma_0 (= 1\text{Pa})$  across the whole plate. Within the ligament this can be represented (shown as a dotted blue line) by a linear stress profile that has the same force and bending moment relative to the centre of the remaining ligament. The linear stress, representing the applied load effect on the ligament, at the crack tip is  $\sigma_a$ .

For  $\sigma_0 = 1\text{Pa}$  applied stress the mean stress on the ligament is 2Pa and the bending stress is 6Pa. The bending stress is large owing to, at  $a/w = 0.5$ , the eccentricity between the centre of the applied load (at  $a/w = 0.5$ ) and the centre of the ligament (at  $a/w = 0.75$ ).



a) Modified Paris and Sih

b) Actual applied load,

Figure 3-16 Stress distributions and linear equivalent stresses for  $a/w = 0.5$   
(Stress: Pa)

Interestingly  $Y = 1.12 \cdot \frac{\sigma_a}{\sigma_{si}}$  is a good predictor of Fett's (Fett, 1998) results

for the  $Y$  values for a uniform applied stress as shown in Figure 3-17. The error is shown in Figure 3-18; the maximum error is about 3%.

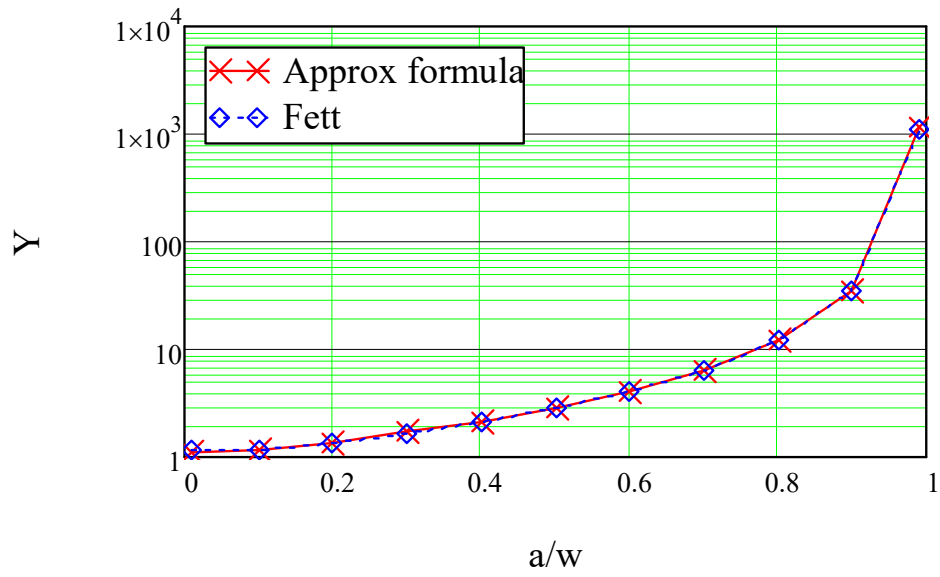


Figure 3-17 Comparison of approximate method and Fett (1998) for applied axial stress.

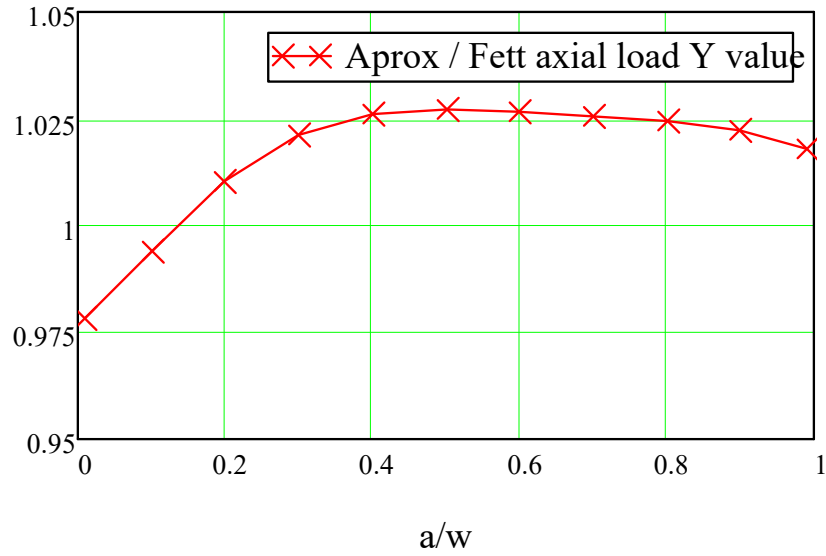


Figure 3-18 Estimated / Fett axial load Y value

### 3.4.4 Application of the method to a plate subject to in-plane bending

The method can easily be applied to a bending case as well. The Modified Paris and Sih part is unchanged but the linearized crack tip stress is different, it

is simply  $\sigma_a = \frac{\sigma_m}{\left(1 - \frac{a}{w}\right)^2}$  where  $\sigma_m$  is the maximum bending stress of, 1Pa,

applied the plate edge.

The formula  $Y = 1.12 \cdot \frac{\sigma_a}{\sigma_{si}}$ , then also predicts Fett's (1998) bending  $Y$

value results across the range of  $\frac{a}{w}$  as shown in Figure 3-19, with a maximum error of 6.5%, as shown in Figure 3-20.

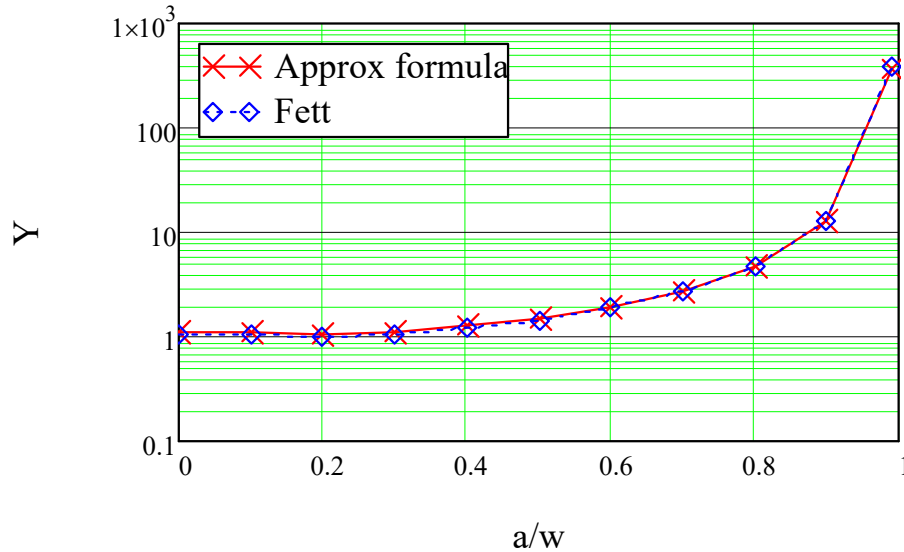


Figure 3-19 Comparison of approximate formula method  $[Y = 1.12 \cdot (\sigma_a / \sigma_{si})]$  and Fett (1998) for applied bending stress.



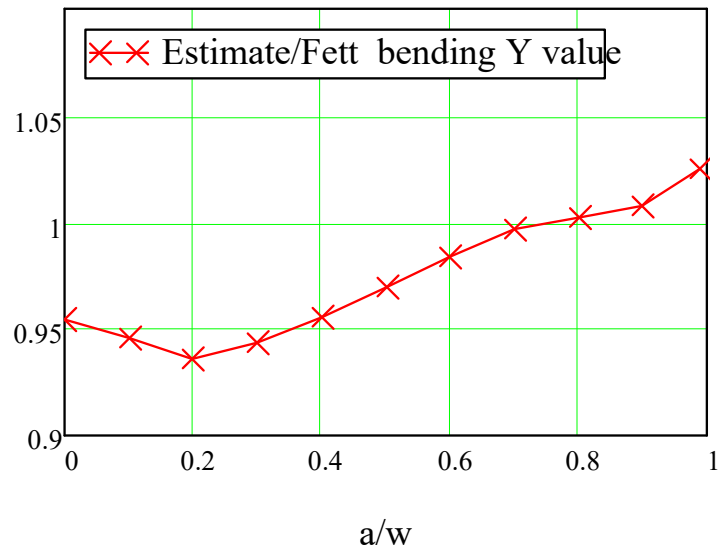


Figure 3-20 Approximate formula method / Fett in-plane bending Y value

The error for the bending case is larger than for the axial tension case although it decreases to zero at  $a/w = 0.8$ . It is possible that this is because the reference singular stress is also largely bending at  $a/w = 0.8$ , whilst the crack length/plate width is not excessive. This suggests that an improved formula might treat the ligament axial force and ligament bending moments slightly differently but, as the present assumptions work quite well, that has not been investigated further.

### 3.5 Conclusion

It is interesting that the linearized stress at the crack tip in a finite width plate and a linearized stress associated with a semi-infinite plate can be used to estimate SIFs for both tension and bending cases applied to a finite width plate.

Choosing the reference stress as a linearized stress in the ligament is an unconventional way of calculating stress intensity factors and the results are only approximate but, if the method can be applied to more complicated geometry, it has the benefits for 'back of the envelope calculations', checking more complicated analyses and use in reliability analysis that the PhD is attempting to find. In the next chapters the method will be applied to a flat plate with a thickness change, a T section (plate and flat stiffener) and a connection between a plate stiffened by an angle stiffener and a transverse stiffened structure.

## Chapter 4 Cracks growing through a change of plate thickness

### 4.1 Introduction

In most published work on stress intensity factors (SIFs), the crack grows in a constant thickness plate, however it is very common that a crack grows into a different thickness plate, see Figure 4-1. Also at a junction of plates in different planes a crack meets a change in stiffness which will have some similarity with a change in thickness; this is studied, for a T section, in Chapter 5.

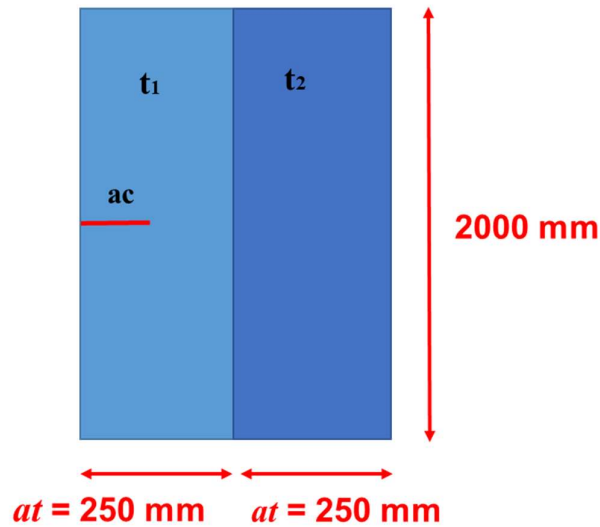


Figure 4-1 Crack growing into different thickness plates

For this chapter the model configuration studied is as in Figure 4-2, which shows an oblique view of the plates. The thickness of  $t_1$  is defined as 12mm. The

thicknesses of  $t_2$  are defined as 48mm, 24mm, 12mm, 6mm and 3mm separately. The width of each plate is 250mm. “ $ac$ ” represents the real crack size for I-shape plate with thickness change. The thickness change occurs at a crack length of  $ac = 250\text{mm}$ , in the calculations in this section this length is given the symbol  $at$  and is used to non-dimensionalize the crack length.

The lengths of the plates are both 2000mm, with the crack at the centre of the length.

Except for the thickness change, the modelling was as for the constant thickness plate in Chapter 3: The Young’s modulus and Poisson’s ratio are 210GPa and 0.3 respectively. The tension stresses applied on the 500mm long sides of the model are both 10MPa. For one side of membrane loading, there is X, Y and Z direction constrains at one keypoint and X, Y direction constrains at the opposite keypoint. For the other side of loading, there is only Y-direction constrain at the middle of line. Small cracks are completely in the  $t_1$  plate. When the crack size is larger than 250mm, it means the cracks are growing into the  $t_2$  plate. The crack lengths adopted in the model to calculate SIF values were initially 100mm, 200mm, 250mm, 300mm, 350mm, 400mm and 450mm. Later more crack size were analysed to better understand the crack behaviour around the thickness change.

$t_1$ [mm]	$t_2$ [mm]
12	48
	24
	12
	6
	3

Table 4-1 Thickness data

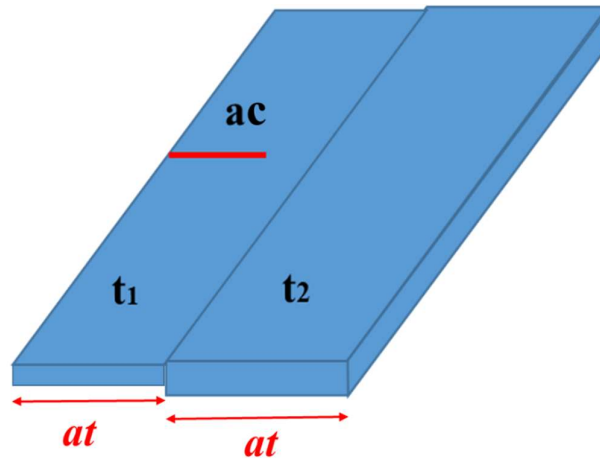


Figure 4-2 View of plates and (through thickness) crack

Stress Intensity Factors, considering step increases in crack length, have been calculated using FEA, for 2-D model with a refined mesh in ANSYS using shell elements (SHELL93) or 3-D model with solid elements (SOLID95) of ANSYS.

The SIF is based on the deflection of nodes on the crack faces, as described in Section 2.4.10.2. The nodes used in the SIF calculation are always in the same plate thickness as the crack tip. This requires a very fine mesh when a crack has just penetrated into the second plate thickness.

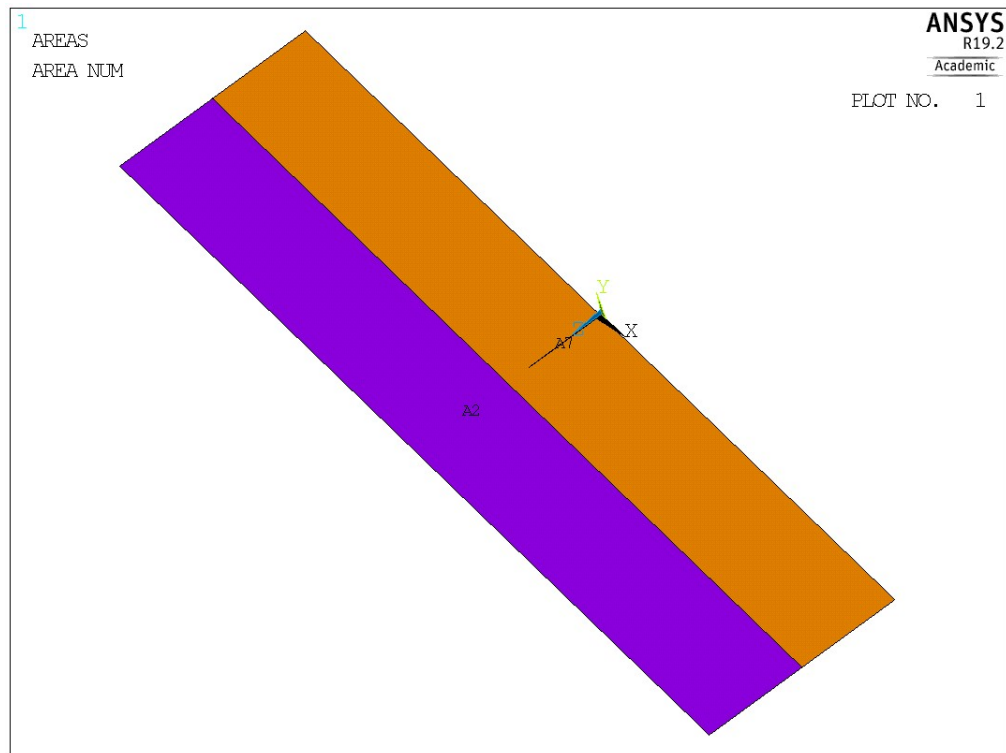


Figure 4-3 Crack growing through  $t_1$  plate

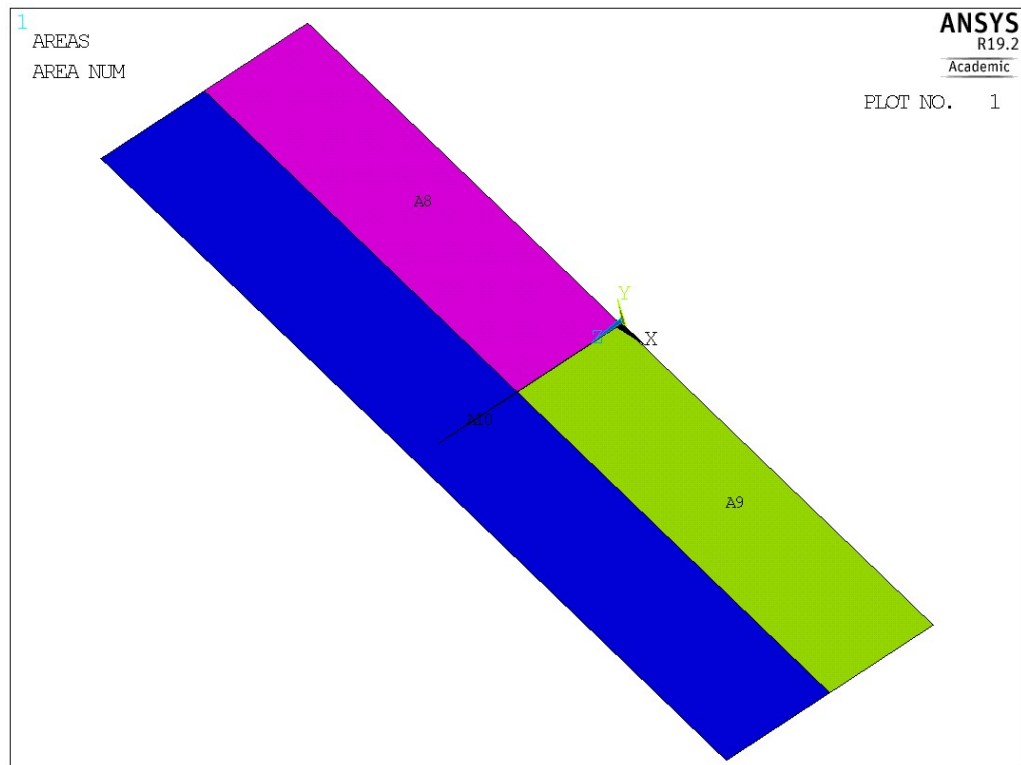


Figure 4-4 Crack propagating through  $t_2$  plate

## 4.2 Flat plate with thickness change, results

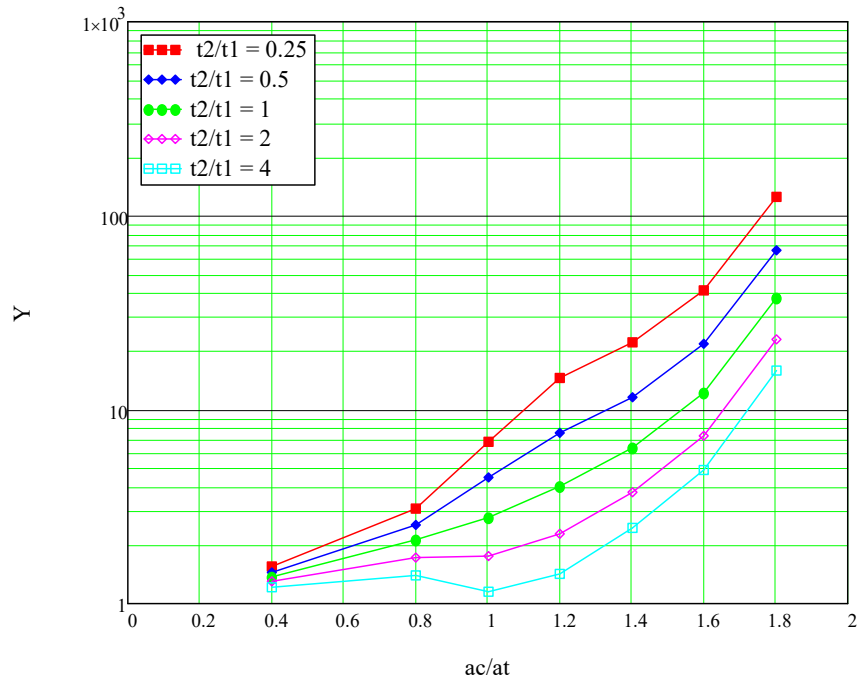


Figure 4-5 SIF values for crack growing in different thickness plates

Figure 4-5 shows the  $Y$  value for the different  $t_2/t_1$  thickness ratios plotted against crack length / first plate width. It can be seen that in the constant thickness,  $t_2=12\text{mm}$  curve (green colour), the  $Y$  corresponds to the case analysed the previous chapter. With a thinner  $t_2$  plate, at any crack length, there are higher  $Y$  values and vice versa.

To better understand the SIF values near the thickness change, more analyses are required and these are introduced in Section 4.4.



### **4.3 Estimation of SIF values for crack growing through a change in thickness**

It was desired to obtain a formula that would reasonably represent the results that had been obtained for the crack growing into a change of thickness. Three formulae were developed, as described in Appendix C (method 1) and in the following parts of this Section (methods 2 and 3). The third method gave the best fit to the data and appears to be a reasonable basis for estimating the effect of thickness changes in different ratios of plate thickness to plate width than have been considered here.

#### **4.3.1 Estimation of SIF values for crack growing through a change in thickness: Second empirical method**

This part introduces a better empirical estimation of  $Y$  values for a crack growing towards or through a change in the plate thickness. Using the model with a thickness change, the FEA results for the  $Y$  values are shown again in Figure 4-6, where, at the thickness change as  $ac/at=1$ . It should be noted that owing to the method used to estimate  $K$  and  $Y$  values the results are more easily obtained for cracks just reaching the thickness change than just passing the thickness change. The results plotted for  $ac/at = 1$  are for a crack with the crack tip in the plate of thickness  $t_1$ .

It is to be expected, that there is in fact a discontinuity as the crack passes the thickness change at  $ac/at = 1$ . This is also suggested by the trends of  $Y$  curves, sketched as dashed lines in Figure 4-6.

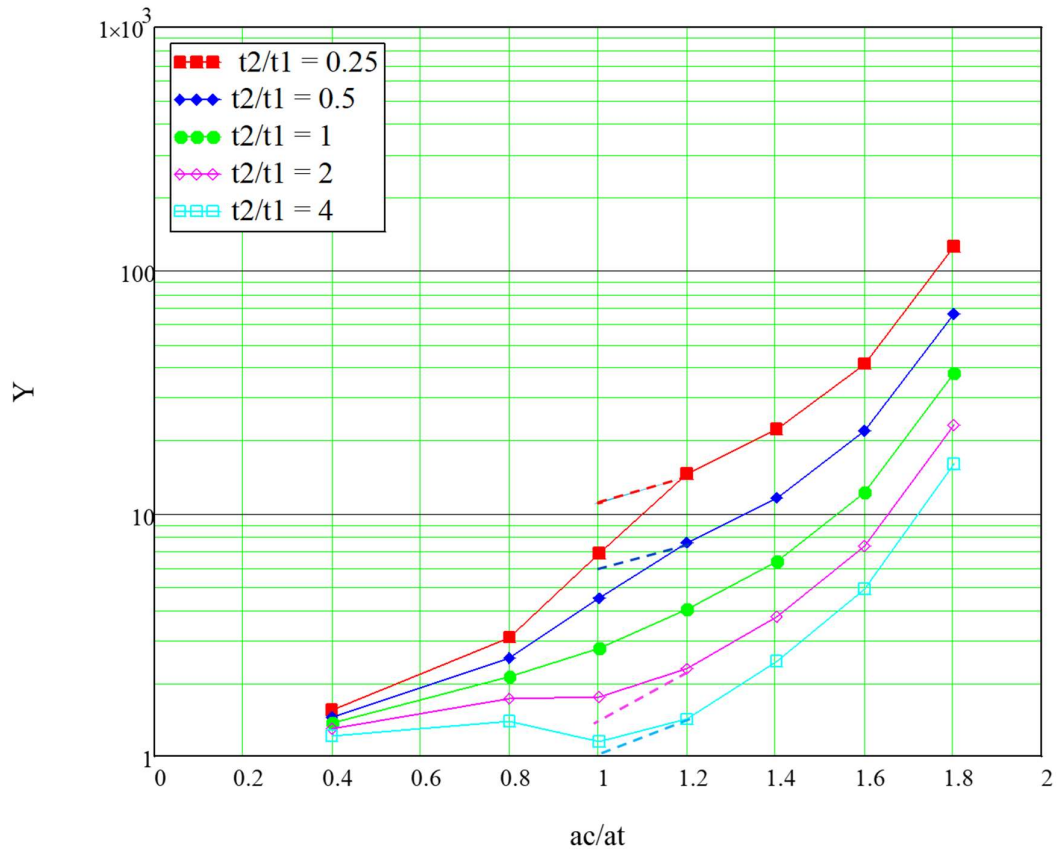


Figure 4-6 The trends of  $Y$  curves at different  $t_1$  and  $t_2$  thicknesses with the step change at  $ac/at = 1$  shown by the dashed lines (Calculated value for  $ac/at = 1$  is only valid for  $ac/at < 1$ .  $Y$  values for more  $ac/at$  values were calculated later and are shown in Figure 4-11)

If the  $Y$  values, from Figure 4-6, for the plate with a thickness change is divided by the  $Y$  values for a constant thickness plate ( $t_1/t_2=1$ ), the results are as shown in Figure 4-7. Figure 4-7 shows that there is an approximately exponential decay in the ratio of  $Y$  values either side of the change in thickness.

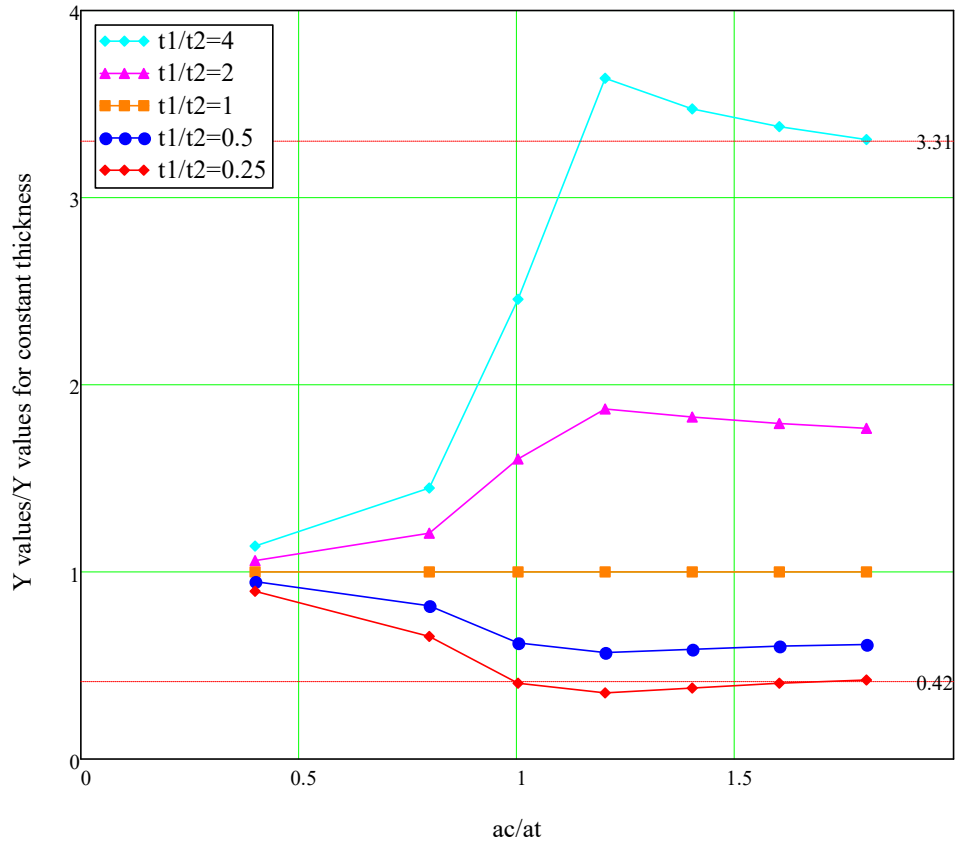


Figure 4-7 Y-value ( $Y$ ) for a plate with a thickness change divided by Y-value in a constant thickness (12mm) plate ( $Y_c$ ) for the same crack length from Figure 3-17 (Note this does not show the extrapolation to the cases where the crack has just penetrated the changed thickness)

An approximate fit for  $Y/Y_c$  curves by trial and error can be approximated to be as  $Ye$ ,

For  $ac < at$ :

$$Ye(ac) = \left[ \left( \frac{t_1}{t_2} \right)^{0.67} - 1 \right] \cdot e^{3 \left[ \left( \frac{ac}{at} \right)^3 - 1 \right]} + 1 \quad (4.1)$$

And for  $ac > at$ :

$$Ye(ac) = \left[ \left( \frac{t_1}{t_2} \right)^{0.95} - 1 \right] \cdot e^{-0.35 \left[ \left( \frac{ac}{at} \right)^{0.4} - 1 \right]} + 1 \quad (4.2)$$

A comparison of the approximate fit  $Ye(ac)$  and the FEA results is shown in Figure 4-8. Approximate and FEA of  $Y$  values/ $Y$ -constant thickness values for a crack as, in thickness  $t_1$ , it approaches and passes a change in the plate thickness to  $t_2$ .

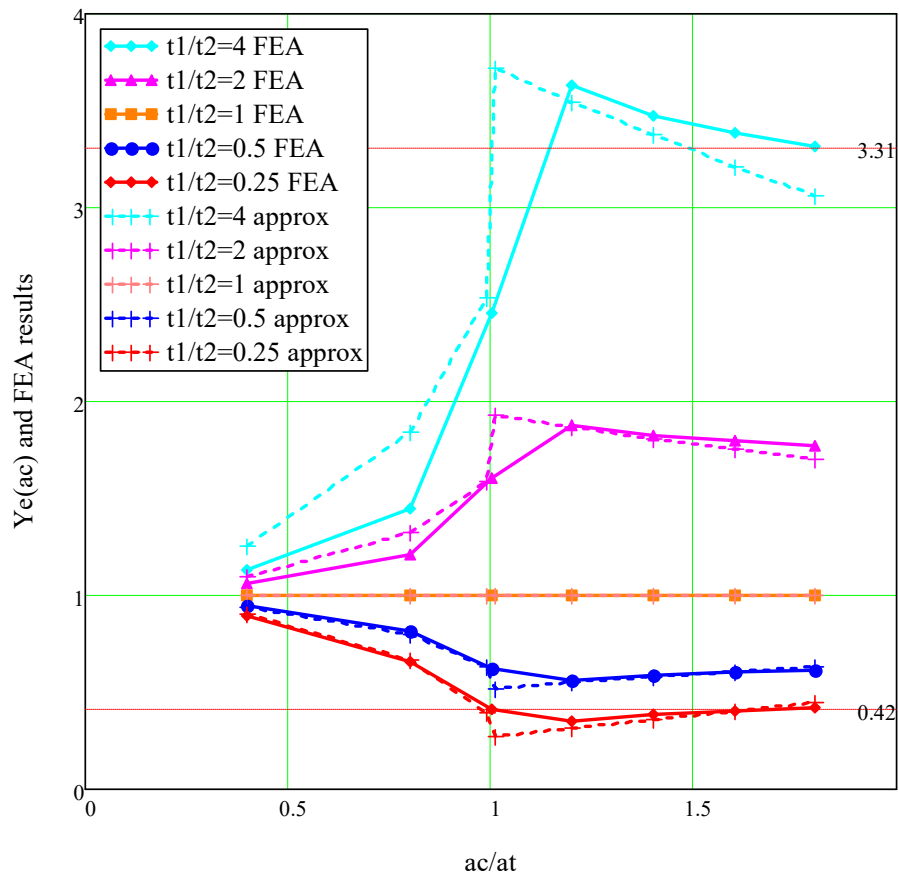


Figure 4-8 Approximately of  $Y_e$  (dashed lines) and FEA (solid lines) of  $Y/Y$ -constant thickness values ( $Y/Y_c$ ) for a crack from  $t_1$  to  $t_2$  (Note the approximate values allow for the step in the  $Y$  value at the change in thickness using  $Y_e$  [Equations (4.1) and (4.2)], that was not calculated for  $ac/at$  just greater than 1 in the FEA)

The comparison of the estimated  $[Y_e(ac) \cdot Y_c(ac)]$  and FEA values for  $Y$  values themselves are also shown, with a vertical log axis, in Figure 4-9.  $Y_c(ac)$  is the curve about  $Y$  values for the case of  $t_1=t_2=12$  mm.

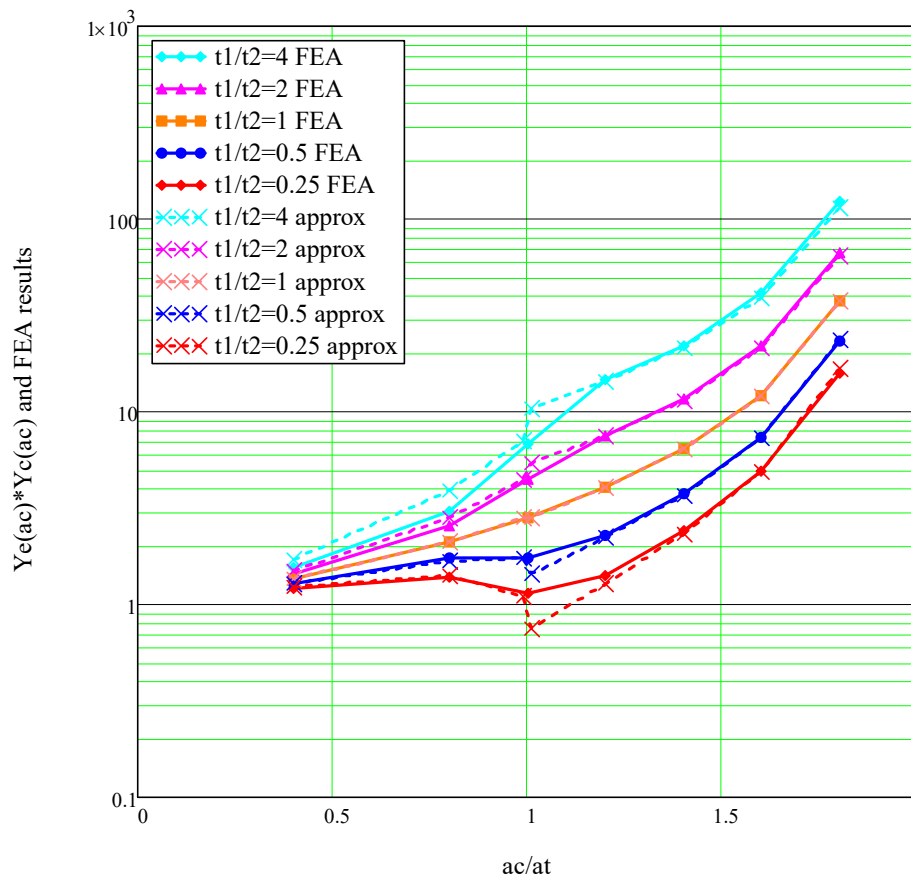


Figure 4-9 Approximate (dashed lines) and FEA (solid lines) of  $Y$  values for a crack from  $t_1$  to  $t_2$ , log vertical axis (Note approximate values are extrapolated back to the step in the  $Y$  value at the change in thickness, using the function  $Y_e$  [Equations (4.1) and (4.2)], that was not calculated for  $ac/at$  just greater than 1 in the FEA)

It was clear that more analyses were needed around  $ac/at = 1$ .

## 4.4 Investigation of $Y$ values for more crack lengths around $W/2$

For plate thickness changes at  $W/2$  ( $a = at = 250\text{mm}$ ) and for the different  $t_1/t_2$  the SIFs are investigated around  $W/2$  to see whether there is a smooth change or a jump (that was expected) in the  $Y$  value as crack length changes from less than  $W/2$  to more than  $W/2$ .

Figure 4-10 shows the changes of SIF values for plate thicknesses change and Figure 4-11 presents the  $Y$  changes for crack lengths around  $W/2$ . It is seen that for  $t_2=t_1$  plate thickness, the  $Y$  curve is very smooth for crack length around 250mm (Orange Curve). For the ratio of  $t_2/t_1=4$  (Red Curve) and  $t_2/t_1=2$  (Blue Curve) thicknesses, the  $Y$  curves decrease after the thickness change. However, the ratio of  $t_2/t_1=0.5$  (Pink Curve) and  $t_2/t_1=0.25$  (Cyan Curve) thicknesses,  $Y$  curves increase when the crack length is bigger than  $W/2$  because for these two curves, the thickness with  $t_2$  plate is much smaller than  $t_1$  plate.

Note that the method used for calculating the SIF values, based on the deformations of the crack surfaces, is only reasonable when the deformations used in the calculation are in the same thickness of plate, so the SIF values for crack sizes of less than  $W/2$  are easily calculated but SIF values when the crack is slightly larger than  $W/2$  are estimated by extrapolation as superimposed on Figure 4-10.

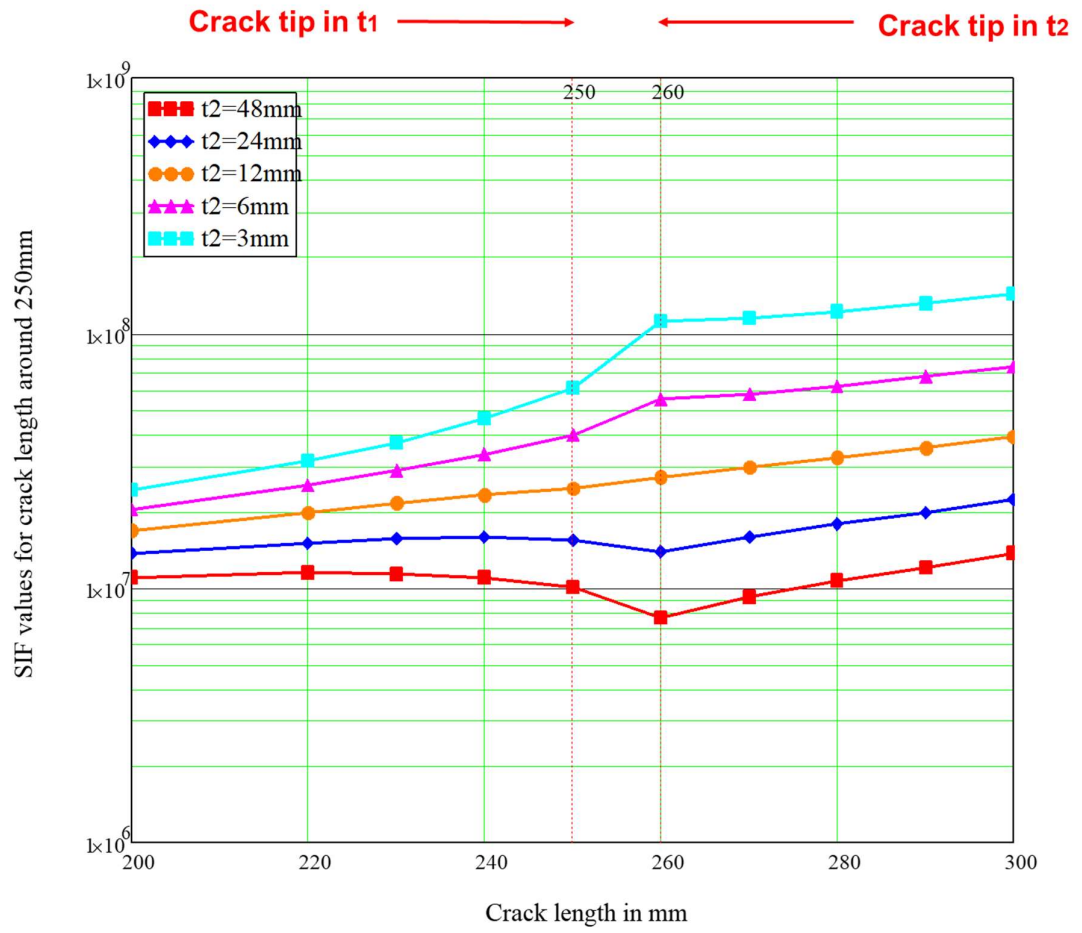


Figure 4-10 SIF values for crack lengths around  $W/2$  for different  $t_2$  thicknesses



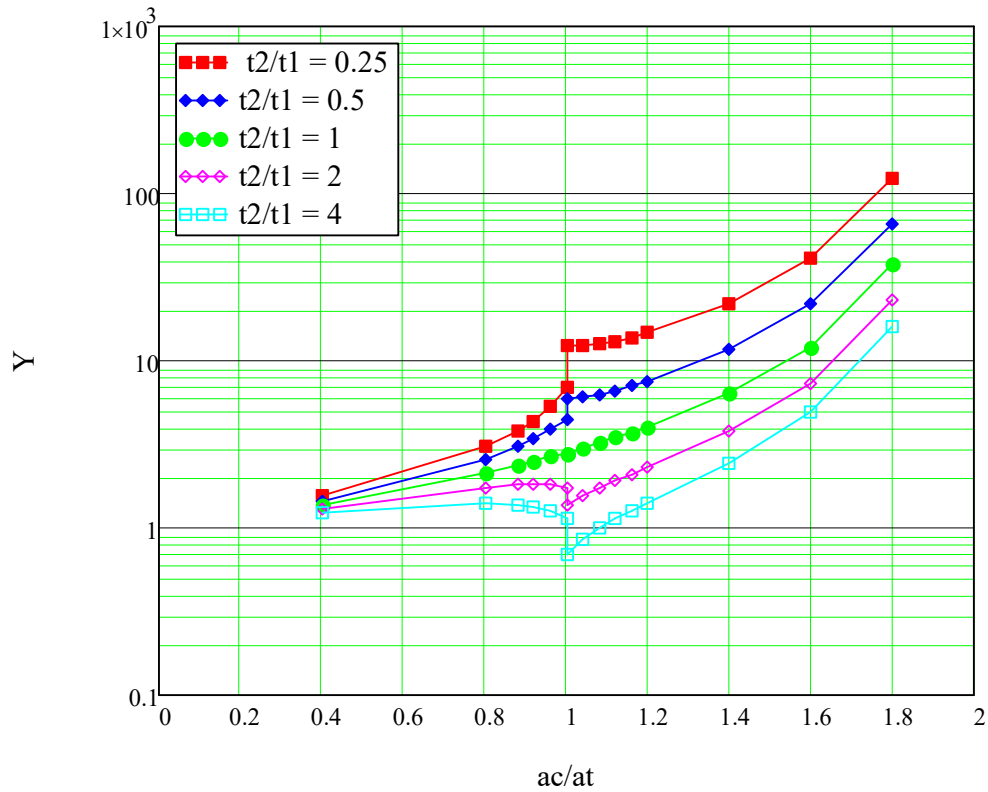


Figure 4-11  $Y$  values for crack lengths around  $at$

Note values for  $a/at$  in thickness  $t_2$  have been extrapolated from the values  $ac/at = 1.04$  and  $1.08$

From Figure 4-11, it can be concluded that the values of  $Y$  are in inverse proportion to the plate thickness  $t_2$ .

Plotting the  $Y$  values results just before the crack reaches the thickness change ( $at=250\text{mm}$ ) against the ratio of thickness, the  $Y$  values are quite

accurately estimated by  $\frac{Y}{Y_c} = \left(\frac{t_1}{t_2}\right)^{0.65}$ . Where  $Y_c$  is the constant thickness  $Y$

values ( $t_2/t_1=1$ ) for the same crack length, as shown in Figure 4-12.

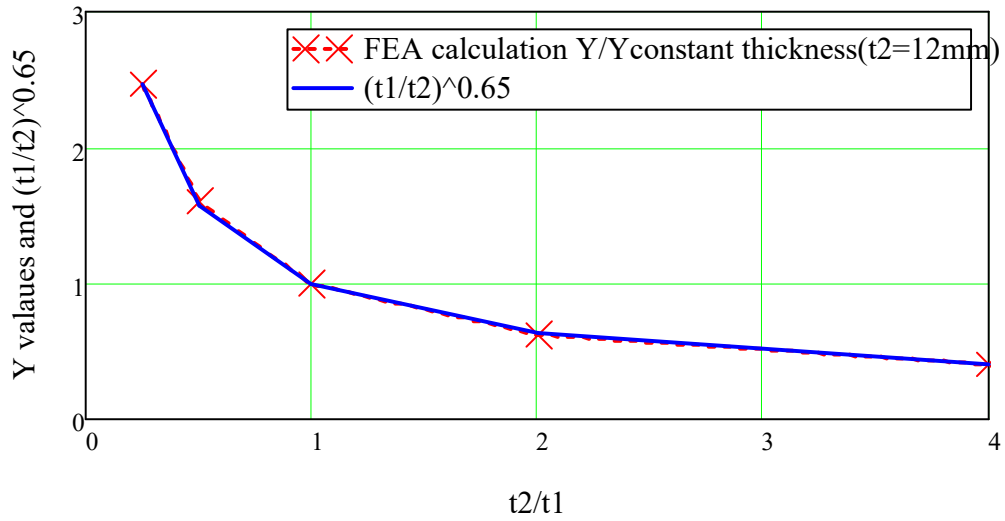


Figure 4-12 Ratio of  $Y$  value for changing in thickness to  $Y$  value for constant thickness just before crack reaches the thickness change

Just after the crack has entered the change of thickness, the  $Y$  values

change and a reasonable approximation is found to be  $\frac{Y}{Y_c} = \left(\frac{t_1}{t_2}\right)^{0.95}$ , see Figure

4-13.

It can be regarded as if the plate thickness doubles, the  $Y$  values, in comparison with a constant thickness plate roughly halves.

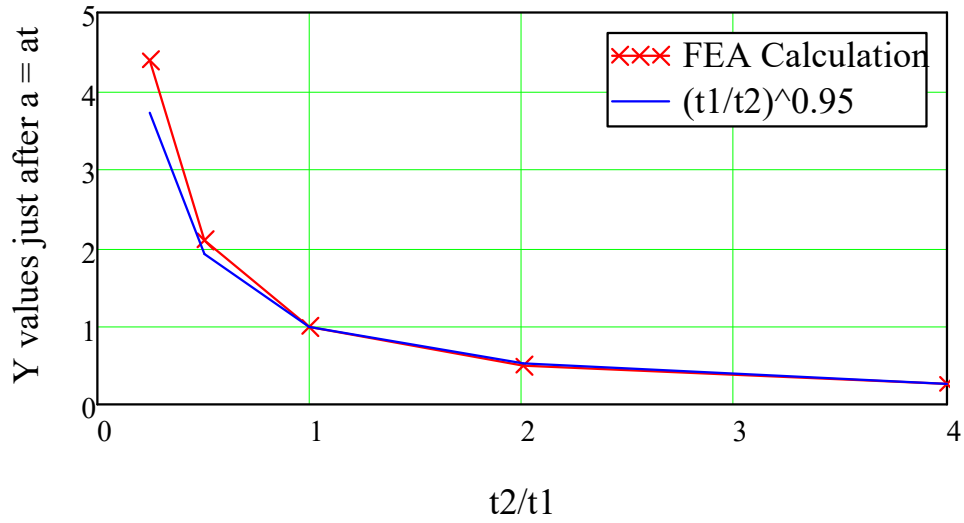


Figure 4-13 Ratio of  $Y$  values for the crack just after it enters the thickness change

With these extra analysis results, by trial and error, an approximate fit for  $Y$  values was found to be,

For  $ac < at$ :

$$\begin{aligned}
 Y(ac) &= Y_e(ac) \cdot Y_c(ac) \\
 &= \left\{ \left[ \left( \frac{t_1}{t_2} \right)^{0.67} - 1 \right] \cdot e^{3 \left[ \left( \frac{ac}{at} \right)^1 - 1 \right]} + 1 \right\} \cdot Y_c(ac) \quad (4.3)
 \end{aligned}$$

And for  $ac > at$ :

$$\begin{aligned}
 Y(ac) &= Y_e(ac) \cdot Y_c(ac) \\
 &= \left\{ \left[ \left( \frac{t_1}{t_2} \right)^{0.95} - 1 \right] \cdot e^{-0.35 \left[ \left( \frac{ac}{at} \right)^{0.4} - 1 \right]} + 1 \right\} \cdot Y_c(ac) \quad (4.4)
 \end{aligned}$$

Whilst this formula was better than the first empirical formula it still needed improving.

The thickness change is now accounted for by including the actual thickness  $t_1$  and  $t_2$ , in the calculation method described for the flat plate in Section 4.4. Considering the crack size near the thickness change ( $a_c=250\text{mm}$ ), as in Figure 4-8 and Figure 4-9, this gave the results of  $Y/Y_c$  shown in Figure 4-14 and Figure 4-15 with the  $Y$  scale being linear and logarithmic respectively.

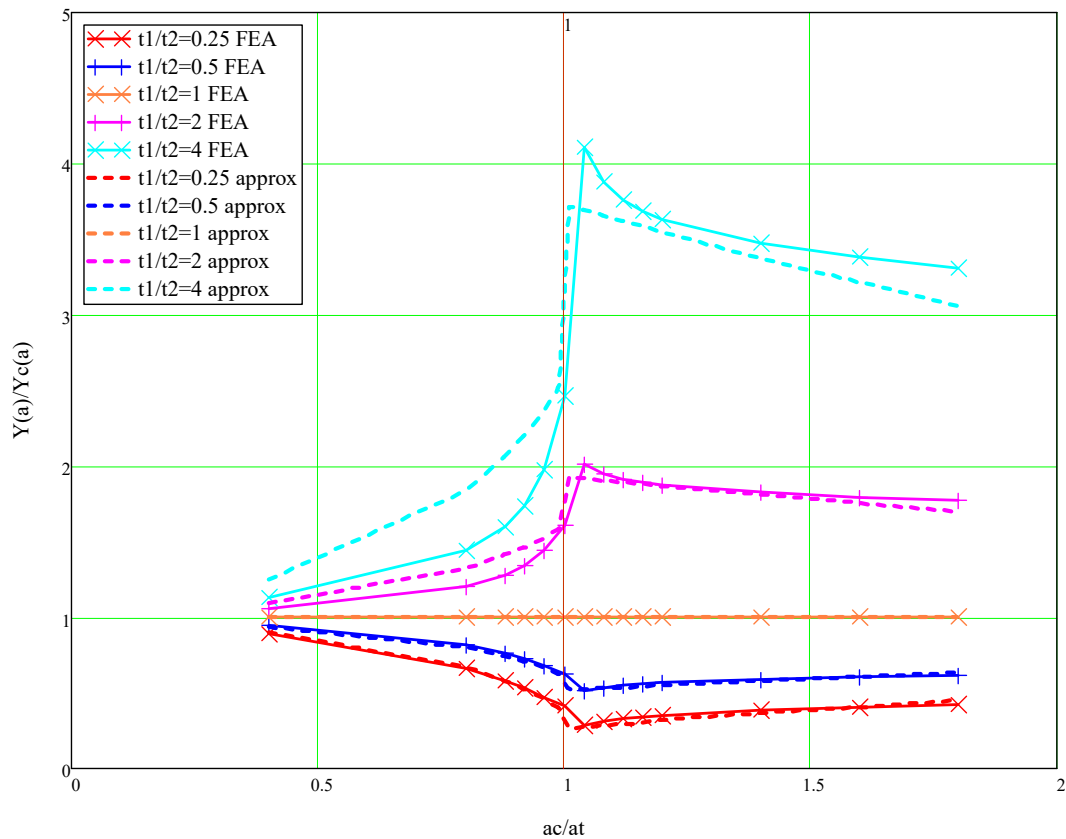


Figure 4-14 Comparison of approximate and FEA results for  $Y/Y_c$  for edge cracked plate with thickness change from  $t_1$  to  $t_2$

The results of  $Y$  for different  $t_2$  thickness are shown in Figure 4-15.

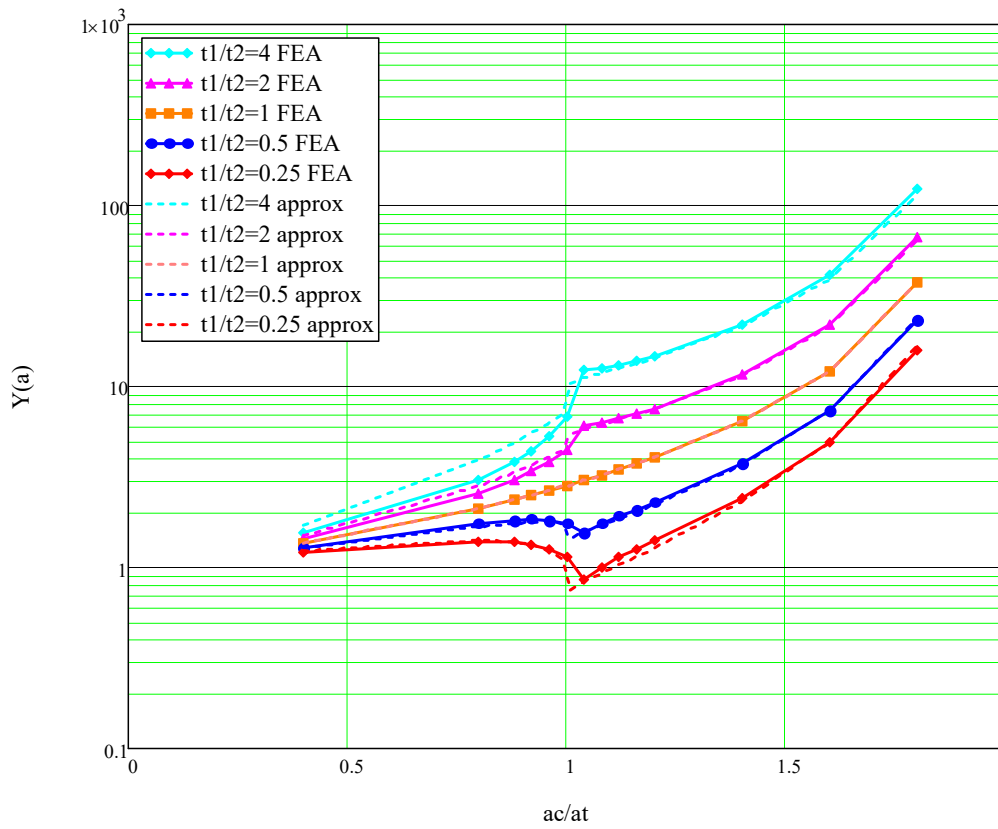


Figure 4-15 Comparison of approximate  $Y$  and FEA results for  $Y$  for edge plate with thickness change from  $t_1$  to  $t_2$

The results have the correct trends but the empirical equations still need to be improved. It appears that a better fit could be obtained if different formulae were derived for  $t_1/t_2 > 1$  and  $t_1/t_2 < 1$ , but that has not been done in this work.

Practical thickness change ratios at simple plate butt welds in ships are typically not as severe as those used for this analysis and the accuracy is better for the smaller ratios so the results should be useful. However at junctions of several plates the large thickness ratios would apply so, although multiple plate further complicates the calculation, it is worthwhile trying to further improve the prediction formulae for this simple thickness change case.

#### 4.4.1 Estimation of SIF values for crack growing through a change in thickness Third empirical method

The previous Method 2, for estimating the  $Y$  values as a crack crossed a plate with a thickness change, used the  $Y$  results for a constant thickness plate ( $Y_c$ ) and multiplied them by a factor ( $Y_e$ ) that corrected for the effect of the step in the thickness.

Method 3 returns to the relatively simple empirical derivation of the  $Y$  values for a constant thickness plate (using the ratio of linearized remaining ligament stress to linearized singular stress in a semi-infinite plate, as described in Chapter 3) and applies the method to the plate with the thickness change.

From the applied loading, the stress at the crack tip is again calculated, assuming linear stress distributions through the remaining ligament of the cracked section, but now acting on the actual cross section by using the actual area and first and second moments of area section properties allowing for the thickness change.

The singular stress is calculated using the same equation [Equation (3.5)] as in Chapter 3 (with  $Y = 1$ ) but it is now applied to the actual local thickness. Whilst this is difficult to justify, it is not unreasonable because when the crack is in  $t_1$  the transverse-to-crack deformations in the plate with thickness  $t_2$  should be the same as for a constant thickness plate having the same stress. When the crack tip is in  $t_2$  the stresses applied normal to the crack tip will be correct.

Although the transverse stresses applied in-line with the crack tip are the same in the two methods, Poisson's ratio effects will be different so that stresses parallel to the crack tip will not be the same as in the constant thickness or semi-infinite case.

It was not obvious that the method would work but it gave results that were quite close to the FEA results. Figure 4-16 shows the results multiplied by 1.04 to get the best average fit. There is still a need for further correction of the results particularly in the vicinity of the thickness change, where the method results in a change of slope, that is almost a step, but it does not result in an actual step that is expected and is evident in the FEA results.

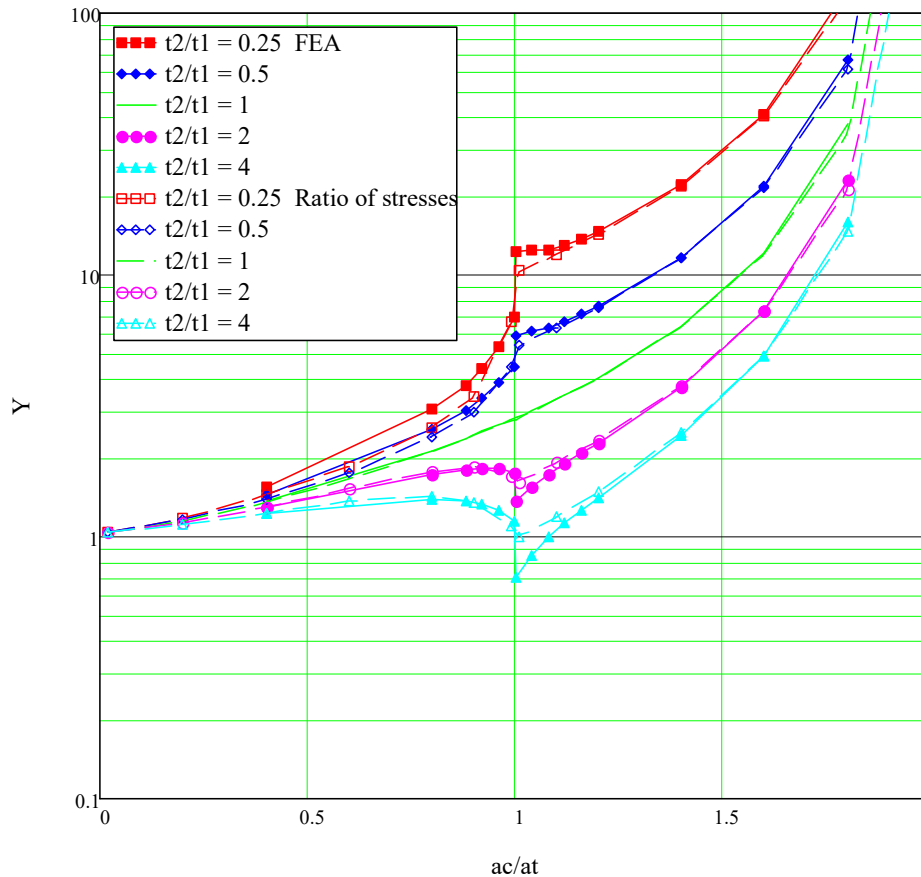


Figure 4-16  $Y$  from simple linearized stress ratio calculation based on actual thicknesses

By plotting the ratio of the FEA results / Linear structural analysis results the form of the required correction ratios was determined by eye and simple

correction equations were fitted. Separate fits were made for  $ac < at$ ,  $ac > at$ ,  $t_2 < t_1$  and  $t_2 > t_1$ .

For  $ac > at$  the correction is simply an exponential decay to 1.

For  $ac < at$  there the form of the correction also involves a linear term.

The corrections are shown in Figure 4-17 and Figure 4-18.

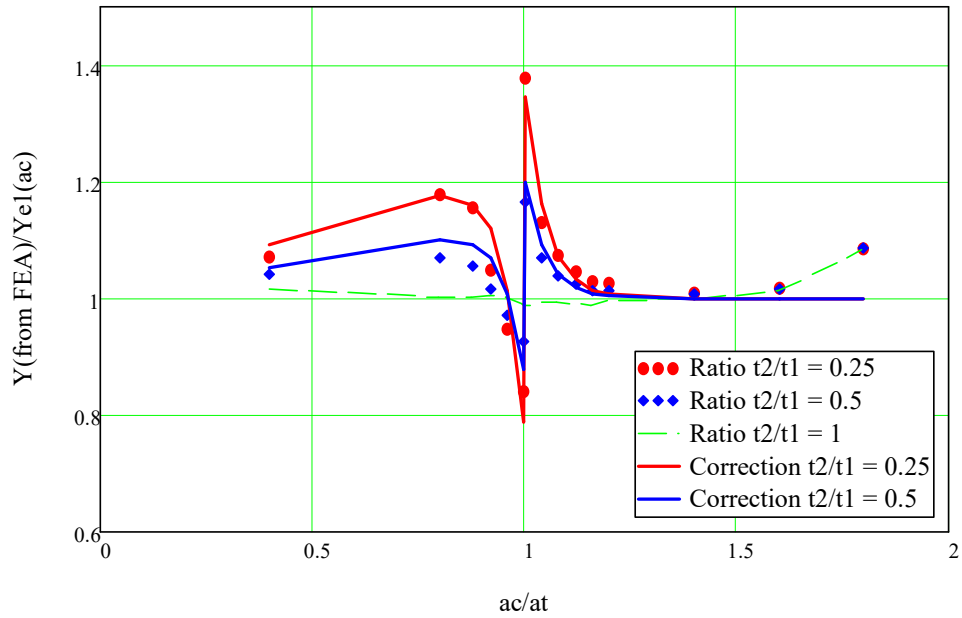


Figure 4-17 Ratios of FE to Linear stress variation calculation  $t_2/t_1 < 1$  and empirical correction  $[Ye1(ac)]$  [Equation (4.5)]



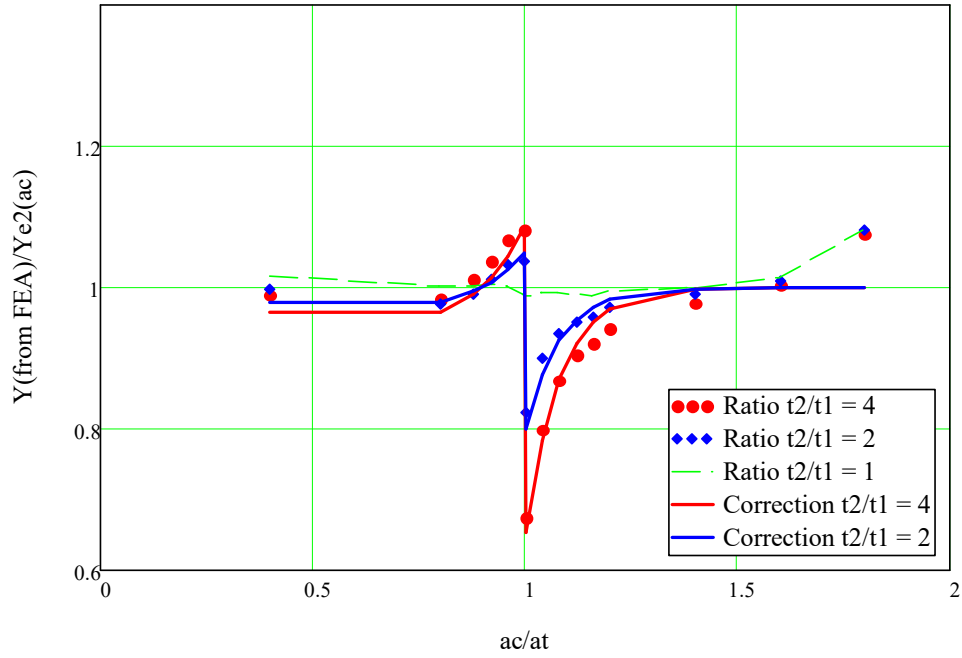


Figure 4-18 Ratios of FE to Linear stress variation calculation  $t_2/t_1 > 1$  and empirical correction  $[Ye_2(ac)]$  [Equation (4.6)]

The correction equations are:

For  $t_2/t_1 < 1$

$$Ye_1(ac) = \begin{cases} -0.45 \cdot e^{20 \left( \frac{ac-at}{at} \right)} + 1 + 0.225 \cdot \frac{ac}{at}, & \text{if } ac < at \\ 0.35 \cdot e^{-20 \left( \frac{ac-at}{at} \right)} + 1, & \text{if } ac \geq at \end{cases} \quad (4.5)$$

For  $t_2/t_1 > 1$

$$Ye_2(ac) = \begin{cases} -0.18 \cdot e^{7.5 \left( \frac{ac-at}{at} \right)} + 1 + 0.09 \cdot \frac{ac}{at}, & \text{if } ac < at \\ 0.35 \cdot e^{-12.5 \left( \frac{ac-at}{at} \right)} + 1, & \text{if } ac \geq at \end{cases} \quad (4.6)$$

With the exponential thickness change correction [Equation (4.5) and Equation (4.6)] applied the comparison of the corrected simplified method and the FEA is shown in Figure 4-19 with,

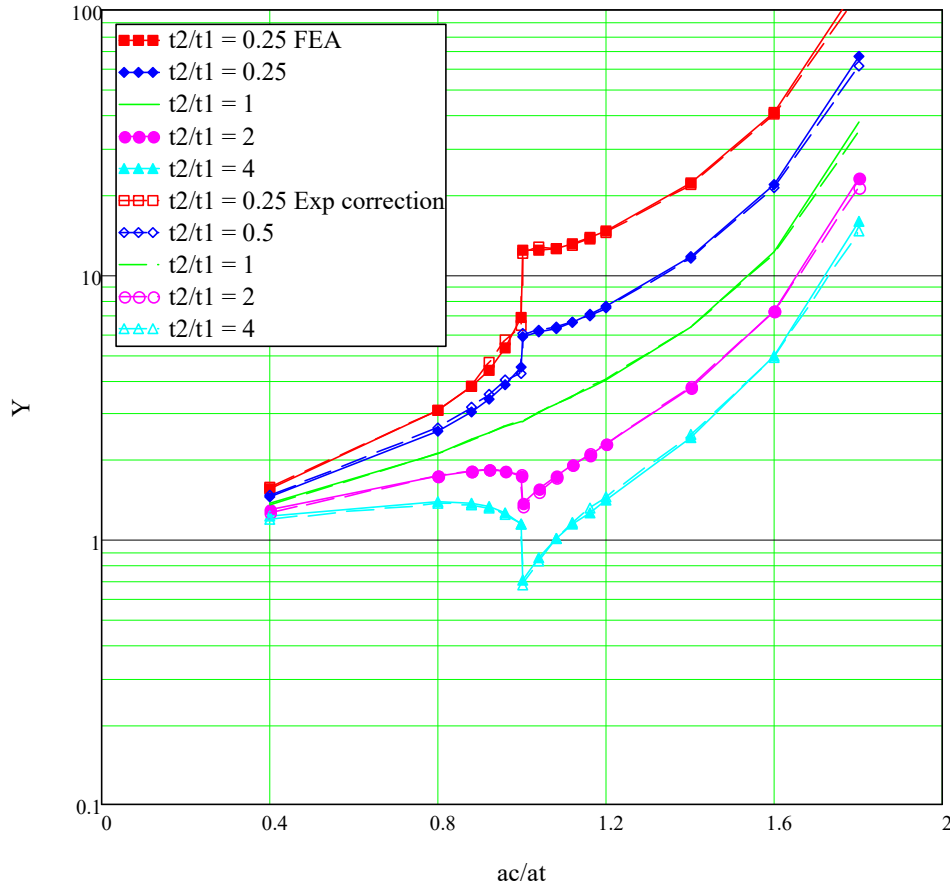


Figure 4-19 Estimation of  $Y$  values for thickness changes, using linearized stresses of the remaining ligament with actual thicknesses and empirical correction equations [Equation (4.5) and Equation (4.6)].

The error: FEA result / Simple method [Equation (4.5) and (4.6)] is shown in Figure 4-20. For  $0.2 < ac/at < 1.6$  the maximum error is less than 7%. As the crack approaches the far face of the model the error increases. This is not surprising as the difference between the finite plate and the semi-infinite case is

likely to be large here as a result of the highly stressed area at the crack tip in the semi-infinite case being outside the finite size of the case of interest and Poisson's ratio effects again being different. Note that these results are compared with FEA results whereas in the previous chapter the ligament stress method results were compared with Fetts results. Fetts results and the FEA diverged as the crack approached the far face. This method fitted Fett, (1998) in that region better than its fit to the FEA. That results in the larger error, as the crack approaches the far face, than in the constant thickness results presented in the previous chapter.

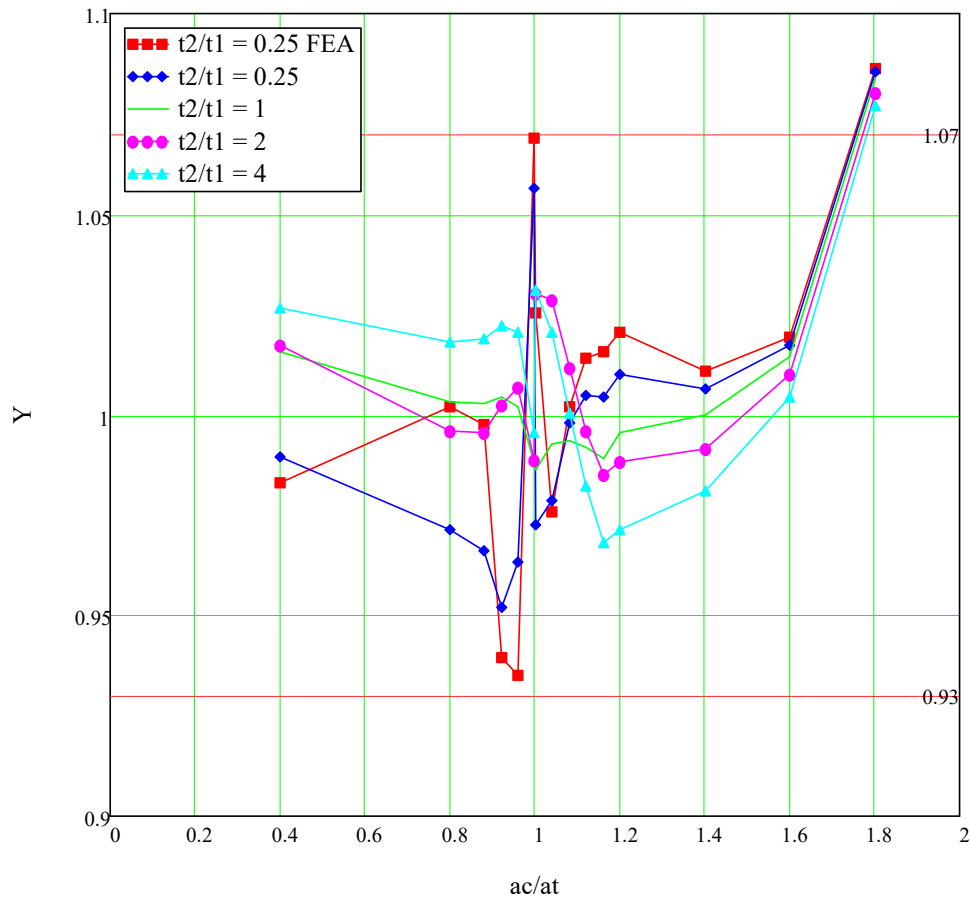


Figure 4-20 Ratio of FEA results / simple method (Applied ligament linearized stress/semi infinite linearized singular stress, with Equation (4.5) and (4.6) correction) results

## **4.5 Conclusion**

The second and third methods in this chapter estimation to estimate  $Y$  values based on the ratio of the linearized stress in the remaining ligament from the applied load to the linearized stress at the crack tip from the semi-infinite plate singular stress pattern results in a good first estimates of the variation of  $Y$  as a crack moves across a plate made up of two thicknesses of material.

The third simplified method of estimating the  $Y$  values, based on linearized applied and singular stresses on the remaining ligament and using the actual structural thicknesses provides the best simplified method results. It is also potentially more versatile for dealing with more complicated structural arrangements. It still requires an empirical correction at the thickness change.

The second method, based on linearized applied and singular stresses on the remaining ligament but using constant structural thicknesses and correcting for the thickness changes separately also provided good results. It has the advantage that the calculations required for the singular stress distribution could be done once and then referred to for later analyses. This might be useful when reliability analysis is being performed and the most efficient calculation is needed to save time.

The first method of trying to represent the change in plate thickness by an artificial crack length did not provide useful or accurate results.

Therefore, in this thesis the third method will be applied to the next stage of the work: the T section or plate stiffened panel.

## Chapter 5 Crack growing through “T-shape” connections

To provide insight into the behaviour of a “T” connection, an analysis is performed with a crack growing from the stiffener into the shell plate as shown in Figure 5-1. To allow comparisons with the constant plate thickness flat plate in Chapter 4, the shell plate thickness is, initially, taken as half the thickness, i.e.  $t_2h=t_2/2$ . The thickness of  $t_2h$  is reduced to half size to obtain results that might more easily be compared with the flat plate case. This is based on imagining the shell plate folded back on itself as shown in Figure 5-2. (The new thicknesses of  $t_2h$  plates would be 24mm, 12mm, 6mm, 3mm and 1.5mm respectively).

Model details are shown in Figure 5-3 to Figure 5-7.

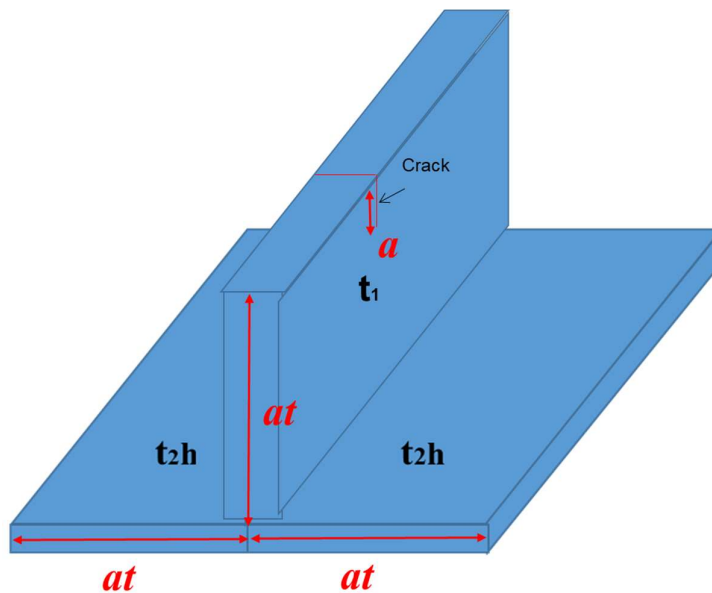


Figure 5-1 Real T-shape structure

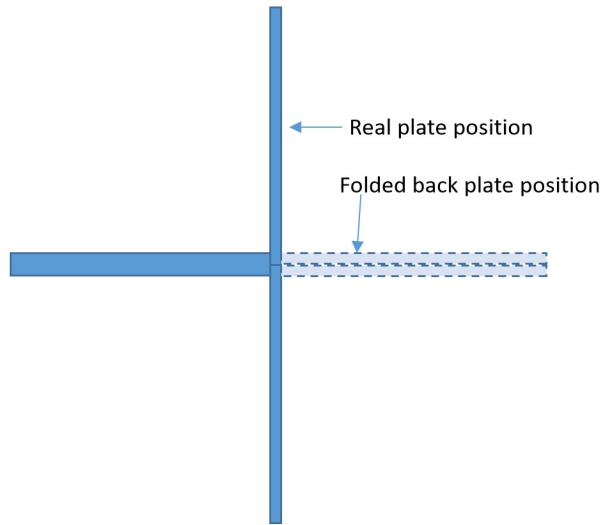


Figure 5-2 Real T structure and equivalent plate for I-shape structure

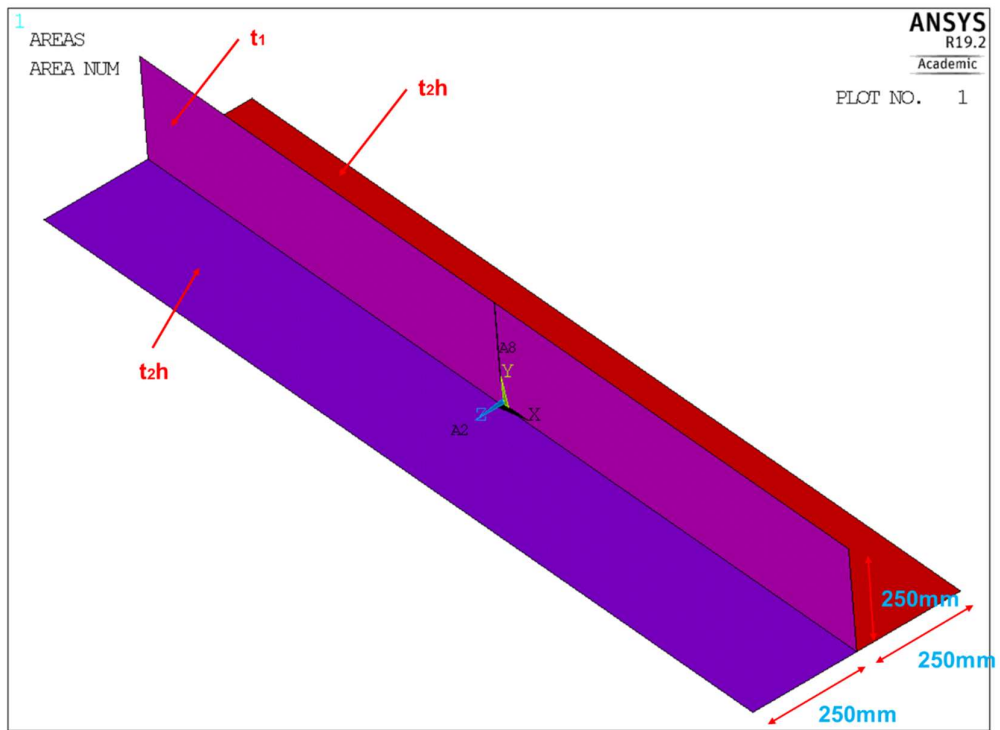


Figure 5-3 Crack growing through  $t_1$  plate

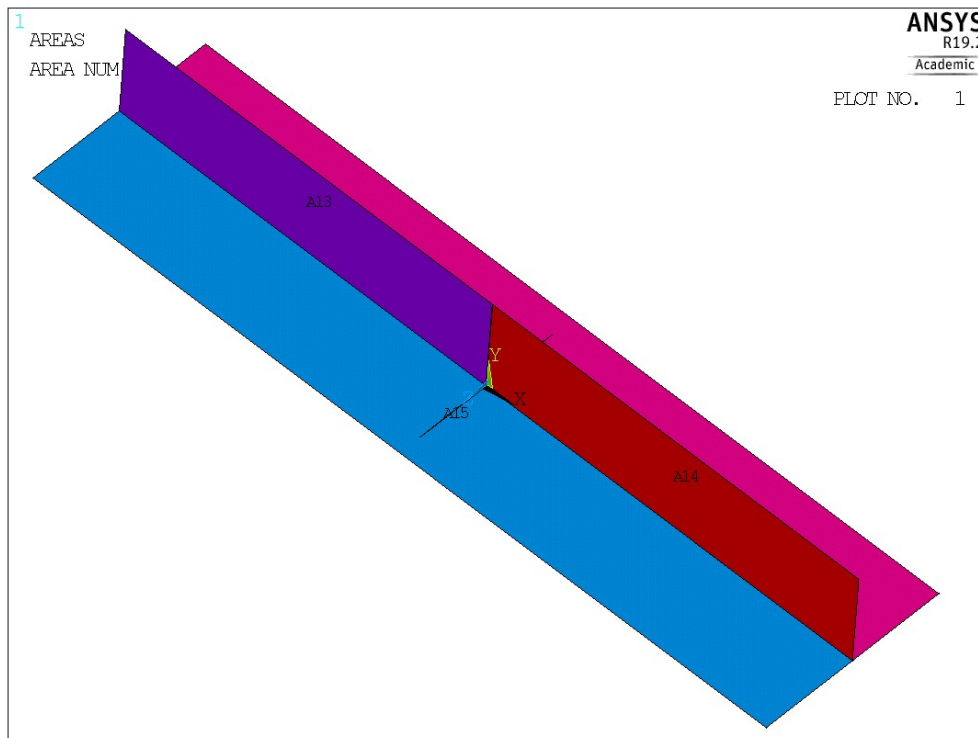


Figure 5-4 Crack propagating through  $t_2h$  plate

Figure 5-3 shows crack growing through  $t_1$  plate, for which the crack size  $a$  is smaller than  $at$ . Figure 5-4 presents crack growing through  $t_2h$  plate with crack length  $a$  is bigger than  $at$ , but smaller than  $2at$ , for which the  $t_1$  plate is completely cracked.

The model set-up and properties are similar to the flat plate described in Chapter 3. The boundary conditions applied on the T-connection is one end is fixed support and the other end is pure tension loading in positive direction of X-axis, see Figure 5-5. The membrane stress loading on the two ends of the structure is 10MPa.

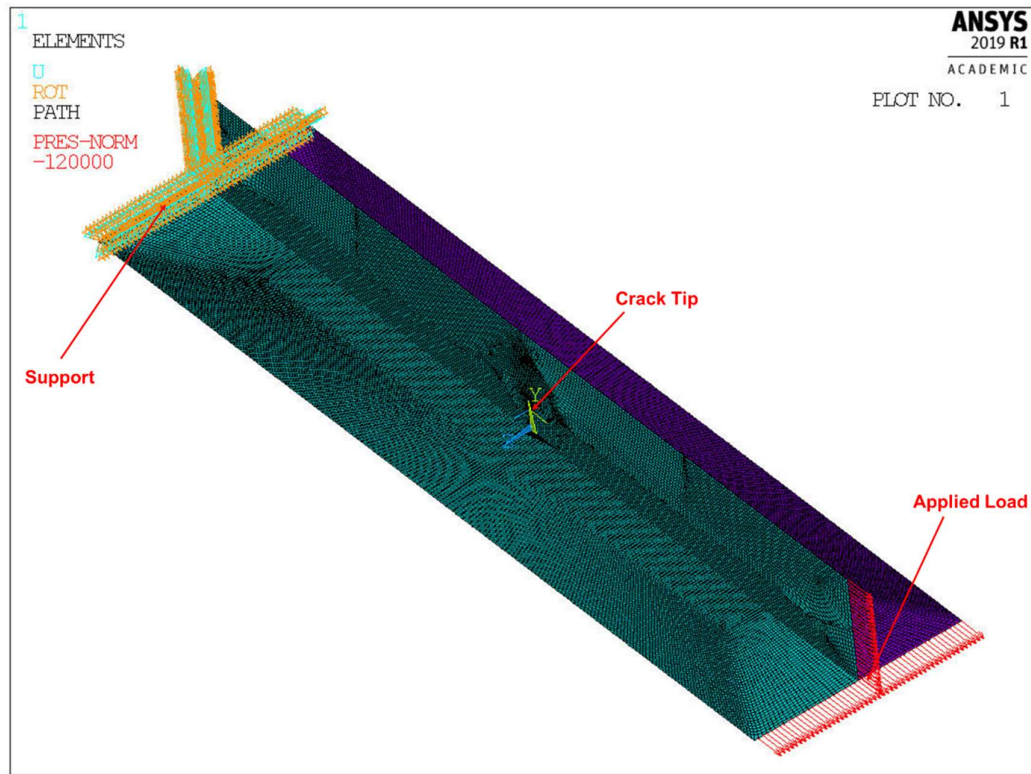


Figure 5-5 General applied loads and supports of T-connection model

The Mesh Details around crack tip is shown in Figure 5-6.



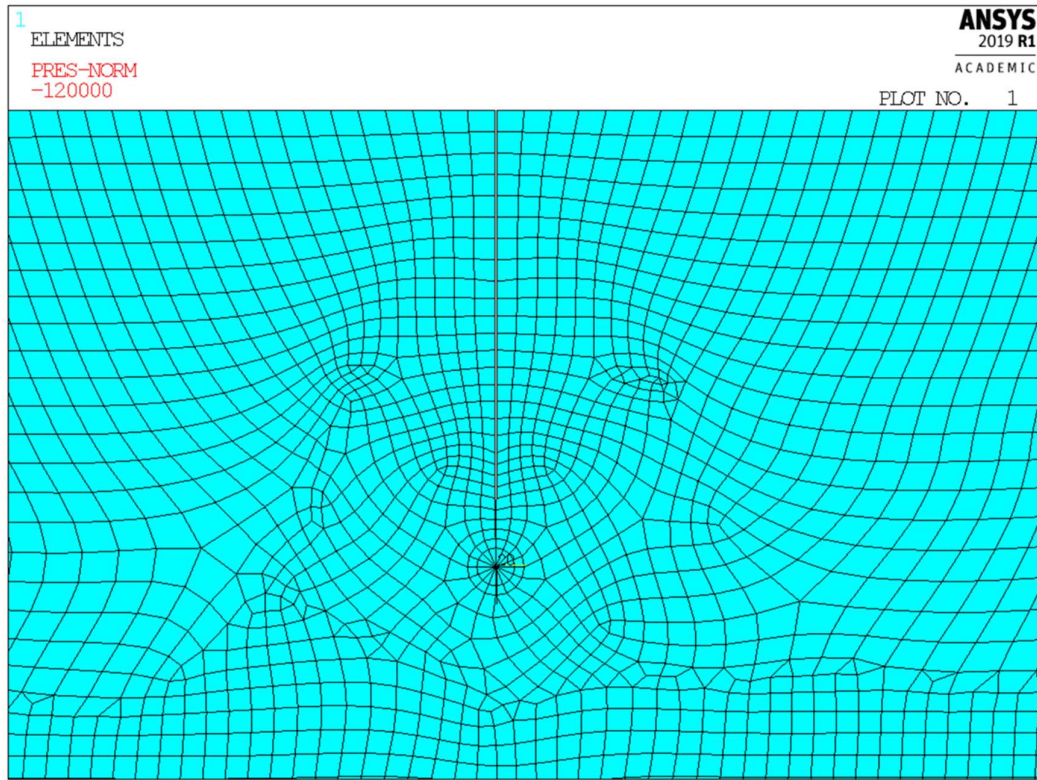


Figure 5-6 Mesh details around the crack tip

## 5.1 Empirical estimation of the $Y$ values for a flat stiffener attached to a panel

The SIF results for the crack growing in a flat plate with a thickness change from  $t_1$  to  $t_2$  are anticipated to provide some guidance for the membrane SIF of a simple stiffened panel with a crack growing from the stiffener outstand edge towards the plate. For comparison with the plate with a thickness change from  $t_1$  to  $t_2$  the stiffener of thickness  $t_1$  is attached to a panel of thickness  $t_2/2$ . This is based on the idea of the plate being folded back on itself as shown in Figure 5-2. It was anticipated that the lateral restraint provided to the crack would be similar, though not identical, for the T and the equivalent flat plate.

Under uniform stress on the T section load, a bending moment is generated in the remaining ligament in the plane of the crack, as for the flat plate. There is no bending moment in the stiffened panel away from the crack.

Note, when the crack breaks through from the stiffener into the plate, as a result of the eccentricity of the load applied to the stiffener relative to the plate, there will be considerable local plate bending. However the very important SIFs associated with that bending are not included in the finite element or theoretical analysis presented in this Chapter. (They are included in the solid element FEA SIF results and the simplified method in Chapter 8.)

The membrane  $Y$  value appears to be difficult to calculate approximately but, as for the flat plate, the surprisingly simple method, based on nominal stresses for the cracked, instead of the conventional, for fracture mechanics, uncracked section was found to give good results, although the method was not as accurate as for the flat plate.

In summary, the approximate method:

- 1) Uses the solution for the stress for a finite crack in an infinite plate (Seif and Kabir, 2016) (Paris and Sih, 1965). This is applied to the remaining ligament and the resulting axial force and moment on the remaining ligament are calculated. From this the sum of the axial stress and engineers' bending stress at the crack tip on the remaining ligament that is consistent with the infinite plate solution and a  $Y$  value of 1.12 for an edge crack on the semi-infinite plate. Note the plate is considered as unfolded for the singular stress distribution but folded for the calculation of the moments and bending stresses, see Figure 5-2.

- 2) Calculate the axial + bending stress in the ligament from the actual applied loads.

3) Estimate the Y value as the result from step 1) divided by the result from step 2).

This then allows the modelling of a stiffened plate with a crack growing down the stiffener and calculates the stress from plate-stiffener intersection, see Figure 5-7. As the panel is folded back at the “*a*” (plate junction) position, it is necessary to investigate the situation of crack length slightly smaller and bigger than “*a*” length. The crack length near the “*a*” position is set up as 490mm and 510mm, see Table 5-1. The total thickness of stiffener plus panel is  $W=1000\text{mm}$ . Therefore the ligament length  $b=W-a$ . The width “*W*”, is the width of stiffener plus half of shell plate:  $W = ds+B/2$ .

Crack Length <i>a</i> (in <i>mm</i> unit)											
10	100	200	300	400	490	510	600	700	800	900	990

Table 5-1 Crack lengths in stiffener model

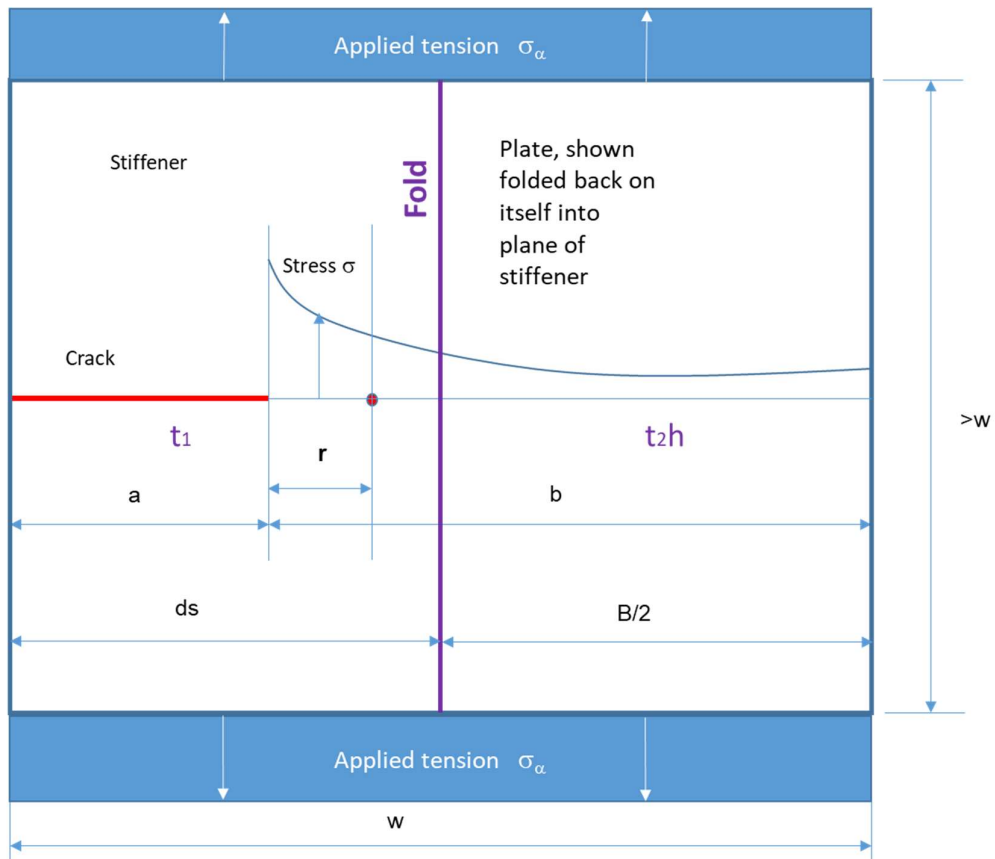


Figure 5-7 Edge crack subject to tension in T-shape model (Applied tension  $\sigma_a = 1Pa$ )

The singular stresses from infinite plate theory. Stress in ligament for a crack in an infinite width plate, the works from Paris and Sih (Paris and Sih, 1965) or Seif and Kabir (Seif and Kabir, 2016) allows for edge crack. After correction to ensure equilibrium, this is assumed to apply to membrane stresses in the folded plate as well.

## 5.2 Results for a T section with $t_2 = t_1 / 2$

On the basis of the above discussion the case for  $t_2 = t_1 / 2$  is shown below. Figure 5-8 shows, on the left the distribution of stress, according to engineers’ bending theory, resulting from the actual applied load; on the right is shown the stress distribution resulting from a crack in a semi-infinite plate. The stresses are only acting on the remaining ligament of the cracked section (i.e., the blue and not the red part). The linear stress distribution has the equivalent force and moment about the centre of remaining ligament (in blue part) with Paris and Sih ligament stress.

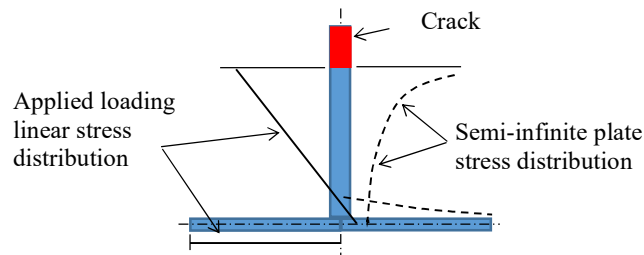


Figure 5-8 Stresses from applied external loads acting on remaining ligament  $\sigma_a$  (left side) and semi-infinite plate singularity  $\sigma_i$  (right side)

These stresses are shown in more detail, for the crack extending 20% of the stiffener depth, for the singular stress distribution, in Figure 5-9 to Figure 5-11 and for the applied unit stress loading in Figure 5-12 to Figure 5-13. In these figures the plate – stiffener intersection is at 1 on the horizontal axis. 0 to 1 corresponds to the stiffener and 1 to 2 to the plate (where the stresses in the flange are symmetric so stresses only in one flange are shown).

The cracked semi-infinite plate singular stress distribution, truncated at the edge of the shell plate is shown in Figure 5-9.

Figure 5-10 shows the mean stress for the singular stress distribution (i.e. the constant stress that results in the same force as the singular stress distribution). The mean singular stress is unity on a semi-infinite plate but because only the part of the distribution from the crack tip to the far end of the shell plate is considered the mean of the singular stress distribution for the stiffened plate is greater than 1.

Figure 5-11 shows the linear bending stress that has the same moment as the singular stress distribution after the mean stress has been subtracted.

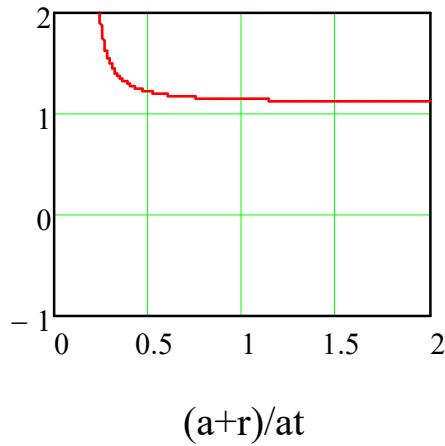


Figure 5-9 Stress from singularity before linearization ( $\sigma_y$ ) (Stress: Pa) plotted against (non-dimensional) distance through the remaining ligament

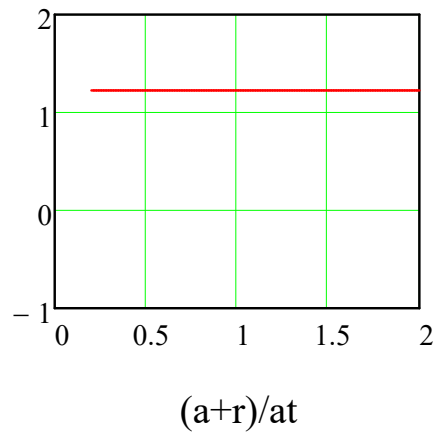


Figure 5-10 Mean stress from singular stress on cracked section ( $\sigma_{si\mu}$ )  
(Stress: Pa)

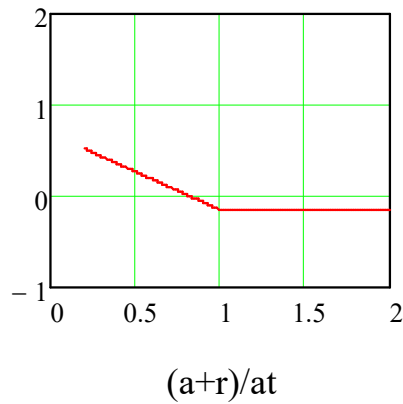


Figure 5-11 Bending stress from singular stress on cracked section ( $\sigma_{bmsi}$ )  
(Stress: Pa)

Figure 5-12 shows the mean stress on the cracked section ligament for an applied unit stress on the end of the stiffened plate. This is higher than the unit applied stress at the end of the stiffened plate as a result of the crack that reduces the sectional area.

Figure 5-13 shows the bending stress on the cracked section caused by the applied unit stress on the uncracked end of the stiffened plate. The moment is caused by the eccentricity of the load relative to the centroid of the cracked section. The bending stress is calculated from engineers' bending theory.

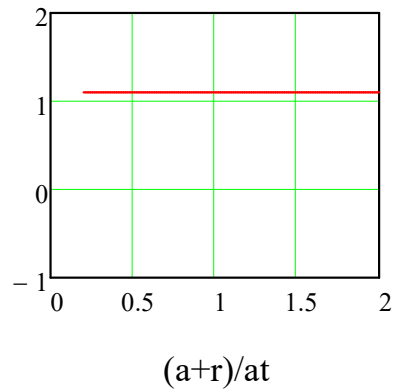


Figure 5-12 Mean stress from applied load on cracked section ( $\sigma_u$ ) (Stress: Pa)

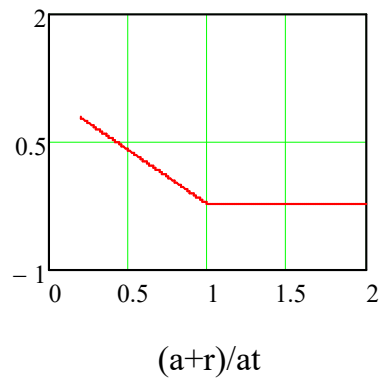


Figure 5-13 Bending stress from applied load on cracked section ( $\sigma_{bma}$ ) (Stress: Pa)



Y calculation method is to consider the stress correction ratio multiplied by 1.12. The stress ratio in the ligament is,

$$\begin{aligned} \text{Ratioh} &= \frac{(\text{mean ligament stress} + \text{linear bending ligament stress}) \text{ from applied nominal stress on T section}}{(\text{mean ligament stress} + \text{linear bending ligament stress}) \text{ equivalent to the singular ligament stress}} \\ &= \frac{\sigma_{\mu a} + \sigma_{bma}}{\sigma_{si\mu} + \sigma_{bmsi}} \text{ calculated at the crack tip} \end{aligned}$$

Calculate the Y values using ratio of underlying mean stress plus the bending stress at crack tip.

$$Y_{nh} = 1.12 \cdot \text{Ratioh} \quad (5.1)$$

Comparison of approximate formula, Equation (5.1) with FEA results is shown in Figure 5-14.

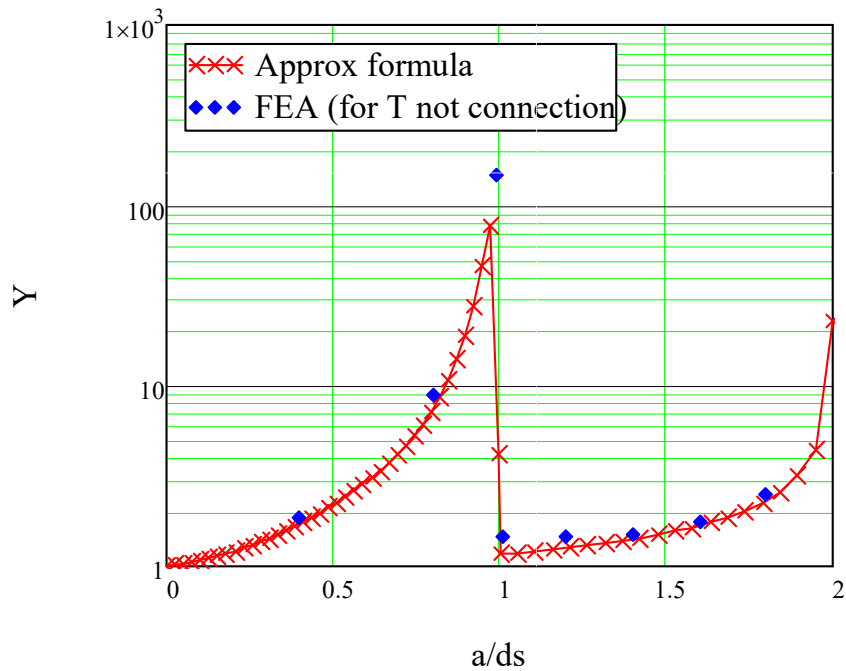


Figure 5-14 Approximate analysis of the T section [using Equation (5.1)] compared with FEA results ( $t_2/t_1=0.5$ )

Comparison of the FEA and formula results shows a reasonable agreement for the two points for  $a/ds < 1$ . The method underestimates the  $Y$  values for  $a/ds > 1$ .

In the calculations for Figure 5-14 it was assumed that the remaining web and full width of the shell plate act as a T section beam to resist the moment caused by the eccentric forces on the cracked section.

The resistance is divided between

- 1) The web acting with the membrane effect of the shell plate as a flange
- 2) The bending stiffness of the shell plate based on  $p \cdot \frac{B \cdot t^3}{12}$  (where  $p$  is the proportion of the width of the plate that is effective)

The moment resisted by the web and flange membrane stresses and the moment resisted by the shell plate bending are in proportion to their cross sectional stiffnesses based on their second moments of area. However because the crack is localized and, according to the simple theory, there are step changes in these stiffnesses, the actual stiffnesses that determine the load sharing will differ from the simple assumption. This is primarily important as the crack is about to break through from the web to the flange, i.e. as  $a/ds$  approaches 1.

Investigation of  $a/ds$  approaching 1 shows that the SIF is very dependent on the assumptions about the relative effective bending stiffness of the shell plate and the cracked stiffener web with the shell plate acting as a flange. If the effective width is 20% of the overall plate width, then the results change to those shown in Figure 5-15. Figure 5-16 shows results for the effective bending width being 60% of the full plate width. (If the shell plate was infinitely thin then the  $Y$  value would correspond to the case of a crack growing through a finite width plate and would become infinite.)

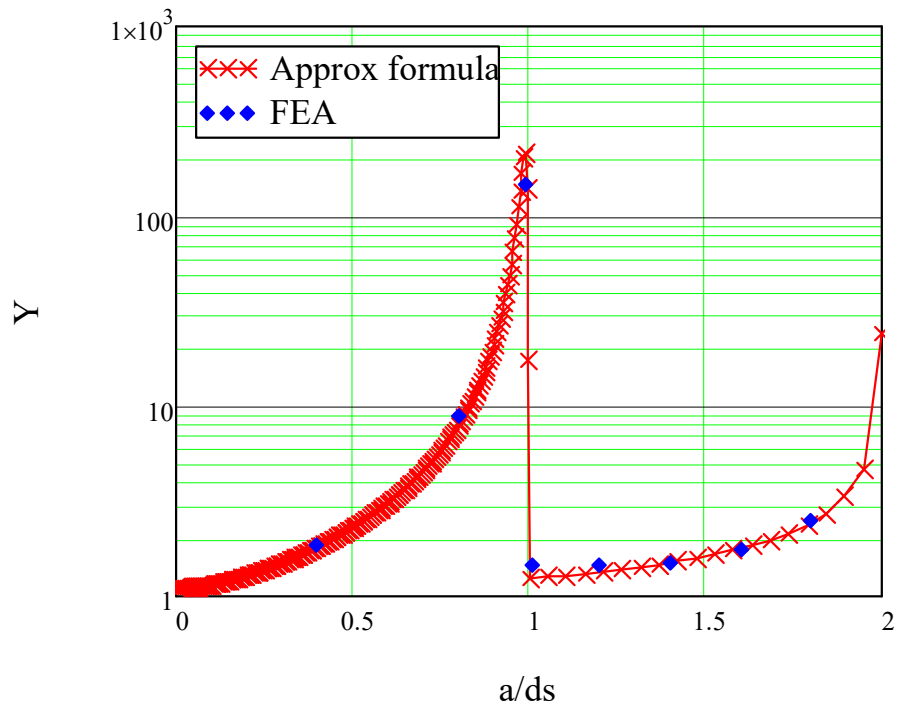


Figure 5-15 Approximate analysis of the T section compared with FEA results ( $t_2/t_1=0.5$ ), effective width of shell plate in bending =  $0.2 \cdot B$

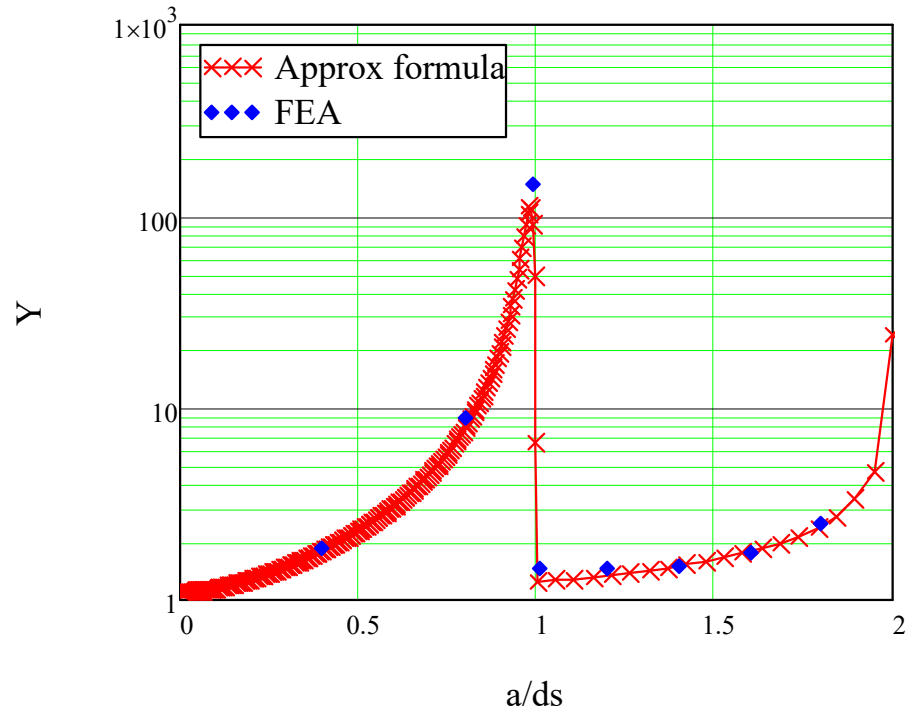


Figure 5-16 Approximate analysis of the T section compared with FEA results ( $t_2/t_1=0.5$ ), effective width of shell plate in bending =  $0.6 \cdot B$

As the stresses are changing rapidly around  $a/ds = 1$  it is helpful to plot more approximate formula points. The results near  $a/ds = 1$  are shown in more detail in Figure 5-17. The calculated peak  $Y$  value occurs at about  $a/ds = 0.98$ . The  $Y$  value then reduces because the applied loads are taken by shell plate bending which results only in a small membrane SIF.

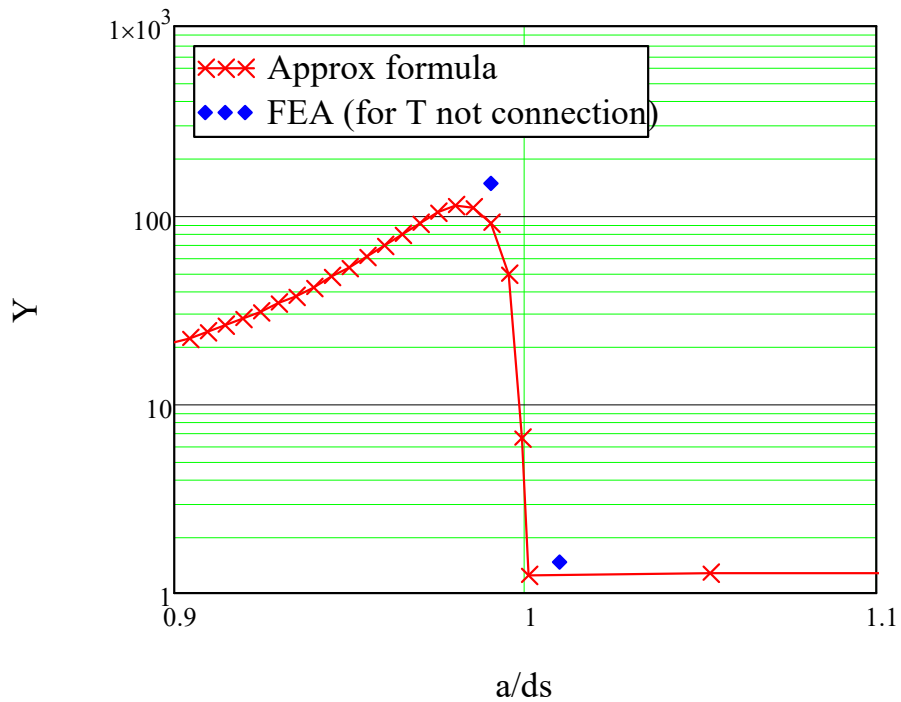


Figure 5-17 Approximate analysis of the T section compared with FEA results region around  $a/ds = 1$  ( $t_2/t_1=0.5$ ), effective width of shell plate in bending =  $0.6 \cdot B$

### 5.3 Crack Growing in a T connection with different ratios of, stiffener to shell plate thickness

The model topology used in the previous section was rerun with different values of  $t_2h/t_1$ , as shown in Table 5-2. The shell plate thicknesses are half the values used for the flat plate ( $t_2h$ ) to allow comparison with the flat plate results, as discussed at the beginning of this chapter.

$t_1h$ [mm]	$t_2h$ [mm]	$2t_2h/t_1h$	$t_2h/t_1h$
12	48/2	4	2
	24/2	2	1
	12/2	1	0.5
	6/2	0.5	0.25
	3/2	0.25	0.125

Table 5-2 Thickness data

Each thickness ratio was analysed for cracks growing through the stiffener web and plate, as for the  $t_2/t_1 = 0.5$  case analysed above. The exponential correction terms derived for the flat plate were applied but with  $2 \cdot t_p$  (i.e.  $2 \cdot t_2$ ) used in place of  $t_p$ , to recognize the effect of the shell plate extending on each side of the stiffener web.

Figure 5-18 shows the membrane or centre plane  $Y$  values for the five thickness ratios with 0.6 of the plate widths used in the calculation of the shell plate bending stiffness. The approximate analysis results are shown as solid lines and the FEA results as points.

Note:

1. The  $Y$  values increase dramatically as cracks approach the connection of the stiffener to the web. As the shell plate thickness tends to zero the  $Y$  value would become infinite, as for a crack about to break through the far side of a finite plate.

2. Once the crack has broken into the shell plate the membrane  $Y$  value becomes very small, however in reality the forces are now resisted by

plate bending and the bending SIF and  $Y$  values would be large. Bending is not considered in this chapter but is studied in Section 8.2.

3. The  $Y$  values for as  $a/ds$  approaches 1 are under-estimated, for  $t_2 < t_1$  and overestimated for  $t_2 > t_1$ .

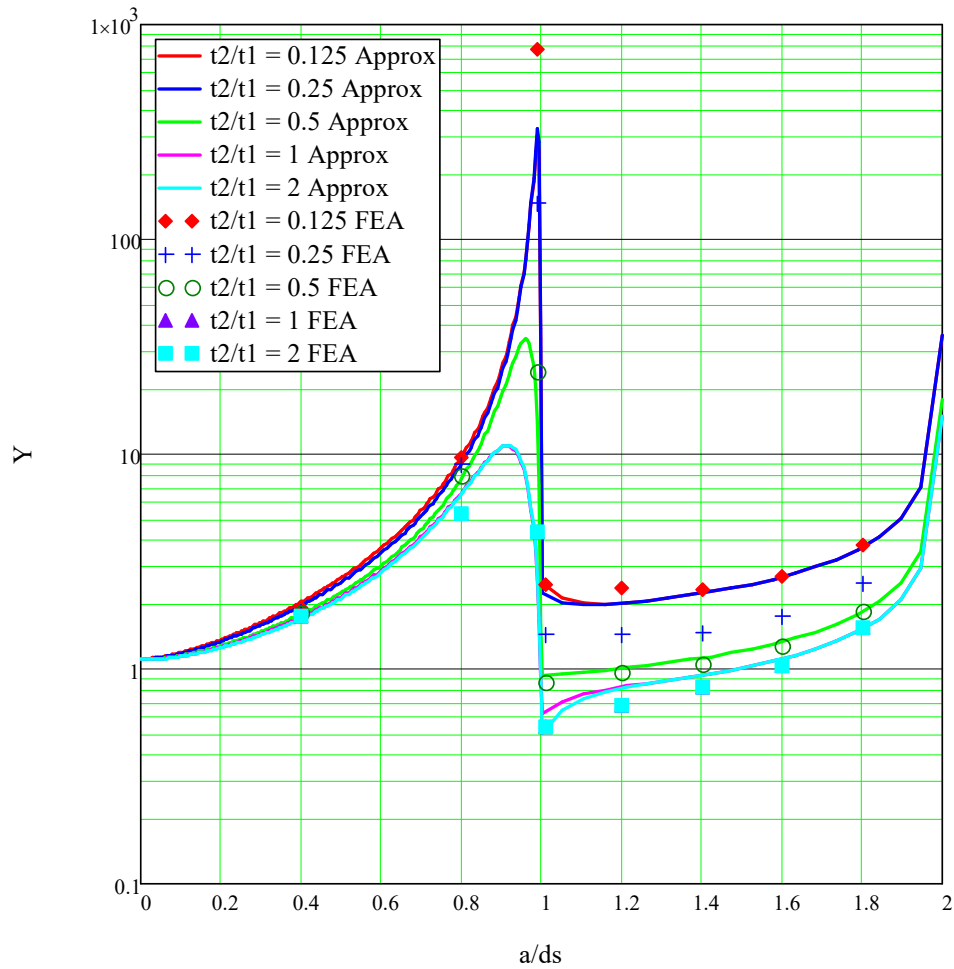


Figure 5-18  $Y$  values for different shell plate / stiffener thickness

The effect of web to shell plate thickness ratio is most likely caused by the bending moment taken by the web and shell plate as a beam and the bending moment taken by the shell plate in bending not being subject to a step change

from the uncracked section but being dependent on the material either side of the crack plane as well as on the crack plane itself, as indicated in Figure 5-19 (i.e. engineers’ bending theory, which assumes a prismatic section, is insufficient here).

Indeed a simple (but incorrect) analysis could argue that the system comprises an uncracked section, an infinitesimally short cracked section and another uncracked section. If analysed in this way the stiffness of the cracked section would not affect the overall stiffness of the cracked stiffened plate.

The above analysis is wrong because the crack affects the stiffness over a finite length, not just over its own length. The shell plate will be less stiff than the engineers’ bending theory predicts because, for a crack nearly reaching the shell plate, the very localized plate bending at the web will spread to a larger length of plate further away from the web. The stiffener web stiffness will also not suddenly change from the full uncracked section to the cracked section stiffness, because the stress flow will be modified either side of the crack, and will appear less stiff as a result.

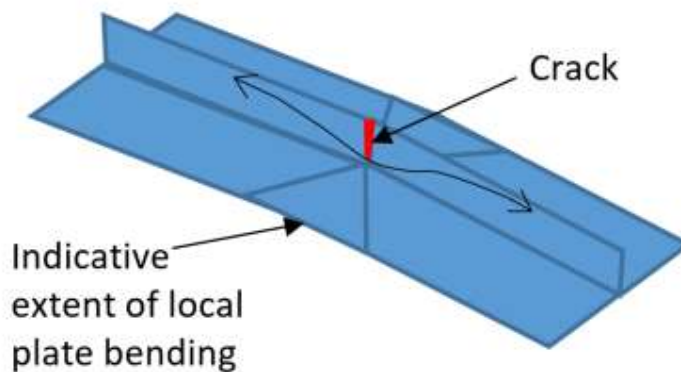


Figure 5-19 Local behaviour of shell plate in bending and web stresses concentrating in the remaining ligament



Simply analysing the above effects is difficult but it is reasonable that a relative stiffness correction, based on the relative thickness should be applied. This correction was applied as a shell plate bending effective width factor (although as discussed above it would seem that more accurately it is a relative stiffness effect). The correction that was found to work reasonably well was:

$$\text{Effective Width} = 0.8 \cdot \left( \frac{t_2}{t_1} \right)^{1.2} \cdot B \quad (5.2)$$

where  $B$  is the shell plate width. The results are shown in Figure 5-20.

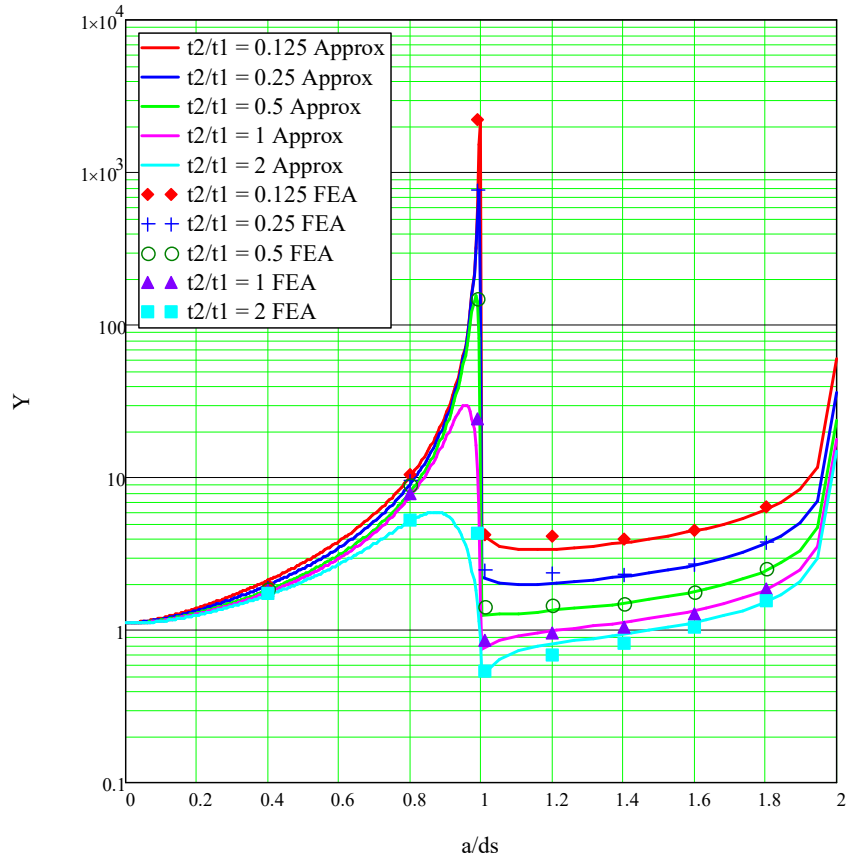


Figure 5-20  $Y$  values with additional shell-plate/web relative thickness correction ( $Y$  in log-scale)

Comparison of the simple approximate method, with the thickness ratio correction, and the FEA results shows that the simple method appears to capture the important behaviour. The error between the results is show in Figure 5-21,

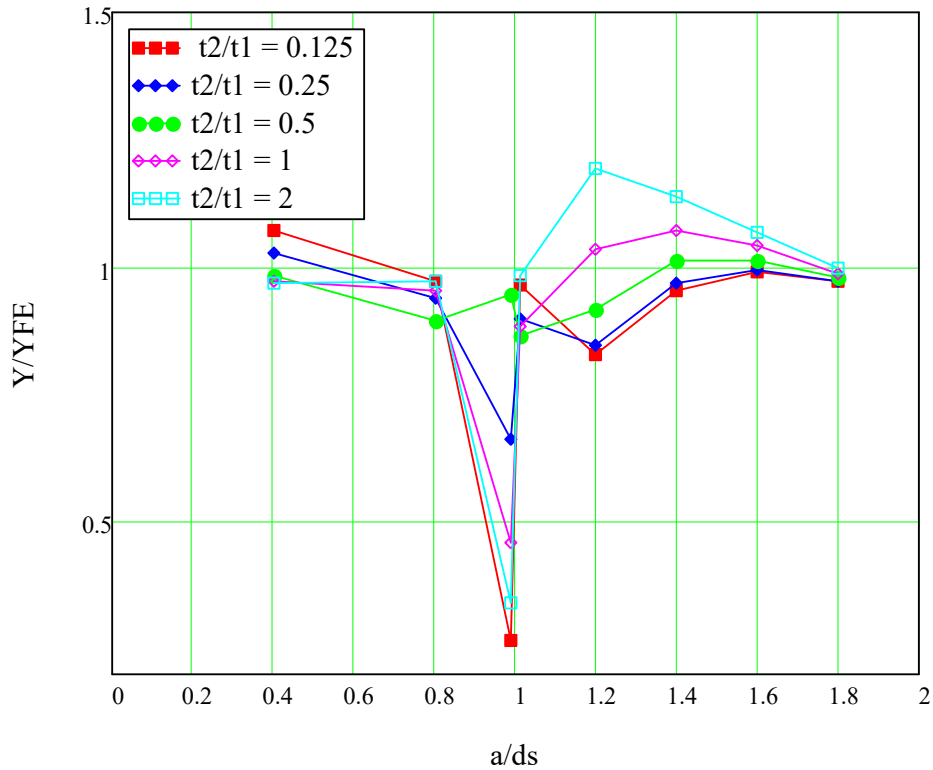


Figure 5-21 Ratio of  $Y$  values Approx/FEA result

The comparison appears to be poor as  $a/ds$  approaches 1 and poorer than suggested by Figure 5-20. This is because the FEA and approximate methods do not predict the maximum  $Y$  values at exactly the same  $a/ds$  and  $Y$  is changing very rapidly in that region. For  $t_2 < t_1/2$  Figure 5-20 shows that the error between the maxima as  $a/ds$  approaches 1 is actually less than 20%. For  $t_2 \geq t_1/2$  there are

not enough FEA analysis results to compare the maxima (however the next section provides more detailed analyses for a stiffener with  $t_2 = t_1$ ).

Away from the stiffener plate connection, the approximate method, based on:

- 1) The simply calculated linear ligament stress at the crack tip
- 2) An adjustment for thickness change
- 3) An adjustment for shell plate local bending to remaining T section relative stiffness gives results that are within 20% of the FEA value. This is too large a difference for using the approximate results in place of more detailed FEA but would be sufficiently accurate to provide a useful check on the results of a more complicated analysis, for roughly estimating likely behaviour and, with some calibration, the method could be used for reliability analysis. So the T section results appear to meet the objectives of the work, as set out in the introduction and in the next section the method is applied to a connection detail that is typically found ship hull structure.

## **Chapter 6 Study of longitudinal stiffener connection to transverse structure with shell elements and membrane-only fracture mechanics elements**

### **6.1 Single stiffener model**

This structural analysis is of a connective detail with these dimensions shown in Figure 6-2. A crack is grown from the initial position at the intersection of the plate and frame stiffeners, in two directions: through the stiffener flange and through the stiffener web to the shell plate.

The Y values for the crack tip in the flange are a little smaller than for the crack tip in the web see, Figure 6-6 and Figure 6-7; as a simplifying approximation it was assumed that the crack extended symmetrically from the initial position so that the length in the flange equalled the length in the web until the flange cracked through.

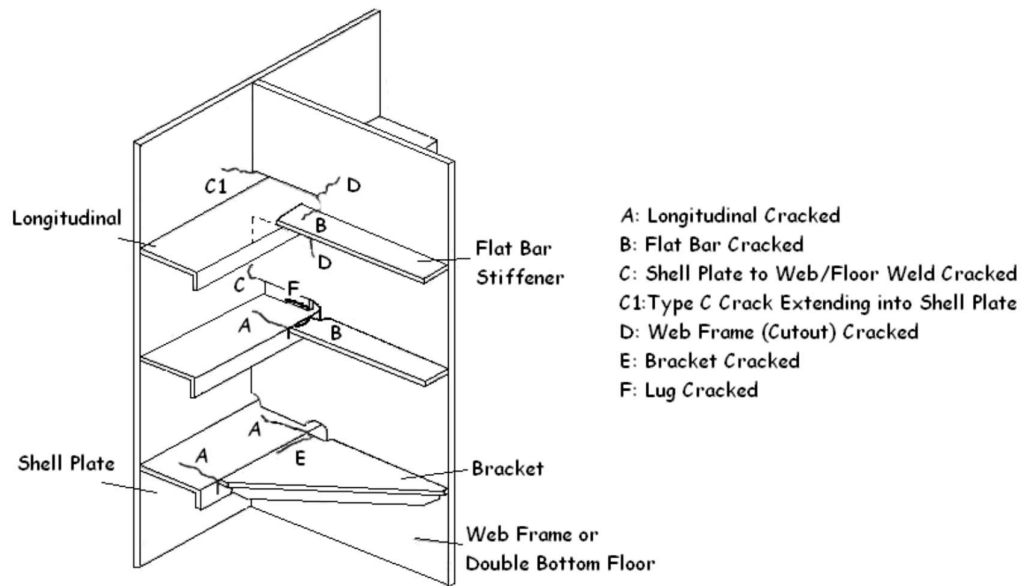


Figure 6-1 Illustration of stiffener structure on ship connection (Lou, 2013)

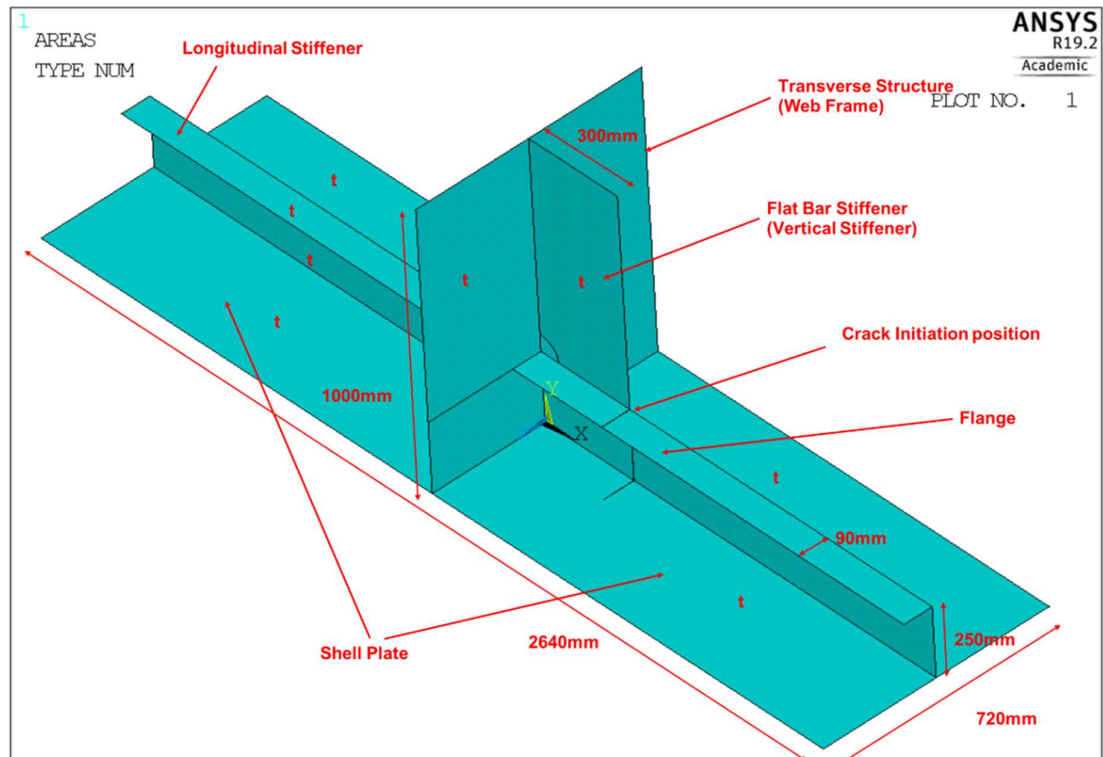


Figure 6-2 Illustration of longitudinal cracked and shell web cracked  
(Thickness  $t=12\text{mm}$ )

The analyses are performed initially with a shell elements (Shell 63) and membrane fracture mechanics elements around the crack tip as shown in Figure 6-3 to Figure 6-5 (later analyses use solid elements in Chapter 8). There are symmetric boundary conditions applied on the front and back sides of structure and the Y-direction fixed loading applied on top side, see Figure 6-3.

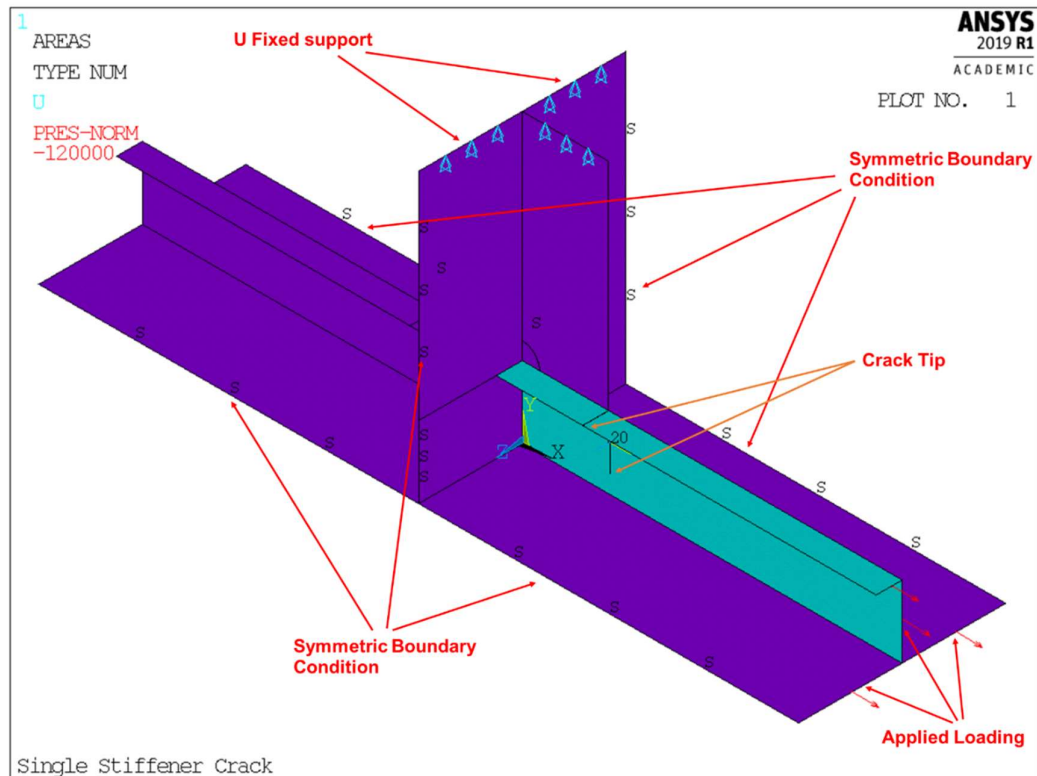


Figure 6-3 Applied symmetric Boundary Conditions and loadings (10MPa)  
 (Note: U-Fixed support means there is no displacement in Y direction, which is the movement in Y direction has been fixed)

The stiffener on the cracked side of the connection is not restrained at the loaded end (it is effectively a cantilever, and the symmetry boundary conditions along the side of the plate will not cause or resist a bending moment in the stiffener between the load and the crack). So as the stiffener cracks through the applied bending moment that results from the eccentricity of the load relative to the centroid of the remaining ligament of material on the cracked section can be calculated from simple statics. Whilst this is not representative of a real structure it is useful for trying to understand the behaviour of the connection detail. The simplified analysis methodology could be adapted to account for different

boundary conditions, although this might require some further ‘beam analysis’ as the more realistic boundary conditions would result in a statically indeterminate structure.

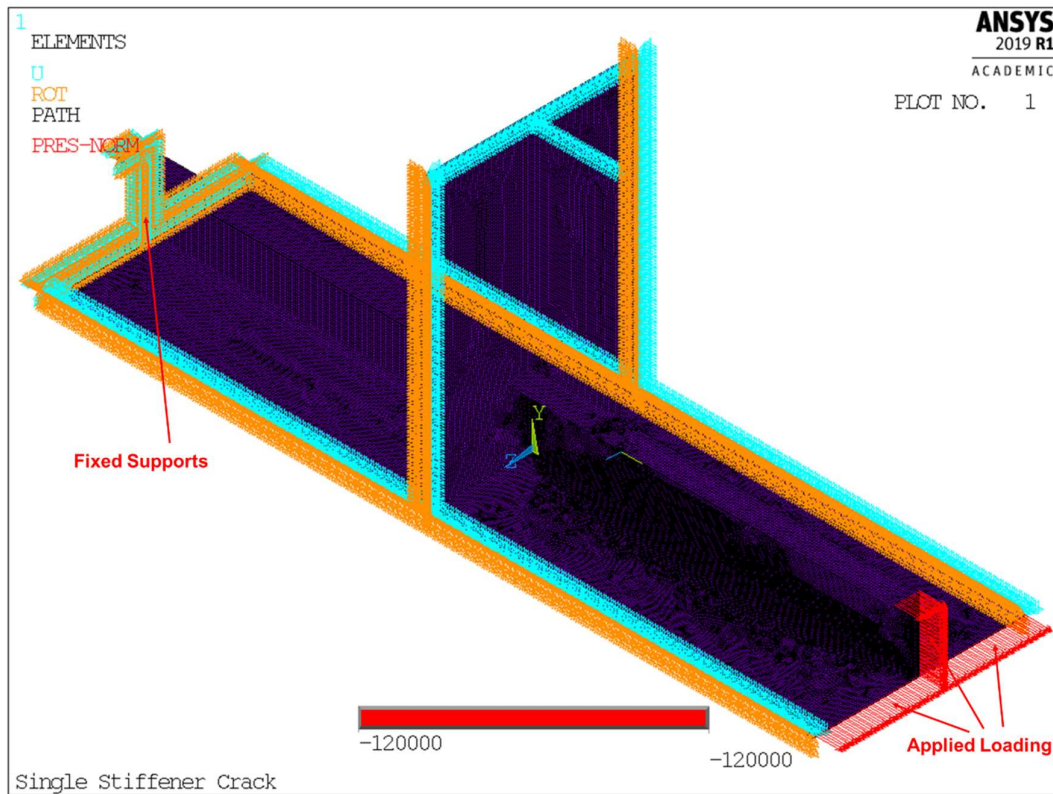


Figure 6-4 Details of mesh, fixed support, and applied loadings (10MPa)



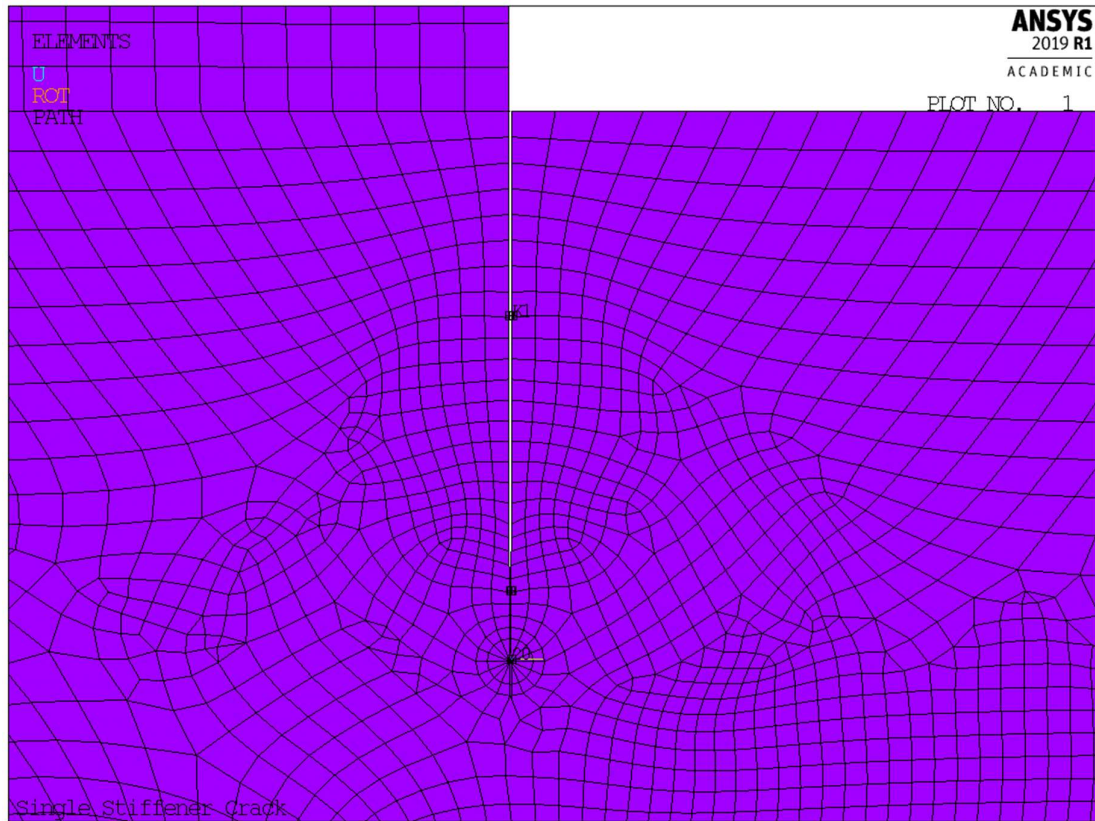


Figure 6-5 Mesh details around crack tip (Stiffener Model)

The  $Y$  curve on single stiffener cracked structure is shown in Figure 6-6. The  $Y$  value drops very dramatically when the crack length is bigger than 250mm, because the shell panel bending effect on  $Y$  is not included in this results (the effect is included in the solid element analysis in Chapter 8). The tendency of  $Y$  is similar to the T-shape model but,

1) At small crack sizes  $Y$  is larger because it influenced by the singularity introduced by the right-angled corner between the frame stiffener and the shell plate stiffener.

2) There is a noticeable kink at  $bf/ds = 1$ , where the stiffener flange breaks.

3) The membrane  $Y$  value, just after the stiffener web cracks through (at  $a/ds = 1$ ), drops to about 1 more gradually. This has not been investigated further but may be a result of the loading that was originally on the stiffener flange.

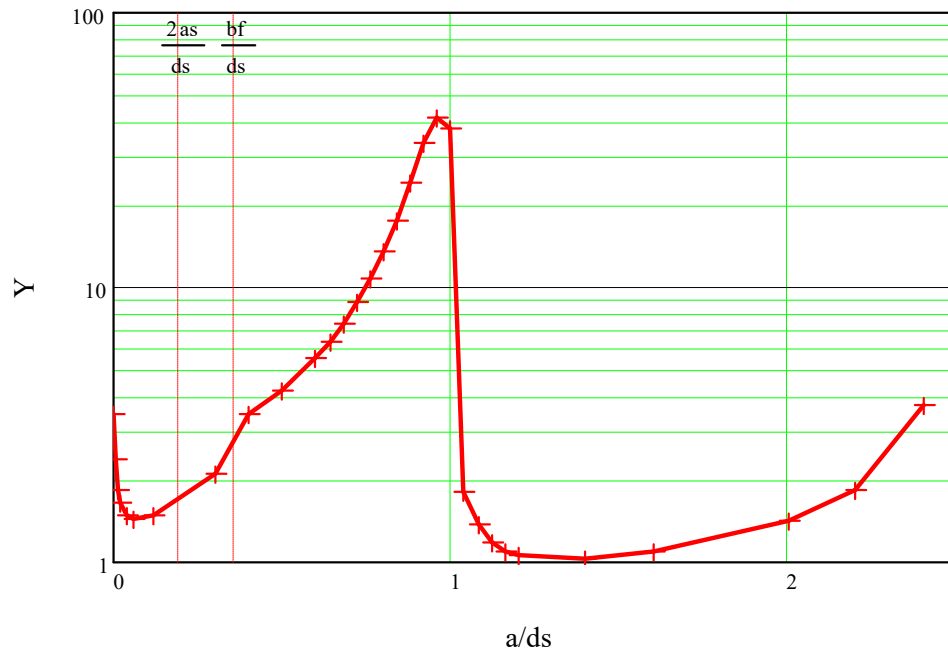


Figure 6-6 Membrane  $Y$  curve for crack in web and shell plate of single stiffener structure under tension loading

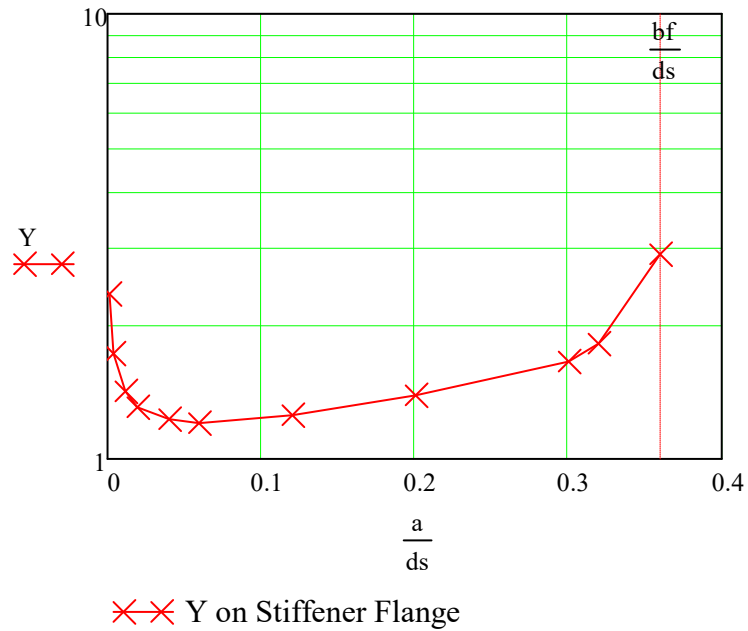


Figure 6-7 Membrane  $Y$  curve for crack in flange of single stiffener structure under tension loading

## 6.2 Simplified numerical model

### 6.2.1 Method based on the T section analysis

Figure 6-8 shows membrane  $Y$  values calculated using an extended method described for the T section method and the FEA results for the single stiffener structure. Only the  $Y$  values for the crack growing through the web and shell plate have been calculated here.

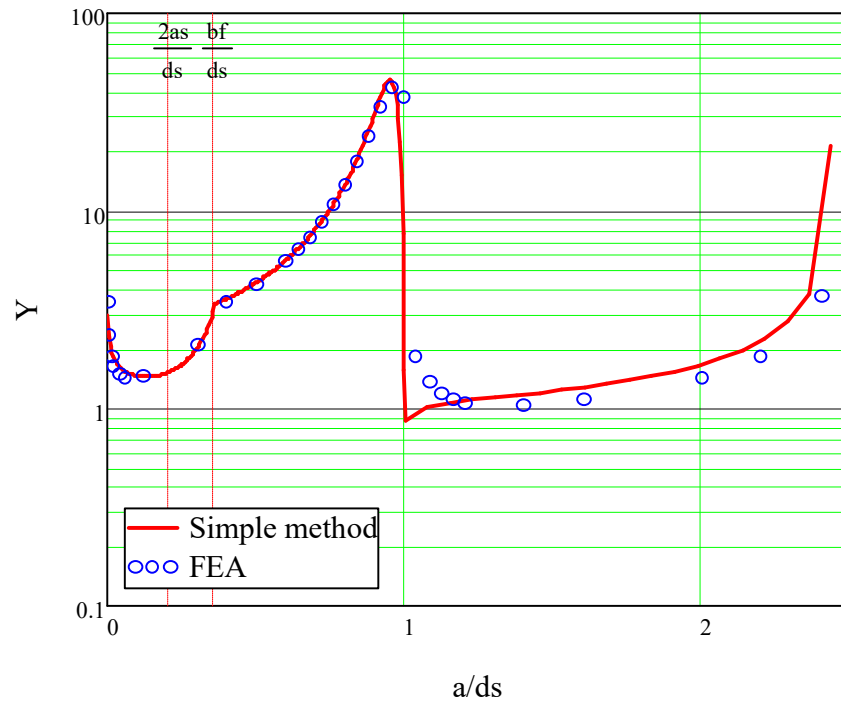


Figure 6-8 Comparison of  $Y$  values between stiffener simple method (including  $ae$ ) and FEA

The extensions to the T section method are:

- 1) The additional corner singularity caused by the right angle intersection of the longitudinal and frame stiffeners is represented by an additional effective crack length “ $ae$  value” (Lou, 2013) of the connection length  $(600\text{mm}) / 25 = 24\text{mm}$ .

$$\text{Then } K = Y \cdot \sigma \cdot \sqrt{\pi \cdot (a + ae)}$$

$Y$  = value calculated without the singularity effect of the frame stiffener,

$a$  = actual crack size,

$ae$  = additional effective crack size which increases from 0 to  $as$  over  $2as$  as described in Section 2.4.8.,

$as$  = connection length/25 = 0.6m/25 = 24mm. Note that a better fit to the FE results was obtained without allowing for the effect of considering the shell stiffener flange folded down and effectively increasing the web thickness. Because all the plates have the same

thickness this would have reduced the  $as$  value by  $\frac{1}{\sqrt{2}}$  to 17mm.

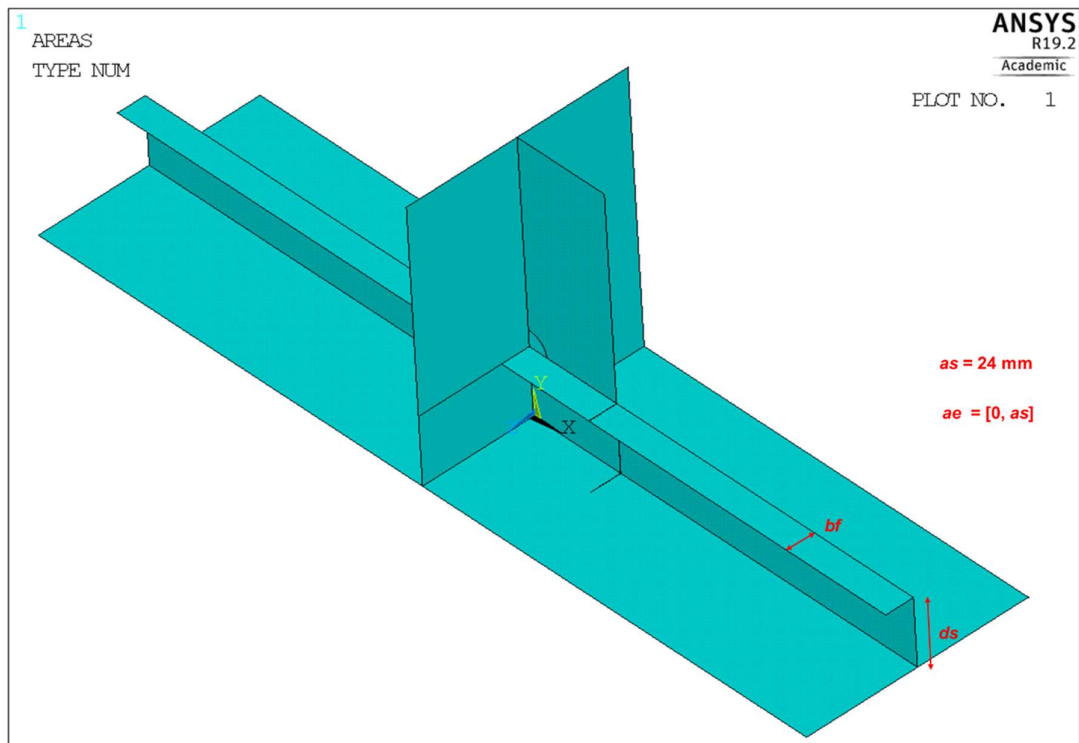


Figure 6-9 Graphical descriptions of some parameters

Although  $ae$  affects  $Y$  over the whole range of  $a$ , the important effect is where  $ae$  is significant in comparison with  $a$  i.e. for smaller cracks, as shown in Figure 6-10.

The simple method for  $Y$  calculations with  $ae$  is  $Y = \frac{K_I}{\sigma \cdot \sqrt{\pi \cdot (a + ae)}}$ , and

comparatively simple method without  $ae$  is  $Y = \frac{K_I}{\sigma \cdot \sqrt{\pi \cdot a}}$ .

The calculation of  $ae$  is discussed in more detail in Section 6.2.2.

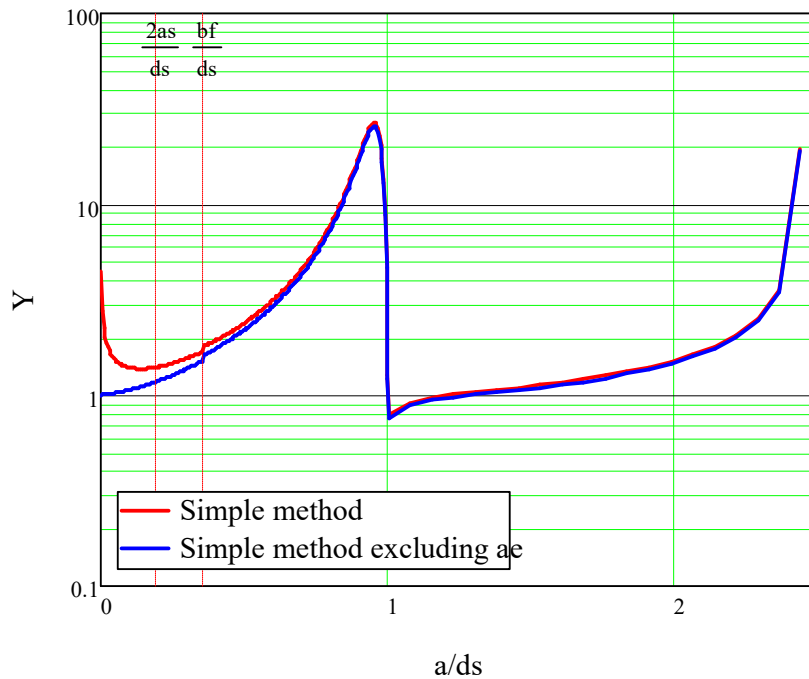


Figure 6-10 Comparison of  $Y$  values with and without  $ae$  values to account for the singularity introduced by the frame stiffener to plate stiffener right angle connection

- 2) The effect of the flange was accounted for by:
  - a. Including the flange section when calculating the applied stresses and assuming, as in the FEA, that the flange cracks propagated at the same speed as the web cracks (so that the

flange cracked completely when the web crack was 90mm long).

- b. Using a  $Y$  value for the reference singular stress distribution of 1 before the flange cracks through and 1.12 after it cracks through. This roughly accounts for the crack effectively becoming an edge crack when the flange breaks through.

The combined effect is seen, in Figure 6-8 at  $bf/ds = 1$ , the kink where the flange breaks is modelled reasonable well by the simple method.

After the flange breaks through the simple model follows the FEA results until shortly before the crack, at 250mm, breaks through to the shell plate. Around the breakthrough  $Y$  is not very accurate, particularly in the precise crack length associated with the maximum  $Y$  value. There is also some difference between the solid element model and the shell model in this region, with  $Y$  in the solid element model being more sharply peaked and slightly higher than in the shell model.

Immediately after the crack breaks through from the web to the plate the trend in  $Y$  is not predicted correctly. The FEA results show the  $Y$  value dropping sharply but then rounding off to about 1, whereas the simple method shows a sharper drop to below 1. Here the T section predictions were better than for the connection detail. It is not obvious why there is a difference here, although in practice plate bending will dominate the membrane effect once the crack has broken through to the shell plate, as discussed in Chapter 7.

This area, around the crack breakthrough into the plate, clearly requires more work. And in reality the crack will not break through in the simplified way, with the line of the crack tip assumed normal to the plate surface, in the FEA and in the simplified method.

Above  $a/ds = 1.2$  the membrane  $Y$  values are underestimated by the simple model.

Overall, particularly before the crack breaks through into the plate, the comparison of the simplified model and FEA results is surprisingly good.

## **6.2.2 Modelling the intersection of the shell and frame stiffeners**

### **6.2.2.1 Comparisons of simplified formulae and $ae$ with Hasebe and Ueda (1981)**

As discussed in Section 2.4.7 a right angled corner results in a singularity, even without a crack, and a simple method needs to take into account the interaction between the geometric corner singularity and the crack singularity.

There are two convenient solutions that are relevant to approximating problem, shown as A) in Figure 6-8:

- B) A crack propagating from the edge of a semi-infinite plate with a stress field representing a corner
- C) A semi-infinite crack growing in an infinite plate with a stress field representing a corner



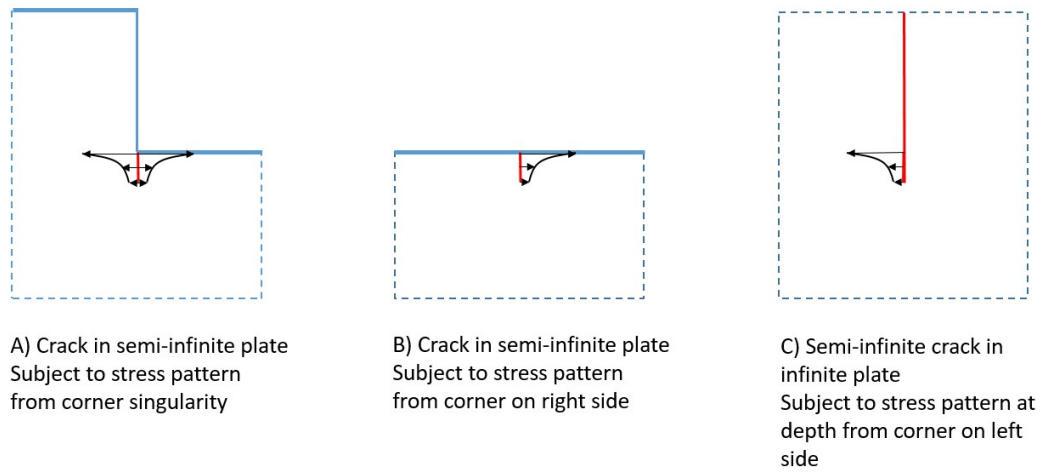


Figure 6-11 Approximation of corner crack by semi-infinite plate and infinite plate cracks

The stress field is defined as described in Section 2.4.7.1.

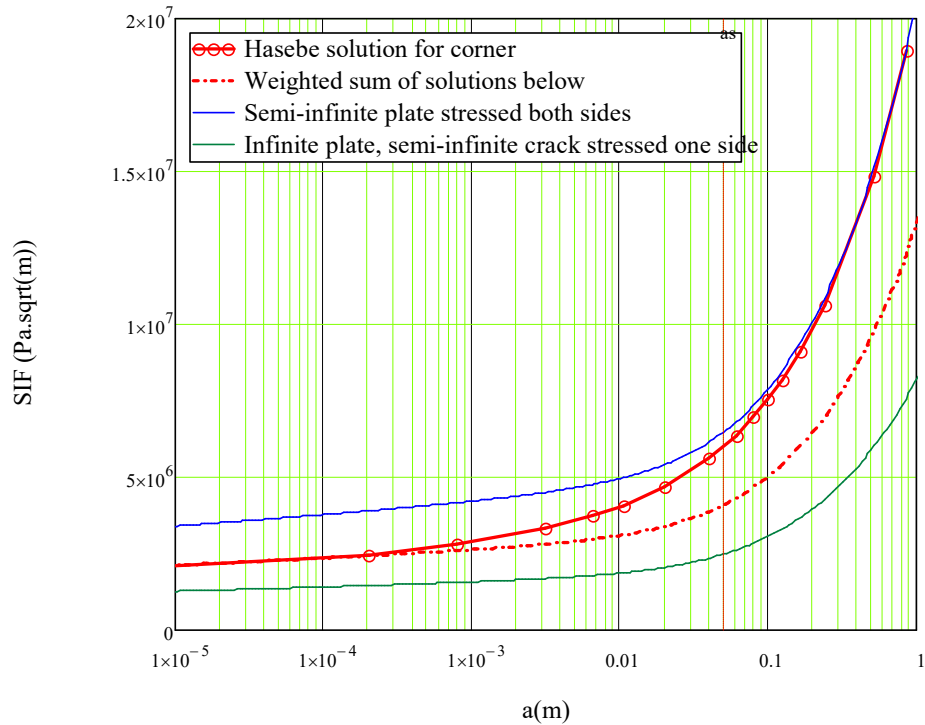


Figure 6-12 Result of approximation of corner crack by semi-infinite plate and infinite plate cracks (step height = 0.1m,  $as \approx 0.05m$ )

Figure 6-12 compares the results of simplified models and the Hasebe results (solid red line).

When the crack is large the formulation of Hasebe and Ueda (1981) tend to the blue curve in Figure 6-12 (semi-infinite plate with both faces of the crack subject to stress Figure 6-11A),

$$K_I = 1.1215 \cdot \sigma \sqrt{\pi \cdot a} \quad (6.1)$$

When the crack is small the crack tends to the red dashed curve in Figure 6-11. This corresponds to:

$\frac{1}{2} \times$  (semi-infinite crack one face stressed, Figure 6-12C) + Figure 6-11 (semi-infinite plate one faces stressed, Figure 6-11B).

Note that the  $\frac{1}{2}$  indicates that the overall contribution of the semi-infinite crack, when the crack is small, is equivalent to half the stress on one face. This was an interesting result – it was guessed that the result might be the simple addition of C) and B). Note that there is not a unique solution to the contribution of the two parts as there are proportions of two values to add together to match the Hasebe and Ueda (1981) result and, for instance, multiplying both cases C and B by 0.35 would also give a good fit when the crack is small.

Whilst this provides an interesting insight into the behaviour of a step or right angled connection the alternative simple method of reducing  $ae$  to 0 as the crack size tends to zero is much simpler and is used here. Xu., Lou and Barltrop (Xu et al., 2013) proposed a power formula for the reduction. This, for a  $qt$  value of 2 (value of  $a/as$  where  $ae = as$ ), is plotted with the Hasebe and Ueda (1981) in Figure 6-13. Note that the Xu et al.(2013) power formula is not a particularly good fit. An exponential formula:

$$ae = \left[ 1 - \left[ e^{-6(a_c)^{0.4}} \right] \right] \cdot as \quad (6.2)$$

was found to give a better fit to the Hasebe and Ueda (1981) but lacked the advantage of a well defined cut-off for the small crack effect (it had been hoped that a simple  $[a+\text{constant } ae]$  solution could be used as this would allow a closed-form crack growth calculation to be used, which speeded up reliability calculations (Barltrop (2020) private communication).

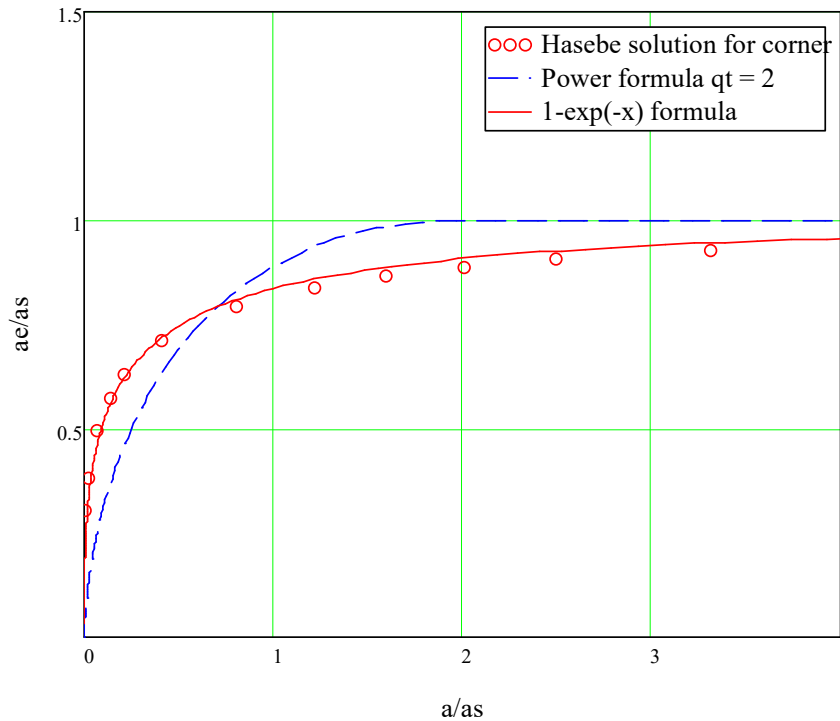


Figure 6-13 Behaviour of  $ae/as$  at small  $a/as$

### 6.2.2.2 Calculation of $ae$ compatible with finite element results and simplified analysis method

The  $ae$  value is calculate using the FEA  $Y$  values ( $Y_{fea}$ ) and the simple method excluding  $ae$  values ( $Y_{sf}$ ), see Figure 6-10.

$$ae = a \cdot \left( \frac{Y_{fea}}{Y_{sf}} \right)^2 - a \quad (6.3)$$

The result is shown by the red circles in Figure 6-14. An  $as$  value of 24mm appeared to be a reasonable estimate. The larger and smaller  $ae$  values either side of the flange cracking through are probably related to the flange cracking through.  $as = 24\text{mm}$  is the frame stiffener connection length (600mm)

divided by 25. From Xu et al. (2013) and considering the stiffener flange folded down to the web it seemed reasonable to consider the frame stiffener as having half the thickness of the combined web and flange. This would result in the estimate for  $as$  being  $\frac{600mm}{25} \cdot \sqrt{\frac{12mm}{2 \times 12mm}} = 17mm$  however the fit to the  $Y$  values of using  $as = 24mm$  was better.

The power formula, exponential [Equation (6.2)] and a linear approximation [Equation (6.3)] are given for comparison. Although the bi-linear fit appears quite good it significantly under-estimates the SIF values at low  $a/as$ , which is where the effect of  $ae$  is most important. The power formula, with  $qt = 2$ , and  $as = 24mm$  was found to give a good fit at small  $a/as$  [Equation (2.28)] and produced a reasonable fit to the  $Y$  values at larger  $a/as$ , as shown in Figure 6-14.

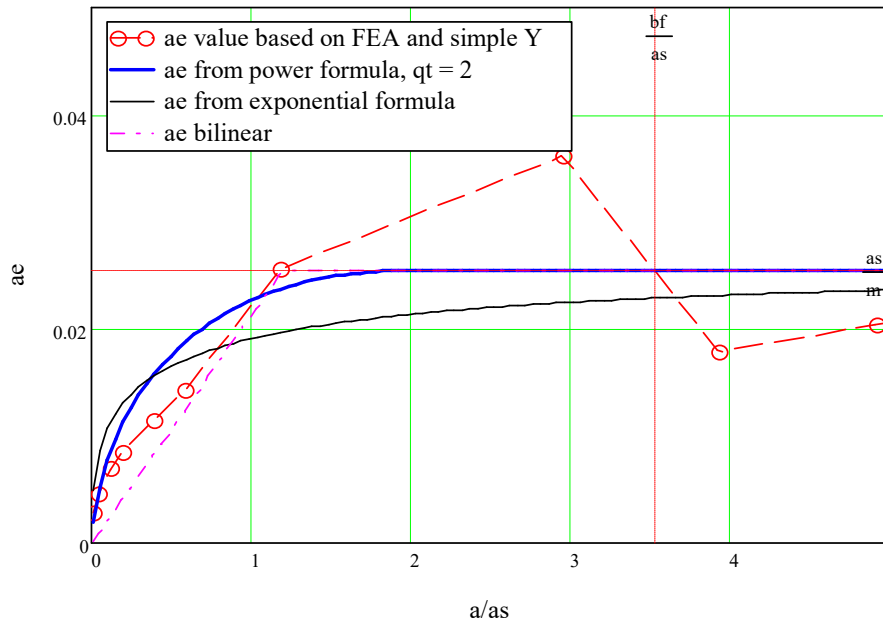


Figure 6-14  $ae$  calculated from FEA with simple method and power and exponential approximations to Hasebe and Ueda (1981) results (non-dimensionalized by  $as = 24mm$ )

It is not clear whether the difference between the  $ae$  values that fit the Hasebe results and those that fit the connection FEA results are physically significant, for example the higher than expected  $as$  value could be a result of the stiffener flange being less effective as a result of its finite width that is much smaller than the connection length of the frame stiffener, or just a result of the approximate, ligament linear-stress, method that is fitted to the FEA results.

More fundamentally the behaviour of the intersection of the frame stiffener with the shell stiffener flange and web may be quite different to the cruciform plate for which the  $ae$  method was derived. Figure 6-15 shows the  $ae$  value from the FEA compared with the power formula and the exponential formula but with  $as = 17\text{mm}$ . There is some indication that the  $as$  method may be valid for  $a/as < 0.4$  but that there is another effect that becomes important after that.

For small cracks up to about 25mm (in this case about equal to  $as$ ) that may be considered to define the fatigue life an alternative fit has been noted (Barltrop and Xu, 2011). This is discussed in Section 6.2.5 and is used in Chapter 9.

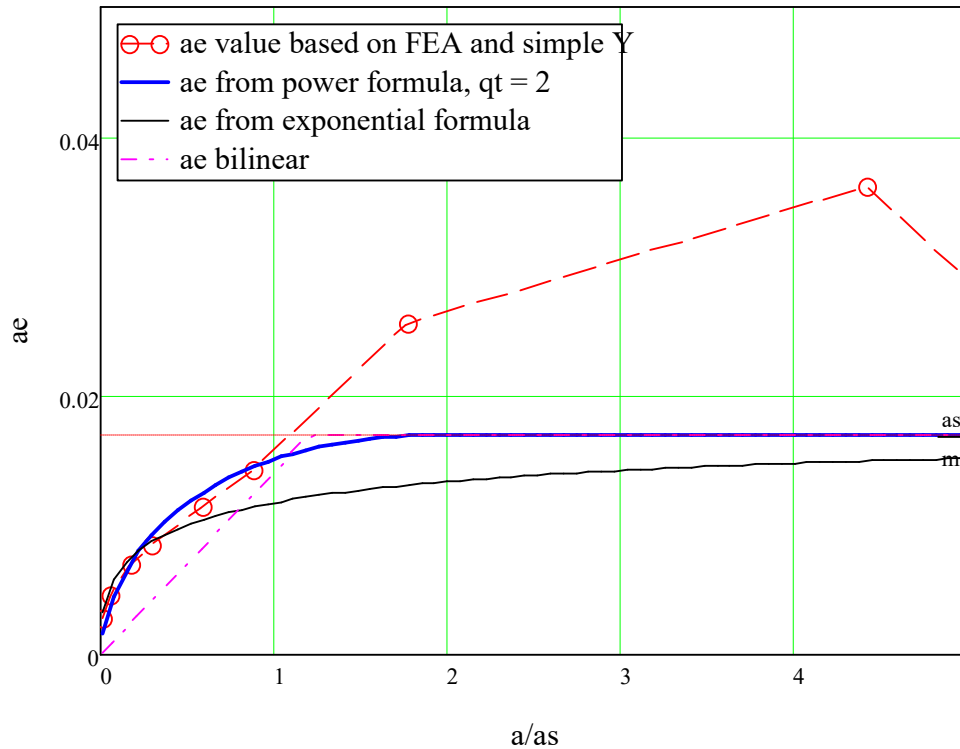


Figure 6-15  $ae$  calculated from FEA with simple method and power and exponential approximations to Hasebe's results (non-dimensionalized by  $as = 17\text{mm}$ )

To understand the behaviour of the crack at the stiffener intersection finite element analyses with different plate thickness ratios and different flange widths might help, however that would extend the work of this PhD too much so instead, in the following sections, two further cases are considered:

1. with the transverse frame removed
2. with the shell stiffener flange removed

### 6.2.3 Effect of flange and transverse frame on Y values

To better understand the effect of the various parts of the connection on the Y values in the stiffener web, analyses were repeated with:

- a) The transverse frame removed but with the connections remaining in place.
  - b) The flange removed (with the transverse frame reinstated).
- Analyses were performed up until the flange broke through.

#### 6.2.3.1 Effect of transverse frame on Y values

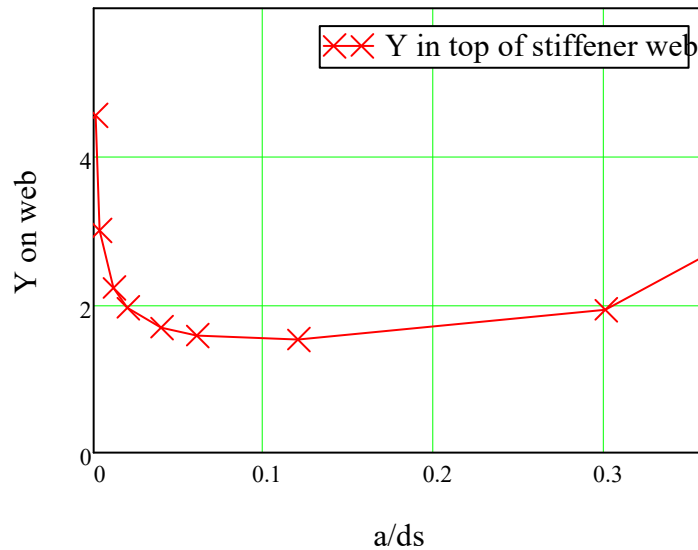


Figure 6-16 FE analysis with frame and flange

Results with the transverse frame removed are shown in Figure 6-17



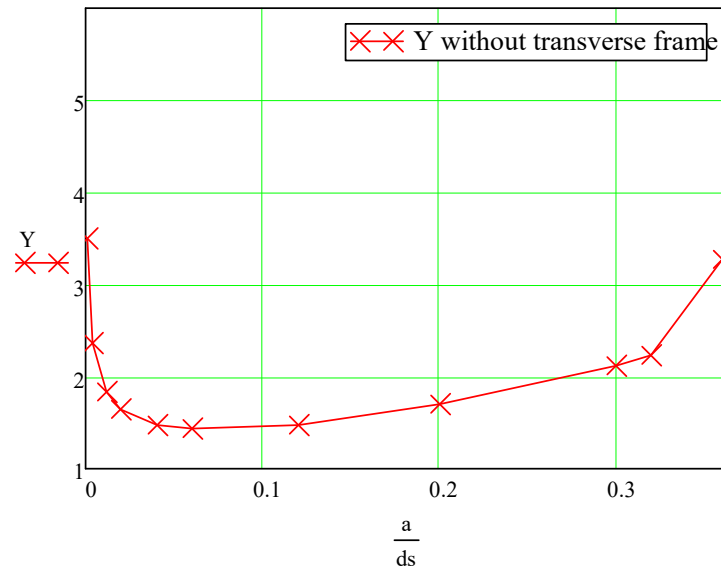


Figure 6-17 FE analysis with transverse frame removed

These analyses demonstrate that (as expected) the transverse frame does not affect the Y value for the connection subject to axial load.

### 6.2.3.2 Effect of shell stiffener flange on Y values

FEA results without the flange are shown and compared with the simple method using  $as = 24\text{mm}$ , exponential equation, in Figure 6-18. For this case the expected value of  $as$ , from Xu et al (2013) is the connection length /25 = 24mm.

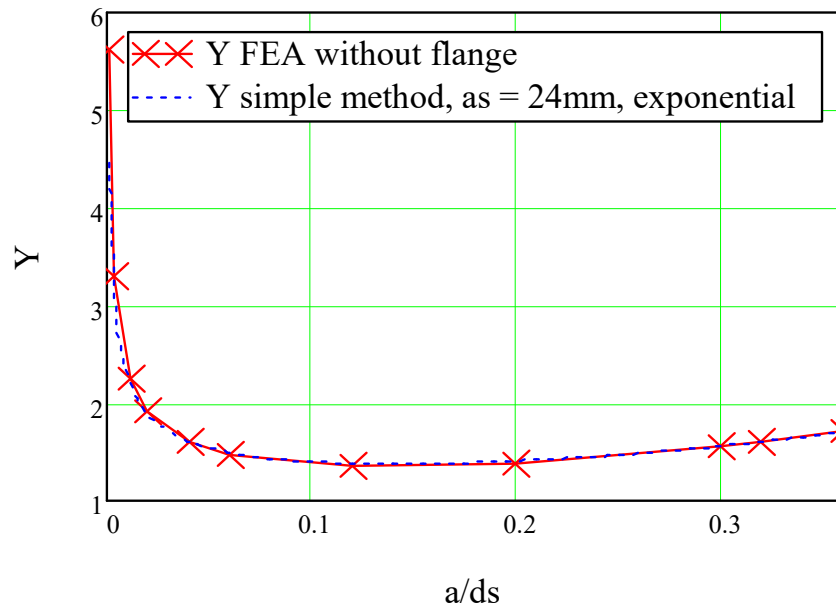


Figure 6-18 FE analysis and simplified method with flange removed

With no flange the initial  $Y$  value (which, for fatigue, will be the most important) is increased, in comparison with the case with a flange, but the increase in  $Y$  as the flange breaks through is avoided.

Using the FEA results in conjunction with the simple model, with  $a_s=0$  the  $ae$  values required to match the results are calculated and shown in Figure 6-19.

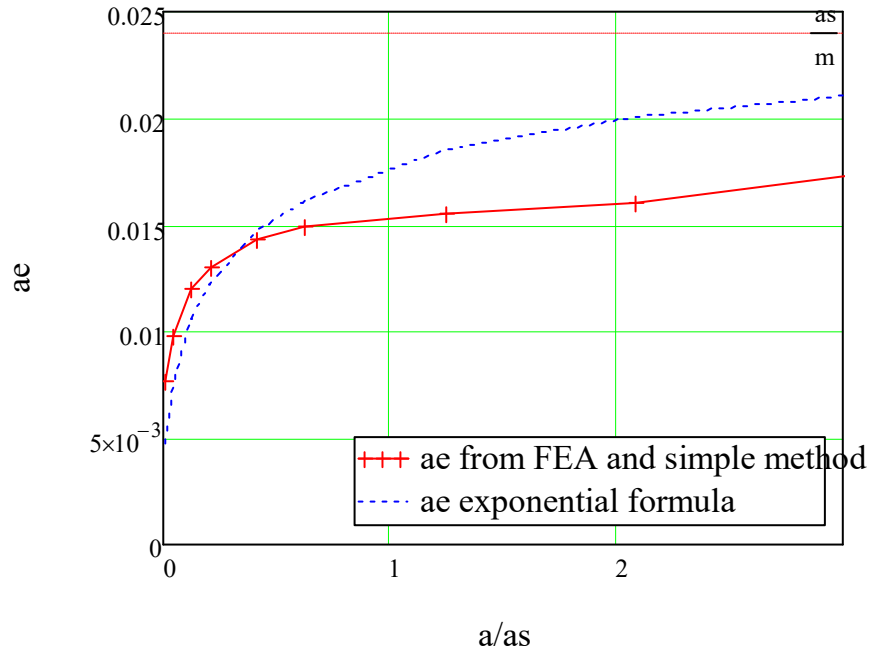


Figure 6-19 Flange removed  $ae$  values

Figure 6-19 shows that  $ae$  is only moderately well predicted by  $as =$  connection length/25 and the exponential formula. It appears that this is a useful first approximation but that more work is needed if the effect of the right angle in structural connections is to be adequately estimated using simple formulae.

#### 6.2.4 Single stiffener shell model subject to stiffener bending

A bending case was also run in ANSYS. The results are shown in Figure 6-20.

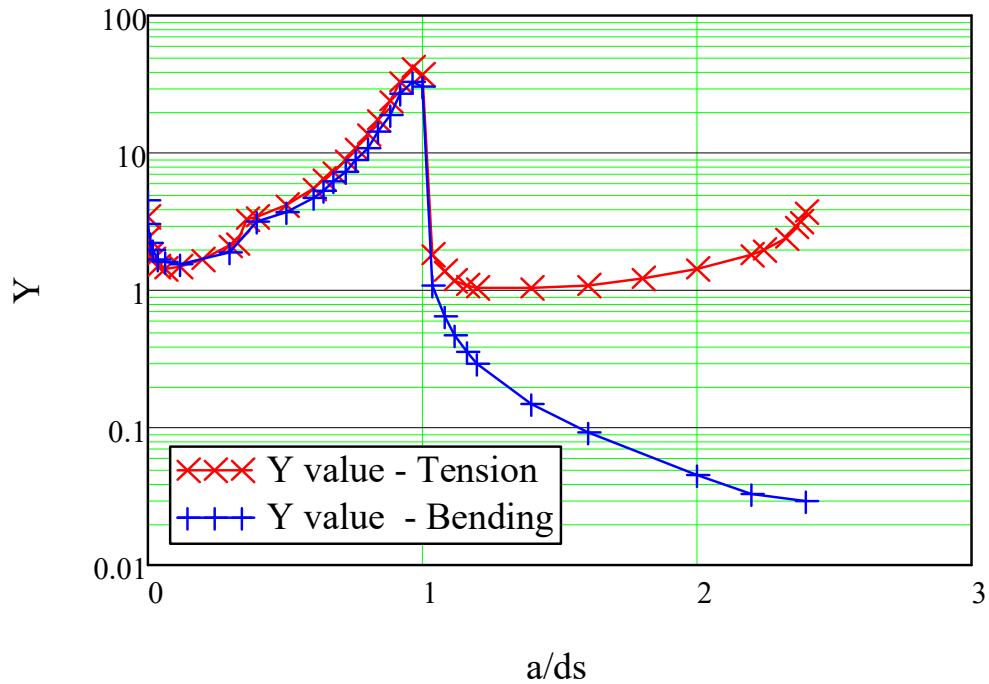


Figure 6-20 Y comparison for bending moment and tension loading on single stiffener

It is noticed that the membrane  $Y$  from the bending moment case does not, as expected, drop to zero immediately the plate stiffener cracks through to the plate at  $a/ds = 1$ . A drop to zero is expected because there is a net moment to the plate with no net axial force.

The non-zero  $Y$  value for  $a/ds > 1$ , is probably caused by a distribution of membrane stress in the plate which totals a zero force but is not the zero stress that a simplified analysis would suggest. The bending case is not considered further in this thesis.

The results are compared with the simple method in Figure 6-21.

The modification to the simple method, from the tension case, involved simplifying the code by replacing the combination of applied force and eccentric bending moment, that increased as the crack grew down the web, with the constant applied bending moment on the remaining ligament.

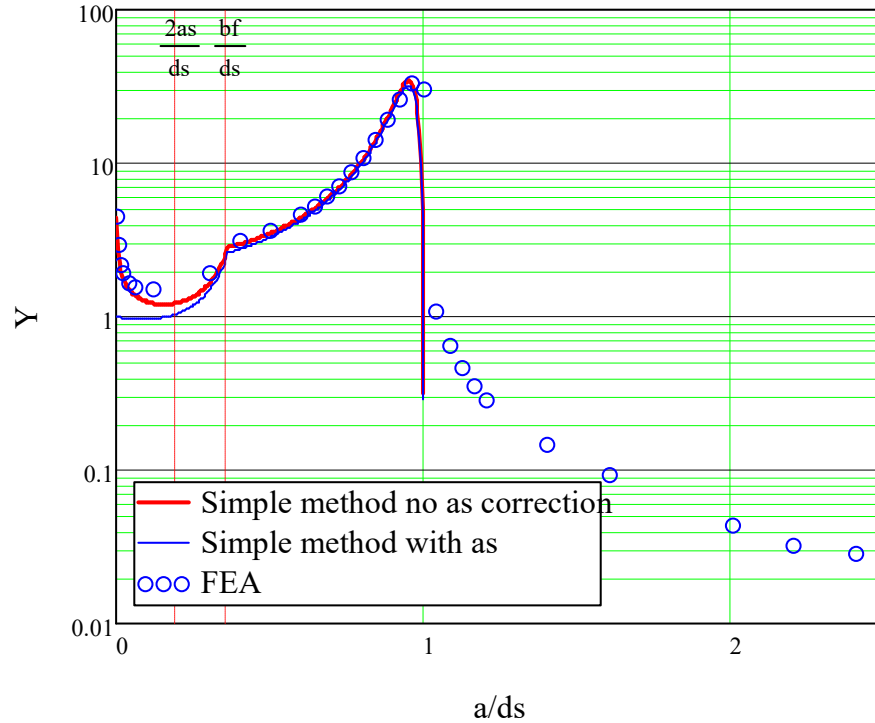


Figure 6-21 Membrane  $Y$  comparison for bending moment case  $as = 24\text{mm}$

The agreement is good after the flange has broken and until the crack breaks through into the plate where the reasons discussed above the bending  $Y$  values would become dominant but are not calculated here. The  $as$  value of 24mm gives a first approximation to the  $Y$  values for small cracks. The methodology is therefore shown to work well for a bending moment as well as for tension applied to the shell stiffener.

### 6.2.5 SIFs for small cracks

For design purposes an S-N calculation with an SCF is usually the most convenient way of demonstrating sufficient fatigue strength. In laboratory experiments there is not a single criteria for deciding the end of life of a specimen being tested but with small specimens the end of life is usually clear e.g. as a marked loss of stiffness or a visible large crack. Very arbitrarily the fatigue life of the large structural details, analysed here, may be taken to correspond to the time to grow a crack from an initial size of 0.15mm to a final size of 25mm.

The SCF has been related to the stress distribution  $as$  value which can itself be related to the fracture mechanics  $ae$  value and  $Y$  value.

Barltrop and Xu (2011) note that the  $as$  value for a simple cruciform outstand (or a step in the edge of a plate) can be calculated from  $as = \text{minimum of } H/2 \text{ or } L/25$  where  $H$  is the height of the outstand and  $L$  is its length. For small cracks less than  $as$  in size, a reduction factor has to be applied as the  $as$  value overestimates SIFs in that region. It was hoped that the outstand calculation method would also usefully apply to connections between longitudinal and transverse stiffened plates (as analysed in this section). However Barltrop and Xu found that, for small cracks, the outstand formula did not give satisfactory results and that a better method used an  $as$  of  $L/190$  in conjunction with an SCF of 1.4. The connection detail analysed in this work is similar to that analysed by Barltrop and Xu so it is not surprising that a similar conclusion is drawn here, as shown in Figure 6-22. Where the apparent

$$\text{crack size} + ae = \frac{K^2}{\pi \cdot \sigma^2}.$$

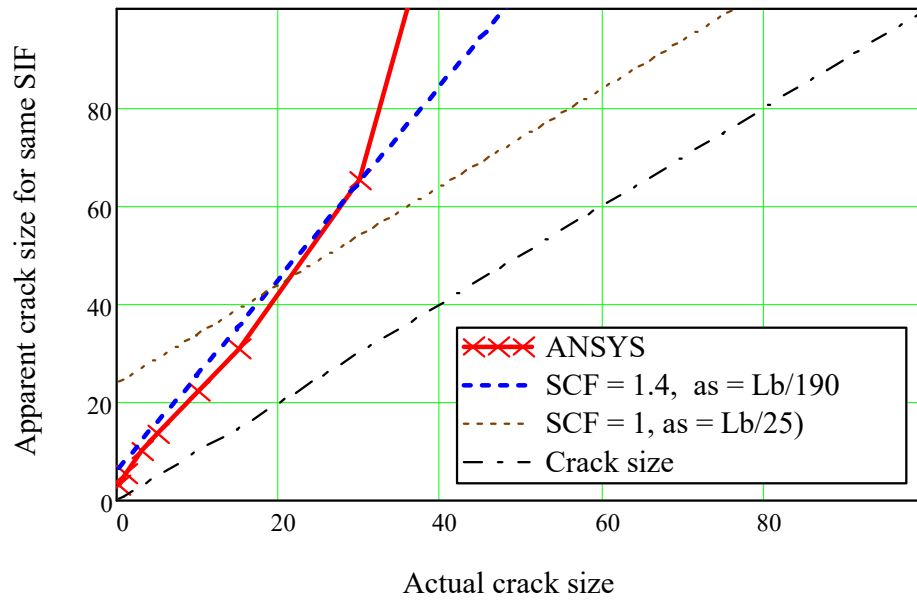


Figure 6-22 Apparent crack size ( $a+ae$ ) for small cracks relevant to typical design fatigue life calculation

This combination of SCF and  $as$  is used in Chapter 9 to estimate an overall SCF that can be used in S-N fatigue analysis.

### 6.3 Conclusion for estimation of Y values in connections

The simple analysis, without allowing for the corner singularity at the transverse frame to shell stiffener connection, works well for crack sizes larger than the flange width (although the applicability limit should probably be in terms of the frame stiffener depth or  $as$ ). For smaller crack sizes the simple analysis under-predicts the Y value. This is where the  $ae$  effect and the way in which  $ae$  increases from 0 to its full value of  $as$  can allow for the corner singularity and is dominant. The formula by Xu et al (2013) that was derived for

a flat cruciform plate only gives a first approximation to this case of the frame stiffener connecting a flange and web plate. This needs further investigation but is not considered further in this thesis. It should also be noted that this calculation is related to a simplified geometry. Where the corner singularity is most important there is also in reality the complication of the three dimensional geometry of the intersection of frame stiffener and shell stiffener with finite plate thicknesses and weld profile all affecting the SIFs.

Nevertheless the simplified method corrected by a simply calculated *as* value and additional crack size, *ae*, does give a useful estimate of *Y*.



## **Chapter 7 Study of three longitudinal stiffener connections to transverse structure with shell elements and membrane-only fracture mechanics elements**

This analysis was performed to study the beneficial effect of load redistribution to stiffeners, adjacent to the cracked stiffener and the reduction in SIFs that result.

### **7.1 Finite element analysis of the three stiffener model**

The dimensions of the model are shown in Figure 7-1. Note there is only a crack in the central stiffener.

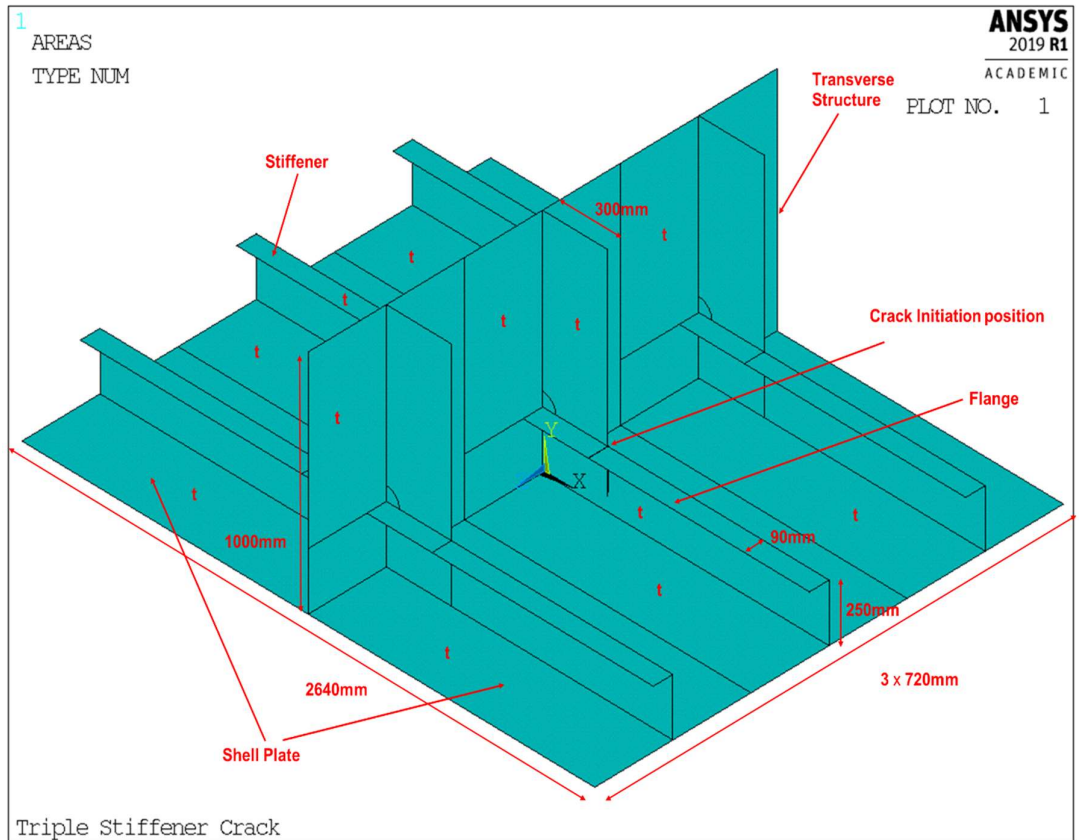


Figure 7-1 Dimensions and Thickness ( $t=12\text{mm}$ ) of triple stiffeners model

The boundary conditions and loading applied (10MPa) on the triple stiffeners are as shown from Figure 7-2 to Figure 7-4. There are symmetric boundary conditions applied along the front and back sides of structure and the Y-direction fixed loading applied on top side, see Figure 7-2.

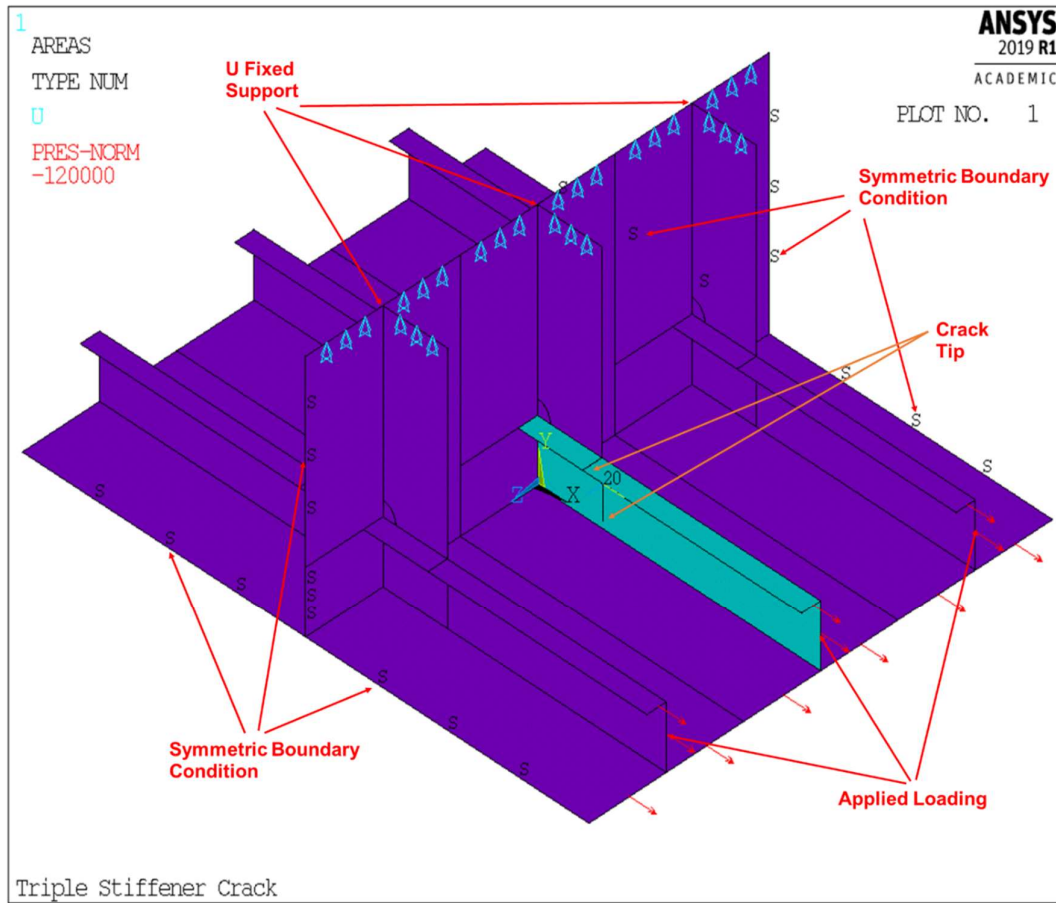


Figure 7-2 Applied symmetric Boundary Conditions and loadings (10MPa)

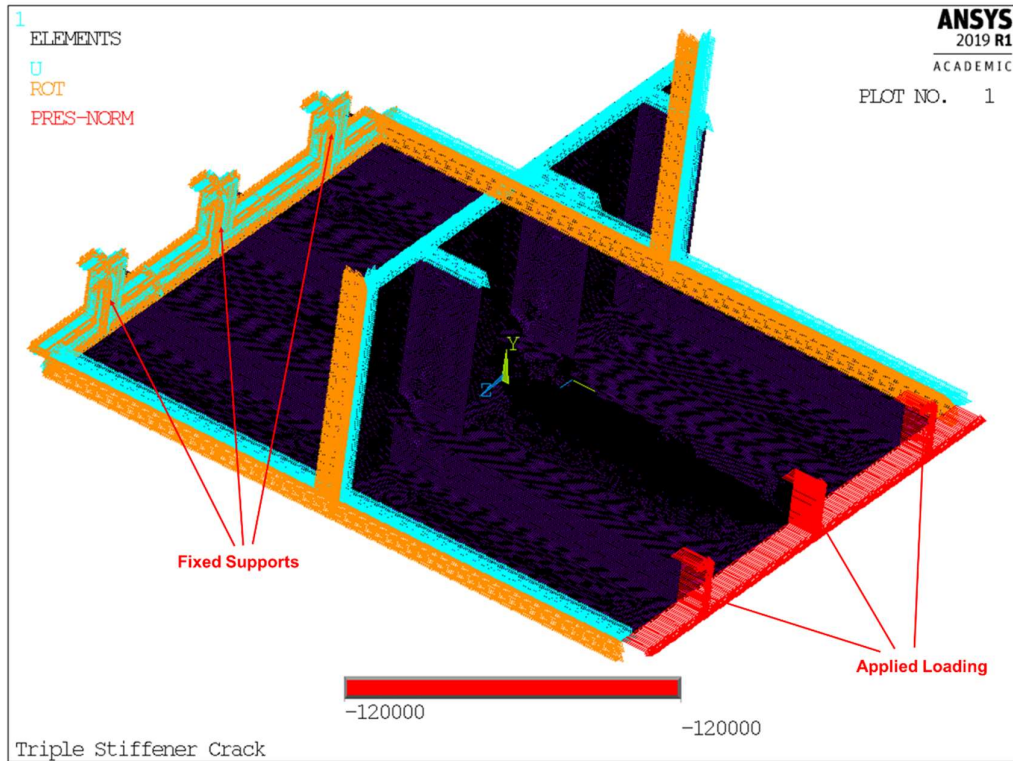


Figure 7-3 Details of mesh, supports, and applied loadings (10MPa) for three stiffeners model

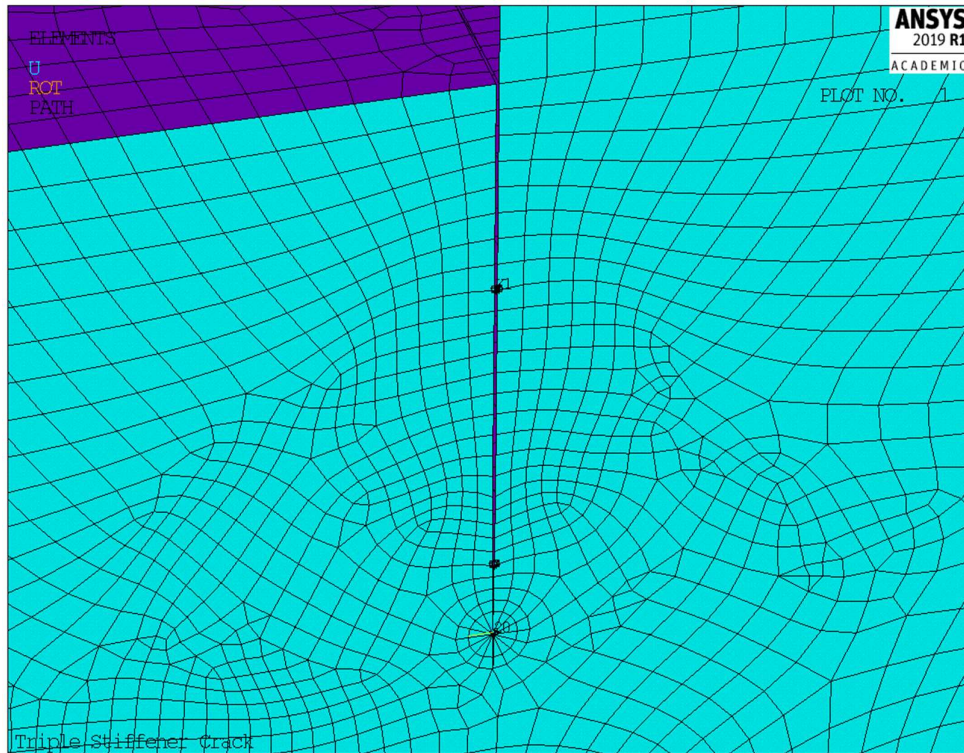


Figure 7-4 Mesh Details around crack tip

The results are shown in Figure 7-5, along with the previous results for a single stiffener.

Until the stiffener flange cracks through  $a/ds = 0.36$  the triple and single stiffener results are essentially the same. For larger cracks the benefit of the support from the adjacent stiffeners are clear; reducing the maximum  $Y$  value from 41.8 to 12.2.

After the web has cracked through, the membrane  $Y$  values in the shell late are also lower in the triple stiffener structure and the sudden increase as the crack approaches the plate edge, after  $a/ds = 2$  in the single stiffener model, does not occur as the plate edge is further away.

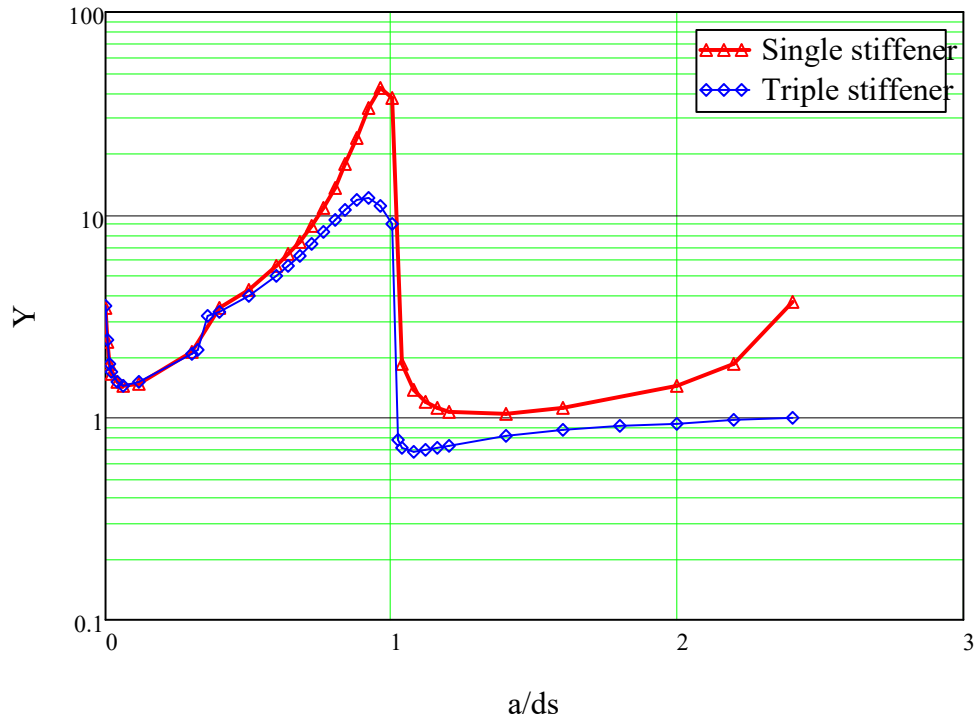


Figure 7-5 Y for crack on triple and single stiffener under tension loading

## 7.2 Simplified analysis of the three stiffener model

A common situation will be that only one stiffener of a group of parallel stiffeners has seriously cracked. The one cracked stiffener will be supported, to some extent, by the shell plating spanning transversely across to the adjacent stiffeners, as shown in Figure 7-6. The relative stiffness of this transverse support to the stiffness of the cracked stiffener section becomes important.

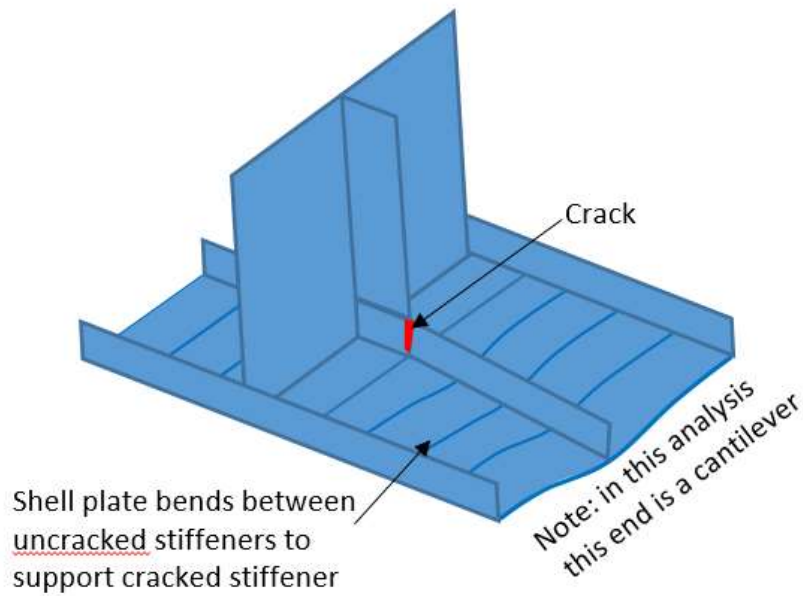


Figure 7-6 Shell plate bending supporting a cracked stiffener

The support to the stiffener provided by the plate is calculated:

For the stiffener the cracked section 2nd moment of area is  $I_r$  and the effective length of the cracked section, is taken as  $h$ .

Then the moment ( $M_s$ ) rotation relationship in the vicinity of the crack is:

$$\theta = \frac{M_s}{E \cdot I_r} \cdot h \quad (7.1)$$

And for a large crack in the stiffener web, with the rotation assumed concentrated in this length  $h$  around the crack the displacement  $\delta_0$  of the end of the stiffener, at  $L_c$  from the crack is:

$$\delta_0 = \theta \cdot Lc = \frac{Ms}{E \cdot I_r} \cdot h \cdot Lc \quad (7.2)$$

or,

$$Ms = \frac{E \cdot I_r}{h \cdot Lc} \cdot \delta_0 \quad (7.3)$$

For the shell plate spanning as an encastre beam between the uncracked stiffeners (in practice it will be less rigidly fixed than encastre but this is a useful starting point).

Consider a transverse strip of plate of transverse length  $2B$  and elemental length  $dx$  supporting the shell plate stiffener at distance  $x$  from the crack. The moment ( $Mt$ ) induced in the stiffener for a displacement  $\delta_0$  at the end of the stiffener is:

$$\Delta M = \frac{192 \times E \cdot I_p}{(2B)^3} \cdot \frac{\delta_0 \cdot x}{Lc} \cdot x \cdot dx \quad (7.4)$$

Integrating with respect to  $x$  over the length of the cantilever ( $Lc$ )

$$M_t = \frac{192 \times E \cdot I_p}{(2B)^3} \cdot \frac{\delta_0}{Lc} \cdot \frac{Lc^3}{3} = \frac{8 \times E \cdot I_p}{B^3} \cdot Lc^2 \cdot \delta_0 \quad (7.5)$$

Therefore, the overall stiffener-moment to end-deflection relationship is:

$$M = \left( \frac{E \cdot I_r}{h \cdot Lc} + \frac{8 \times E \cdot I_p}{B^3} \cdot Lc^2 \right) \cdot \delta_0 = \frac{E}{h \cdot Lc} \cdot \left[ I_r + I_p \cdot \left( \frac{8 \times E \cdot Lc^2}{B^3} \right) \cdot \left( \frac{h \cdot Lc}{E} \right) \right] \cdot \delta_0 \quad (7.6)$$



$$M = \frac{E}{h \cdot Lc} \cdot \left[ I_r + I_p \times 8 \times h \cdot \left( \frac{Lc}{B} \right)^3 \right] \quad (7.7)$$

Or the effective stiffener 2nd moment of area is,

$$I_r + I_p \times 8 \times h \cdot \left( \frac{Lc}{B} \right)^3 \quad (7.8)$$

to fit the above method to the FE analysis results  $h$  was found to be about 80mm or about  $6.5tp$ .

The results are shown in Figure 7-7,

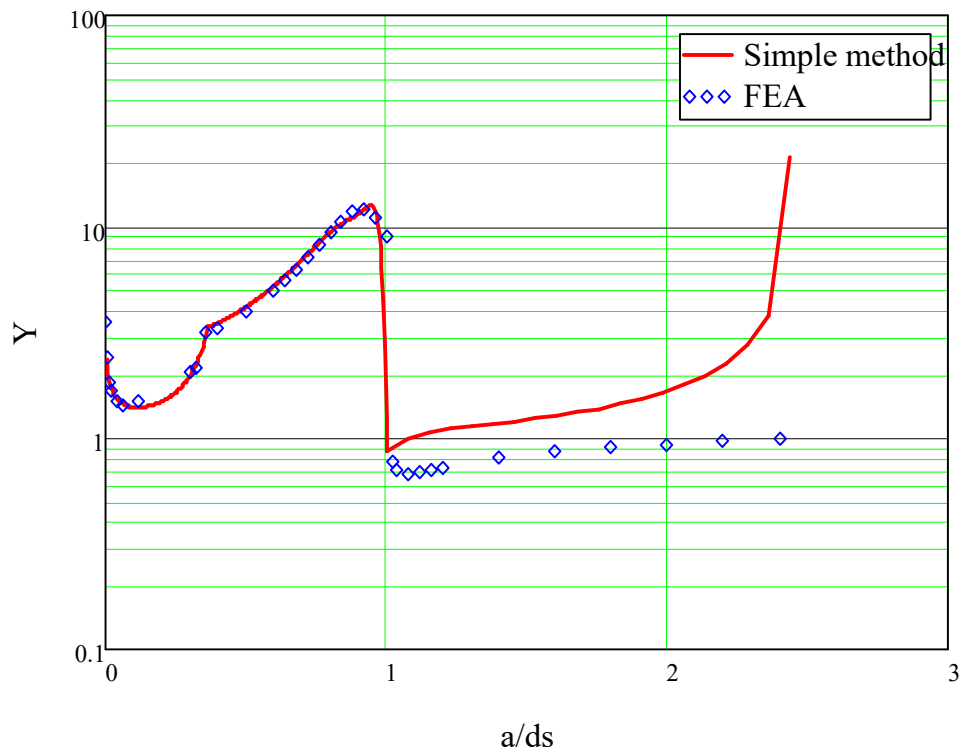


Figure 7-7 Comparison of  $K$  values from simplified model and FEA with moment redistribution through plating to side stiffeners

The redistribution of the bending moment gives good results until the crack breaks through the shell plate, after that, and until a crack length corresponding to nearly complete cracking of the shell plate the simplified method overestimates the  $Y$  value because:

- 1) The method does not account for the compression induced in the shell plate by the bending of the adjacent stiffeners as they support the cracked stiffener. However an approximate investigation, based on the moment shed to the adjacent stiffeners and the resulting compression induced in the plate, showed that it could only explain about half the overestimate of  $Y$  after the stiffener web had cracked through.
  
- 2) No account has been taken of the redistribution of the applied axial force to the outer longitudinals. There was not an obvious way of estimating the axial redistribution effect. It was found that a reasonable fit for  $a/ds > 1$  was obtained by assuming that, after the stiffener was cracked through, 15% of the cracked stiffener axial force was redistributed to the adjacent stiffened plate and that the area of the cracked stiffened plate included 10% of the area of the adjacent stiffener and plate, so overall about 25% of the axial force was redistributed, compared with 32 % of the area of one stiffener and its associated plate, or 11% of the overall area, being lost as the crack breaks through into the shell plate. (Splitting the redistribution effect in this way was found to give the best fit to the FE analysis and avoided the increase in the  $Y$  value as the crack reached the now artificial plate edge half way between the stiffeners.)

However the estimated  $Y$  value now, incorrectly, drops rapidly as the crack is about to break through to the edge of the central stiffened panel. This is a result of the simplified analysis being based on a single stiffener and

associated plate with increased area accounting for some of the redistribution of the applied load but the singular stress pattern being applied to the cracked area of the single stiffener and associated plate. It may be better to account for the larger area in both the applied stress and singular stress calculation, it would need to be considered if the crack was to be modelled as it approached the adjacent stiffeners but that has not been pursued further in this thesis.

The improved result is shown in Figure 7-8.

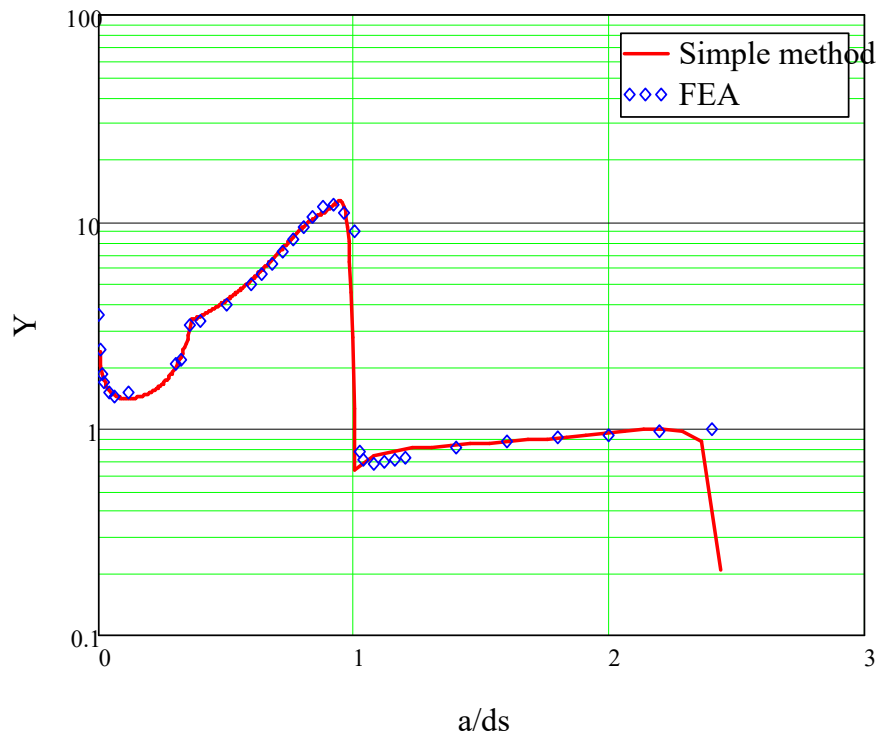


Figure 7-8 Comparison of  $K$  values from simplified model and FEA with moment and axial force redistribution

For practical purposes the assumption that the membrane  $Y$  value = 1 is conservative but probably satisfactory once the crack breaks through into the plate.

The bending  $Y$  value is an order of magnitude higher and is discussed in Chapter 8.

### **7.3 Conclusion of three stiffener simplified modelling**

The simplified method for the assessment of a crack at a connection between a single longitudinal stiffener and transverse supporting structure has been extended to allow the assessment of three parallel stiffeners with the central stiffener cracked.

Before the crack breaks through to the shell plating, the most important effect that is taken into account is the redistribution of the stiffener bending moment that results from the eccentricity of the load as applied to the cracked structure.

Redistribution of axial load and the effect of the moment generated in the uncracked stiffeners on the  $Y$  values were found to be important after the crack had grown into the shell plating.

Overall, with the extensions to allow for moment and force redistribution, the method continues to work well, especially up till the crack breaks through the web into the shell plate.

## **Chapter 8 Study of a longitudinal stiffener connection to transverse structure with solid elements and solid fracture mechanics elements**

### **8.1 The solid model**

This model had the same dimensions as the shell connection model described in Chapter 6 but, for the shell plate, uses solid elements instead of shell elements.

Shells are a mathematical simplification of solids which are thin in comparison with their other dimensions. In Finite Element Analysis, shell elements can often provide sufficient accuracy. Unfortunately, for the calculation of SIFs associated with plate bending, there is not a suitable shell element in ANSYS. The flat plate fracture mechanics elements and associated SIF calculation methodology only consider membrane axial stress/deflection and do not include bending effects. Whereas this may be sufficient for some structures or for some small defects, the bending related SIF will become important in the T section and connection analyses as soon as the plate bends significantly, roughly when the crack has propagated through the stiffener and into the plate.

Solid elements overcome this problem as there are associated elements that can be used for the calculation of the plate surface SIFs that are affected by both membrane and bending stress. The analyses presented in this section therefore use solid elements including solid fracture mechanics elements and related methodology to allow bending as well as membrane effects to be considered by calculating SIFs on the element's structural faces as well as on the

centre of the elements. The solid element model of the stiffener is shown in Figure 8-1. Thickness, boundary conditions are as for the shell model shown in Figure 8-2 to Figure 8-4. The applied stress was 100MPa whereas for the shell model 10MPa was used. (The actual stress does not matter as the results are presented as  $Y$  values.)

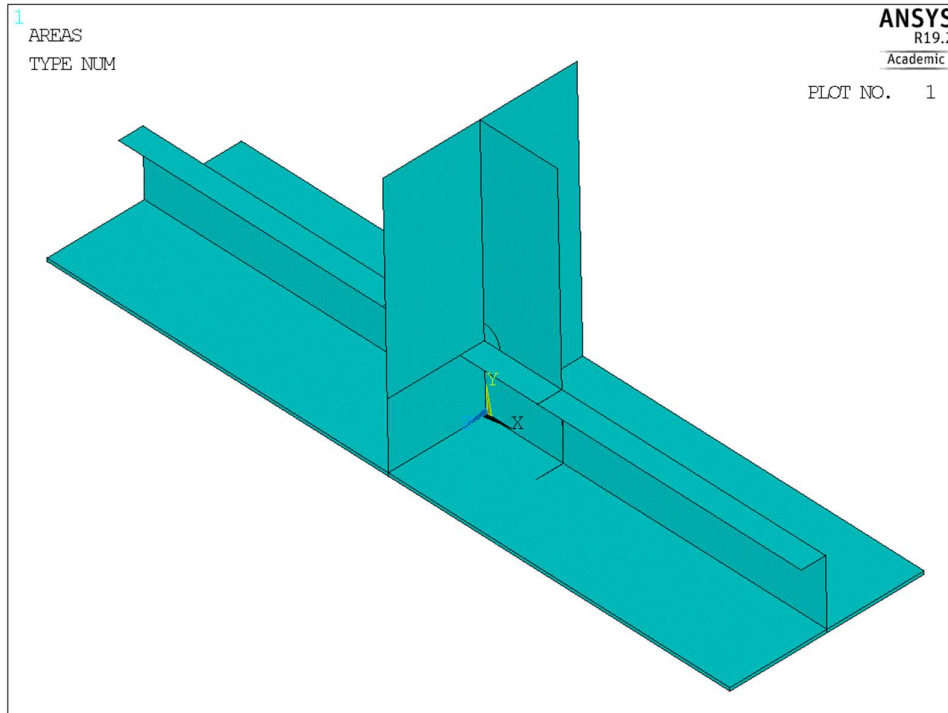


Figure 8-1 Single Stiffener model with solid elements modelling the shell plate

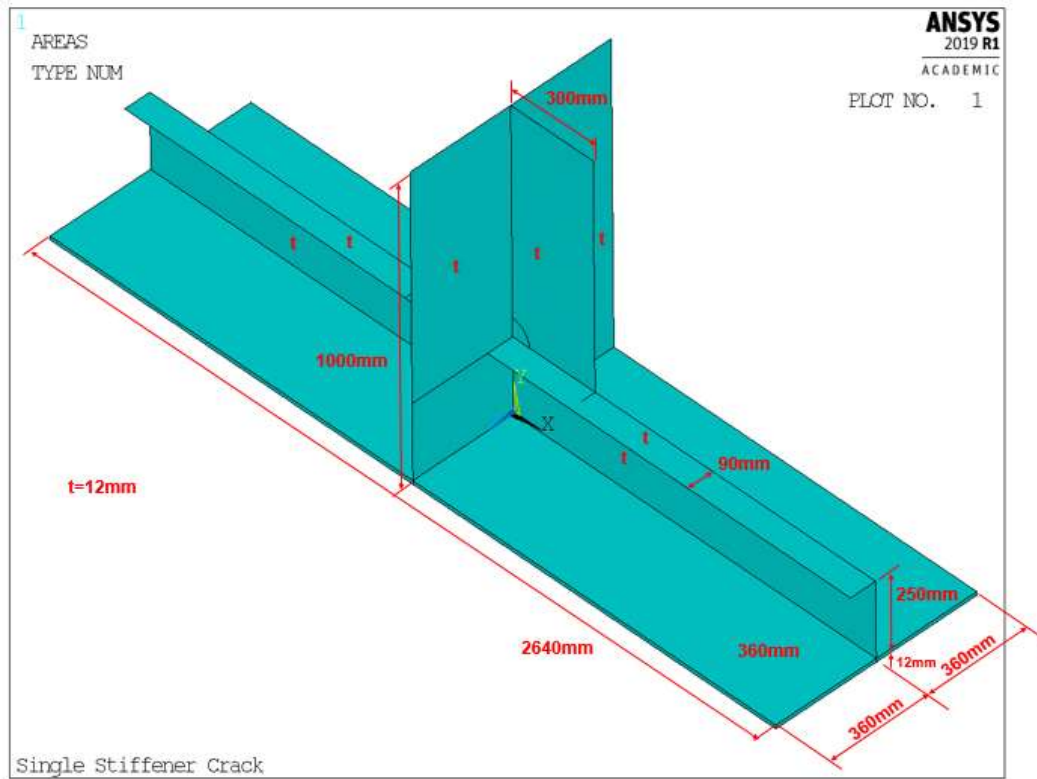


Figure 8-2 Dimensions and Thickness ( $t=12\text{mm}$ ) of solid elements model

The boundary conditions and loading applied on the single stiffener with solid element type are as shown in Figure 8-3. There are symmetric boundary conditions applied along the front and back sides of structure and the Y-direction fixed loading applied on top side.

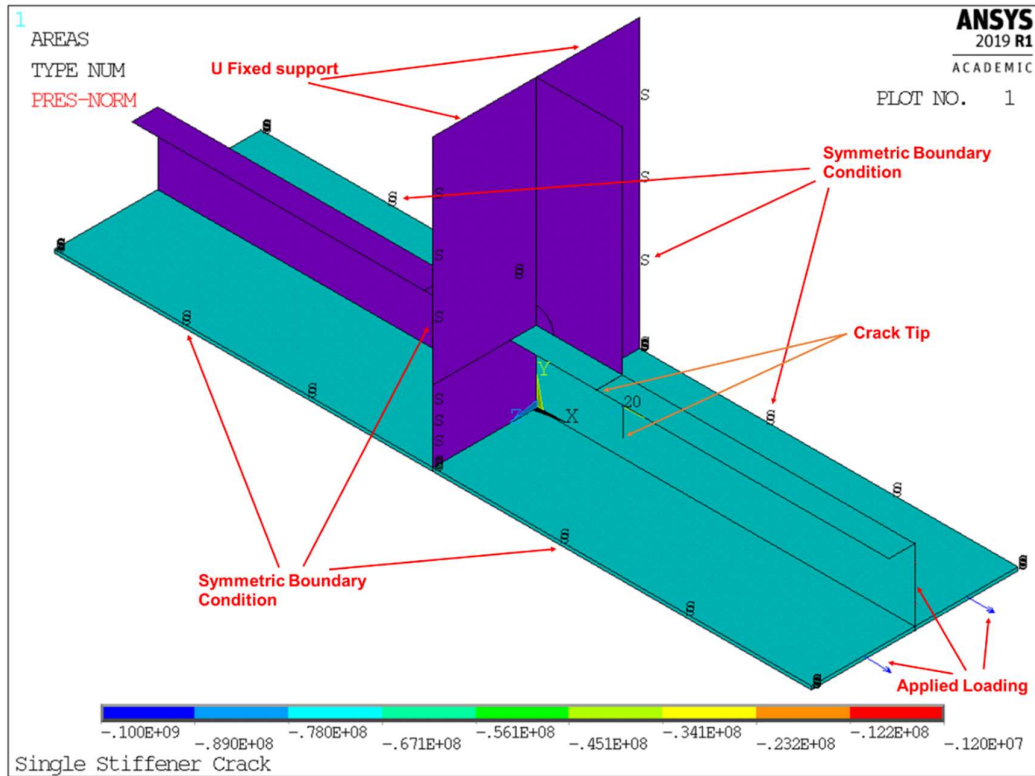


Figure 8-3 Applied boundary conditions and loading (100MPa) on solid elements

As for the shell model, the stiffener on the cracked side of the connection is not restrained at the loaded end and the symmetry boundary conditions along the side of the plate will not cause or resist a bending moment in the stiffener between the load and the crack. Therefore, as the stiffener cracks through the applied bending moment that results from the eccentricity of the load relative to the centroid of the remaining ligament of material on the cracked section can be calculated from simple statics.



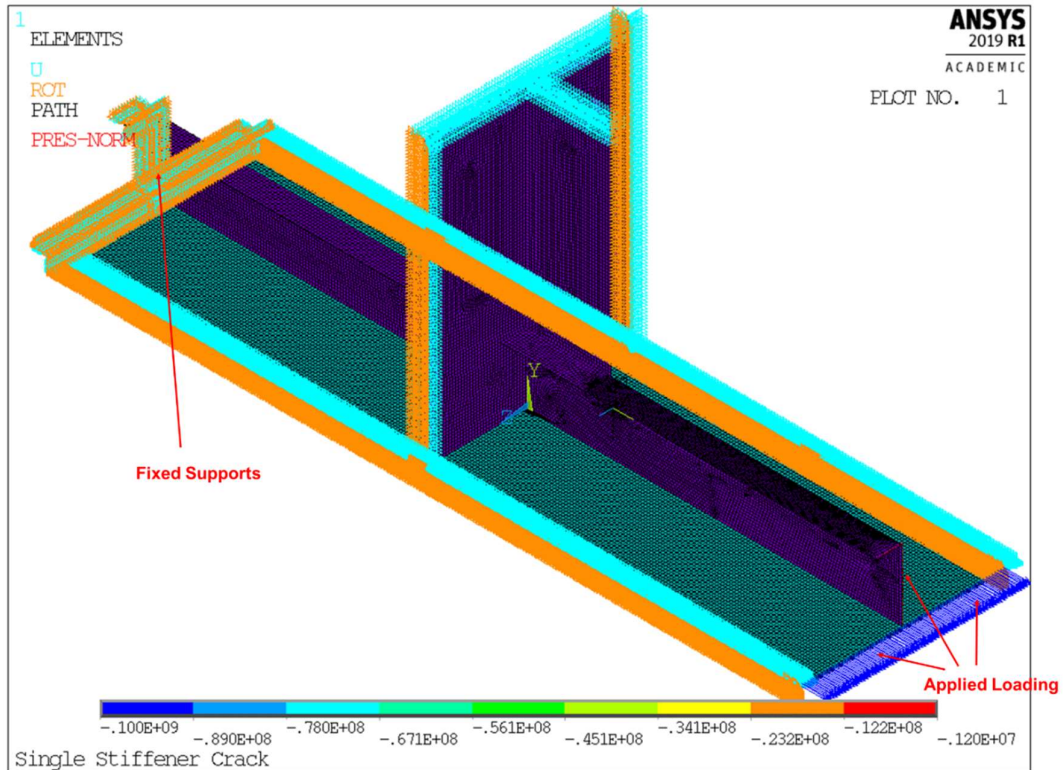


Figure 8-4 Details of mesh, support, and applied loadings (100MPa) on solid elements model

Figure 8-5 shows the  $Y$  results for shell model and middle plane in the solid model are, for  $a/d_s > 0.3$  in good agreement. For  $a/d_s < 0.3$  the shell element SIFs are about 15% greater than the solid element mid plane values. This is probably caused by the difference between the thin shell ‘zero thickness geometry’ and the actual geometry which is modelled with the solid elements. However this difference is likely to be acceptable for practical purposes, especially as the simpler shell model is conservative in comparison with solid model which is expected to be the more accurate. Overall this demonstrates that shell element modelling is satisfactory providing only the membrane SIFs are important.

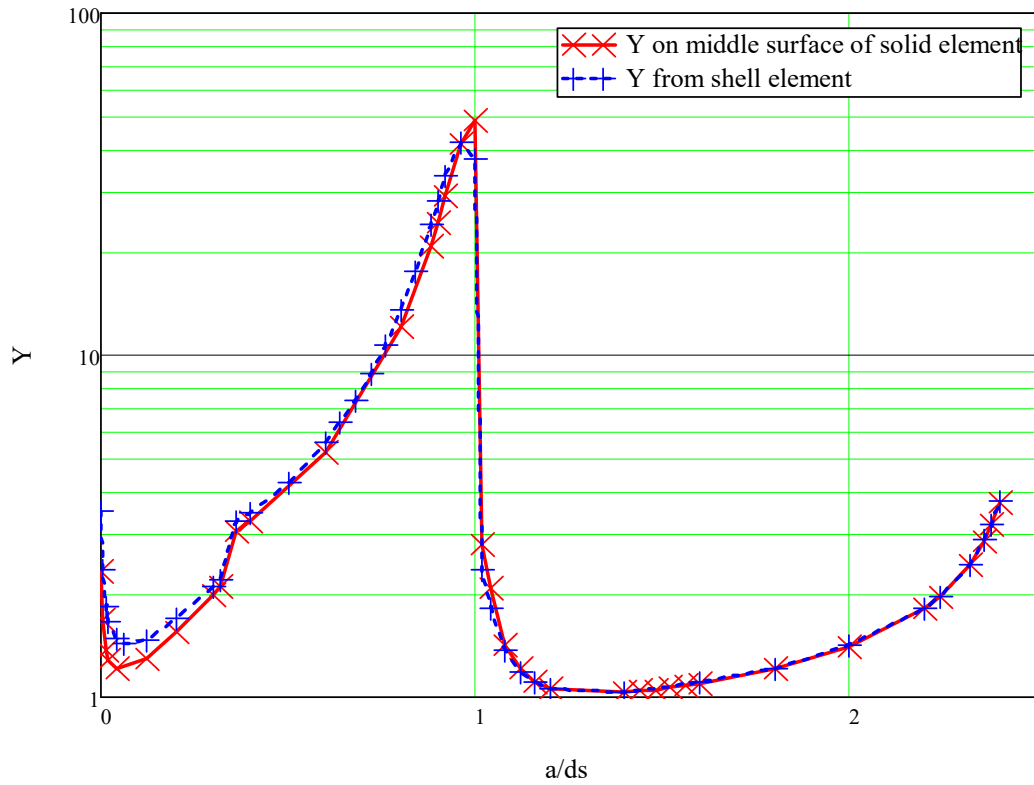


Figure 8-5 Comparisons of  $Y$  values for shell model and middle plane with solid model

For this structure and load that is the case until the crack breaks through into the plate. After the crack breaks into the shell plate the bending effect is clearly dominant, as shown in Figure 8-6.

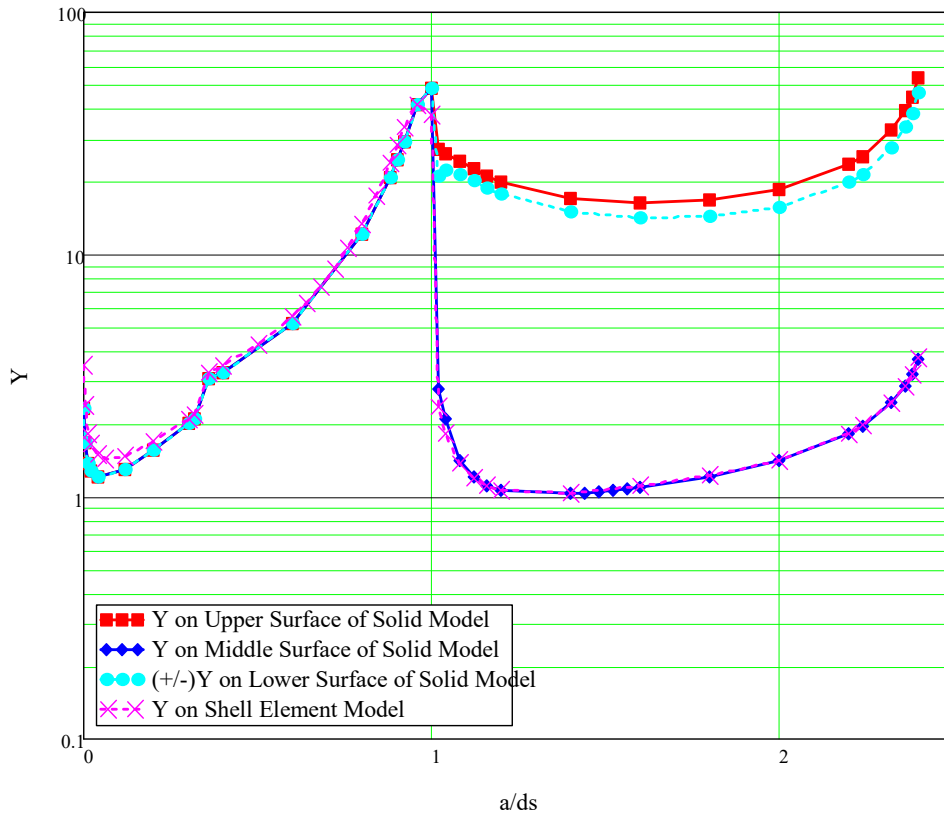


Figure 8-6 Absolute Y values for different planes in solid model and shell model type (see Figure 8-7 for definition of surfaces)

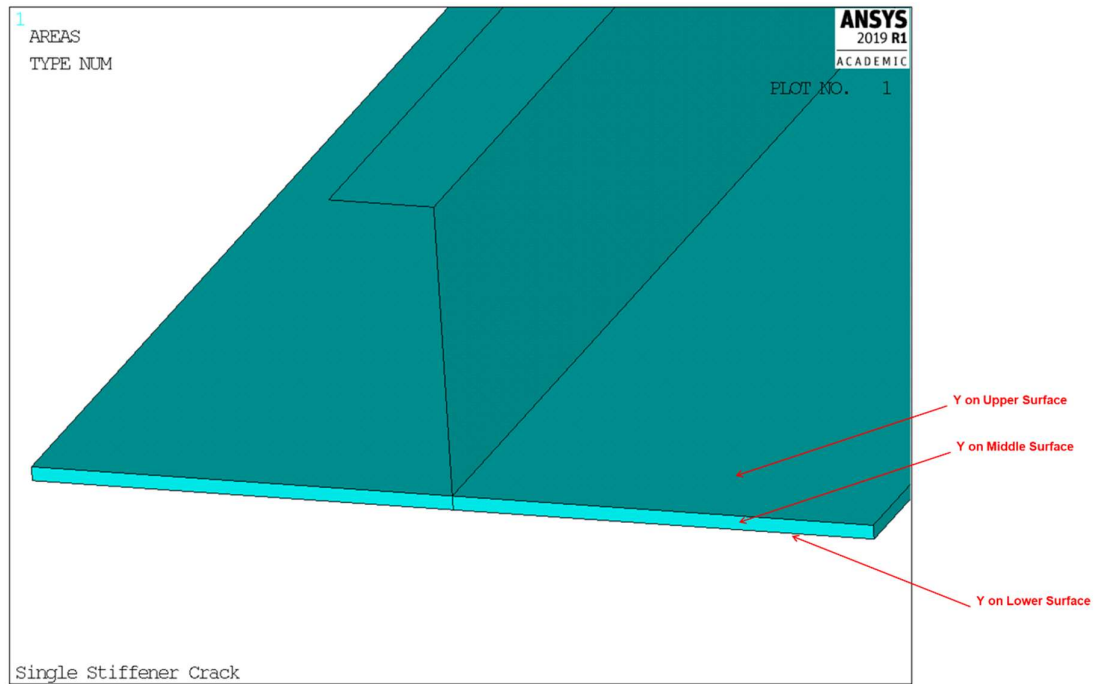


Figure 8-7 Description of Y on Upper/Middle/Lower Surface of Solid Model

Using solid elements the SIFs and hence  $Y$  values can be calculated along the crack tip from one plate surface to the other. In Figure 8-6, the results for the two plate surfaces are shown. Whilst the crack is in the stiffener  $Y$  shows negligible difference at the two crack surfaces.

Once the crack breaks through into the shell plate a very large  $Y$ , associated with plate bending occurs. This is because the shell has to bend to maintain the equilibrium. The SIFs and hence the calculated  $Y$  values output by ANSYS are always positive but, arguably, should be positive on the stiffener side of the shell plate and a negative SIF on the opposite side.

Note that the analysis performed is linear, so on the tension side of the crack the crack faces separate. However on the compression side the surfaces

are predicted to overlap. This clearly cannot happen in practice but a non-linear analysis would be required to model the crack closing and the surfaces not overlapping. An analysis of this type for a simple plate is included in Appendix B but the method has not been applied to a stiffener connection in this work.

There is likely to be some transverse bending in the stiffener flange and web as a result of the asymmetry of the stiffener flange, however that affect will be more important when there is a moment applied to the stiffener and appears to be small in this case.

For the crack sizes after the breakthrough to the shell plate, the average value of the ratio between upper SIFs (bending + membrane stresses) and middle SIFs (membrane only) is, after allowing for the correct sign of the SIF, in the interval 12 to 17.5, see Figure 8-8.

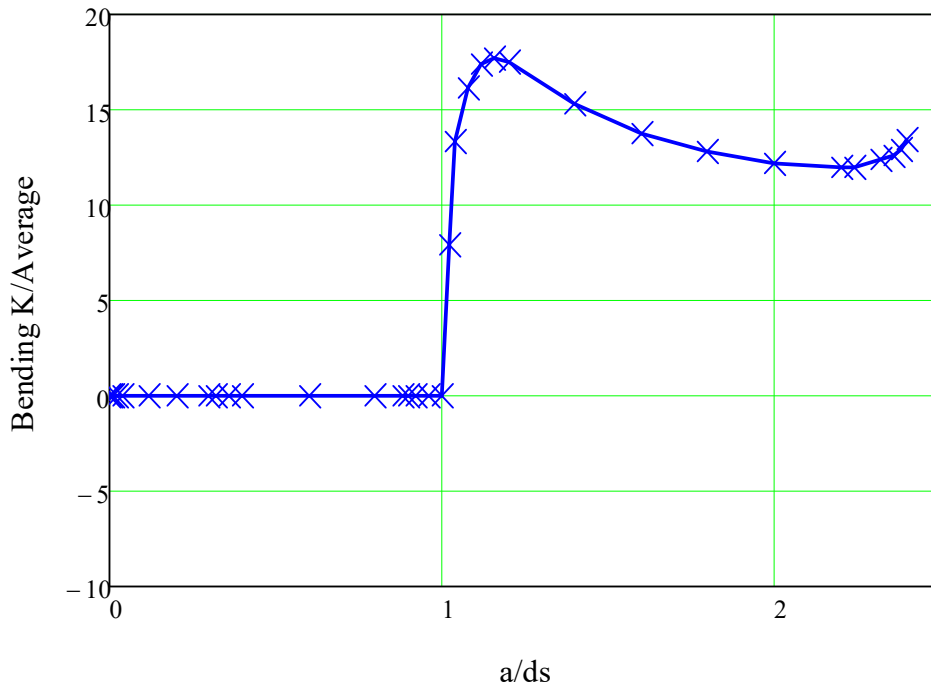


Figure 8-8 Ratio between bending  $Y$  values and average  $Y$  values (Bending  $Y$  value is  $(Y_1 - Y_2)/2$ , where  $Y_1$  and  $Y_2$  are the opposite surface  $Y$  values)

## **8.2 Prediction of the bending SIFs in the plate after the stiffener has broken**

It has already been shown that good estimates of SIFs or  $Y$  values can be obtained until the stiffener is close to cracking through. The estimation of SIFs after stiffener the cracking through, when the crack is crossing the shell plate and resulting in a lot of bending is now investigated.

This case is not usually interesting at the design stage because the design fatigue limit state will be reached with smaller cracks. It is, however, of interest when performing structural reliability analysis and considering the failure probability associated with overall hull girder failure or leakage of fuel/cargo which may result from this type and extent of cracking. If there was sufficient information available to properly understand the state of a ship casualty, it would also be of interest when assessing how the casualty is breaking up. Whilst, even in the recent past, that detailed information would not usually have been available, drones are capable of providing more information and so these types of calculation may become relevant when deciding how to deal with a casualty.

1  
DISPLACEMENT  
STEP=1  
SUB =1  
TIME=1  
DMX =2.3992

**ANSYS**  
2019 R1  
ACADEMIC

PLOT NO. 1

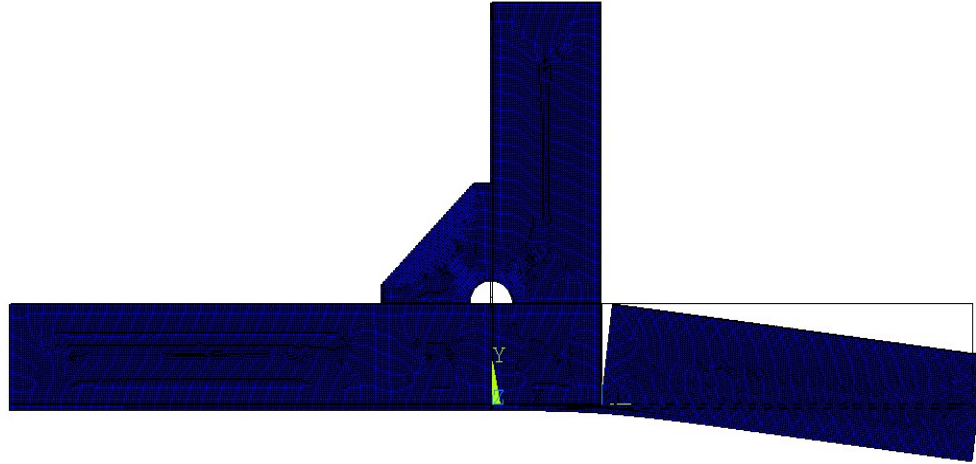


Figure 8-9 Connection with the stiffener just completely cracked

Owing to the loading and stiffness effects after the stiffener breaks (Figure 8-9), the prediction of the bending SIFs is difficult. However, for the linear case, where material overlap in the compressive part of the crack is permitted, a relatively simple formula, based on SIF solutions (Paris and Sih, 1965) Equations (8.1), that was empirically fitted to the bending SIF from ANSYS:

$$K = f_r \cdot \sigma_b \cdot \left[ f \cdot \sqrt{\pi \cdot (a - ds + as)} + \frac{1.0 \cdot (1 - f) \cdot W}{\sqrt{\pi \cdot (a - ds + as)}} \right] \cdot \left[ \frac{1}{1 - \frac{a - ds + as}{(0.5 \cdot W) + as}} \right]^p \quad (8.1)$$

Where

$a$  = crack length measured from the web flange intersection

$a_s$  = empirical additional crack length (25mm)

$d_s$  = stiffener depth (250mm)

$W$  = plate width (720mm)

$\sigma_b$  = applied average bending stress on shell plate surface

$f$  = empirical factor on the moment that is uniformly distributed over the plate width = 0.6

$1-f$  = empirical factor on moment concentrated at the middle of the plate / crack = 0.4

$fr$  = empirical factor = 0.5

$p$  = empirical power to increase  $K$  as it approaches the plate edge

There is no guarantee that this formula will work with other dimensions of stiffener and plate but it is interesting that to approximately fit the ANSYS calculated SIFs it was helpful to apportion (using  $f$  and  $1-f$ ) solutions for moments both distributed uniformly over the plate and concentrated at the centre of the shell plate i.e. in line with the stiffener which, at its broken end, might be expected to result in a local concentration of applied moment.

The overall empirical factor  $fr$  may account for the stiffeners either side of the cut preventing bending in the plate and reducing the amount of strain energy stored in the plate but this has not been demonstrated in this work.

The factor  $p$ , which would be 1 for a simple edge crack.



The result, including the simplified formula membrane stress, is shown in Figure 8-10.

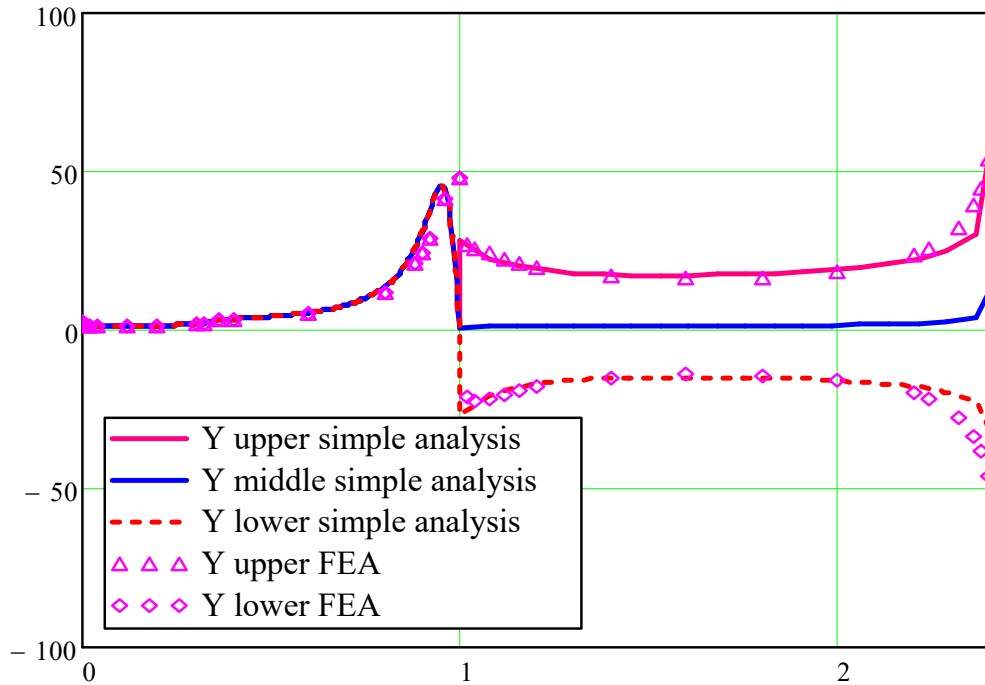


Figure 8-10 Y values, including plate bending (linear scale)

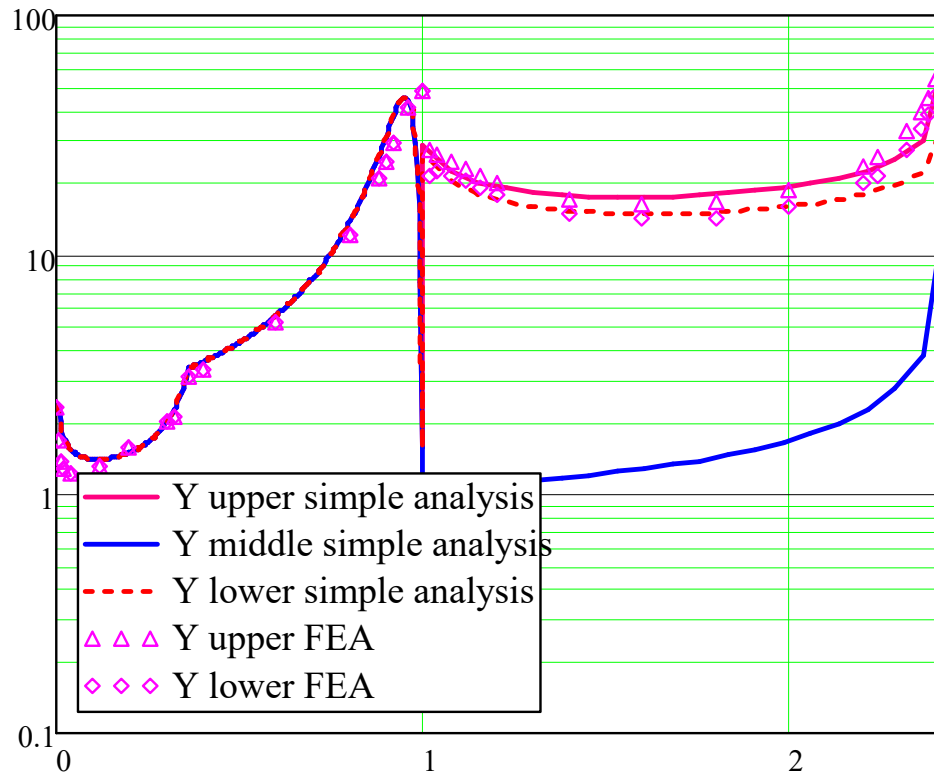


Figure 8-11 Y values, including plate bending (log scale)

Even though the empirical estimate contains three empirical coefficients, it is not highly accurate but it does demonstrate the observed behaviour, probably includes some of the physical behaviour and could lead to a better estimating formula. Note that the method used is linear and does not account for crack closure, which should reduce the plate bending Y values.

### **8.3 Conclusions for simplified modelling of connection with plate bending included**

The solid element and shell element models predicted very similar  $Y$  values when the crack was confined to the stiffener but the shell elements and related membrane-only fracture mechanics elements could not include the effect of the plate bending stress once the crack penetrated the shell plating and the stiffener was broken.

The solid element model was able to handle the crack extending into the shell plating. However the linear model used did not account for partial crack closure and this is likely to have overestimated the  $Y$  values.

The methodology for predicting the membrane  $Y$  values, derived in Chapter 6, was satisfactory for predicting the centre plane  $Y$  values of the solid model.

A physically based but nevertheless highly empirical formula was derived to approximate the bending  $Y$  values, excluding crack closure, when the crack is in the shell plate.

## Chapter 9 Comparison of Stress Concentration Factors calculated using stress extrapolation and singularity strength estimation

The ship component analysed is shown in Figure 9-1. The crack starts in the stiffener outstand at the flange web junction. The numerical results were obtained using ANSYS. The unit system was defined consistently as length-*m*, time-*s*, mass-*kg*, force-*N* and stress-*Pa*, 2D elements (Shell63) were used as bending effects were expected to be small until the crack broke through from the stiffener into the plate. Around the structural connections there were very fine densities of mesh.

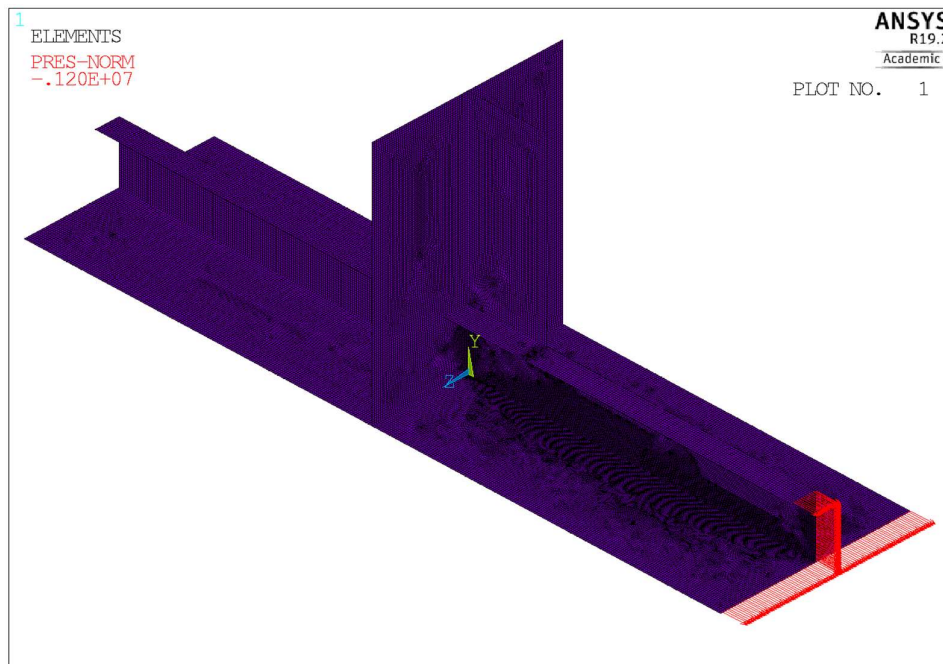


Figure 9-1 Principal fine mesh model of the ship components

## **9.1 SCF Assessment from LEFM**

The nominal stress range for the location where the fatigue assessment is being conducted may need to be modified to account for local conditions that affect the local stress at that location. The ratio of the local to nominal stress is definition of the Stress Concentration Factor (SCF). Depending on specific situations, different SCF may apply to different nominal stress components and while it is most common to encounter SCF values larger than 1.0, therefore signifying an amplification of the nominal stress, there are situations where a value of less than 1.0 validly exists.

Weld defects, cold laps and undercuts of varying size and shape, are often present at the weld toe in welded joints. As illustrated previously, weld defects were found in the majority of the batches analyzed and together with the variation in local weld geometry, this will increase the scatter in the fatigue data.

The hot-spot stress is the structural stress at the weld toe. It is usually necessary to determine it by extrapolation from the stress distribution approaching the weld. The hot-spot stress method is to use the S-N curve approach obtain the results from tests on actual welded joints. Nominal stress is easy to define in simple laboratory specimens. However in real structures, the presence of gross structural discontinuities, non-uniform stress distributions and through-thickness stress gradients can be complex that the nominal stress is no longer obvious. Experimental and numerical (e.g. FEA) stress analysis methods are capable of providing detailed information about the stresses arising near welded joints. Stresses are dropping as the distance from the corner is getting bigger, at the end it will drop even lower than the nominal stress. This is because close to the corner, stresses increases due to the stress concentration caused by

the corner, within a small distance the stresses are much higher than the nominal stress.

The SCF prediction methodology is illustrated in the method of a crack propagating from an initial size (0.25mm) to a size corresponding to design failure of the component and several definitions are possible for the final crack growing through the plate width seemed reasonable, considering the thickness of the ship hull plates applied in practice.

At the moment the most common method to get the SCF is the linear extrapolation method. The hot-spot stress at the corner is obtained by linear extrapolating the stresses at  $\frac{1}{2} t$  and  $\frac{3}{2} t$  away from the corner.

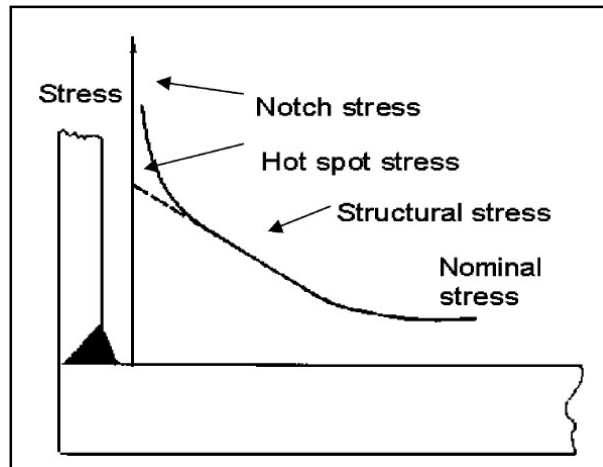


Figure 9-2 Stress distribution approaching a welded joint and the definition of the hot-spot stress (Maddox, 2003)

Normally cracks occur at the connection weld areas. To define the maximum stresses in the connection weld areas, the SCF (or  $K_t$ ) is considered. This coefficient takes into account the existence of irregularities and

discontinuities in the structure which leads to a higher stress in this area than the nominal stress.

$$SCF = \frac{\sigma_{\max}}{\sigma_0} \quad (9.1)$$

— $\sigma_0$  is the nominal stress for the fracture mechanics calculations

— $\sigma_{\max}$  is the maximum stress at the discontinuity

The sharp corners are singularities and it means these sharp corners have an infinite stress. However FEA method will generally not predict an infinite stress and the actual predicted peak stress will depend on the element size and will generally increase as the element size decreases (as shown in Figure 9-2).

The existing guidance on determination of sharp corner stresses is in terms of linear extrapolating stresses based on a number of plate thickness  $t$  away from the singularity to the corner; for example, some Classification Societies recommend the linear extrapolation from  $0.5t$  and  $1.5t$ , See Figure 9-3.

A simple analysis might suggest that the infinite stress would result in a structure with inadequate ultimate and fatigue strength but that is not the case because materials can resist localized high stresses. Indeed when a structure contains a crack it also has infinite stresses at crack tip according to the linear theory and fracture mechanics methods are normally applied in fatigue crack growth of cracked structures (Xu and Barltrop, 2007a).

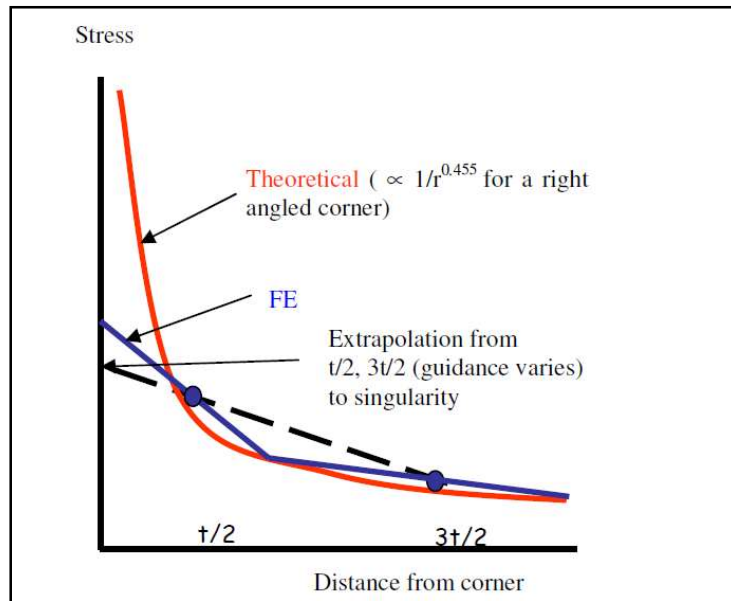


Figure 9-3 Typical existing guidance on determining sharp corner stresses (Maddox, 2001)

## 9.2 Comparison of the different models

For the 2-D models with right angled and 135 degree corner, there is previous work has given the method for the estimation of  $as$  to calculate the stress distribution without doing the FEM analysis on structures. However, in reality, 3-D models are more generally used in real engineering structures. Therefore it would be interesting to focus on to investigate the stress distribution at 3-D model corners and try to find the stress concentration factors for different 3-D structures with FEM Analysis and estimate the stress singularity at the sharp corners, see Figure 9-4 and Table 9-1.



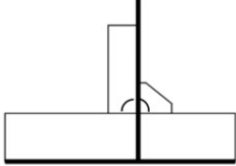
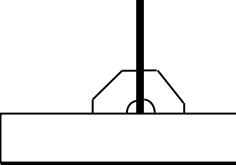
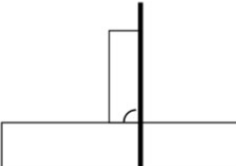
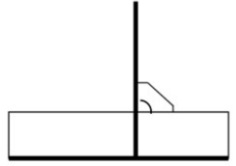
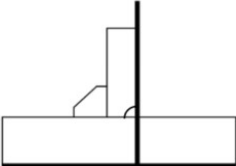
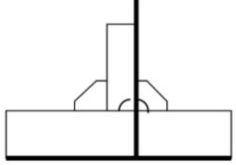
<p>Model 1 <math>L_c = 600\text{mm}</math></p>	
<p>Model 2 <math>L_c = 600\text{mm}</math></p>	
<p>Model 3 <math>L_c = 300\text{mm} - 60\text{mm} = 240\text{mm}</math></p>	
<p>Model 4 <math>L_c = 300\text{mm} - 60\text{mm} = 240\text{mm}</math></p>	
<p>Model 5 <math>L_c = 600\text{mm} - 60\text{mm}</math></p>	
<p>Model 6 <math>L_c = 900\text{mm}</math></p>	

Table 9-1 Different models of the single stiffener structure showing connection length:  $L_c$

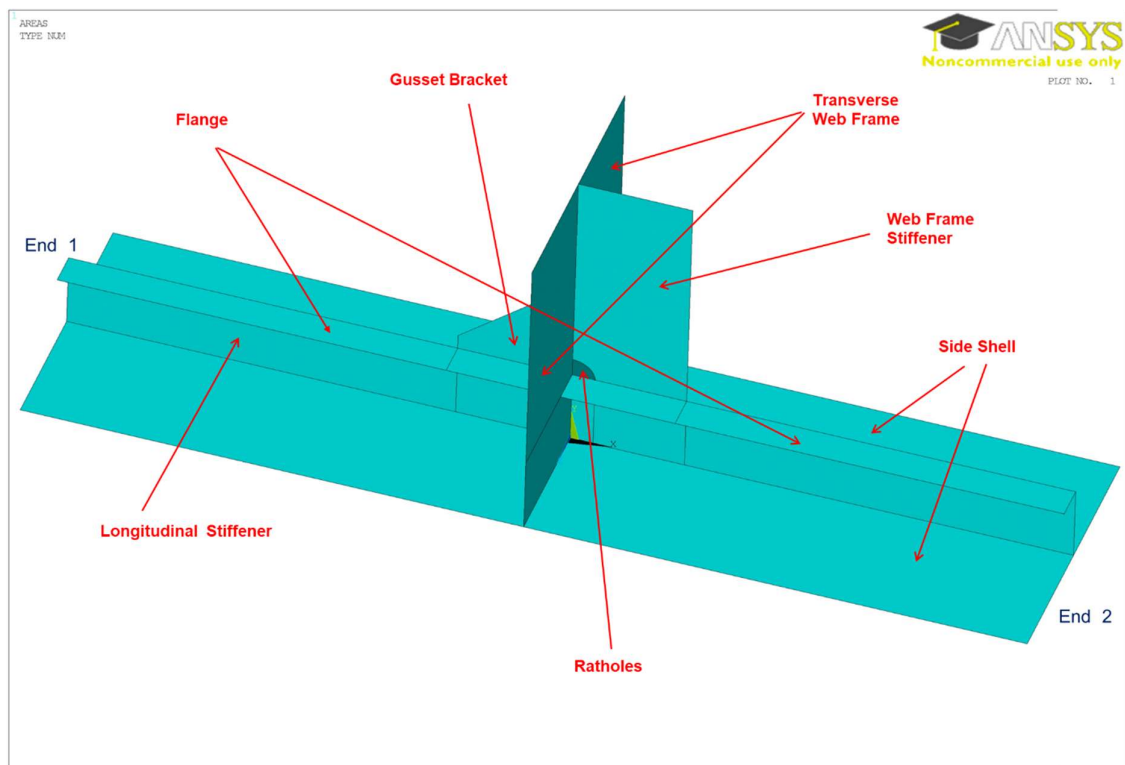


Figure 9-4 Structure parts definition in 3-D coordinates

The stresses along Y and Z axis on the coloured lines (X, Y and Z) will be calculated and saved in the FEA, they are called as stress lines, see Figure 9-5. The SCF values will be calculated based on the stress lines. The two Y lines (in blue) start from the bracket corner and vertical stiffener corner separately in Model 1. The tension and bending moment cases focus on the X-direction stresses on Line Y.

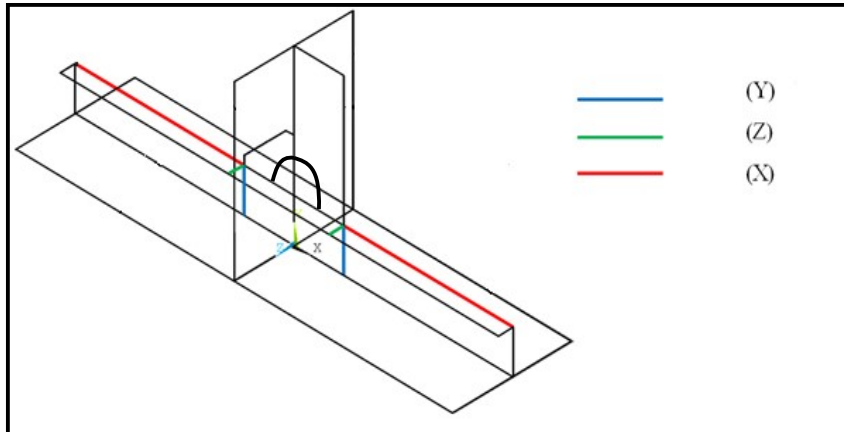


Figure 9-5 Localization of the stress lines (X, Y and Z direction)

### 9.3 Results and Analysis

The comparisons of displacement plots for Mode 1 under different loading cases are given in Figure 9-6, Figure 9-7 and Figure 9-8.

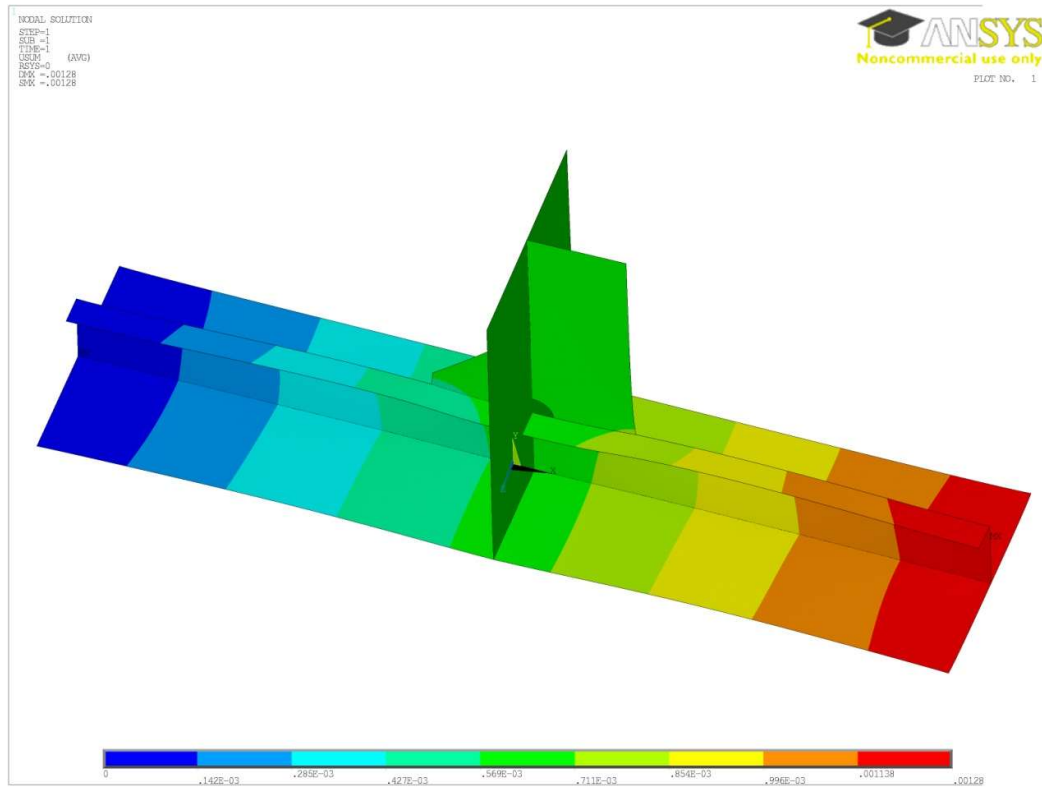


Figure 9-6 Displacement Plot under Tension Loading

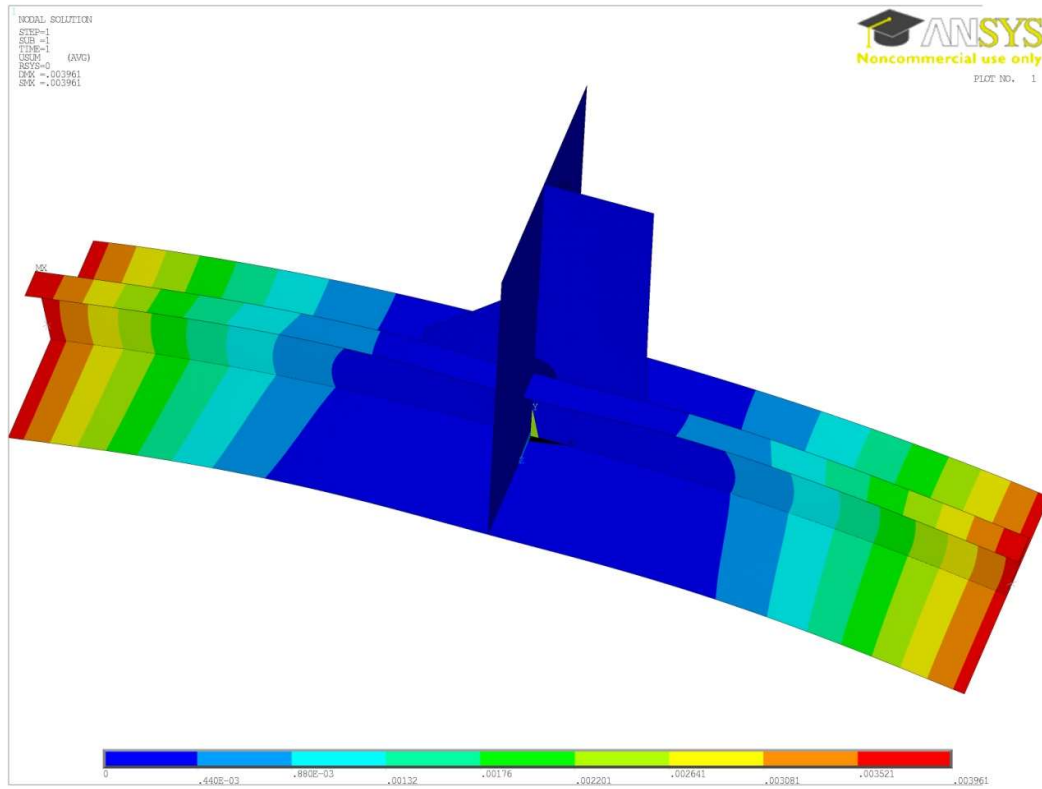


Figure 9-7 Displacement Plot under Pure Bending Loading

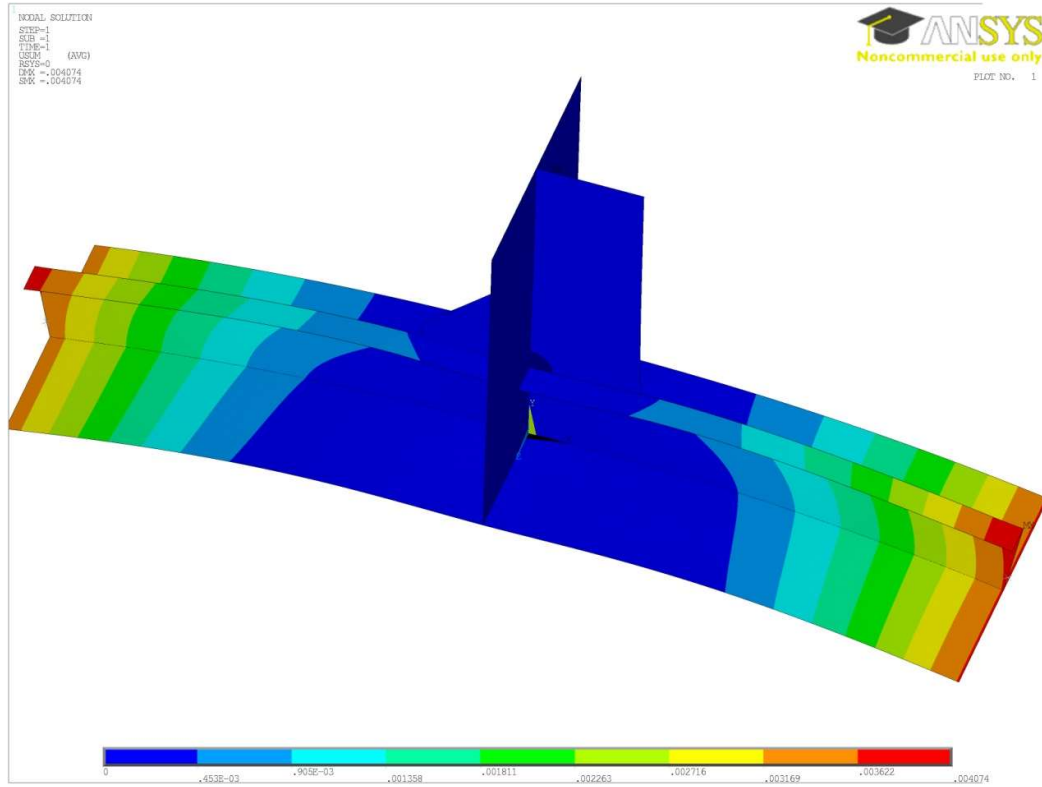


Figure 9-8 Displacement Plot under Tension and Bending Combined Loading

For Model 1, the stress contour plots for each corner under tension loading are shown below with a zoom-in picture showing the stress concentration at each corner. It can be seen that the maximum stress and minimum stress (in negative signal) at the bracket corner and vertical stiffener corner, occur separately.

Chapter 9 Comparison of Stress Concentration Factors calculated using stress extrapolation and singularity strength estimation

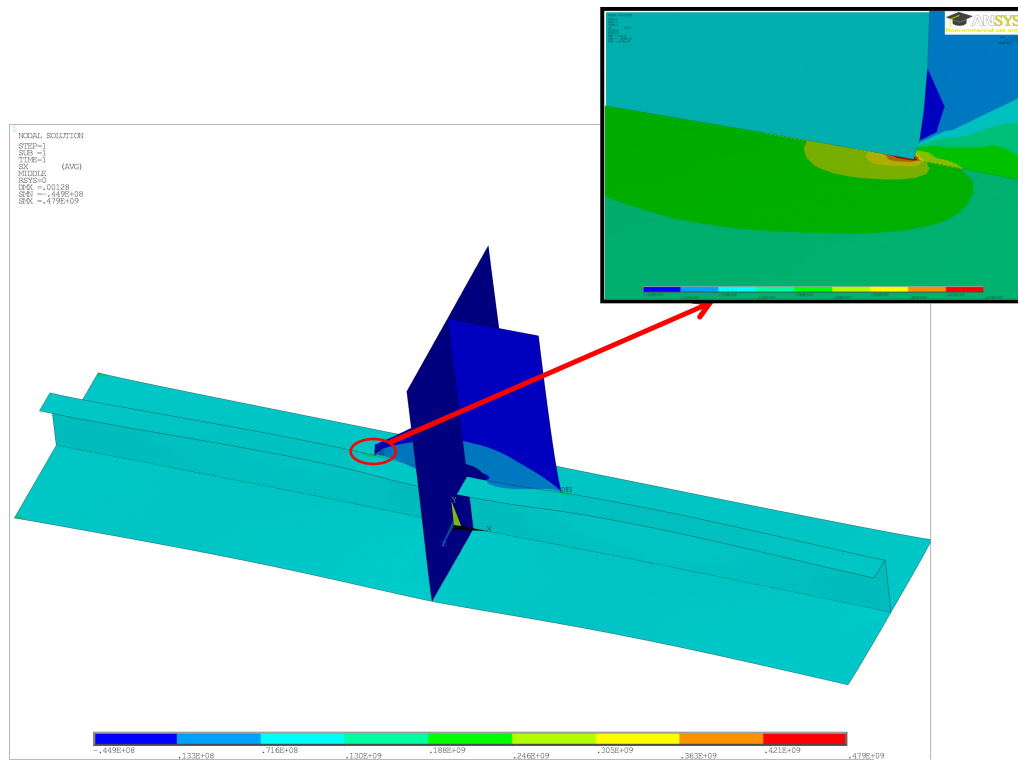


Figure 9-9 Stress Concentration at bracket corner in Model 1 (Max Stress)

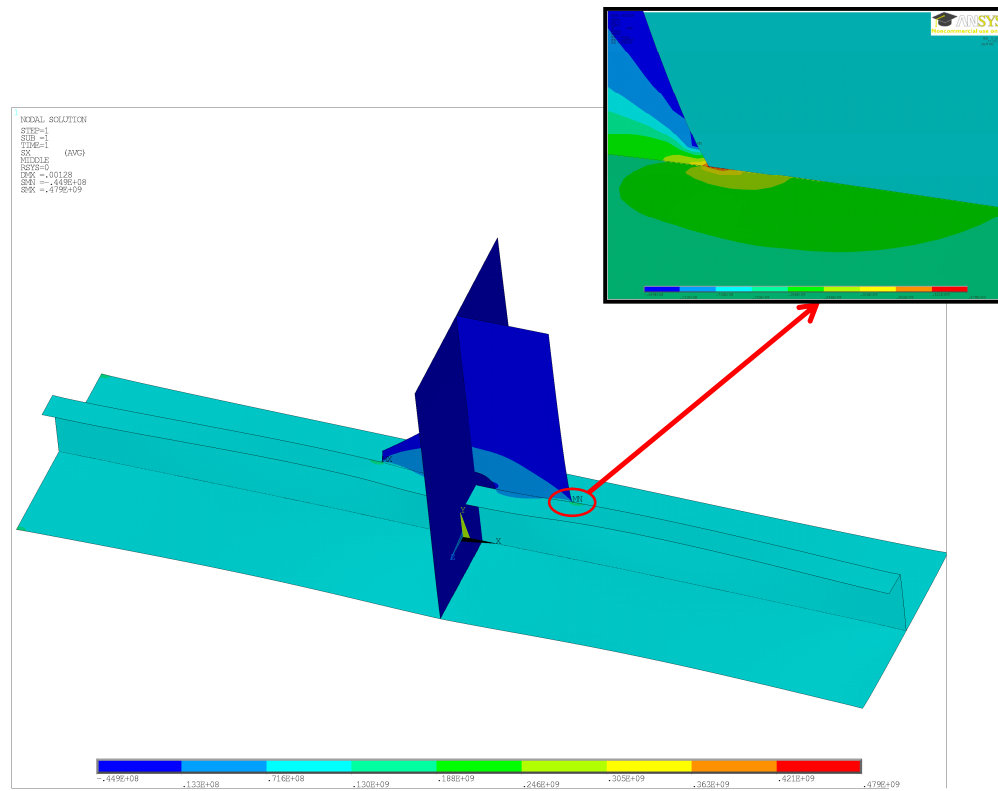


Figure 9-10 Stress Concentration at vertical stiffener corner in Model 1 (Min Stress)

The stress distribution curves at each corner on different  $Y$  lines under tension are given in Figure 9-11. Because Model 2 is supported symmetrically structure with its bulkhead, the two stress distribution curves for  $Y$  lines in Model 2 are nearly coincide. Based on Figure 9-11, it can be seen that the stress from Model 6 Left and Model 6 Right are the highest showing higher stress concentration and stresses from Model 3 and Model 4 giving the lowest stresses with the same loading, comparing with other models. Stress concentrations in Model 1, Model 2 and Model 5 are very close and slightly less than the stresses from Model 6.



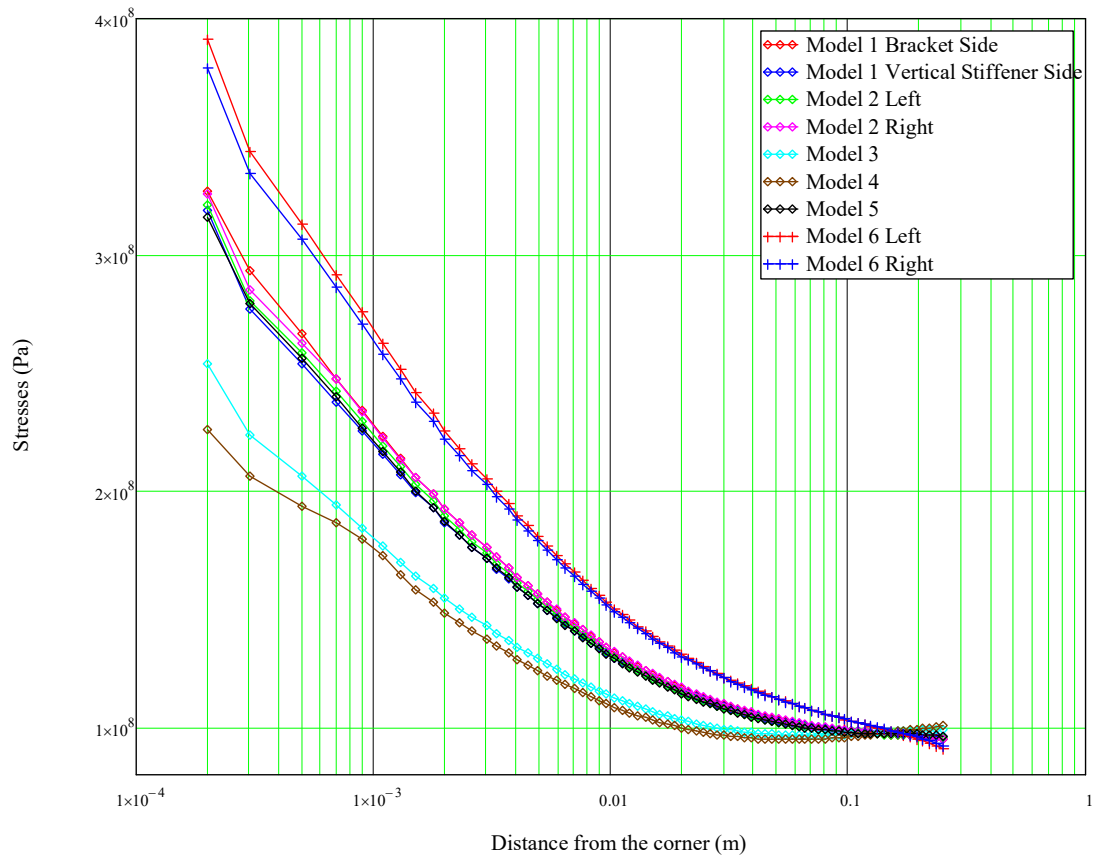


Figure 9-11 Stresses on Line Y (Stress Line on longitudinal stiffener) under tension loading nominal stress= 100MPa

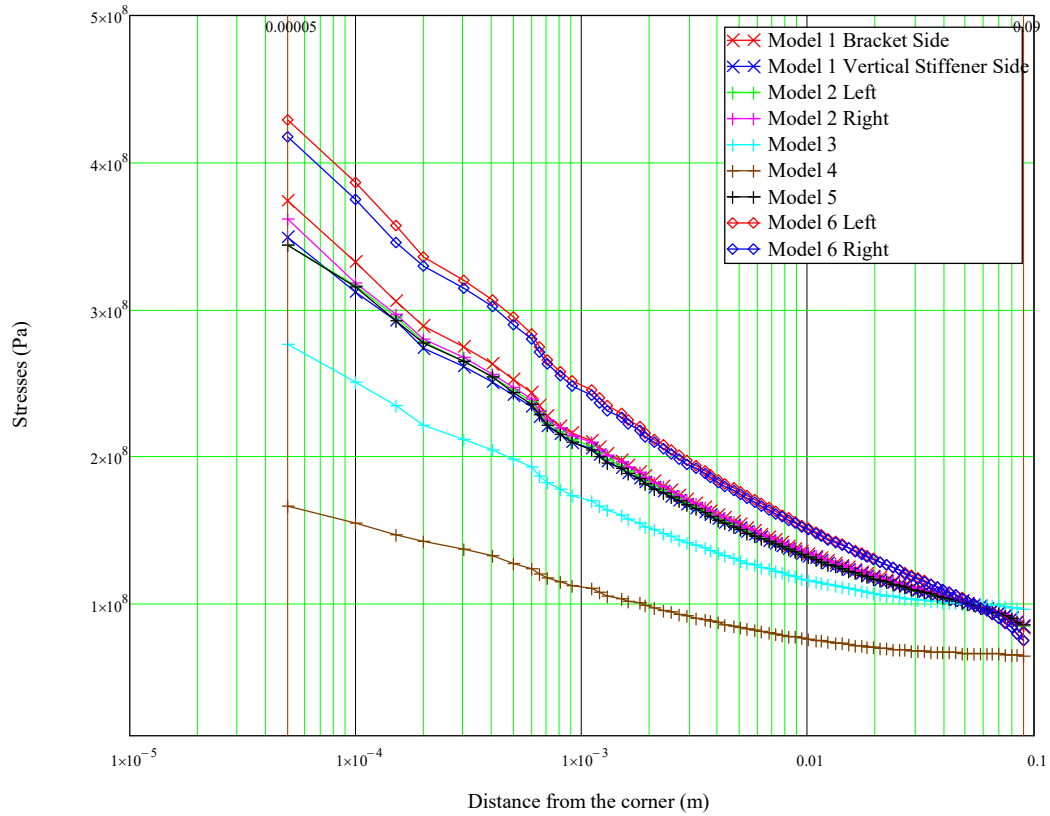


Figure 9-12 Stresses on Line Y under Bending Moment  
(nominal flange stress = 100MPa)

It is interesting to compare the shape of the tension curves with the theoretical curve [Equation (2.24)] for a notch,

$$\sigma(x) = \frac{\sigma_0(as+x)}{\left[ \left( 2 \left( \frac{1}{2p} \right) \cdot x \cdot as \left( \frac{1}{p} - 1 \right) \right)^q + x \left( \frac{q}{p} \right) \right]^{\frac{p}{q}}} \quad (9.2)$$

where,  $q = 3p - 0.5$

This is done in Figure 9-13, where the black curve with solid diamonds shows the shape of the power = 0.455 stress distribution which was expected for a right angled corner. It is found that a power of 0.25 is a better (though not good) fit. This suggests that the stress concentration effect is less than for a coplanar attachment (0.25 corresponds to a coplanar attachment with an angle greater than 135 degrees whereas 0.455 corresponds to a 90 degree angle).

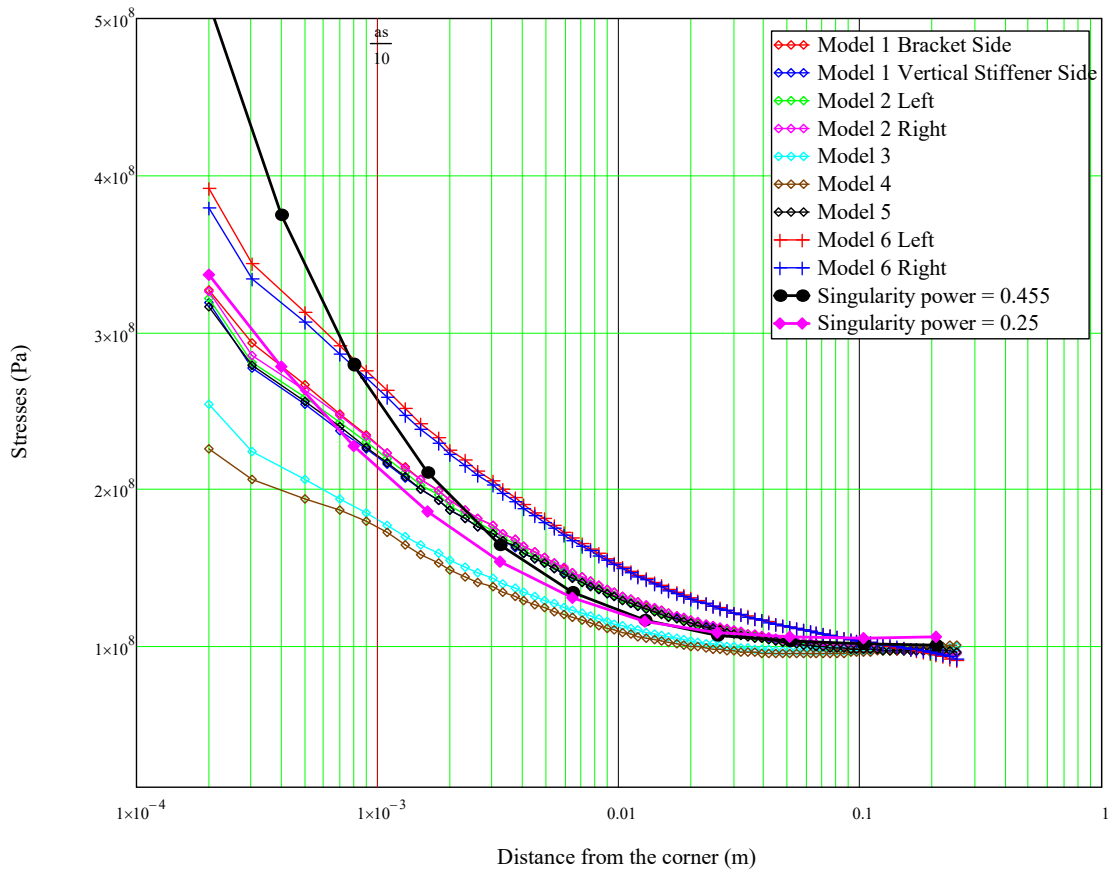


Figure 9-13 Stresses on Line Y under Tension, compared with  
 1) expected decay for a corner ( $p = 0.455$ ) and  
 2) better (though not good) fit ( $p = 0.25$ )

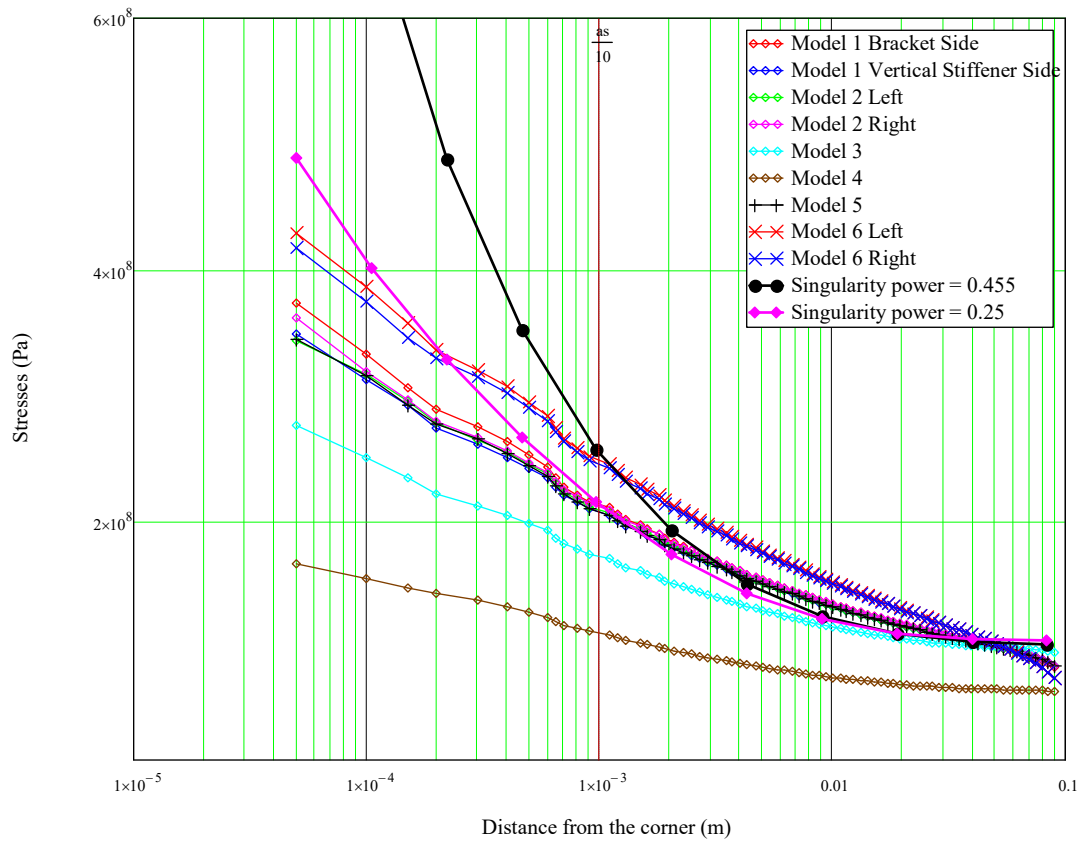


Figure 9-14 Stresses on Line Z (on Flange) under Tension, compared with  
 1) expected decay for a corner ( $p = 0.455$ ) and  
 2) better (though not good) fit ( $p = 0.25$ )

This confirms the findings of the SIF based calculation that the connection between the angle shell stiffener and the frame stiffener is behaving differently to a coplanar attachment to the edge of a plate.

In the next section the estimation of SCFs, for the connection is considered.

## 9.4 SCFs from stress extrapolation

The Hot-Spot stresses at the crack corner and the SCF values, obtained by extrapolation from points  $3t/2$  and  $t/2$  away from the corner, to the corner for each model with tension loading, showing in Table 9-2 (The position of Right side and Left side is based on description in Table 9-1).

Model	1-Right	1-Left	2	3	4	5	6-Left	6-Right
$\sigma_{t/2} (MPa)$	149.1	146.0	147.0	124.2	119.6	145.6	172.1	170.3
$\sigma_{3t/2} (MPa)$	118.4	111.0	117.0	104.3	101.0	116.4	133.4	133.4
$\sigma_{hst} (MPa)$	164.5	163.5	162.0	134.1	128.9	160.3	191.5	189.1
SCF	1.645	1.635	1.62	1.341	1.289	1.603	1.915	1.891

Table 9-2 Hot-Spot Stress and SCF for each Model under Tension Loading

Chapter 9 Comparison of Stress Concentration Factors calculated using stress extrapolation and singularity strength estimation

Model	1-Right	1-Left	2	3	4	5	6-Left	6-Right
$\sigma_{1/2} (MPa)$	148.0	145.5	146.1	125.3	81.55	144.9	167.5	169.0
$\sigma_{3/2} (MPa)$	120.2	119.1	119.0	107.6	70.7	118.5	132.8	132.8
$\sigma_{hsb} (MPa)$	161.8	158.8	159.6	134.2	86.97	158.1	185.2	187.1
SCF with nominal Flange Stress	1.618	1.588	1.596	1.342	0.87	1.581	1.852	1.871

Table 9-3 Hot-spot Stress for each Model under Bending Moment (nominal flange stress = 100MPa)

The SCF results in Table 9-2 and Table 9-3, are compared with values determined from the dimensions and  $as = \text{connection length}/25$

## 9.5 Estimation of stress concentration factors SCFs

For the different stiffener configurations studied in this chapter, the SCFs estimated from the stress distributions, using  $\frac{3}{2} t$ ,  $\frac{1}{2} t$  extrapolation to the corner, on lines parallel to the shell stiffener and normal to the shell stiffener were given in Section 9.4.

The SCFs are now simply estimated from the  $as$  values (shown in Table 9-1) using the formulae given in Section 2.4.7.1.  $\left( as = \frac{L}{25} \cdot \left( \frac{tfs}{tw + tf} \right)^{0.5} \right)$  as discussed there, the  $SCF_p$  formula was derived for a simple cruciform and the  $SCF_r$  formula was an adaption for an angle stiffener connection (that was based on the assessment of the SIFs at small crack sizes).

$$SCF_p = 0.55 \cdot \left( \frac{as}{mm} \right)^{0.48} + 0.9 \quad (9.3)$$

$$SCF_r = 1.4 \times 0.55 \cdot \left( \frac{\frac{25}{190} \cdot as}{mm} \right)^{0.48} + 0.9 \quad (9.4)$$

The results from the FEA are compared with the two SCF prediction formulae in Figure 9-15.

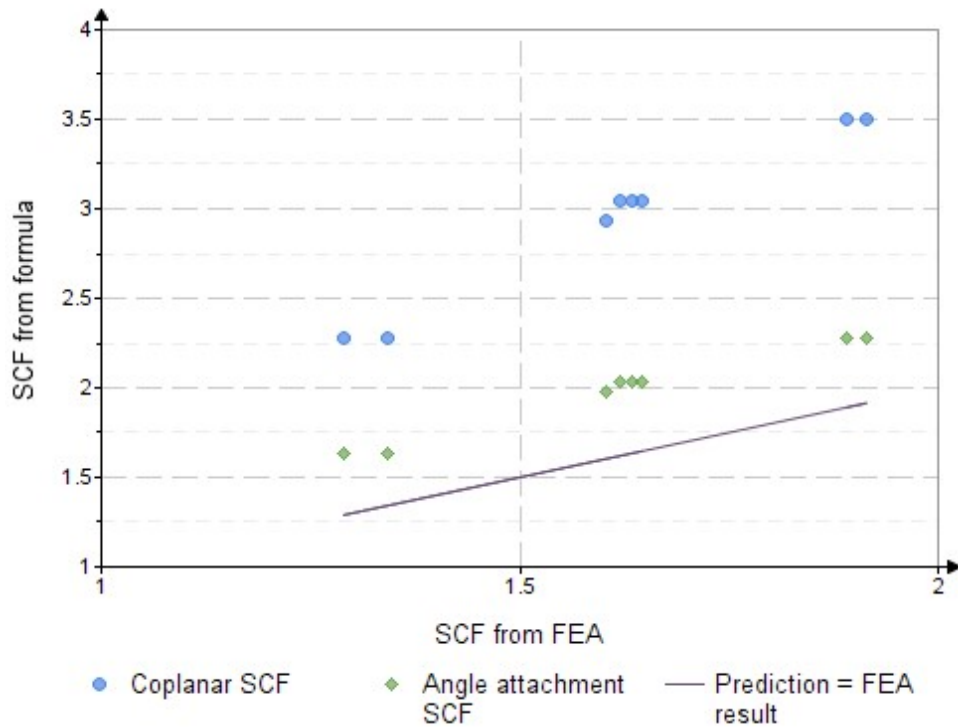


Figure 9-15 FEA SCF results ( $SCF_{fe}$ ) extrapolated on transverse (y) line compared with predictions from the cruciform formula ( $SCF_p$ ) and the revised stiffener connection formula ( $SCF_r$ )

The results show an over prediction of the FEA SCF values by 1.7 to 1.88 for the cruciform SCF formula, which is not surprising as the stress concentration was seen in the previous section to be less than for a cruciform. Using the revised formula that is more applicable to this detail and based on parameters that fit SIF results from Barltrop and Xu (2011) the method still overestimates the SCF but only by 1.2 to 1.26.

Considering the very different methods used for the SCF calculations:

1. extrapolation of stresses from the FEA compared with



2. estimation of the  $as$  value from the dimensions combined with a formula based on Paris Law crack growth calculations

The stiffener connection formula is providing interesting results and with some work, considering different relative thicknesses and stiffener depths and flange widths a practical formula could probably be derived.

## **9.6 Conclusions related to stresses and SCFs in stiffener connection**

The stress concentration and decay in an angle shell stiffener web, that has a right angled connection to a frame plate stiffener, are quite different in size and nature to a coplanar edge attachment with a right angled corner. This was unexpected and at present is not explained.

However the connection length can be used to calculate an  $as$  value in a similar way to the calculation for an edge connection. That  $as$  then, for the cases considered here, where the shell stiffener is unchanged but the connection to the frame stiffener changes, can predict the SCF using a simple formula. The more general case, where the dimensions of the stiffener change, has not been studied here but it seems likely that a general formula could be derived for the general case.

## **Chapter 10 Conclusions and Recommendations**

### **10.1 Introduction**

The main objective of the thesis is to study the behaviour of a crack propagating through a longitudinal shell stiffener to transverse frame stiffener connection and into the shell plate. Of particular interest are the effects on the SIF:

1. at changes of plate thickness,
2. as the crack grows through the stiffener flange and web,
3. as the crack grows into the shell plating,
4. the localized effect of the right angled corner at the intersection of the stiffeners had been studied by others but this work showed that there is more work required for those local areas.

The intention was to develop simplified methods as a means to determine SIFs and also SCFs.

Whilst the methodologies that have been derived can still be improved, they are expected to make a useful contribution for the following purposes:

- a. Providing some insights into the stress patterns which is important for analysts setting up finite element analyses (where complicated stress variation may only be able to be represented by linear variation in each element and too coarse a mesh will not be able to follow the true stress variation.
- b. Approximately check more detailed Finite Element Analysis.

- c. Making quick assessments of SIFs for preliminary and ‘back of the envelope’ checking purposes.
- d. Reliability modelling, where quick solutions for the effects of different geometry in different parts of a structure and the effect of corrosion on thicknesses are needed and with some calibration from limited number of analyses in the important failure regions that affect reliability may be accepted.

This chapter draws the main conclusions from the work undertaken to highlight the significant achievements. The chapter also proposes work in order to improve and better understand the methodology, so that it can be applied confidently to reliability analysis, structural fatigue life and fracture assessment.

## 10.2 General Conclusions

The method presented here provides an effective approximate method for estimating the SIF at changes of plate thickness and for cracks growing at a longitudinal stiffener to transverse stiffener connection into a plate. The method can be applied for screening (selecting locations for more detailed analysis) and approximate checking of detailed finite element (FE) analysis.

Understanding the nature of the effect of crack growing into different plate thicknesses should also help the FE analyst set up a better model because the analyst will have an advance idea of the likely model behaviour and the approximation involved in analysing one of several parallel stiffeners when only one may, in the first place, be cracked.

Some general observations are:

- a) Using a simple analysis,  $Y$  values can be determined surprisingly well, for cracks growing in finite size flat plates (compared with Fett (Fett,

1998) and FEA) and through longitudinal to transverse stiffener connections (compared with FEA).

- b) The simple analysis uses the ratio of linearized remaining ligament stresses that result from:
- a. the actual applied loading and
  - b. the load corresponding to the cracked semi-infinite plate singular stress distribution ((Paris and Sih, 1965) or, more recently, Seif and Kabir (Seif and Kabir, 2016)) applied to the remaining ligament and simply truncated to the size of the ligament. Note:
    - i. When, as for the stiffened plate, the remaining ligament is not coplanar the singular stress distribution simply follows the semi-infinite plate values calculated as if the plating was unfolded to a flat plate.
    - ii. When there is a thickness change the singular stress distribution (not for instance the force per unit length) is applied either side of the thickness change.
    - iii. The calculated axial and moment load does allow for the actual (unfolded) geometry of the plate.
  - c) When there is a thickness change normal to the crack propagation direction, the SIF reduces when there is thicker plate ahead of the crack tip and vice versa. The effect needs to be superimposed on the calculation from List a) and takes the form of an exponentially decaying correction on both sides of the thickness change that results in a step change of SIF at the thickness change. Because SIFs are quantities that are effectively per unit plate thickness a step change in inverse proportion to the plate thicknesses might have been expected but the actual change appears to be closer to the inverse ratio of the square roots of the thicknesses (perhaps because the SIF is determined by the stresses in the vicinity of the crack tip and not just the crack tip).

- d) In a simple, single stiffener or connection, the membrane SIF values drop dramatically after the stiffener crack extends into the plate. This is because the applied loading is now resisted by plate bending and so the bending SIF becomes dominant.
- e) There are similarities between the membrane behaviour a plate with a thickness change from  $t_1$  to  $t_2$  and a stiffener-plate T-connection with a crack growing from the stiffener of thickness  $t_1$  into a plate of thickness  $t_2/2$ . However the constants in the formulae are different. This shows the thickness correction formulae are not universal and that more work is needed here to better understand that effect.
- f) The additional SIFs caused by plate bending can be estimated from a plate bending solutions. Note that in practice crack closure on the compression side during bending (and axial force) is likely to be important.
- g) Shortly before a crack grows from a stiffener web into the plate the relative membrane stiffness of the remaining ligament and the bending stiffness of the plate are important and can be taken into account approximately, as shown in this thesis.
- h) When, as in the usual case, there are multiple stiffeners side by side and a crack is only growing through one stiffener the lateral support from the adjacent, intact, stiffeners needs to be taken into account and again some guidance is provided for assessing this support effect.
- i) Existing guidance (Xu et al., 2013) using structural dimensions to determine ‘ $as$ ’ for estimating the effect of right angled corners on SIFs overestimates the SIFs for small cracks and SCFs (for crack growth to 25mm) at the right angled connection between a longitudinal angle stiffener and a transverse stiffener. However, whilst still using the same ‘ $as$ ’ calculation a modification to the small crack SIF given by Barltrop and Xu (Barltrop and Xu, 2011) not only provides a better fit to the SIF but allows a better formula for estimating the SCF.

Overall, the methods provide a useful way of estimating  $Y$  values or SIFs in stiffened plating. However more work is required, particularly related to finding a universal method that will account for thickness change.

### **10.3 My Contributions from this study**

The research has made the following contributions which should be useful to practicing engineers as well as leading to observations that will be of interest to fracture mechanics academics:

1. An alternative and unconventional formula for calculating the SIF in a cracked finite width plate subject to in plane tension and in-plane bending has been developed in terms of the stresses on the remaining ligament.
2. Formulae for SIFs as a crack grows through, and normal to, a change in plate thickness have been developed.
3. Simple analysis methods for cracks growing through the outstand of a plate stiffener to the plate connection have been developed, as an extension to the method in 1.
4. Simple analysis methods for cracks growing from a connection between longitudinal and transverse structure have been developed as an extension to 1 and 3.
5. 1. to 4. have been modelled using shell and solid FEA and a considerable data base of results produced.
6. SIFs from the FEA have been compared with those from the simple analysis methods.
7. SCFs in stiffened connections with different connection details have been predicted using conventional extrapolation methods and from predicted singularity strengths based on the dimensions of the connections.

## 10.4 Proposals for future research

Although this research has extended previous work e.g. by Lou, Xu and Barltrop (Xu et al., 2013) and has made substantial progress related to SIF and SCF calculation in ship details there is still a lot of work that could be done that is not only relevant to ship structures but to other stiffened plated structures such as steel bridges and pressure vessels.

1. Why does the ligament stress method work – it seems reasonable but can it be given a sound theoretical basis?
2. Why is the formula for  $as$  and SCFs different for longitudinal – transverse structure connections than for simple steps on the edge of a plate? Is this the result of the flange or the constraint from the perpendicular plating?
3. Can methods be developed to represent, in a simple way, the 3-D, finite thickness behaviour of a crack growing into an intersection of plates?
4. This work has been based around, mainly statically determinate, behaviour of a cantilevering stiffener. Methods need to be developed to model continuous stiffness and the longitudinal load redistribution that will occur as a stiffener cracks.
5. Work needs to be done to simply model the effects of out of plane loads caused by pressure fluctuations on the hull which have, in the past, caused serious fatigue problems. This loading can also result in cracks that grow through connections in a direction through the frame stiffener that is parallel to the longitudinal shell stiffener. This type of cracking should be investigated.
6. Other locations in longitudinal – transverse structure connections, such as the numerous ratholes should be investigated.

7. Other types of detail, such as corners in transverse frames, transverse corners in holds of bulk carriers, transverse connections without transverse stiffeners should be investigated.
8. Residual stresses in these connections will affect fatigue and fracture and methods of assessment should be derived.
9. All the methods should be calibrated for use within structural reliability analysis where environmental factors: salt environment and coatings/coating decay and thickness loss warrant further investigation and their interaction with stress levels (as material is lost) and changes in material properties need to be properly understood.
10. After further development the method needs to be reviewed to determine whether it is suitable for use within reliability modelling or whether alternatives, such as running a limited number of detailed finite element analyses and interpolating/extrapolating from them, provide a more efficient and/or more accurate analysis.



## Chapter 11 References and Bibliography

1977. *Avondale Launches 165,000-DWT Tanker For Standard Oil (Ohio) Alaskan Service* [Online]. Available: <https://magazines.marinelink.com/Magazines/MaritimeReporter/197710/content/avondale-launches-165000dwt-210807> [Accessed].

1988. *Structural Casualty Study* [Online]. Available: <https://www.dco.uscg.mil/Our-Organization/Assistant-Commandant-for-Prevention-Policy-CG-5P/Inspections-Compliance-CG-5PC-/Office-of-Investigations-Casualty-Analysis/Marine-Casualty-Reports/> [Accessed].

ACADEMY, U. S. N. 1996. FRACTURE OF MATERIALS. *EN380 Naval Materials Science and Engineering Course Notes*.

AHMED, B. A. & ALSHAMMA, F. A. 2016. Strain Behavior at Crack Tip in Thin Plate Using Numerical and Experimental Work. *Engineering and Technology Journal*, 34, 513-526.

ANDERSON, T. L. 2017. *Fracture mechanics: fundamentals and applications*, CRC press.

ARSHAD, M. 2015. *Liberty Ship Failures* [Online]. Available: <https://metallurgyandmaterials.wordpress.com/2015/12/25/liberty-ship-failures/> [Accessed].

BAO, R., ZHANG, X. & YAHAYA, N. A. 2010. Evaluating stress intensity factors due to weld residual stresses by the weight function and finite element methods. *Engineering Fracture Mechanics*, 77, 2550-2566.

BARLTROP, N. 2014. FATIGUE: S-N CURVES & CYCLE COUNTING. *Inspection & Survey Part 2*.

BARLTROP, N. & XU, L. Structural reliability including response to breaking wave loads and the assessment of cracks in connections. 1st International

Conference of Maritime Technology and Engineering, MARTECH 2011, 2011. 289-319.

BATE, A. 1999. THE TAPS TANKERS: DEALING WITH THE DOUBLE DEADLINES. *Marine Digest*.

BOARDMAN, B. 1990. Fatigue resistance of steels. *ASM International, Metals Handbook. Tenth Edition*, 1, 673-688.

BS, B. S. 2000. Guidance on methods for assessing the acceptability of flaws in metallic structures. *British Standards Institution*.

BUECKNER, H. F. 1987. Weight functions and fundamental fields for the penny-shaped and the half-plane crack in three-space. *International Journal of Solids and Structures*, 23, 57-93.

BV 2016a. Rules Notes NR 445 Rules for the Classification of Offshore Units. *Paris: Bureau Veritas*.

CALLISTER, W. D. & RETHWISCH, D. G. 2018. *Materials science and engineering: an introduction*, Wiley New York.

CICERO, S., MADRAZO, V. & CARRASCAL, I. 2012. Analysis of notch effect in PMMA using the Theory of Critical Distances. *Engineering Fracture Mechanics*, 86, 56-72.

CICERO, S., MADRAZO, V., CARRASCAL, I. & CICERO, R. 2011. Assessment of notched structural components using failure assessment diagrams and the theory of critical distances. *Engineering fracture mechanics*, 78, 2809-2825.

DNV, G. 2015. Class guideline DNVGL-CG-0129:“fatigue assessment of ship structures”. *DNV GL, Oslo*.

DNV, G. 2017a. Class guideline DNVGL-CG-0129:“fatigue assessment of ship structures”. *DNV GL, Oslo*.

DNVGL-RP-0416 March 2016. Corrosion protection for wind turbines.

DONG, P. 2001. A structural stress definition and numerical implementation for fatigue analysis of welded joints. *International Journal of Fatigue*, 23, 865-876.

FETT, T. 1998. *Stress intensity factors and weight functions for special crack problems*, FZKA Karlsruhe.

FRANKLIN, P. 1993. *Fatigue design of oil tankers: a design approach*. Virginia Tech.

FRICKE, W. 2002. Recommended hot-spot analysis procedure for structural details of ships and FPSOs based on round-robin FE analyses. *International Journal of Offshore and Polar Engineering*, 12.

FRICKE, W. 2003. Fatigue analysis of welded joints: state of development. *Marine structures*, 16, 185-200.

FRICKE, W. & KAHL, A. 2005. Comparison of different structural stress approaches for fatigue assessment of welded ship structures. *Marine structures*, 18, 473-488.

FRICKE, W. & PETERSHAGEN, H. 1992. Detail design of welded ship structures based on hot-spot stresses.

GARBATOV, Y., ÅS, S., BRANNER, K., CHOI, B., DEN BESTEN, J., DONG, P., LILLEMÄE, I., LINDSTROM, P., DE SOUZA, M. L. & PARMENTIER, G. Committee III. 2: Fatigue and Fracture. 20th International Ship and Offshore Structures Congress (ISSC 2018), 2018. CRC Press, 441-547.

GRIFFITH, A. 1920. "The phenomenon of rupture and flow of solids", *Philosophical Transaction of the Royal Society of London*.

GÜRGEN, S., KUŞHAN, M. C. & DILTEMİZ, S. F. 2016. Fatigue failure in aircraft structural components. *Handbook of Materials Failure Analysis with Case Studies from the Aerospace and Automotive Industries*. Elsevier.

GURNEY, T. R. 1979. *Fatigue of welded structures*, CUP Archive.

HASEBE, N. & UEDA, M. 1981. A crack originating from an angular corner of a semi-infinite plate with a step. *Bulletin of JSME*, 24, 483-488.

HELLEN, T. 2001. *How to undertake fracture mechanics analysis with finite elements*, NAFEMS.

HOBACHER, A. 1996a. Fatigue design of welded joints and components. International Institute of Welding. Abington Publishing, Cambridge, UK.

HOBACHER, A. 1996b. *Fatigue design of welded joints and components: Recommendations of IIW Joint Working Group XIII-XV*, Woodhead Publishing.

HOBACHER, A. 2016. *Recommendations for fatigue design of welded joints and components*, Springer.

HUGHESI, O. & FRANKLIN, P. 1993. Rationally-Based Fatigue Design of Tankers.

J, D. 2008. Liberty cargo ship [EB/OL]. [ww2ships.com](http://ww2ships.com).

JANSSEN, M., ZUIDEMA, J. & SUN, R. W. 2004. H. Fracture Mechanics. London: Spon Press.

LOU, B. 2013. *A geometric method of fatigue SCF and fracture SIF assessment*. University of Strathclyde.

MADDOX, S. 1975. An analysis of fatigue cracks in fillet welded joints. *International Journal of Fracture*, 11, 221-243.

MADDOX, S. Recommended hot-spot stress design SN curves for fatigue assessment of FPSOs. The Eleventh International Offshore and Polar Engineering Conference, 2001. International Society of Offshore and Polar Engineers.

MADDOX, S. 2003. Review of fatigue assessment procedures for welded aluminium structures. *International Journal of Fatigue*, 25, 1359-1378.

MANAN, A. 2008. *Fracture mechanics analysis of multiple edge cracks*. University of London.

- NEUBER, H. 1958. Theory of notch stresses; principles for exact calculation of strength with reference to structural form and material: US Atomic Energy Commission. *Office of Technical Information Report AEC-4547*.
- NIEMI, E., FRICKE, W. & MADDOX, S. J. 2006. *Fatigue analysis of welded components: Designer's guide to the structural hot-spot stress approach*, Woodhead Publishing.
- PARIS, P. & ERDOGAN, F. 1963. A critical analysis of crack propagation laws.
- PARIS, P. C. & SIH, G. C. 1965. Stress analysis of cracks. *Fracture toughness testing and its applications*. ASTM International.
- PRADANA, M. R., QIAN, X. & SWADDIWUDHIPONG, S. 2017. Simplified Effective Notch Stress calculation for non-overlapping circular hollow section K-Joints. *Marine Structures*, 55, 1-16.
- QIAN, X. 2016. Fracture representation and assessment for tubular offshore structures. *Handbook of Materials Failure Analysis with Case Studies from the Oil and Gas Industry*. Elsevier.
- REGISTER, L. 2016a. Rules and Regulation for the classification of ships, part 3, ship structures. July.
- REGISTER, L. S. 2009. ShipRight Design and Construction: Fatigue Design Assessment - Level 1 Procedure Structural Detail Design Guide. *London, UK: Lloyd's Register Group Limited*.
- REGISTER, L. S. 2015. ShipRight 2014.2 User Guide FDA Level 2 Spreadsheet. *London, UK: Lloyd's Register Group Limited*.
- REGISTER, L. S. 2016b. ShipRight 2014.2 User Guide FDA Level 2 Assessment. *London, UK: Lloyd's Register Group Limited*.
- REGISTER, L. S. 2016d. ShipRight Design and Construction: Fatigue Design Assessment - Level 3 Procedure Guidance on Direct Calculations. *London, UK: Lloyd's Register Group Limited*.

REGISTER, L. S. June 2015. ShipRight Design and Construction: Fatigue Design Assessment - Application and Notations. London, UK: Lloyd's Register Group Limited.

RONGRONG, J. 2007. *Stress intensity factors for ship and offshore structural details*.

ROYLANCE, D. 2001a. Introduction to fracture mechanics.

ROYLANCE, D. J. M. I. O. T., CAMBRIDGE 2001b. Introduction to fracture mechanics. 1.

SCHIJVE, J. 2009. Residual stress. *Fatigue of structures and materials*, 89-104.

SCHÜTZ, W. 1996. A history of fatigue. *Engineering fracture mechanics*, 54, 263-300.

SEIF, A. E. & KABIR, M. Z. 2016. The general form of the elastic stress and displacement fields of the finite cracked plate. *Journal of Theoretical and Applied Mechanics*, 54, 1271-1283.

SEIFI, R. 2012. K and J-Integral Variations Due to Residual Stresses in Welded Plates. *Transactions of the Indian Institute of Metals*, 65, 239-249.

SHAH, R. 1976. Stress intensity factors for through and part-through cracks originating at fastener holes. *Mechanics of crack growth*. ASTM International.

SHEN, W.-C. 2015. Stress Field and Fatigue Strength Assessment of Ship Welded Joints Based On Singular Strength Theory. *Wuhan University of Technology, Wuhan*.

SHEN, W., LIANG, G., LI, C. & LIU, E. 2020a. A simplified method to predict the local stress field and N-SIF of V-shaped notch. *Engineering Fracture Mechanics*, 107096.

SHEN, W., QIU, Y., YAN, R., XU, L. & LIU, E. 2020b. A simplified method for evaluating singular stress field and fatigue strength of U-shaped notch. *Marine Structures*, 72, 102770.

- SIH, G. 1973. Handbook of stress intensity factors: Bethlehem. Pa., Lehigh University, Institute of Fracture and Solid Mechanics.
- SIH, G. C., PARIS, P. & ERDOGAN, F. 1962. Crack-tip, stress-intensity factors for plane extension and plate bending problems.
- SIPES, J., MACDONALD, J., BOWEN, M., COJEEN, H., SALERNO, B., MAXHAM, J. & BAXTER, J. Report on the Trans-Alaska Pipeline Service Tanker Structural Failure Study. Proceedings of the Maintenance, Inspection, and Monitoring Symposium, 1991.
- STANDARD, B. 2014. Guide to fatigue design and assessment of steel products, BS 7608: 2014. The British Standards Institution, London, UK.
- TANEJA, A. 2016. Historical failures and the evolution of Fracture Mechanics.
- TAYLOR, D. 1996. Crack modelling: a technique for the fatigue design of components. *Engineering Failure Analysis*, 3, 129-136.
- TAYLOR, D. 2008. The theory of critical distances. *Engineering Fracture Mechanics*, 75, 1696-1705.
- TAYLOR, D. 2011. Applications of the theory of critical distances in failure analysis. *Engineering Failure Analysis*, 18, 543-549.
- TIPPER, C. E. 1948. *The fracture of mild steel plate: Report No. R. 3*, HMSO.
- VERITAS, B. 1998. Fatigue strength of welded ship structures. *Bureau Veritas, NI*, 393.
- VERITAS, B. 2000. *Rules for the classification of steel ships*, The Bureau.
- WANG, C. H. 1996. *Introduction to fracture mechanics*, DSTO Aeronautical and Maritime Research Laboratory Melbourne, Australia.
- WILLIAMS, M. 1952. Stress singularities resulting from various boundary conditions in angular corners of plates in extension. *Journal of applied mechanics*, 19, 526-528.

WU, X.-R. & CARLSSON, J. 1991. *Weight functions and stress intensity factor solutions*, Pergamon press Oxford.

XU, L. Analysis of sharp corners in structural details. Proceedings of MARSTRUCT'07, the 1st International Conference on Marine Structures, Glasgow, United Kingdom, Advancements in Marine Structures. Paper: P2007-3 Proceedings., 2007.

XU, L. & BARLTROP, N. Analysis of sharp corners in structural details. International Conference on "Advancements in Marine Structures" Marstruct, 2007a.

XU, L. & BARLTROP, N. Analysis of sharp corners in structural details. 1st International Conference on Marine Structures: Advancements in Marine Structure, MARSTRUCT 2007, 2007b. 323-330.

XU, L. & BARLTROP, N. SCF and crack growth analysis of ship connection details. 1st international conference on floating structures for deepwater operations, Glasgow, UK, 2009. 21-23.

XU, L., LOU, B. & BARLTROP, N. 2013. Considerations on the fatigue assessment methods of floating-structure details. *Proceedings of the Institution of Mechanical Engineers, Part M: Journal of Engineering for the Maritime Environment*, 227, 284-294.

YODA, M. 1980. The J-integral fracture toughness for mode II.

ZHANG, W. 2016. Technical problem identification for the failures of the liberty ships. *Challenges*, Volume 7, Page 20.



## Appendix A Validation of ANSYS using Fett (1998)

### A.1 Introduction

The fracture behaviour of cracked structures is dominated by the near-tip stress field. In fracture mechanics most interest is focused on stress intensity factor, which describe the singular stress field ahead of a crack tip and govern fracture of a specimen when a critical stress intensity factor is reached.

In a large numbers cases of stress intensity factor solutions were given, methods for the determination of weight functions were reported and numerical results for a number of crack geometries were compiled

### A.2 Stress intensity factor

For the determination of stress intensity factors the Boundary Collocation Method (BCM) and the weight function procedure can be applied. The stress intensity factor  $K$  is a measure of the singular stress term occurring near the tip of a crack and defined by

$$\sigma_{ij} = \frac{K}{\sqrt{2\pi a}} f_{ij}(r, \varphi) \quad (\text{A.1})$$

where  $r$  and  $\varphi$  are polar coordinates with the origin at the crack tip.

$K$  is the stress intensity factor.

For the loading modes considered in this report, the stress intensity factor  $K_I$  and  $K_{II}$  are expressed as

$$K_I = \sigma^* \times \sqrt{\pi a} F_I \left( \frac{a}{W} \right) \quad (\text{A.2})$$

$$K_{II} = \tau^* \times \sqrt{\pi a} F_{II} \left( \frac{a}{W} \right) \quad (\text{A.3})$$

where  $a$  is the crack length and  $W$  is the width of the component. The value of  $a/W$  represents the relative crack depth  $\alpha$ .  $\sigma^*$  and  $\tau^*$  are characteristic stresses in the component, e.g. the outer fibre stress in a bending bar.

$F_I$  and  $F_{II}$  are called the “geometric function”, sometimes also the “shape function”.  $F_I$  and  $F_{II}$  are functions of the ratio of crack length to the specimen’s width as well as the type of load applied.  $F$  depends on the crack or component geometry as well as on the special load

### A.3 The rectangular plate with an edge crack

The stress intensity factor for pure tension is,

$$K = \sigma \sqrt{\pi a} \cdot Y \quad (\text{A.4})$$

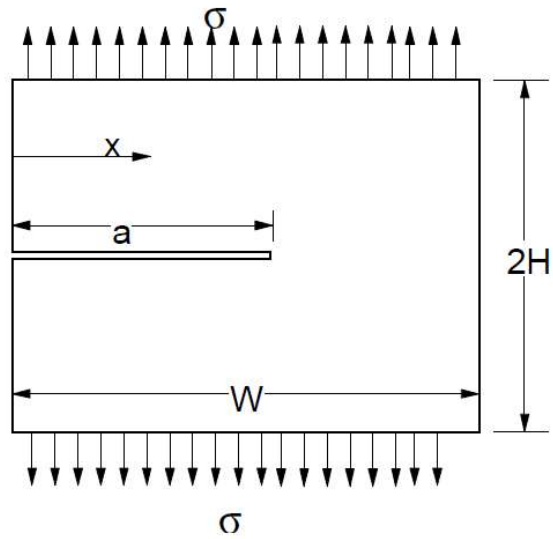


Figure A-1 Crack in rectangular plates under pure tension (Fett, 1998)

Fett listed the geometric factors values in different rectangular plate dimensions (Fett, 1998). I will validate Fett work with my FEA models corresponding to various crack length rates and different plate geometric sizes. The tension loading applied on both sides of rectangular plate is  $10^8$  Pascal.

	H/W=1.5	1.25	1.00	0.75	0.5	0.4	0.3	0.25
$\alpha = 0$	1.1215	1.1215	1.1215	1.1215	1.1215	1.1215	1.1215	1.1215
0.1	1.0170	1.0172	1.0174	1.0182	1.0352	1.0649	1.1455	1.2431
0.2	0.9800	0.9799	0.9798	0.9877	1.0649	1.1625	1.3619	1.5358
0.3	0.9722	0.9723	0.9729	0.9840	1.0821	1.2134	1.4892	1.7225
0.4	0.9813	0.9813	0.9819	0.9915	1.0819	1.2106	1.5061	1.7819
0.5	0.9985	0.9986	0.9989	1.0055	1.0649	1.1667	1.4298	1.7013
0.6	1.0203	1.0203	1.0204	1.0221	1.0496	1.1073	1.2898	1.5061
0.7	1.0440	1.0441	1.0441	1.0442	1.0522	1.0691	1.1498	1.2685
0.8	1.0683	1.0683	1.0683	1.0690	1.0691	1.0734	1.0861	1.1201
1.0	1.1215	1.1215	1.1215	1.1215	1.1215	1.1215	1.1215	1.1215

Table A-1 The values of Geometric function  $Y \cdot (1 - a / W)^{3/2}$  for tension

From Table A-1,  $\alpha$  represents the ratio of crack depth and plate width ( $a/W$ ) and  $H/W$  means the ratio of component height to the component width.

At base of Table A-1, the values of Geometric Function,  $Y \cdot (1 - a/W)^{3/2}$  in different crack depths and  $H/W$  ratios, the values of Geometric Factor  $Y$  is available for calculation. See Table A-2 and Figure A-2

	$H/W=1.5$	1.25	1.00	0.75	0.5	0.4	0.3	0.25
$\alpha = 0$	1.121	1.121	1.121	1.121	1.121	1.121	1.121	1.121
0.1	1.191	1.191	1.192	1.193	1.212	1.247	1.342	1.456
0.2	1.37	1.369	1.369	1.38	1.488	1.625	1.903	2.146
0.3	1.66	1.66	1.661	1.68	1.848	2.072	2.543	2.941
0.4	2.111	2.111	2.113	2.133	2.328	2.605	3.241	3.834
0.5	2.824	2.824	2.825	2.844	3.012	3.3	4.044	4.812
0.6	4.033	4.033	4.033	4.04	4.149	4.377	5.098	5.953
0.7	6.354	6.354	6.354	6.355	6.403	6.506	6.997	7.72
0.8	11.944	11.944	11.944	11.952	11.953	12.001	12.143	12.523
0.9	34.624	34.624	34.624	34.635	34.636	34.704	34.905	35.443
1.0	4429	4429	4429	4429	4429	4429	4430	4433

Table A-2 the values of Geometric factor  $Y$  under tension

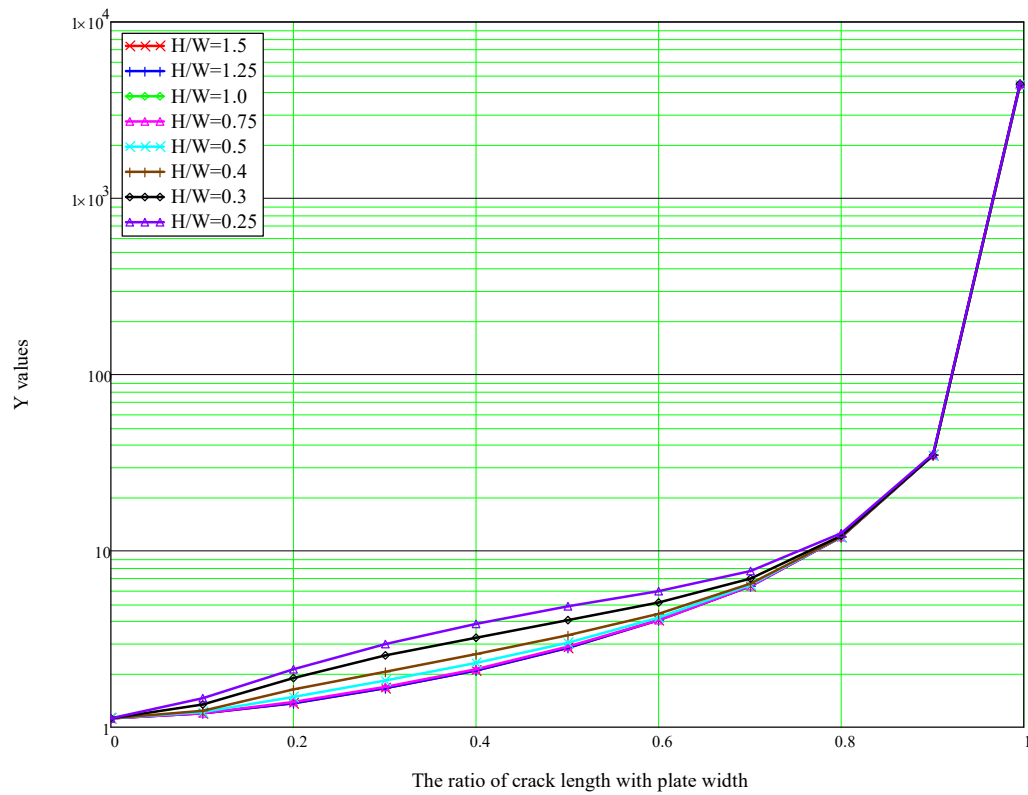


Figure A-2 the values of  $Y$  for various  $H/W$  in Fett work

#### A.4 The SIF values through FEA methods

The stress intensity factor values in  $10^8$  Pa pure tension for  $H/W=1.5$ , 1.25, 1.00 and 0.75 components are,

$\alpha$	$K_I$ with FEA approach			
	1.5	1.25	1.00	0.75
0.0	0.31238E+07	0.31240E+07	0.31238E+07	0.31239E+07
0.1	0.33259E+08	0.33259E+08	0.33264E+08	0.33364E+08
0.2	0.54083E+08	0.54084E+08	0.54114E+08	0.54593E+08
0.3	0.80506E+08	0.80507E+08	0.80569E+08	0.81522E+08
0.4	0.11851E+09	0.11851E+09	0.11858E+09	0.11976E+09
0.5	0.17799E+09	0.17799E+09	0.17804E+09	0.17895E+09
0.6	0.28070E+09	0.28070E+09	0.28069E+09	0.28091E+09
0.7	0.48630E+09	0.48630E+09	0.48625E+09	0.48572E+09
0.8	0.10218E+10	0.10218E+10	0.10217E+10	0.10209E+10
0.9	0.36017E+10	0.36018E+10	0.36018E+10	0.36011E+10
1.0	0.48163E+12	0.48017E+12	0.47300E+12	0.47309E+12

Table A-3 SIF values for components with  $H/W=1.5, 1.25, 1.00$  and  $0.75$  through FEA



The stress intensity factor values in  $10^8\text{Pa}$  pure tension for  $H/W=0.5, 0.4, 0.3$  and  $0.25$  components are,

$\alpha$	$K_I$ under FEA approach			
	0.5	0.4	0.3	0.25
0.0	0.31243E+07	0.31241E+07	0.31241E+07	0.31242E+07
0.1	0.34376E+08	0.35761E+08	0.38619E+08	0.41348E+08
0.2	0.58891E+08	0.64504E+08	0.75731E+08	0.85470E+08
0.3	0.89789E+08	0.10085E+09	0.12358E+09	0.14340E+09
0.4	0.13049E+09	0.14625E+09	0.18182E+09	0.21435E+09
0.5	0.18902E+09	0.20651E+09	0.25236E+09	0.29829E+09
0.6	0.28657E+09	0.30042E+09	0.34626E+09	0.39998E+09
0.7	0.48422E+09	0.48775E+09	0.51385E+09	0.55626E+09
0.8	0.10128E+10	0.10019E+10	0.98462E+09	0.98109E+09
0.9	0.35915E+10	0.35717E+10	0.35074E+10	0.34293E+10
1.0	0.47316E+12	0.47273E+12	0.47331E+12	0.47318E+12

Table A-4 SIF values for components with  $H/W=0.5, 0.4, 0.3$  and  $0.25$  through FEA

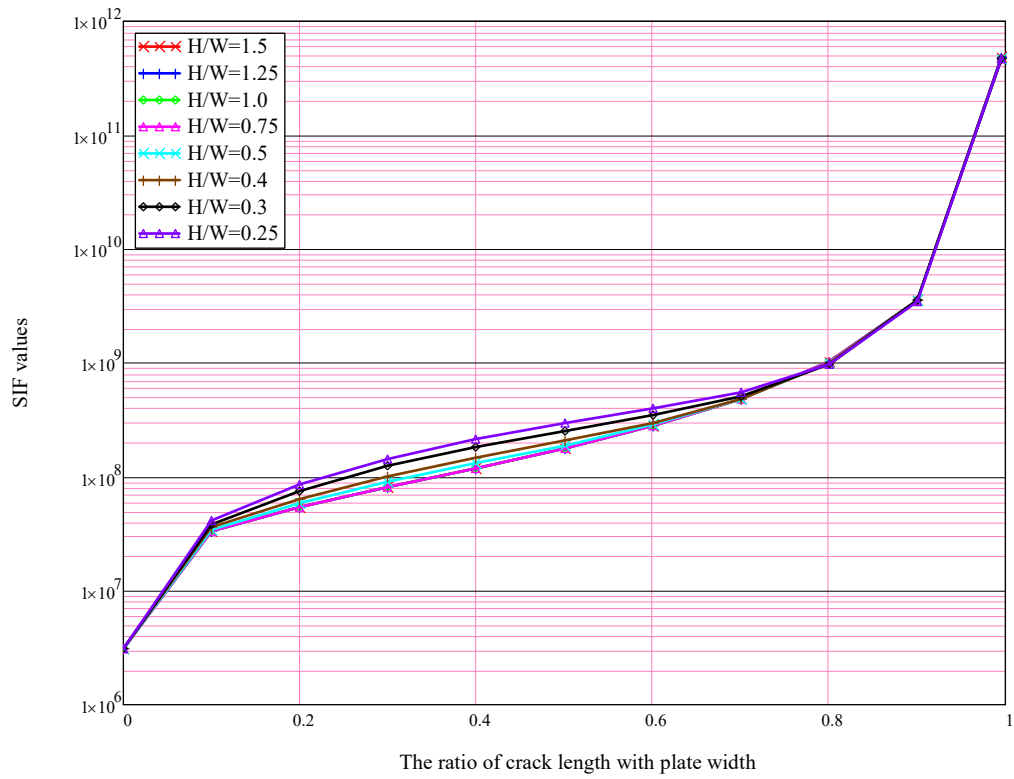


Figure A-3 SIF values for various  $H/W$  ratios in  $Y$ -Log scale from FEA methods

Based on Equation (A.4), there is expression for  $Y$  from known SIF values (K)

$$Y = \frac{K}{\sigma \sqrt{\pi a}} \quad (\text{A.5})$$

The values of  $Y$  from  $K$  with FEA methods can be found in Table A-5.

	$H/W=1.5$	1.25	1.00	0.75	0.5	0.4	0.3	0.25
$\alpha=0$	1.115	1.115	1.115	1.115	1.115	1.115	1.115	1.115
0.1	1.187	1.187	1.187	1.191	1.227	1.276	1.378	1.475
0.2	1.365	1.365	1.365	1.377	1.486	1.628	1.911	2.157
0.3	1.659	1.659	1.66	1.679	1.85	2.078	2.546	2.954
0.4	2.114	2.114	2.116	2.137	2.328	2.609	3.244	3.824
0.5	2.84	2.84	2.841	2.856	3.016	3.295	4.027	4.76
0.6	4.089	4.089	4.089	4.092	4.175	4.376	5.044	5.827
0.7	6.559	6.559	6.558	6.551	6.531	6.578	6.93	7.502
0.8	12.891	12.891	12.889	12.879	12.777	12.64	12.422	12.377
0.9	42.839	42.84	42.84	42.832	42.718	42.482	41.718	40.789
1.0	5435	5418	5337	5338	5339	5334	5341	5339

Table A-5 the values of Geometric factor  $Y$  from Finite Element Analysis methods

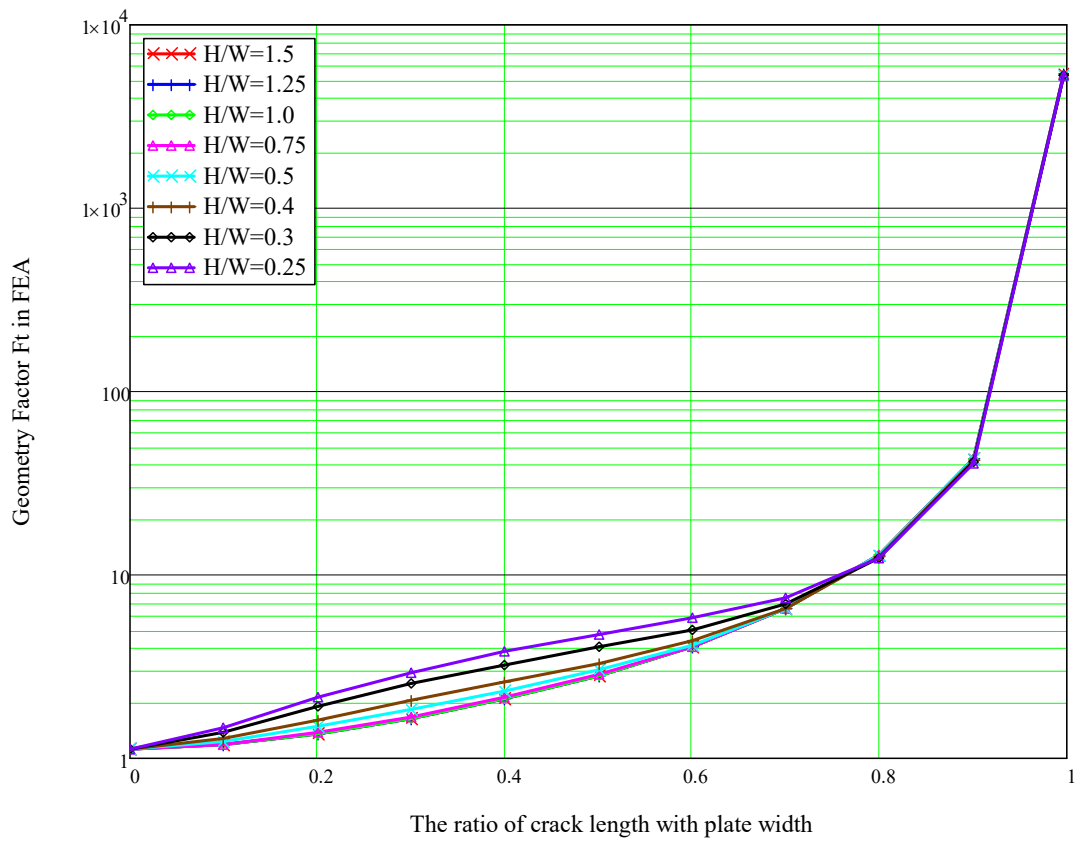


Figure A-4  $Y$  values for various  $H/W$  ratios from FEA methods

Comparing the  $Y$  values with FEA and Fett paper, it is found that the results from two approaches are in good agreement, see Figure A-5.

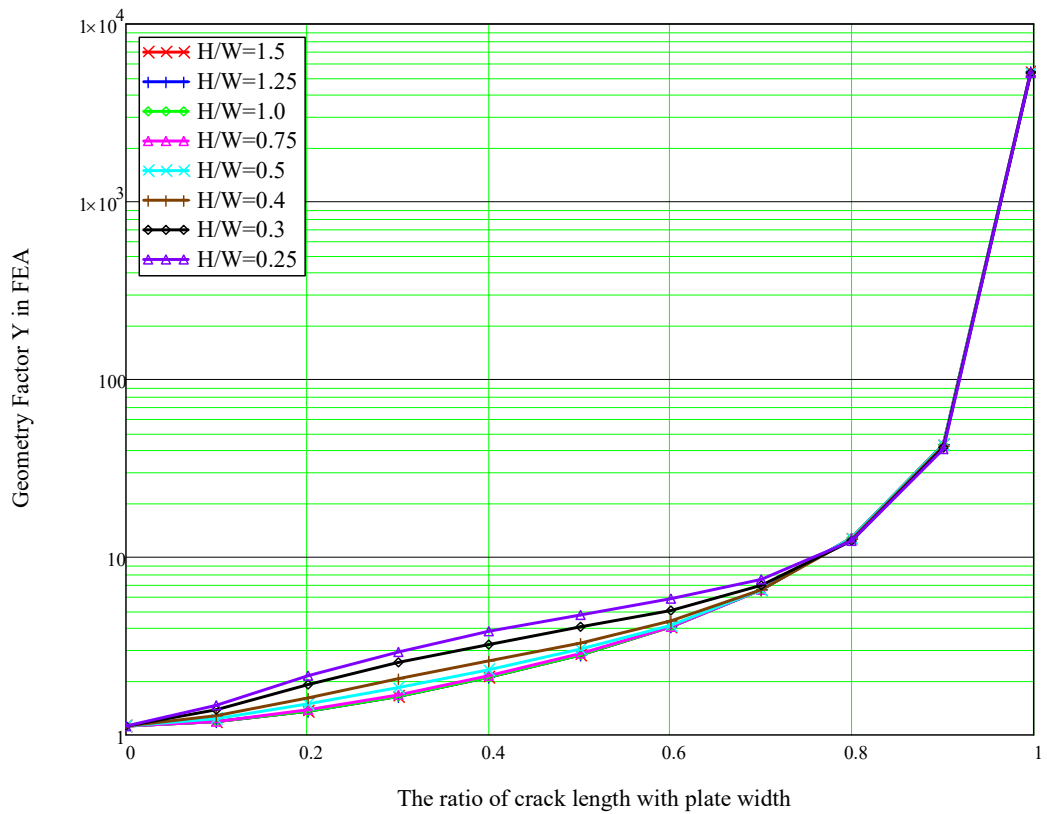


Figure A-5 Comparison of  $Y$  values with FEA and Fett work

## A.5 The SIF results through Fett approach

The SIF values through Fett approach can be calculated on the basis of  $Ft$  values and Equation (A.4), see Table A-6 and Table A-7.

$\alpha$	$K_I$ under Fett method			
	1.5	1.25	1.00	0.75
0.0	0.3143E+07	0.3143E+07	0.3143E+07	0.3143E+07
0.1	0.3338E+08	0.3339E+08	0.3339E+08	0.3342E+08
0.2	0.5428E+08	0.5428E+08	0.5427E+08	0.5471E+08
0.3	0.8058E+08	0.8059E+08	0.8064E+08	0.8156E+08
0.4	0.1183E+09	0.1183E+09	0.1184E+09	0.1196E+09
0.5	0.177E+09	0.177E+09	0.1771E+09	0.1782E+09
0.6	0.2769E+09	0.2769E+09	0.2769E+09	0.2773E+09
0.7	0.4711E+09	0.4711E+09	0.4711E+09	0.4712E+09
0.8	0.9468E+09	0.9468E+09	0.9468E+09	0.9474E+09
0.9	0.2911E+10	0.2911E+10	0.2911E+10	0.2912E+10
1.0	0.3925E+12	0.3925E+12	0.3925E+12	0.3925E+12

Table A-6 SIF values for components with  $H/W=1.5, 1.25, 1.00$  and  $0.75$  through Fett

$\alpha$	$K_I$ under Fett Method			
	0.5	0.4	0.3	0.25
0.0	0.3143E+07	0.3143E+07	0.3143E+07	0.3143E+07
0.1	0.3398E+08	0.3495E+08	0.376E+08	0.408E+08
0.2	0.5898E+08	0.6439E+08	0.7543E+08	0.8507E+08
0.3	0.8969E+08	0.1006E+09	0.1234E+09	0.1428E+09
0.4	0.1305E+09	0.146E+09	0.1816E+09	0.2149E+09
0.5	0.1887E+09	0.2068E+09	0.2534E+09	0.3015E+09
0.6	0.2848E+09	0.3005E+09	0.350E+09	0.4087E+09
0.7	0.4748E+09	0.4824E+09	0.5188E+09	0.5724E+09
0.8	0.9475E+09	0.9513E+09	0.9625E+09	0.9927E+09
0.9	0.2912E+10	0.2918E+09	0.2935E+10	0.298E+10
1.0	0.3925E+12	0.3925E+12	0.3926E+12	0.3929E+12

Table A-7 SIF values for components with  $H/W=0.5, 0.4, 0.3$  and  $0.25$  through Fett



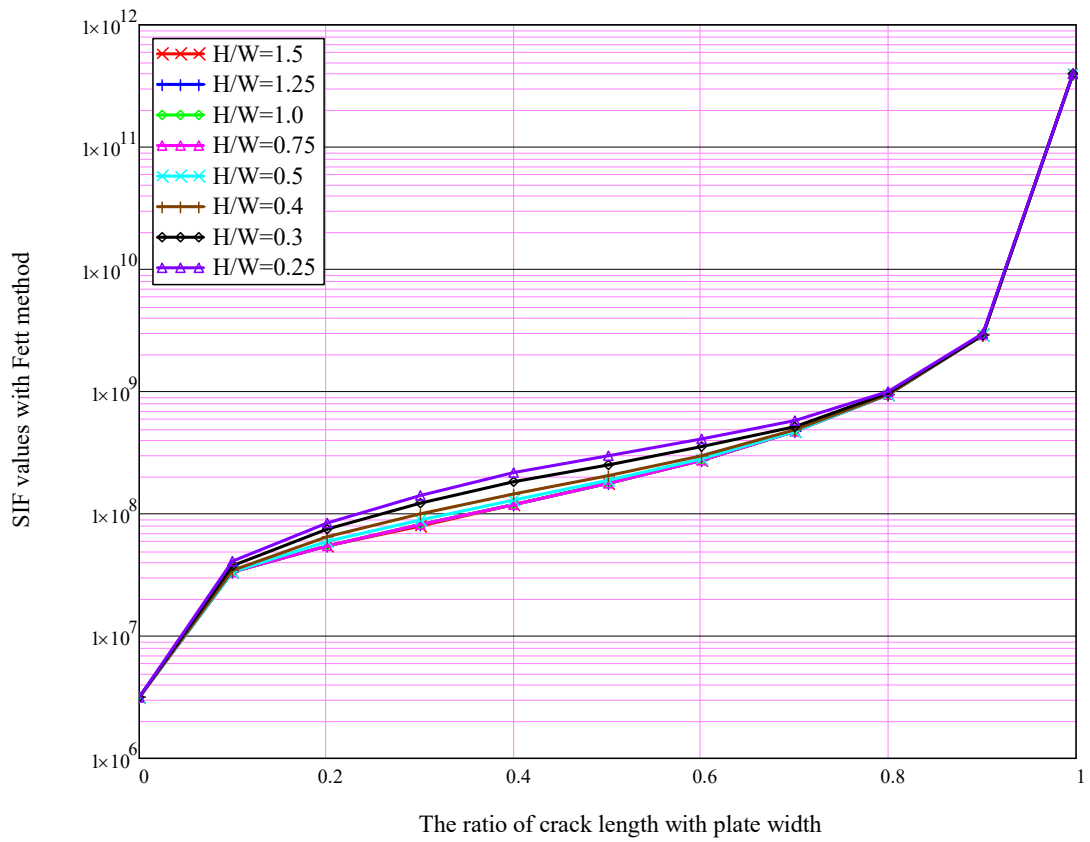


Figure A-6 SIF values for various  $H/W$  ratios from Fett work

Comparing the SIF values between FEA approach and Fett work. The SIF results from FEA method are close approximate to Fett work for all  $H/W$  ratios, see Figure A-7.

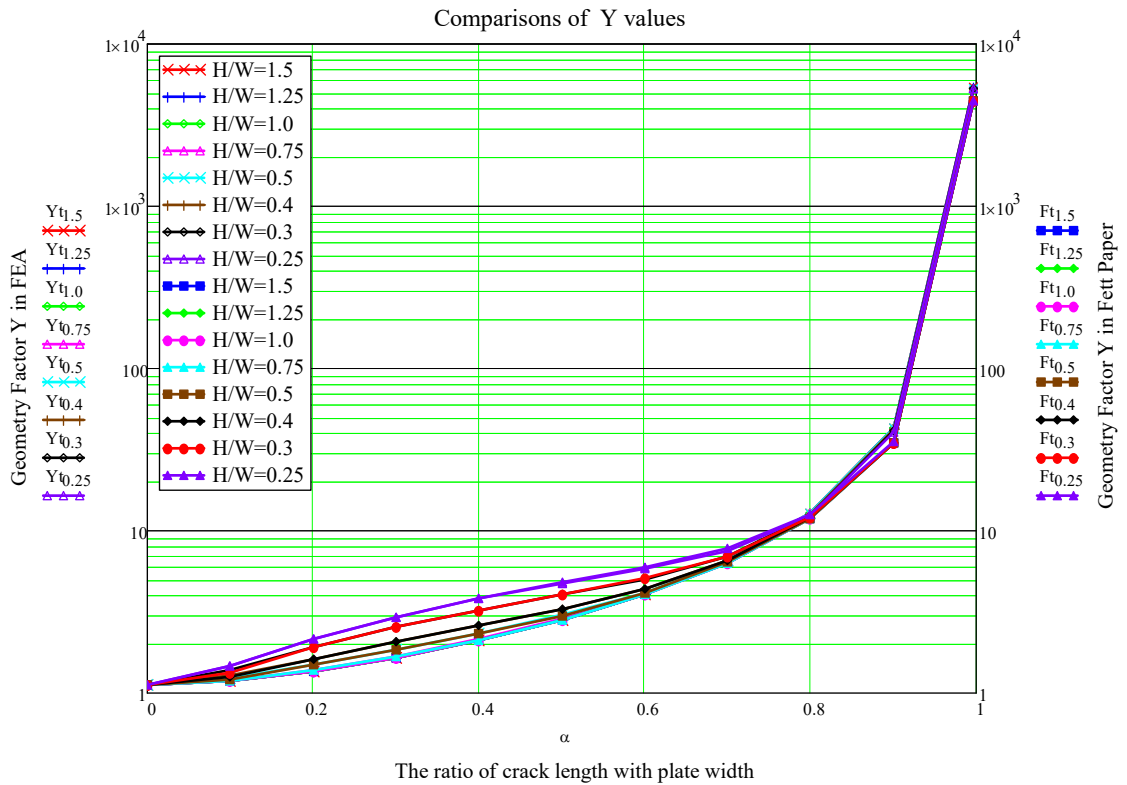


Figure A-7 Comparison of SIF values with FEA and Fett work

## A.6 Conclusion

Different mode-I stress intensity factor values have been compared based on single plate model subject to tension loading.

The comparisons in Figure A-5 and Figure A-7 shows the SIF results are almost identical between the FEA methods and Fett work. The  $F_t$  results from Fett paper can be utilised for the I-Shape Model SIF estimations in single stiffener and triple stiffener models with pure tension loadings.

## **Appendix B Validation of ANSYS plate bending calculation using solid elements (with and without crack closure)**

### **B.1 Three Dimensional Analysis**

The width  $W$  of the plate is 130mm and its height  $H$  is 90 mm, the thickness  $t$  should be much less than  $W$  and the length of the crack on the plate is a 25mm. The Young's modulus and Poisson's ratio is set at 205GPa and 0.3 respectively. The thicknesses are simulated for  $t=10$ mm and 20mm under the illustrated geometries of edge cracks and in these cases,  $W/t=13$  and 6.5 respectively.

There are number of elements used in the crack tip for each thickness to get the stress intensity factor at the different geometric position, see Table B-1. Displacement correlation is used to determine stress intensity factor and the orientations of the local coordinates at the crack tip is shown in Figure B-6.

T(mm)	Elements numbers on the crack front
10	20
20	40

Table B-1 Elements Number on the front crack

The stress intensity factor is normalized as

$$Y = \frac{\Delta K}{\Delta \sigma \sqrt{\pi a}} \quad (\text{B.1})$$

$\sigma$  is the characteristic stress (nominal stress) and  $a$  is the crack length

The non-dimensional solution to a single edge cracked plate under extension loading is,

$$Y_a^0 = 1.122 - 0.231 \left( \frac{a}{W} \right) + 10.550 \left( \frac{a}{W} \right)^2 - 21.710 \left( \frac{a}{W} \right)^3 + 30.382 \left( \frac{a}{W} \right)^4 \quad (\text{B.2})$$

with accuracy of 0.5% for any dimension  $\frac{a}{W} \leq 0.6$  (Janssen et al., 2004).

The normalised stress intensity factor for the double edge cracked plate is,

$$Y_b^0 = \frac{1.122 - 1.122 \left( \frac{a}{W} \right) - 0.820 \left( \frac{a}{W} \right)^2 + 3.768 \left( \frac{a}{W} \right)^3 - 3.040 \left( \frac{a}{W} \right)^4}{\sqrt{1 - \frac{2a}{W}}} \quad (\text{B.3})$$

which is accurate to 0.5% for any dimension  $\frac{a}{W}$ . See Table B-2,

	Geometry	$Y^0$
a	Single Edge Cracked	1.35
b	Double Edge Cracked	1.15

Table B-2 Normalised stress intensity factor for extension loaded,  $Y^0$

When the crack faces are allowed to overlap (no contact considered), the stress intensity factor across the plate thickness is linear and is skew-symmetric about the mid-plane, as expected. When this effect is considered, the stress intensity factor in the crack tip shows a gradient through the thickness of the plate in the tension region and then reduces to zero for the surfaces part in contact, the compression region.

Normally the maximum stress intensity factor for a cracked plate under bending is around 45-50 percent of stress intensity factor in the cracked plate under an extension loading. Obviously it can be seen that the crack-face constant has significant effect on the stress intensity factors ( $K$  values). See Table B-3,

	Geometry	$Y_{\max}$	$Y_{\max} / Y^0$
a	Single Edge Cracked	0.58	0.43
b	Double Edge Cracked	0.56	0.49

Table B-3 The ratio between  $Y_{\max}$  and  $Y^0$

For the same plate thickness, the contact region in the crack tip is coincident for all geometries and it corresponds to about 20% of the crack front length. There is a region of non-linear stress intensity factor in the transition between the opening crack and closed crack because of the non-linear behaviour of the contact.

The comparison of the stress intensity factors for various geometries with  $t=10\text{mm}$  and  $t=20\text{mm}$  are shown in Figure B-2 and Figure B-3 separately. These results were obtained for the no contact case.

In-plane-bending moment means the plate bends in its own plane such as a shear wall with horizontal and vertical forces which are applied to its plane and thus produce in plane bending moments. In plane bending moments do not cause the plate to bend it a way that make a stomach for the plate.

Out-of-plane bending moments are those which are caused by out of plane forces such as a building slab. The forces on the building slab are out of plane and thus they produce out-of-plane bending moments or in other words they make the slab concave down, see Figure B-1. In this work, I applied the out-of-plane bending moments for analysis.

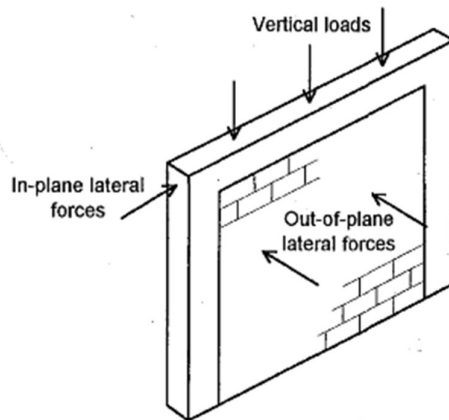


Figure B-1 In-Plane and Out-Plane lateral forces on plate

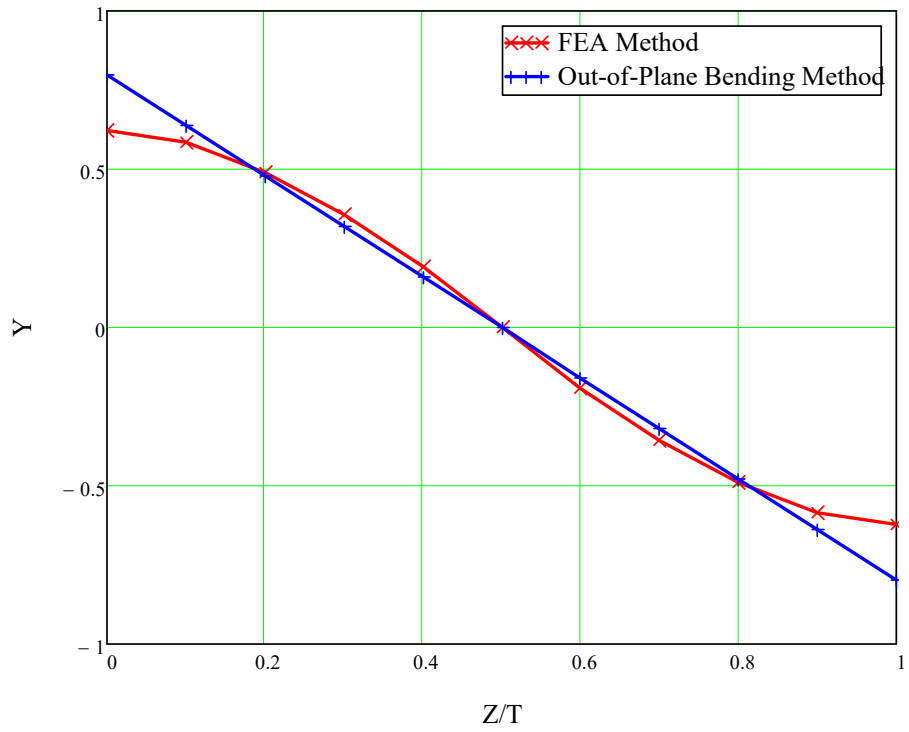


Figure B-2 Normalized geometry factor along the crack front ( $t=10\text{mm}$ )

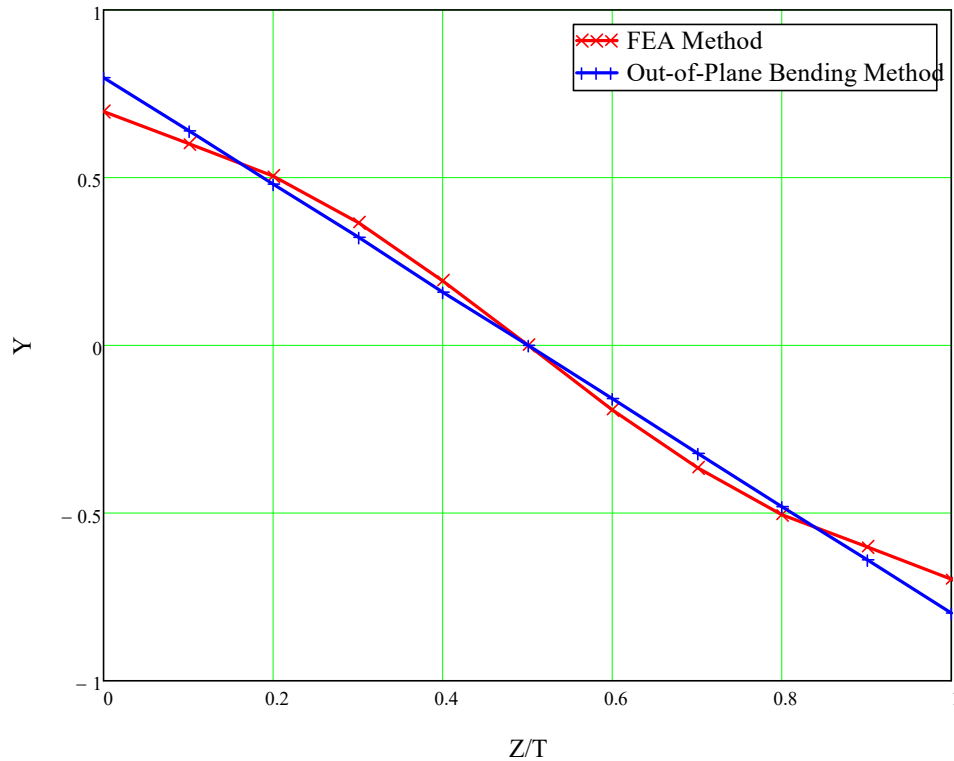


Figure B-3 Normalized geometry factor along the crack front ( $t=20\text{mm}$ )

In finite element analysis (FEA), mesh size is a critical issue. It closely relates to the accuracy, computing time and efforts required for meshing of finite element models, which determines their complexity level. The accuracy of FEA results and required computing time are determined by the finite element size, which is normally named as mesh density. According to FEA theory, the FE models with fine mesh (small element size) yields highly accurate results but may take longer computing time. On the other hand, those FE models with coarse mesh (large element size) may lead to less accurate results but smaller computing time. Also, small element size will increase the FE model's complexity which is only used when high accuracy is required. Large element size, however, will reduce the FE model's size and is extensively used in



simplified models in order to provide a quick and rough estimation of designs. It is being showed the normalized stress intensity factor (SIF) along the crack front in different mesh size (0.8mm and 2mm mesh density) in Figure B-4 and Figure B-5, which proves the diverse mesh size will not making big different results for both no contact region plates (in Figure B-4) and part contact region plates (in Figure B-5).

For the stiffener calculations in Chapter 3, 0.8mm mesh size will be adopted for the parts around crack tip and 2.0 mm mesh size will be suitable for general finite element analysis to improve the accuracy and save calculation time concurrently.

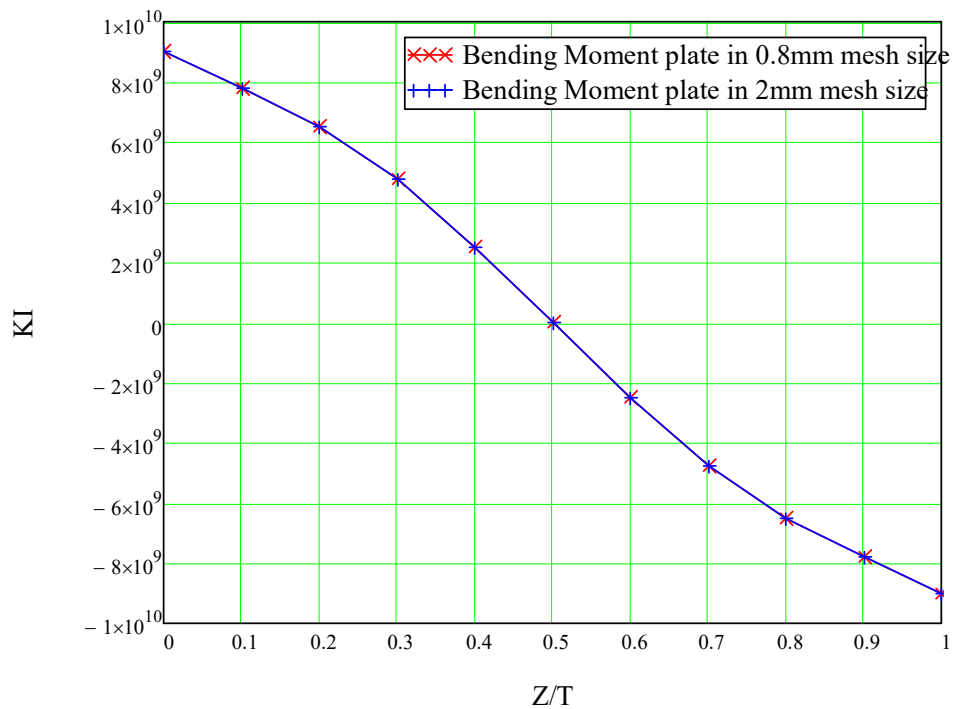


Figure B-4 Normalized SIF for no contact region plates with different mesh sizes

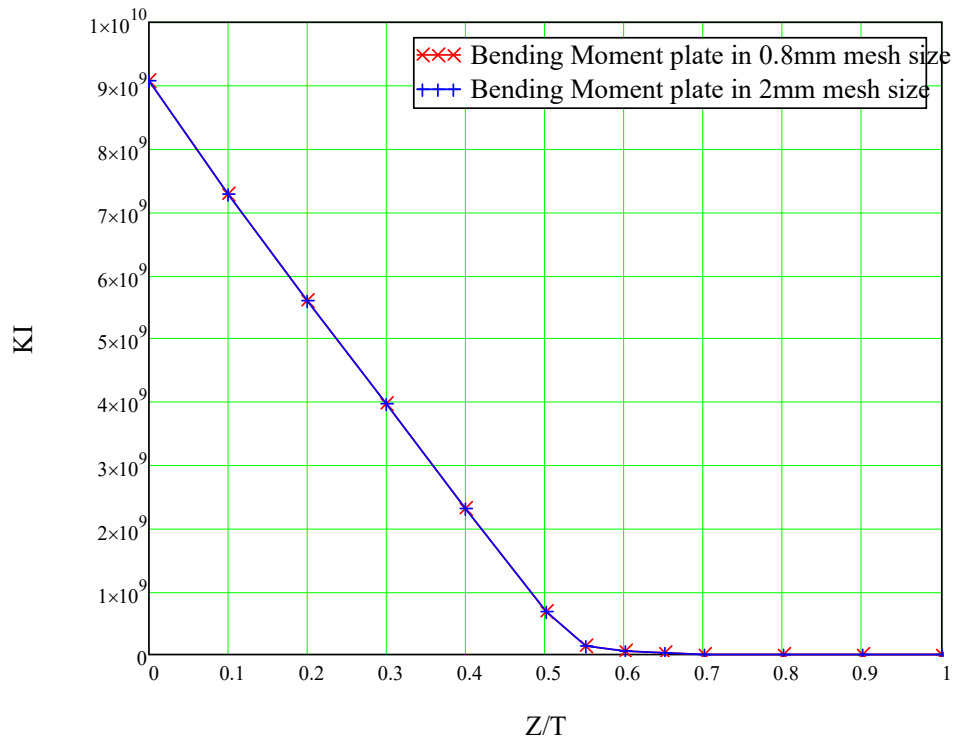


Figure B-5 Normalized SIF for 6mm contact region plates with different mesh sizes

The comparison of the stress intensity factors for various geometries with  $t=10\text{mm}$  and  $t=20\text{mm}$  are shown in Figure 2 and Figure 3 separately. These results were obtained for the no contact case. For these two thicknesses, the contact region is around 30% of the whole thickness. That is for 10mm thickness case the contact part is 3mm and for 20mm thickness case, the contact part is about 6mm. From Figure B-2 and Figure B-3,  $Z/T$  represents the geometric position of crack tips are located and the number of means the ratio of the crack tips position (in z axis) divided by the whole plate thickness ( $t$ ), see Figure B-6.

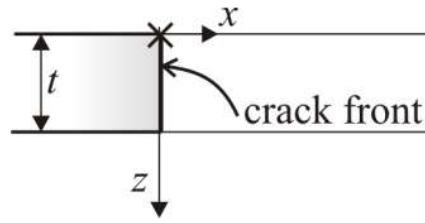


Figure B-6 Coordinate around the crack tip

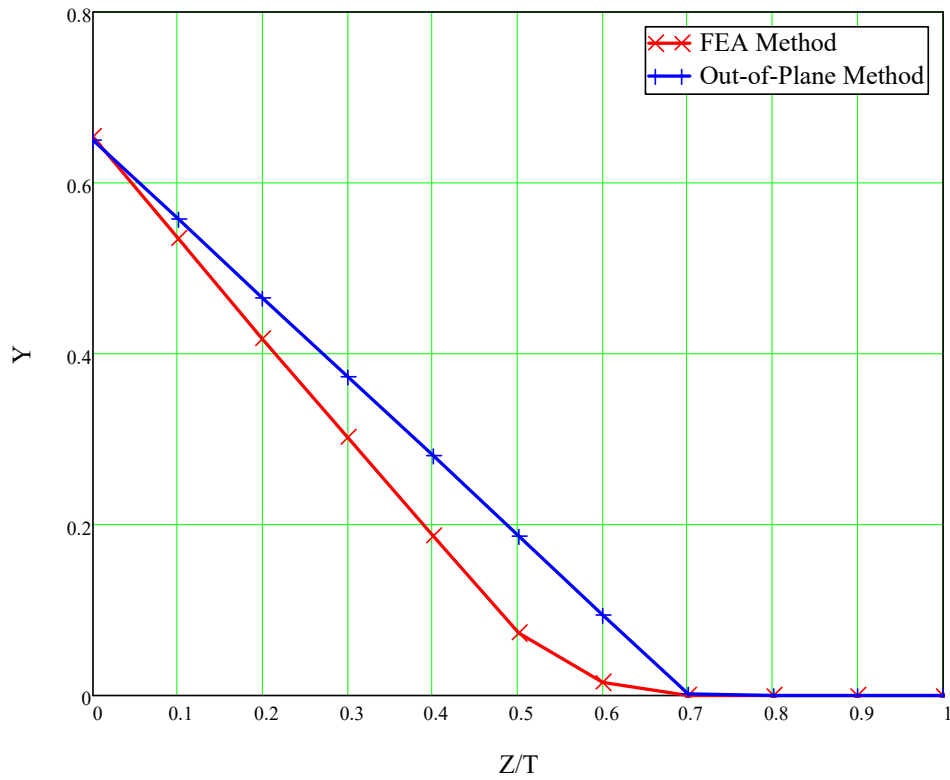


Figure B-7 Normalized geometry factor along the crack front in contact case ( $t=10\text{mm}$ )

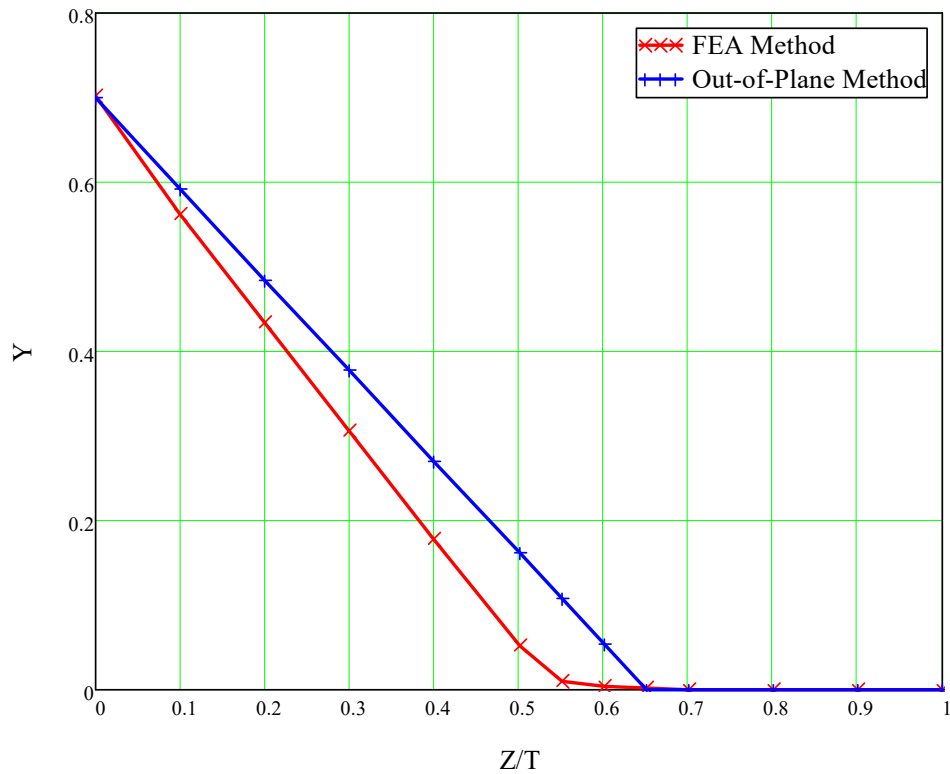


Figure B-8 Normalized geometry factor along the crack front in contact case ( $t=20\text{mm}$ )

Comparing the FEA method and the out-of-plane method, the magnitudes of maximum Geometry Factor values are close for the two methods in 10mm and 20mm thickness cases. When the contact effect is considered, the stress intensity factor in the crack tip shows a gradient through the thickness of the plate in the tension region and reduces to zero where the surfaces are in contact, i.e. in the compression region.

The comparison of the stress intensity factors for various geometries with  $t=10\text{mm}$  and  $t=20\text{mm}$  are shown in Figure B-9. These results were obtained for contact and no contact case.

Appendix B Validation of ANSYS plate bending calculation using solid elements (with and without crack closure)

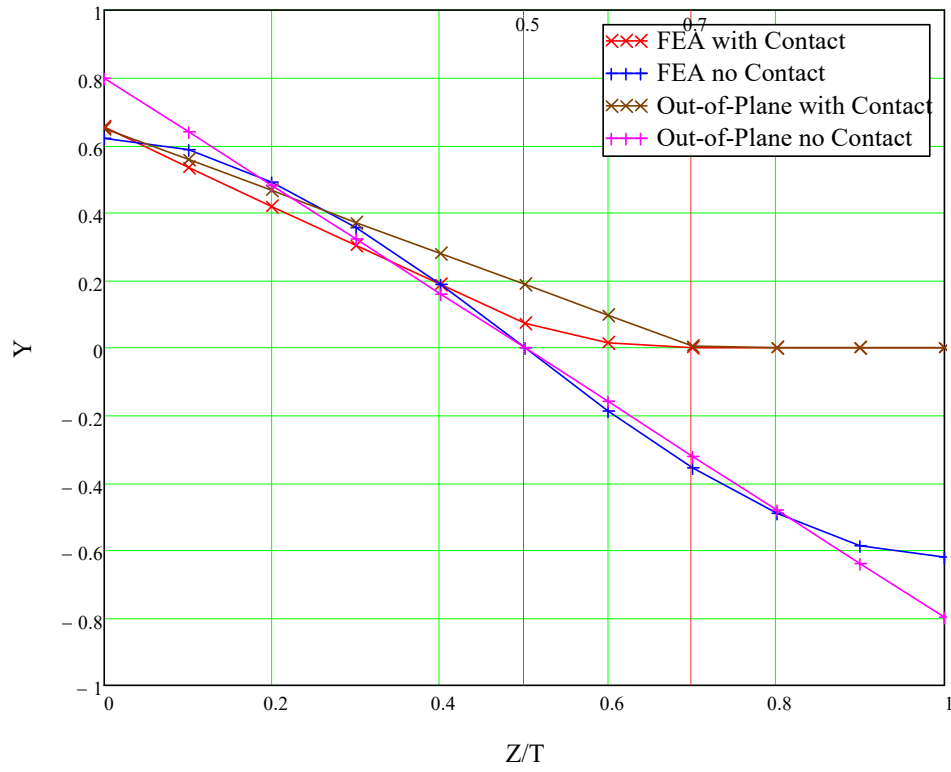


Figure B-9 Normalized Geometry Factor along the crack front in contact and not contact cases ( $t=10\text{mm}$ )

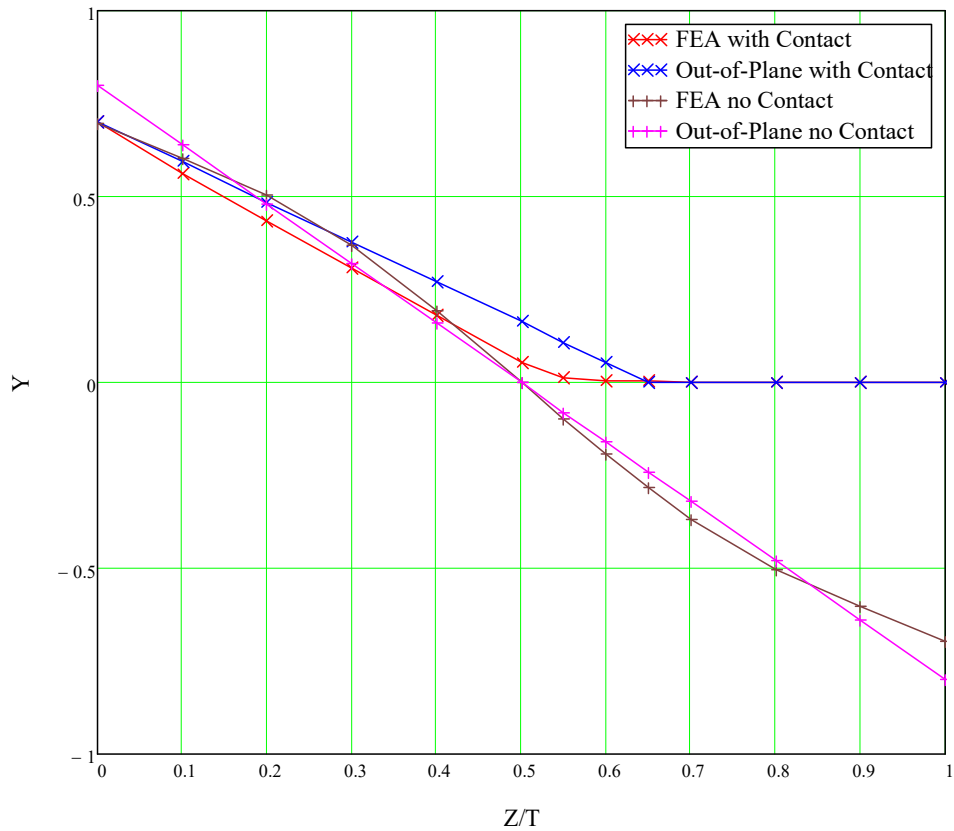


Figure B-10 Normalized Geometry Factor along the crack front in contact and not contact cases ( $t=20\text{mm}$ )

The comparison of the geometry factor for a single edge cracked plate with various thicknesses is presented in Figure B-11 and Figure B-12. As noted in these two figures, the crack opening depends on the thickness. The opening part of the crack front for  $t=20\text{mm}$  is smaller than the opening part for  $t=10\text{mm}$  thickness plate. The magnitude of maximum stress intensity factor for  $t=10\text{mm}$  and  $t=20\text{mm}$  are very close in both contact and no contact cases.

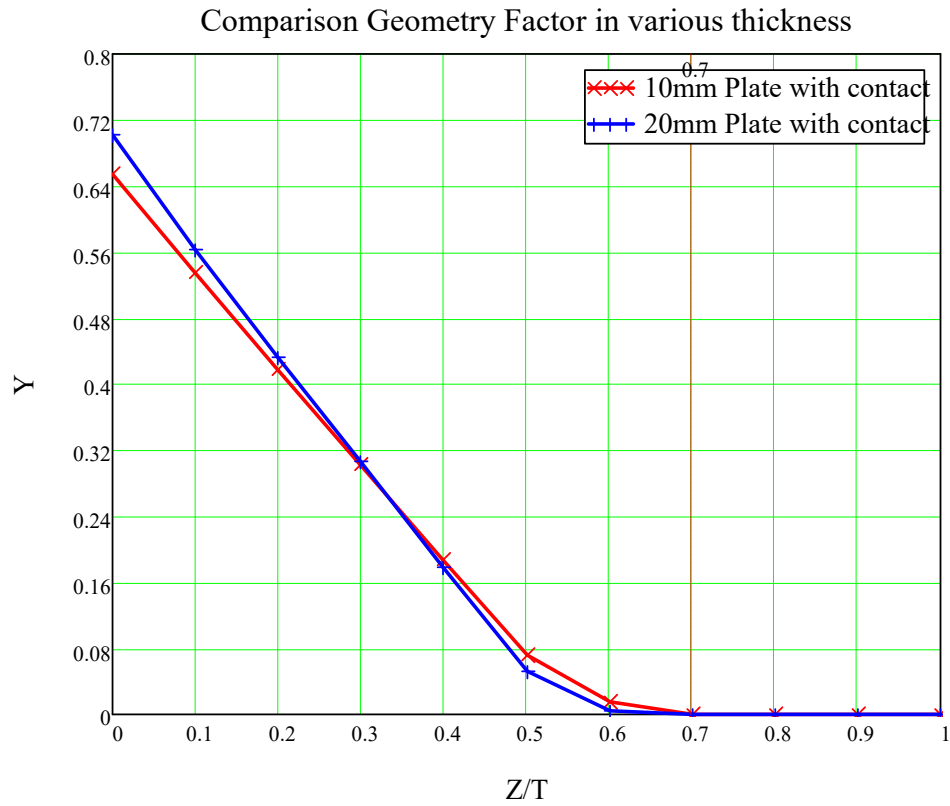


Figure B-11 Geometry Factor for various thicknesses along the contacted crack

For the no contact cases, The  $Y$  factor for  $t=10\text{mm}$  thickness plate is slightly smaller than  $t=20\text{mm}$  which proves that there would be no much differences of SIF values if increasing the plate thickness from 10mm to 20mm.

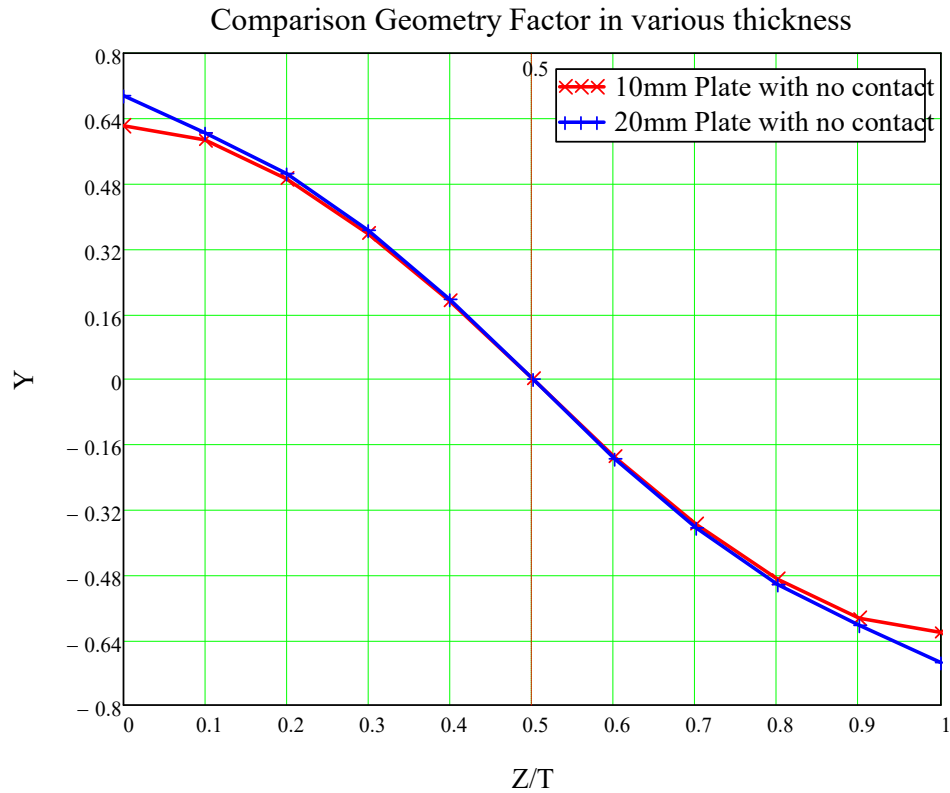


Figure B-12 Geometry Factor for various thicknesses along the non-contacted crack

## B.2 Three-dimensional Analysis under tension loading

For a single edge cracked plate under tension loading, the uniform tensile stress,  $\sigma = 100,000 Pa$ , were used to determine the crack tip SIF values under tension, see Figure B-13.

The stress intensity factor  $K$  is a measure of the singular stress term occurring near the tip of crack and defined by the polar coordinates with the origin which is defined as  $r$  and  $\theta$ .



$$\sigma_{ij} = \frac{K_I}{\sqrt{2\pi a}} f_{ij}(r, \theta) \quad (\text{B.2})$$

Stress intensity factor is effected by the specimen's three dimensional size and the most important, the crack length  $a$ .

Stress intensity factor for pure tension loading, see Figure B-13, is expressed as

$$K_I = \sigma \cdot \sqrt{\pi a} \cdot F_I(a/W) \quad (\text{B.3})$$

$$K_{II} = \tau \cdot \sqrt{\pi a} \cdot F_{II}(a/W) \quad (\text{B.4})$$

where  $a$  is the crack length,  $W$  is the width of the component and  $\sigma, \tau$  is the characteristic stresses in the component.  $F_I$  and  $F_{II}$  are functions of the ratio of the crack length to the specimen's width as well as of the type of load applied.

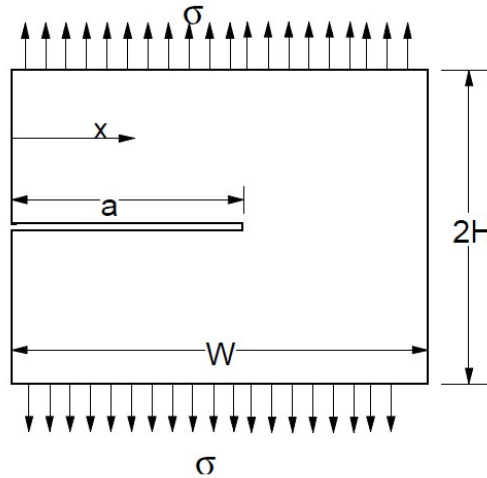


Figure B-13 The regular plate with an edge crack

Table B-4 shows the values of factor  $F_I \cdot (1 - a/W)^{3/2}$  for different plate dimensional size and crack length.  $\alpha$  is the ratio of crack size and plate width,  $a/W$ .  $H/W$  represents the ratio of plate height and plate width. For my model, the values of  $a/W$  and  $\alpha$  are 0.35 and 0.2 respectively. The value of factor  $F_I \cdot (1 - a/W)^{3/2}$  should be in the range of between 1.1625 and 1.3619.

*Appendix B Validation of ANSYS plate bending calculation using solid elements (with and without crack closure)*

	H/W=1.5	1.25	1.00	0.75	0.5	0.4	0.3	0.25
$\alpha = 0$	1.1215	1.1215	1.1215	1.1215	1.1215	1.1215	1.1215	1.1215
0.1	1.0170	1.0172	1.0174	1.0182	1.0352	1.0649	1.1455	1.2431
0.2	0.9800	0.9799	0.9798	0.9877	1.0649	1.1625	1.3619	1.5358
0.3	0.9722	0.9723	0.9729	0.9840	1.0821	1.2134	1.4892	1.7225
0.4	0.9813	0.9813	0.9819	0.9915	1.0819	1.2106	1.5061	1.7819
0.5	0.9985	0.9986	0.9989	1.0055	1.0649	1.1667	1.4298	1.7013
0.6	1.0203	1.0203	1.0204	1.0221	1.0496	1.1073	1.2898	1.5061
0.7	1.0440	1.0441	1.0441	1.0442	1.0522	1.0691	1.1498	1.2685
0.8	1.0683	1.0683	1.0683	1.0690	1.0691	1.0734	1.0861	1.1201
1.0	1.1215	1.1215	1.1215	1.1215	1.1215	1.1215	1.1215	1.1215

Table B-4 Geometric function for tension loading

*Appendix B Validation of ANSYS plate bending calculation using solid elements (with and without crack closure)*

---

The values of normalised geometry factor  $Y$  along the crack front for 20mm thickness no contact plate ( $t=20\text{mm}$ ) in pure tension loading conditions are distributed around 1.2, see Figure B-14.

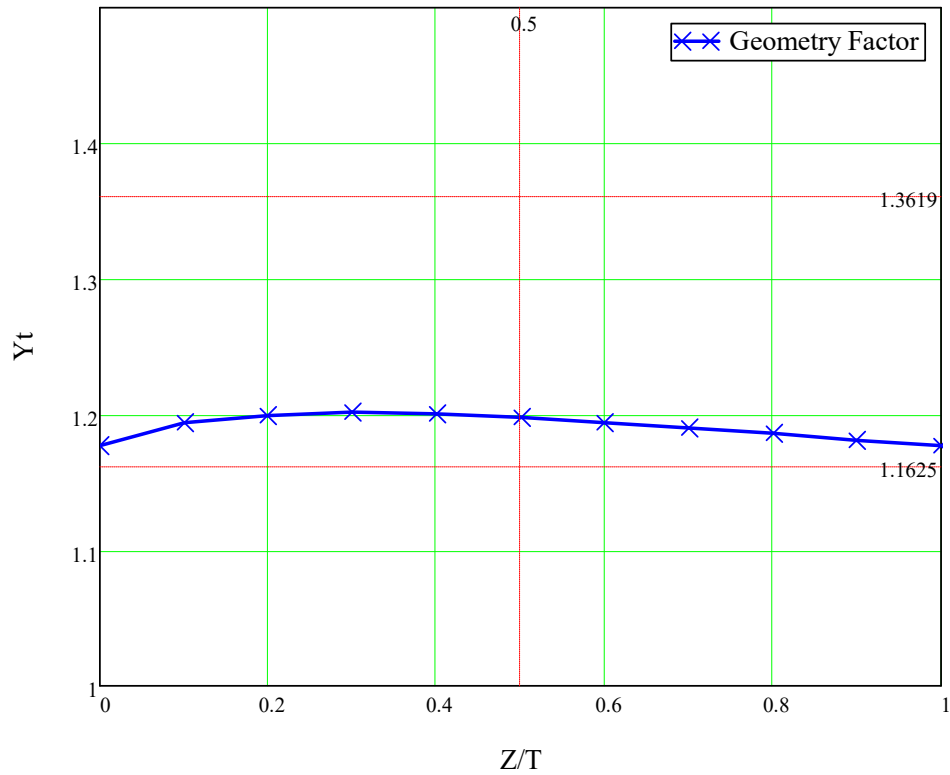


Figure B-14 Geometry Factor in no contact cases in 20mm thickness

The values of normalised geometry factor  $Y$  along the crack front for 10mm thickness no contact plate ( $t=10\text{mm}$ ) in pure tension loading conditions are distributed around 1.2, See Figure B-15.

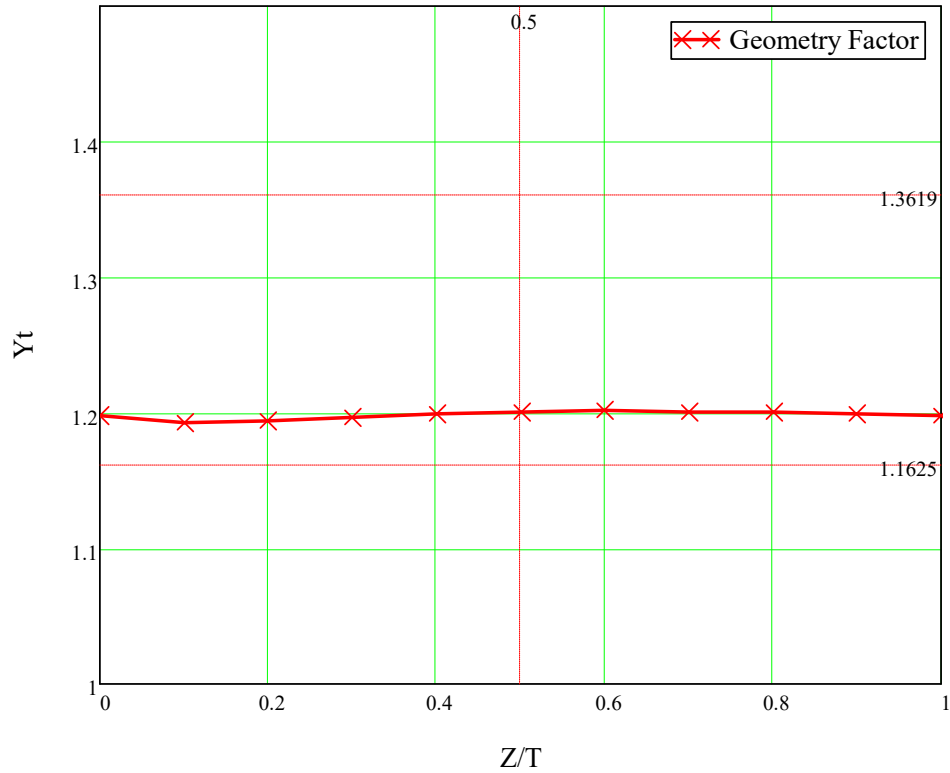


Figure B-15 Geometry Factor in no contact cases in 10mm thickness

Based on the Figure B-16, it is to be found that the values of Geometry Factor  $Y_t$  are both around 1.2 and the results of  $Y_t$  for two different thickness plates ( $t=10\text{mm}$  and  $t=20\text{mm}$ ) has not much variation. Therefore it can be assumed as constant values through the thickness for a finite thickness plate.

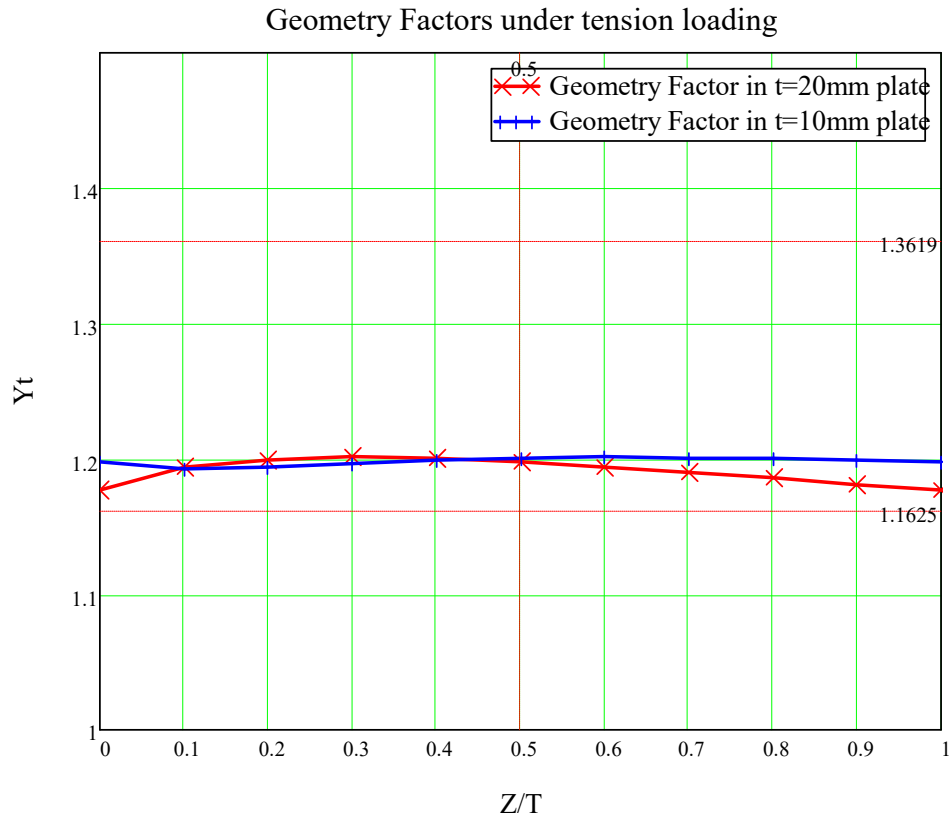


Figure B-16 Comparisons of Geometry Factors in two thicknesses plates

### B.3 Model with Finite Element method

The stress field near the crack tip is singular so that the crack tip stress component tends to infinity. Near the crack tip stress and  $1/x$  ( $x$  is the distance from the crack tip) are proportional. When using ANSYS modelling, in order to reflect this feature, it often uses “fourth node” for processing. The midpoint of the connecting crack tip moves away from the tip 1/4 side location, to better reflect the singular crack tip displacement field. Therefore ANSYS can use SHELL93 and SOLID95 to simulate the crack tip singular element together.

Appendix B Validation of ANSYS plate bending calculation using solid elements (with and without crack closure)

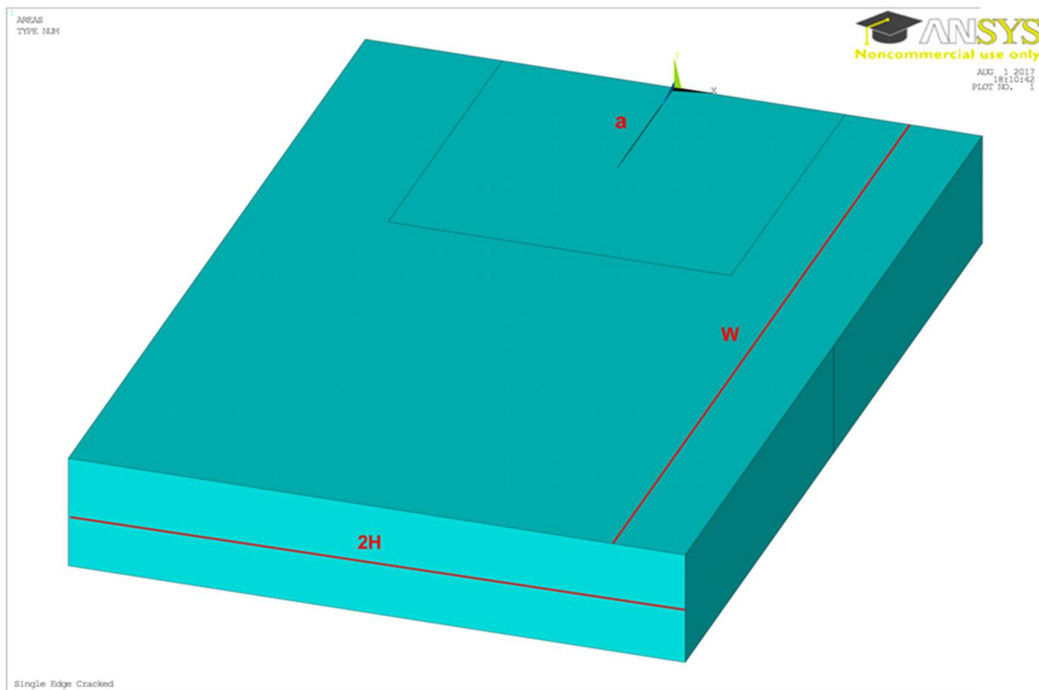


Figure B-17 crack plate calculation model

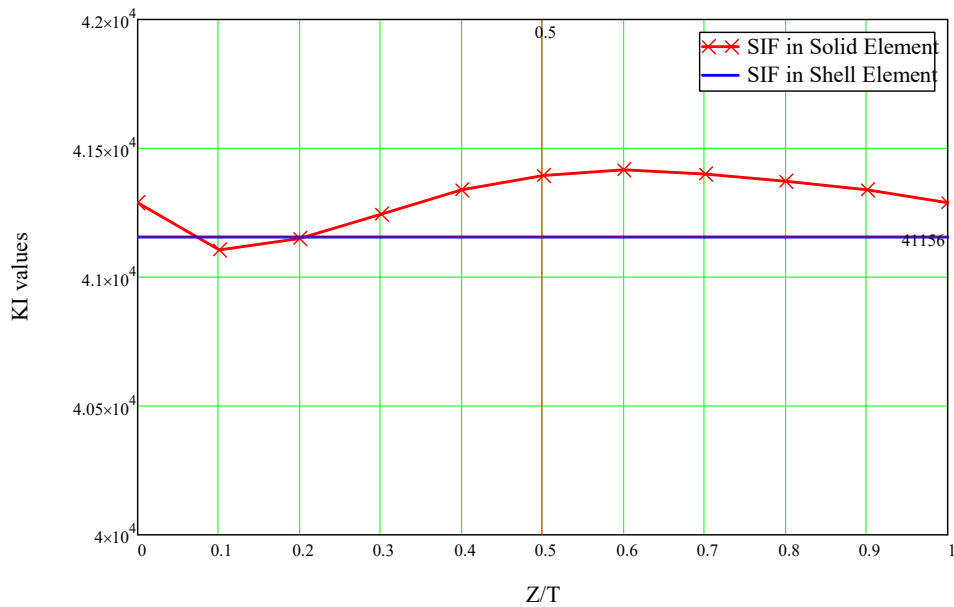


Figure B-18 SIF values for the same model with solid element and shell element

Figure B-18 shows the SIFs calculated for a simple cracked plate with solid elements and shell elements. The SIF value in shell element ( $KI=41156$ ) is close to the values for the upper and lower surface ( $KI=41288$ ) in solid element.

The meshing procedure used for the solid elements started by placing the 2-D mesh elements on the plate surfaces, see Figure B-19, forming the solid mesh between them, using the VSWEEEP command in ANSYS to get the meshes for the whole structure, and then deleting the 2-D elements.

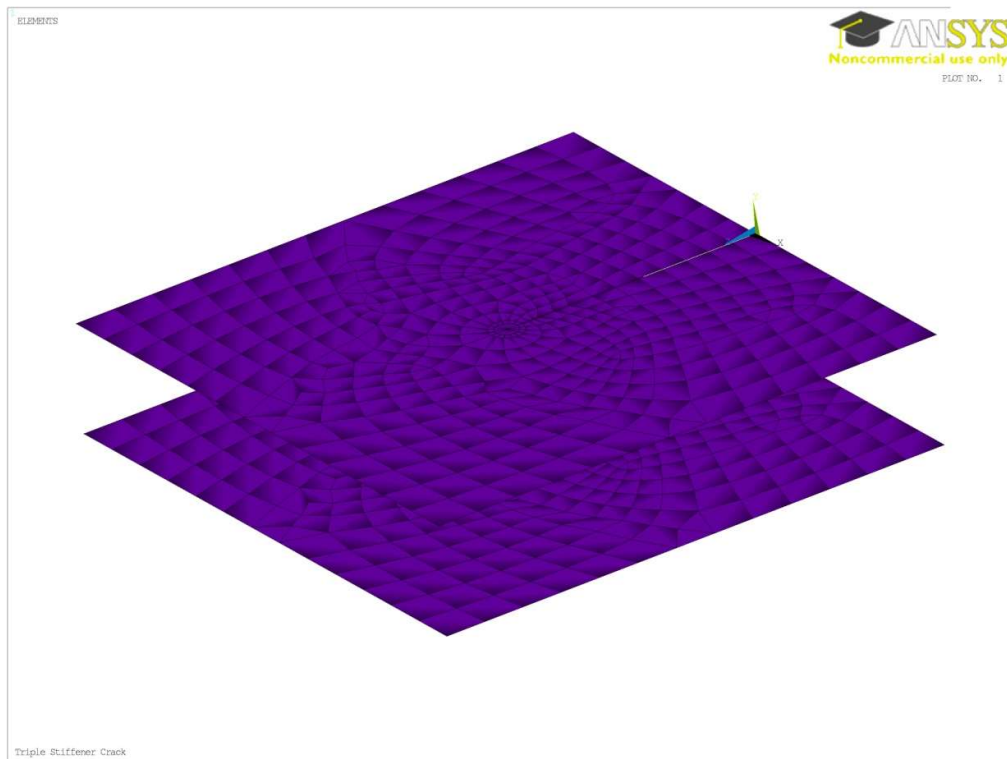


Figure B-19 Meshes on source area and target area



Relatively simple two-dimensional model can be used directly SHELL93 automatic meshing procedure to obtain grid for area entity. In this three-dimensional analysis, it is normally to use the VSWEEP command in ANSYS to get the meshes for the whole volume. In the boundary condition stage, the first step is to constrain all of the left side nodes ( $x = -45/1000$ ) in X, Y, Z and ROTX, ROTY, ROTZ directions. The next step is to apply the uniform tensile stress,  $\sigma = 100,000 Pa$  in X positive direction (red arrows) along every element located in the right side ( $x = 45/1000$ ) of this plate to determine the tension loadings, see Figure B-20.

The first use of KSCON command in PREP7 specifies the concentration keypoint around element to define which area mesh will be skewed. During meshing, elements are initially generated circumferentially about, and radially away, from the keypoint. Lines attached to the keypoint are given appropriate divisions and spacing ratios. Only one concentration keypoint per unmeshed area is allowed. The second use of CSKP command is to define a local coordinate system by three key point locations, which the origin of this coordinate system is located at the crack tip. To locate the origin, to locate the positive X-axis, and to define the positive X-Y plane, this local system becomes the active coordinate system. In the post-processing module POST1, the crack stress intensity factor ( $KI$ ) can use displacement interpolation (KCALC order) method to calculate.

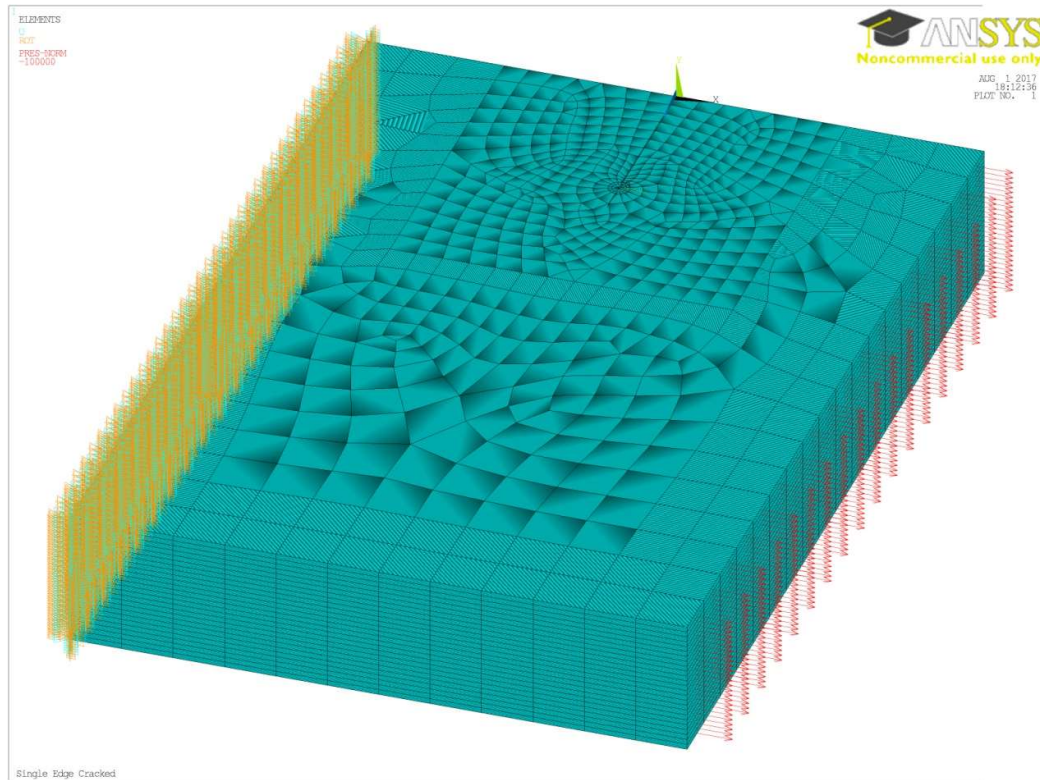


Figure B-20 Boundary Conditions and Tension Loading details

## **B.4 Solid Element Conclusions**

The achievement of this chapter is to check the accuracy of SIF calculations with ANSYS for the thickness in plates and to find out the mesh size for the plate of simple cracking model is suitable in the stiffer calculations.

Plates with a pre-existing “through-the-thickness” crack were studied under the action of a remote bending moment. The dependence of the contact region in the crack tip was investigated, as well as the bending effect on the stress intensity factor.

Two sets of numerical analyses were performed in two different FEA methods. One set uses a single cracked geometry for two different thicknesses under pure bending moment and the second set uses the same cracked geometry under extension loading. The contact region length is around 30% of the thickness for 10mm and 20mm cases.

Results from the two different FEA methods show the similar SIF results. It proves the SIF across the plate thickness is linear and is skew-symmetric about the mid-line of the plate in no contact cases, as expected. When the contact part effects considered, the SIF at the crack tip shows a gradient line through the thickness of the plate in the bending moment and then reduces to zero where the surfaces are close to contact parts.

In the Tension loading, it shows the SIF values are not in big variation through the thickness, therefore it can be assumed to be constant value through the thickness for a finite thickness plate. The Geometry Factor ( $Yt$ ) values in 3-D cracked plate are both assumed as 1.2 for thickness 10mm and 20mm.

## **Appendix C Estimation of SIF values for crack growing through a change in thickness: First empirical method**

Previous work by Xu et al.(Xu et al., 2013) showed that a crack growing from a corner could be approximated by an edge crack plate but with an additional length of crack that represented the effect of the corner. In this section, the possibility of representing the thickness change by a modified crack length is investigated, if this worked it might have led to a convenient analytical crack growth solution. However, whilst the results are presented here for interest, it was not found to be a useful approach and alternative empirical approximations, presented in the following sections were found to be a better approaches.

Figure C-1 shows the results, obtained from FEA, of SIF values for different thicknesses  $t_2$ . In each case  $t_1 = 12\text{mm}$ .

It is to be expected, that there is in fact a discontinuity as the crack passes the thickness change at  $a/at = 1$ . (This is also suggested by the trends of  $Y$  curves, sketched as dashed lines in Figure 4-6.) However at this stage of the work that discontinuity was ignored.

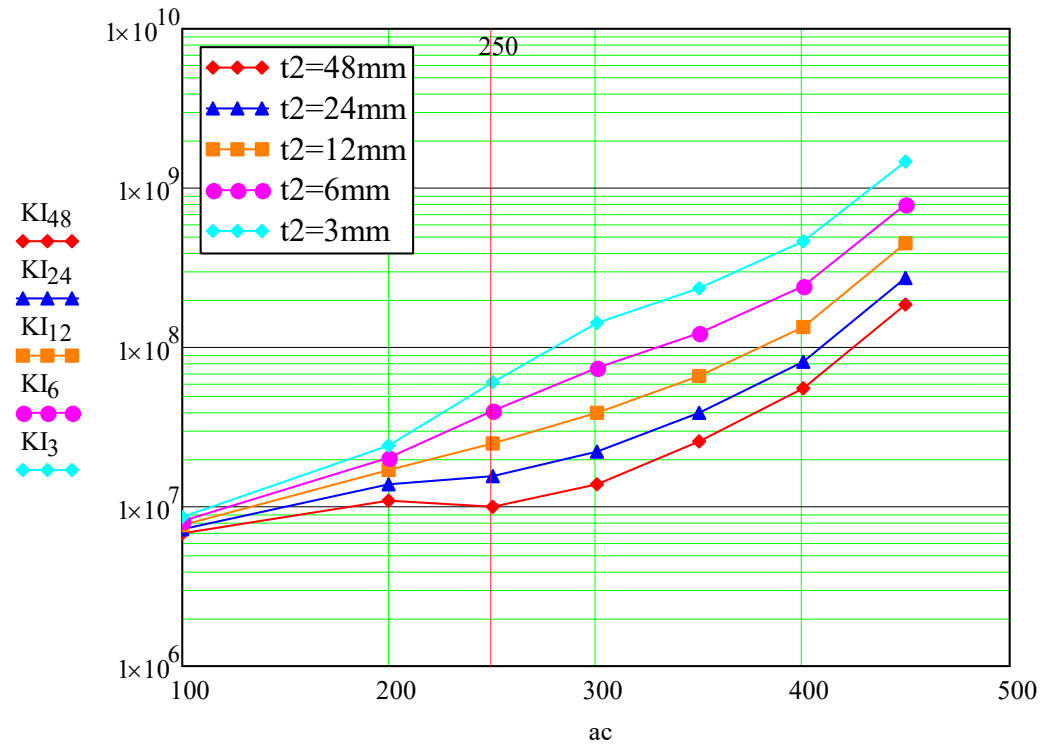


Figure C-1 SIF values for crack growing in different thicknesses plates in flat plate model

Figure C-2, shows the method that was tried to calculate equivalent crack lengths. The blue curve is the constant thickness curve, the red curve is for  $t_2 = 48\text{mm}$  ( $t_2/t_1 = 4$ ). The points A and B have the same SIF and reading down the equivalent crack length on the  $t_2=12\text{mm}$  case for the  $t_2=48\text{mm}$  case is found.

The point A means for the SIF value corresponding to 300mm crack length on  $t_2=48\text{mm}$  cracking plate, the equivalent crack size on  $t_2=12\text{mm}$  crack plate is approximately 165.861mm and therefore the equivalent crack length ratio is  $\frac{165.861}{300} = 0.5529$ . The same situation for point B, the SIF value corresponding to 400mm crack length on  $t_2=48\text{mm}$  cracking plate, the

*Appendix C Estimation of SIF values for crack growing through a change in thickness:  
First empirical method*

equivalent crack size on  $t_2=12\text{mm}$  cracking plate is about 328.843mm and the equivalent crack length ratio is directly  $\frac{328.843}{400} = 0.8221$ . The remaining equivalent crack lengths are calculated for the other plate thicknesses.

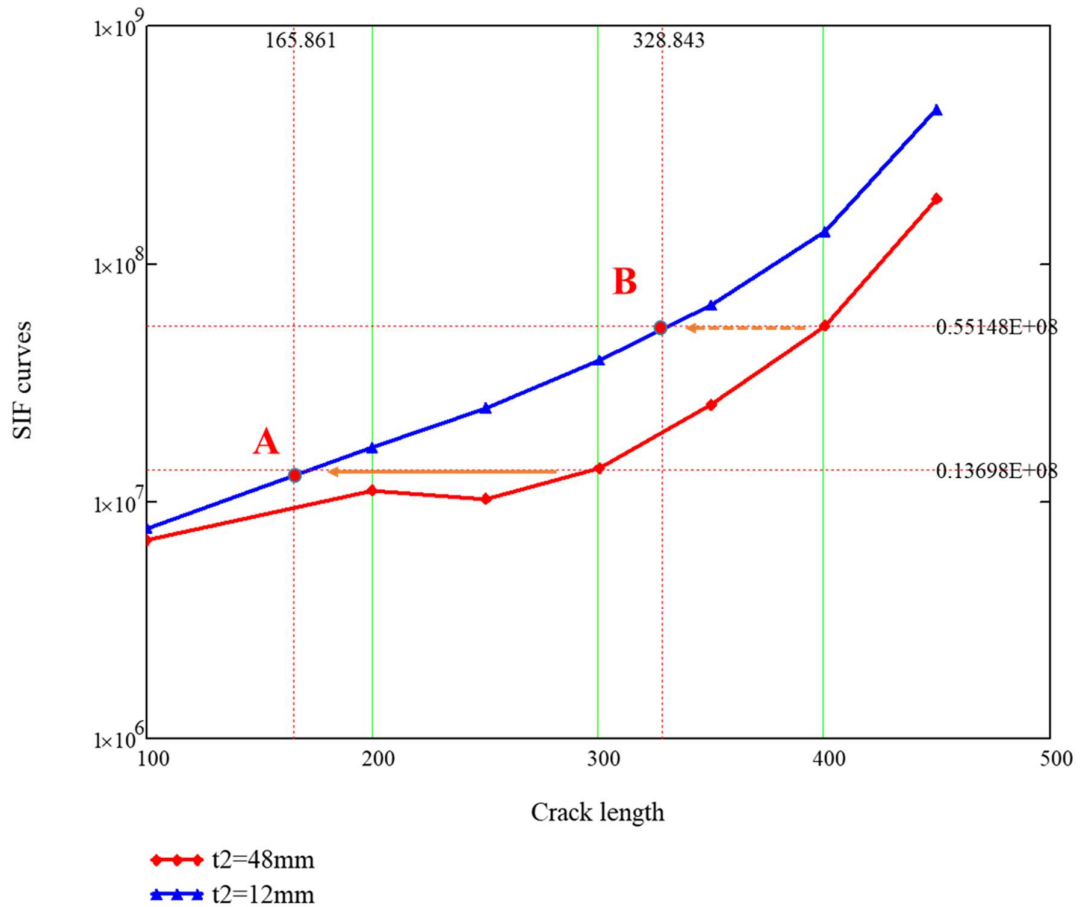


Figure C-2 Estimating equivalent length of crack for the same SIF value

Figure C-3 shows (horizontally) the equivalent,  $t_1 = 12\text{mm}$ , crack length for different plate thicknesses. For constant plate thickness,  $t_2 = 12\text{mm}$ , the equivalent total crack length is the same as the actual crack length, when  $t_2$  is less than  $t_1$  the equivalent crack length is reduced and vice versa.

Appendix C Estimation of SIF values for crack growing through a change in thickness:  
First empirical method

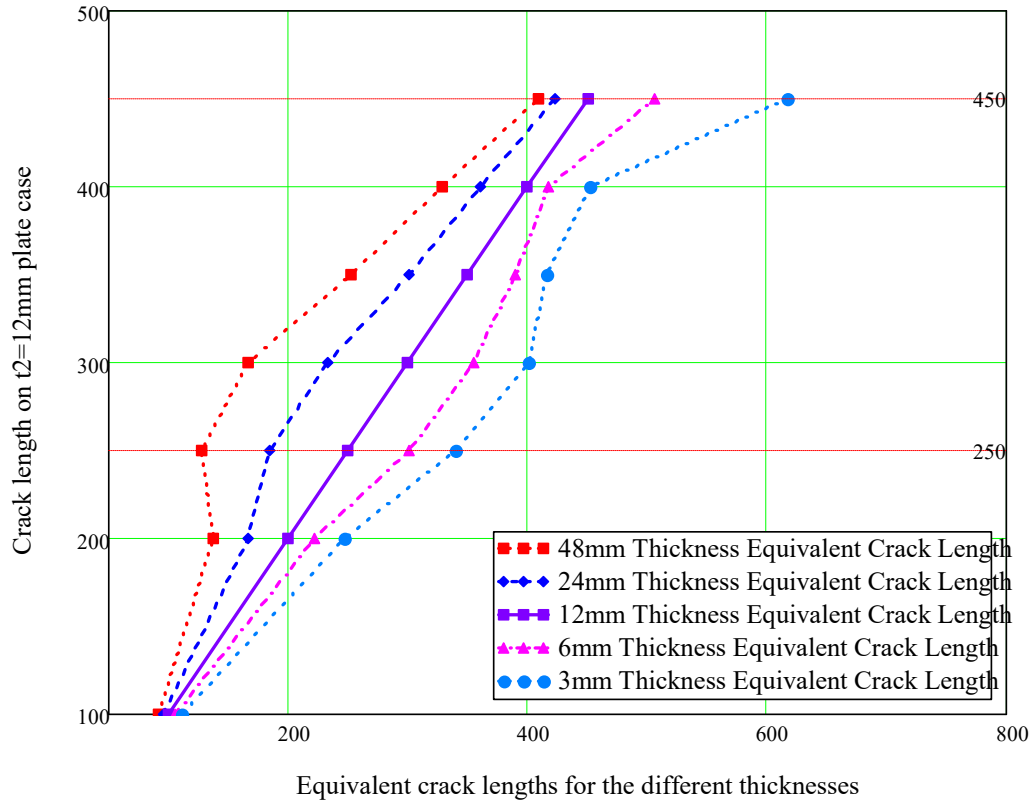


Figure C-3 comparing the equivalent crack length for five thicknesses

Figure C-4 shows the ratio of equivalent crack length to actual crack length for each point in Figure C-3.

Appendix C Estimation of SIF values for crack growing through a change in thickness:  
 First empirical method

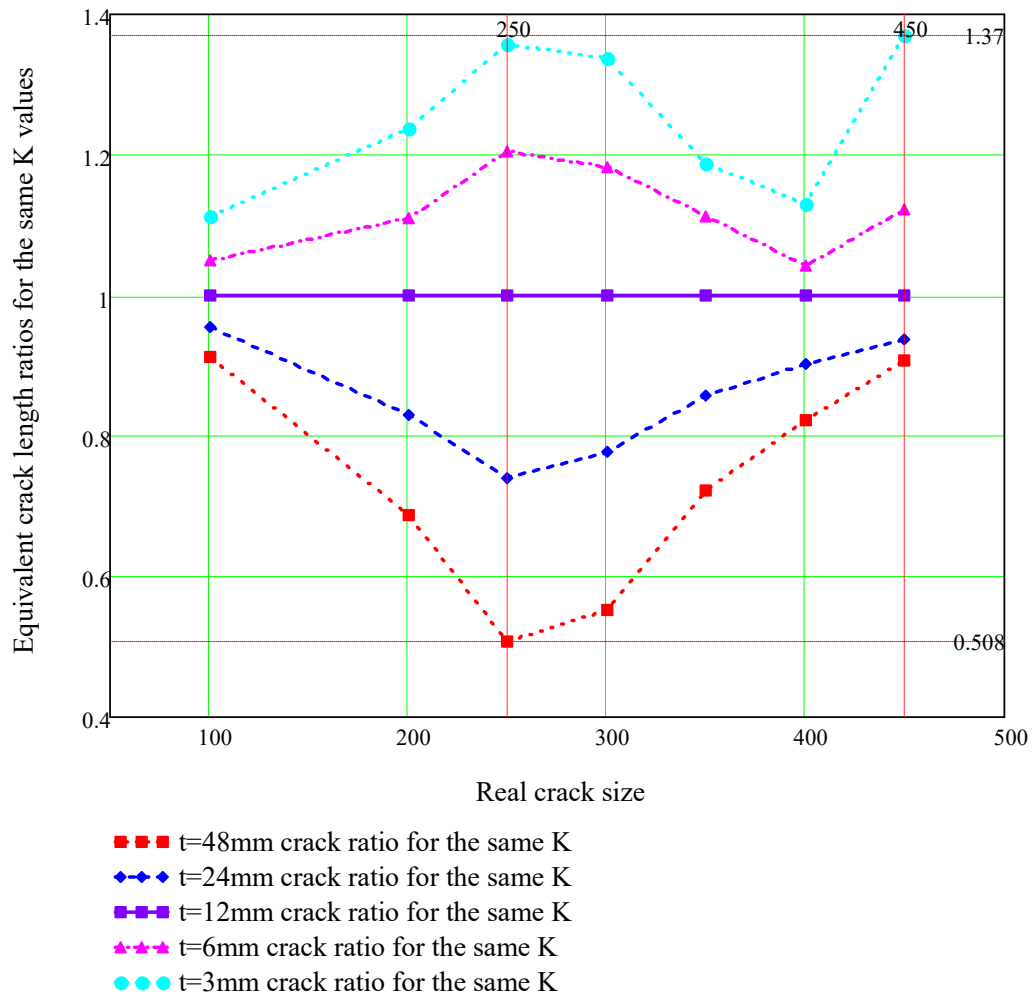


Figure C-4 Equivalent crack length ratios for five thicknesses

Unfortunately the equivalent crack length did not give a simple result.

Excluding the 450mm cracks, the curves in Figure C-4 were approximately fitted using a (1 + normal distribution) equation (simply because of the bell shape).



*Appendix C Estimation of SIF values for crack growing through a change in thickness:  
First empirical method*

---

This led to an estimation formula in the form of  $F\left(\frac{ac}{250}\right) = 1 + Q \cdot \sigma \cdot f\left(\frac{ac}{250}, \mu, \sigma\right)$ , where  $Q$  is a function of  $\frac{t_1}{t_2}$  and  $f\left(\frac{ac}{250}, \mu, \sigma\right)$  is the normal distribution function with the real expectation value  $\mu = 1.1$  and the standard deviation  $\sigma$  is 0.4. The factor of  $\frac{ac}{250}$  is a scale factor that is in the range 0 to 2 and has a value of 1 when the crack tip is at the thickness change.

The results were:

$$F_N\left(\frac{ac}{250}\right) = 1 + Q \cdot \left(\frac{t_1}{t_2}\right) \cdot \sigma \cdot f\left(\frac{ac}{250}, \mu, \sigma\right)$$

when

$$t_1 = 12mm,$$

$$\frac{t_2}{t_1} = 4, \quad t_2 = 48mm, \quad Q = -4.45$$

$$\frac{t_2}{t_1} = 2, \quad t_2 = 24mm, \quad Q = -1.26 \quad (C.1)$$

$$\frac{t_2}{t_1} = 1, \quad t_2 = 12mm, \quad Q = 0$$

$$\frac{t_2}{t_1} = 0.5, \quad t_2 = 6mm, \quad Q = 0.25$$

$$\frac{t_2}{t_1} = 0.25, \quad t_2 = 3mm, \quad Q = 0.22$$

The approximate estimation curve and the FEA data points are shown, for different  $t_2/t_1$  in Figure C-5 to Figure C-8.

Appendix C Estimation of SIF values for crack growing through a change in thickness:  
First empirical method

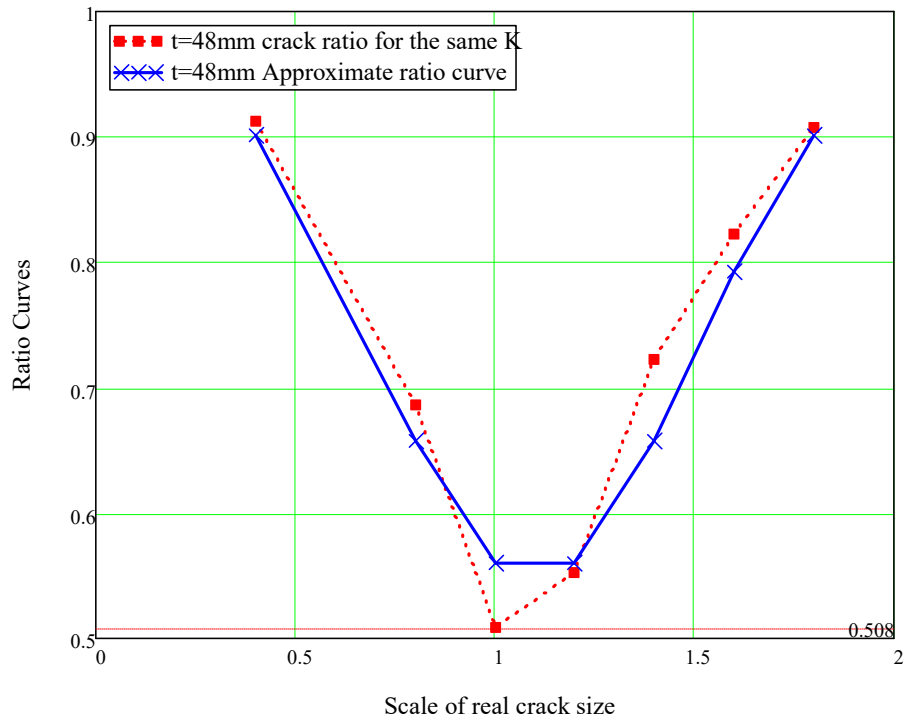


Figure C-5 Estimation of crack length ratio when  $t_2/t_1=4$

Appendix C Estimation of SIF values for crack growing through a change in thickness:  
First empirical method

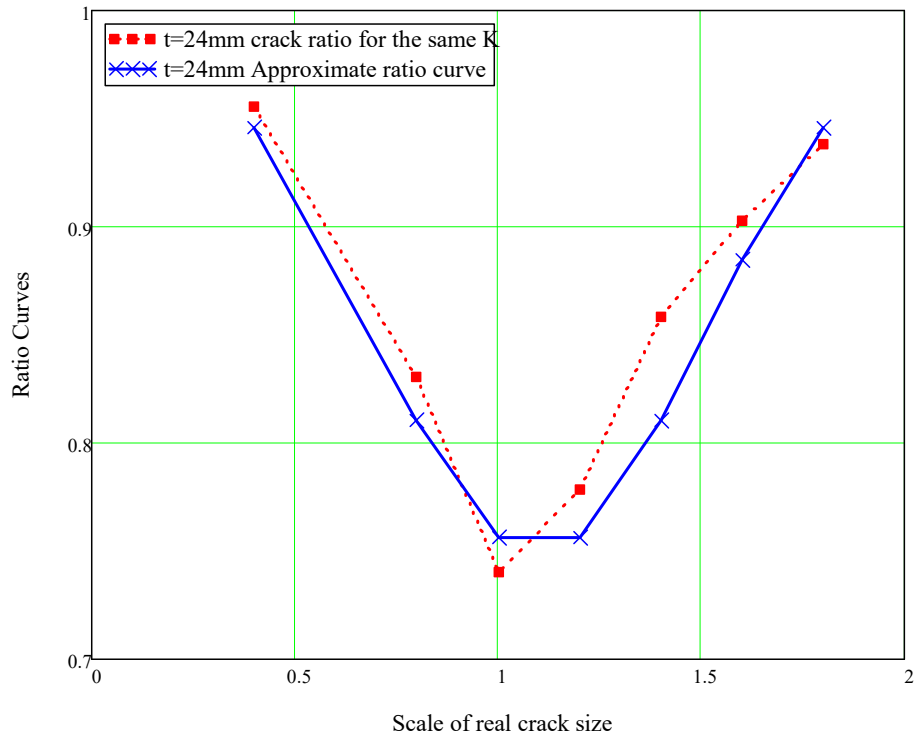


Figure C-6 Estimation of crack length ratio when  $t_2/t_1=2$

Appendix C Estimation of SIF values for crack growing through a change in thickness:  
 First empirical method

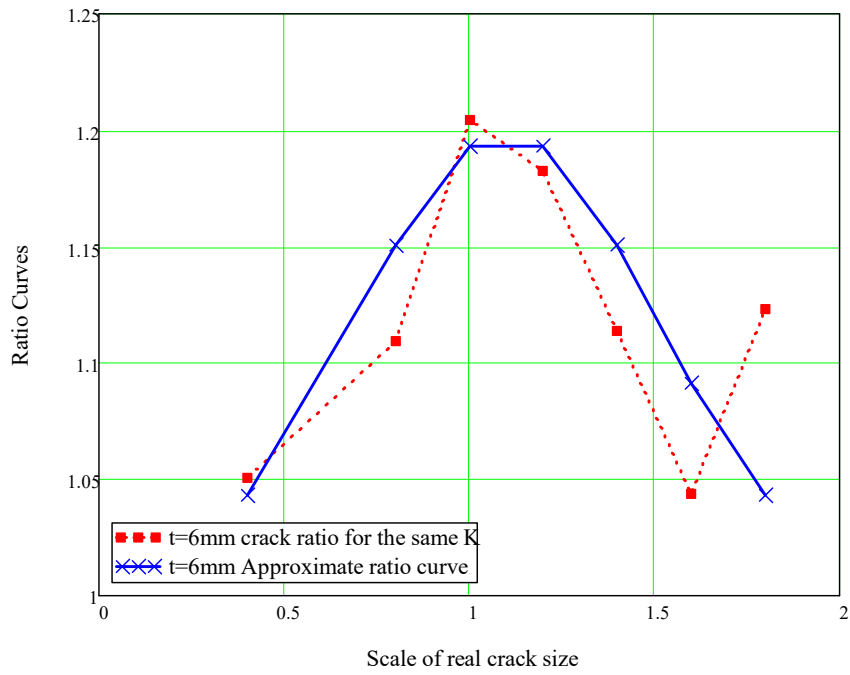


Figure C-7 Estimation of crack length ratio when  $t_2/t_1=0.5$

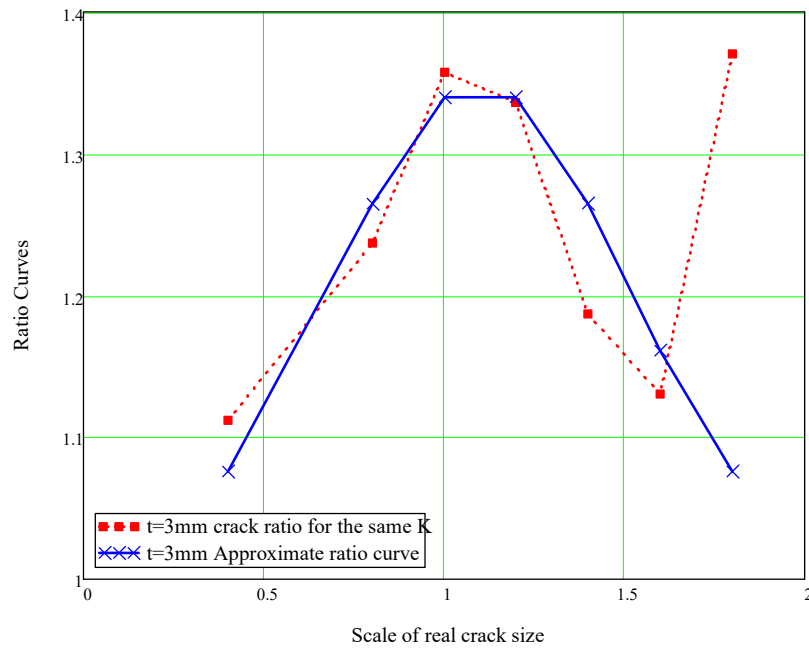


Figure C-8 Estimation of crack length ratio when  $t_2/t_1=0.25$

*Appendix C Estimation of SIF values for crack growing through a change in thickness:  
First empirical method*

---

The equivalent crack growth approach did not lead to a simple method and the simple equation fit to the results was poor, so the method was abandoned.

## **Appendix D References**

FETT, T. 1998. Stress intensity factors and weight functions for special crack problems, FZKA Karlsruhe.

JANSSEN, M., ZUIDEMA, J. & SUN, R. W. 2004. H. Fracture Mechanics. London: Spon Press

XU, L., LOU, B. & BARLTROP, N. 2013. Considerations on the fatigue assessment methods of floating-structure details. Proceedings of the Institution of Mechanical Engineers, Part M: Journal of Engineering for the Maritime Environment, 227, 284-294.